Transitional pipe flow of drag-reducing polymer solutions

UNIVERSITY OF
LIVERPOOL

Acknowledgements

First, my sincerest gratitude goes to my supervisors, Professor Marcel P. Escudier and Dr. Robert J. Poole for the opportunity to work with them on this challenging project. They have provided me with all the resources needed and given me valuable advice and direction without which this thesis would not have been possible.

I am thankful for my association with my colleagues from the Department of Mechanical Engineering, Keith Nickson, Fiona Keegan and Azuraien Japper-Jaafar who have provided me with moral and technical support, particularly, Dr. Keith Nickson, who has also shared my success and disappointments over the period of three years.

I am extremely grateful to all the technical support staff who have contributed to the design and construction of various experimental apparatus, which ensured the success of this work, especially John Curran, Steven Bode and Derek Neary.

I wish to express my appreciation to Professor Fernando Pinho for establishing the initial contact which gave me the opportunity to come to Liverpool and work with Professor Escudier.

I also wish to thank the sponsorship of EPSRC (Engineering and Physical Sciences Research Council) in England and of the Portuguese company Navegadores® for funding my study.

Summary

This report details an experimental pipe-flow investigation covering the laminar, transitional and fully-turbulent regimes with particular attention placed on the transitional regime, for both Newtonian and non-Newtonian liquids; aqueous glycerine, 60% w/w, and three different polymer solutions, 0.03% w/w and 0.125% w/w of a polyacrylamide and 0.15% w/w of a xanthan gum. The non-Newtonian liquids investigated are all drag reducing and shear thinning, the 0.125% polyacrylamide and the 0.15% xanthan gum solutions have similar degrees of shear-thinning but different levels of elasticity. These liquids have shown reasonable resistance to degradation and transparency (optically clear).

The experiments were carried out in a long horizontal glass pipe facility with a length of 23.28 m and a diameter of 100 mm, with the measurements obtained using a laser Doppler anemometer system. For all liquids investigated, detailed measurements of mean axial velocity and velocity fluctuations were obtained at different axial locations along the pipe and for various azimuthal angles.

Within the laminar and turbulent flow regimes the results of the axial velocity and corresponding velocity fluctuations are in good agreement with the literature. Therefore the experimental results for these two flow regimes represent a "validation" of the experimental arrangements and instrumentation used in this work. However, for the transitional flow regime the experiments resulted in significant new observations. Strong velocity profile asymmetries appear in transitional flow for all

non-Newtonian liquids. This effect is not seen for the Newtonian liquid where the flow remains axisymmetric.

For the non-Newtonian liquids, as the Reynolds number increases from the laminar flow region entering the transitional regime the asymmetry of the velocity profile progressively increases, then as the flow leaves the transitional regime approaching the turbulent regime the asymmetry progressively decreases becoming symmetric again at fully turbulent flow. All non-Newtonian liquids investigated exhibit the same variation of the degree of asymmetry with the azimuthal angle. The velocity profiles remain essentially symmetric from the entrance until a particular axial distance along the pipe, and then, the degree of asymmetry suddenly increases and remains at a constant level until the outlet.

Different outlet and inlet flow conditions were imposed by making modifications to the upstream and downstream geometry of the pipe facility in order to isolate, and be able to study the influence of, each particular modification on the axial velocity profiles. However, after these modifications the velocity profile asymmetry and its evolution essentially remained unaltered. The causes of the velocity profile asymmetries observed in non-Newtonian pipe flow within the transitional-flow regime could not be explained, but it has been shown that it is independent of the influence of the inlet and outlet geometry. Consequently, it is hoped that the large amount of experimental data obtained from this work can be used to gain more insight into the mechanism which leads to the asymmetry.

Contents

List of tables

List of figures

Nomenclature

Latin letters

a	constant of the Carreau-Yasuda model
c	polymer concentration (%)
c^*	critical overlap concentration (%)
D	diameter of the pipe (m)
De	Deborah number [λ / T]
Dn	Dean number [$Re(D /(2R_A))^{1/2}$]
Ek	Ekman number [$Ek = \mu_w /(2\Omega\rho D^2 \sin\beta)$]
f	Fanning friction factor [$\tau_w /(1/2\rho U_b^2)$]
G'	storage modulus [$\mu\lambda\omega^2 /(1+(\lambda\omega)^2)$] (Pa)
G''	loss modulus [$\mu\omega /(1+(\lambda\omega)^2)$] (Pa)
k	power-law consistency index ($Pa.s^n$)
L	length of the test pipe used for pressure-drop measurements (m)
L_e	entrance length (m)
m	Cross model exponent
$\dot{m}$	mass flow rate (kg/s)
n	power-law model exponent
N_1	first normal-stress difference (Pa)
N_2	second normal-stress difference (Pa)
N_S	sample size

P_S population average

r radial location within pipe (m)

R radius of the pipe (m)

R_A radius of curvature of the pipe axis (m)

Re Reynolds number [$\rho U_b D / \mu$]

Re_C critical Reynolds number

Re_W Reynolds number [$\rho U_b D / \mu_W$]

Re_{CS} Collins-Schowalter Reynolds number [$\rho U_b^{2-n} D^n / k$]

Re_{MR} Metzner-Reed Reynolds number [$\rho U_b^{2-n} D^n / k \cdot 8(n/(6n+2))^n$]

Re_1 Reynolds number corresponding to onset of transition

Re_2 Reynolds number corresponding to end of transition

S_S population standard derivation

T characteristic time of the deformation process (s)

t_i transit time of a particle across the control volume (s)

u local mean velocity in the axial direction (m/s)

U_b bulk mean velocity [$4\dot{m}/(\rho\pi D^2)$] (m/s)

u_i individual velocity from burst measurements (m/s)

u_m arithmetic average of the velocity data on either side of the centreline (m/s)

u_0 velocity at the centreline of the pipe (m/s)

u' velocity fluctuation (or turbulence intensity) in axial direction (m/s)

u^+ non-dimensional velocity [u / u_τ]

u_τ friction velocity [$(\tau_W / \rho)^{1/2}$] (m/s)

x axial distance from the entrance to the measuring location (m)

y distance from the pipe wall (m)

y^+ non-dimensional distance from the pipe wall [$\rho u_\tau y / \mu_W$]

Z_C confidence coefficient

Greek letters

α coefficient of asymmetry [$\int_0^R (u - u_m) r \cdot dr / \int_0^R u_m r \cdot dr \cdot 100$] (%)

β angle between the pipe axis and the rotation axis of the Earth (°)

$\dot{\gamma}$ shear rate (1/s)

$\dot{\gamma}_W$ wall shear rate (1/s)

Δp pressure drop (Pa)

Δt_i duration of the Doppler signal (s)

$\dot{\varepsilon}$ extensional strain rate (1/s)

λ relaxation time of the liquid [$N_1 / (2\mu\dot{\gamma}^2)$] (s)

λ_C constant which represents onset of shear-thinning in Cross model (s)

λ_{CY} constant which represents onset of shear-thinning in Carreau-Yasuda model (s)

μ viscometric shear viscosity (Pa.s)

μ' dynamic viscosity [G'' / ω] (Pa.s)

μ_E extensional viscosity (Pa.s)

μ_W wall shear viscosity [$\tau_W / \dot{\gamma}_W$] (Pa.s)

μ_0 viscosity at zero shear rate (Pa.s)

μ_∞ viscosity at infinite shear rate (Pa.s)

θ azimuthal angle (°)

ρ fluid density (kg/m^3)

τ shear stress (Pa)

τ_W wall shear stress [$\Delta pD/(4L)$] (Pa)

ω angular frequency (rad/s)

Ω angular velocity of the Earth (7.272x10^{-5} rad/s)

Ψ_1 first normal-stress difference coefficient [$N_1 / \dot{\gamma}^2$] (Pa.s^2)

1 - Introduction

1.1 – Objectives

It is well known that many industries, such as the chemical, pharmaceutical, petroleum and plastics, amongst others, make use of fluid flow in dozens of practical applications. Examples of such applications include drilling operations, injection-moulding, energy provision, delivery of products, etc. The fluids used in such applications can be classified as Newtonian or non-Newtonian. The fundamental knowledge of Newtonian fluid flow in pipes, for example air or water, is regarded as well understood; however, the majority of fluids encountered in such industrial pipe flow systems and under everyday conditions are non-Newtonian. Examples of non-Newtonian fluids are; polymers, paints, cleaning liquids, drilling muds, crude oil, food and pharmaceutical products, blood, etc.

The rheological behaviour of non-Newtonian fluids is more complex than for Newtonian fluids, because the viscosity is not necessarily constant and depends on factors such as the shear rate and the time of shearing. Their rheological behaviour can be classified as purely viscous (i.e. inelastic) or viscoelastic and as time-dependent or non time-dependent, and, as a consequence, non-Newtonian fluids are as likely to differ from each other as from a Newtonian fluid.

Why the flow of a fluid along a straight pipe is typically observed to change from laminar to turbulent as the flow rate is increased has been an ongoing quest for more than a century and is not yet understood in detail even for a Newtonian fluid.

Therefore, any advance towards an understanding of the fundamentals involved in transition from laminar to turbulent flow will have a widespread impact on flows of practical interest. For example, the flow in oil and gas pipelines is often run inefficiently turbulent to avoid the large pressure fluctuations of the transitional regime. Moreover, the control of turbulence is a dream of many engineers and a complete understanding of turbulence is the desire of many scientists (Hof et al (2003)).

Although considerable advances have been made in the last decade in improving knowledge about the transitional mechanism from laminar to turbulent flow for Newtonian fluids in pipes, for non-Newtonian liquids little is known, perhaps unsurprisingly given the inherent additional complexity of non-Newtonian rheological behaviour involved. There is virtually no data available in the literature for transitional pipe flow of non-Newtonian fluids. Identification of the fluid dynamics involved and the relevant fluid properties, to determine possible correlations between fluid dynamics and complex rheological behaviour of non-Newtonian fluids, is needed to understand in more detail the mechanics of transitional pipe flow.

The above considerations, both fundamental scientific interest and numerous practical applications, motivated this work which contributes to a better understanding of non-Newtonian fluid flow in pipes in the transitional regime between laminar flow and fully-turbulent flow. This investigation aims to address this gap in the knowledge by providing detailed observations of the radial distributions of axial velocity for a number of different polymer solutions. Results of

mean and fluctuating velocity were obtained, plus the wall shear stress, for a range of Reynolds numbers from laminar to fully-turbulent flow conditions. A complete study of the rheological characteristics of the different polymer solutions investigated was used to link the fluid flow dynamics with the rheological behaviour.

The underlying motivation for this study was the need to explain an interesting effect observed independently by Escudier and Presti (1996) and Peixinho et al (2005) that for Reynolds numbers within the transition region, the flow of non-Newtonian liquids develop stable asymmetric velocity profiles. For laminar and turbulent flows the velocity profiles are symmetric for both Newtonian and non-Newtonian liquids, although asymmetry due to the Earth's rotation can occur under fully developed-laminar flow conditions for Newtonian fluids of low viscosity. Three groups of researchers (Escudier et al (2005)) jointly published these and additional observations. Recently, Esmael and Nouar (2008) highlighted the velocity profile asymmetry phenomenon by publishing a three-dimensional description of this effect.

1.2 – Literature review

The literature review has been designed in the following manner; the relevant scientific investigations related to pipe flow of non-Newtonian fluids, with emphasis on pressure drop and turbulent drag reduction, are reviewed, followed by a literature survey of transitional pipe flow, firstly for Newtonian and then for non-Newtonian fluids. Finally, the main conclusions of the literature review are presented.

1.2.1 – Pipe flow of non-Newtonian fluids

Turbulent drag reduction is the reduction of friction on the surfaces past which the fluid flows. It has been found that dissolving a small amount of polymer, typically only a few parts per million (ppm) in a solvent, typically water, can drastically reduce the pressure drop (or frictional drag) of turbulent pipe flows. The drag-reduction phenomenon was discovered by Toms (1949) and has subsequently received a lot of attention from many authors, especially in relation to pipe flow because of its practical use in various commercial applications such as efficient pipeline transport of fluids.

Some of the earliest experimental studies were carried out by Metzner and Reed (1955), Dodge and Metzner (1959) and Shaver and Merrill (1959), who developed empirical correlations between friction factor and Reynolds number (*Re*), which were obtained adopting a purely viscous liquid that follows the power-law model (see Section 2.3). Therefore, the proposed correlations were restricted to inelastic and time-independent fluids. A few years later Metzner and Park (1964) produced a correlation for the degree of turbulence suppression (drag reduction) in turbulent flow considering viscoelastic properties. They correlated the drag reduction with the ratio of elastic to viscous stress, i.e. with N_1 / τ_w, where N_1 is the first normal-stress difference, which gives an indication of elasticity, and τ_w is the wall shear stress (see Chapter 2 for further explanation).

Over the past decades numerous studies have been carried out on drag reduction by polymer addition. Review articles of the early works on this subject began to appear

when Lumley (1969) discussed the physical phenomena of drag reduction. Hoyt (1972) provided a comprehensive review of the effect of various solvent-additives on frictional drag and summarised the various theories that attempted to explain the drag-reduction phenomenon. Virk (1975) presented a review based on experimental evidence which showed that turbulent drag reduction can increase due to a number of factors including increased flow rate, increased polymer concentration, increased polymer molecular weight and a decrease in pipe diameter. It was also demonstrated that turbulent drag reduction is limited within two asymptotes, the Prandtl-Karman law and a maximum drag reduction asymptote (now commonly referred to as "Virk's asymptote" or "Virk's maximum drag reducing asymptote"). To describe the mean velocity profiles Virk et al (1970) proposed an important model called the three-layer model, derived from pressure-drop measurements, which comprises of a viscous sub-layer, an interactive zone and a Newtonian plug. The model and the two drag-reduction asymptotes mentioned above will be discussed in further detail in Chapter 4.

In order to investigate the role of elongational (or extensional) viscosity as a crucial rheological property in combination with viscoelasticity, Durst et al (1982) and Gyr (1984) attempted to provide extensional-viscosity models to describe the drag-reduction mechanism. As Matthys (1991) pointed out, extensional viscosity and viscoelasticity are both important and play a major role in turbulent drag reduction. Escudier et al (1999) was one of a few, until then, to report drag reduction experiments including measurements of the shear viscosity and first normal-stress difference as a function of shear rate and also extensional viscosity *versus* strain rate, obtained using the "opposed-jets" technique (Fuller et al (1987)). With both the

viscoelastic and extensional viscosity characteristics available the situation would still not be entirely satisfactory given the batch-to-batch variability of polymers, the influence of mixing, biological and mechanical degradation, ageing, etc.

A number of investigators, for example Tiederman (1989), Pinho and Whitelaw (1990), Pereira and Pinho (1994), den Toonder et al (1997), Escudier et al (1999) and Ptasinski et al (2001), have published extensive detailed experimental measurements in turbulent pipe flow, reporting the effect of polymer additives on various elements of the drag-reducing flows, such as mean velocity distributions, turbulence intensities, and other measurements of the turbulence structure. An important conclusion from these papers was that polymer addictives do not simply suppress the turbulent motion. On the contrary, the stream-wise turbulence intensity can increase while the normal turbulence intensity decreases, meaning that the turbulence structure is changed, rather than simply attenuated.

In spite of the large quantity of experimental data available, the mechanism of drag reduction by polymers still remains unclear. As a consequence, direct numerical simulation (DNS) has been used in an attempt to obtain more insight into the mechanism of polymeric drag reduction. Orlandi (1995) and den Toonder et al (1995) investigated the role of extensional viscosity using "toy" models but their results only produced minor drag-reduction effects. Pioneering viscoelastic DNS work using robust viscoelastic constitutive equations (Sureshkumar et al (1997) was then followed by several others (Dimitropoulos et al (1998), and Housiadas et al (2005), amongst others). Contrary to what is possible with experiments, one can attempt in numerical simulations to isolate certain properties of the polymer by using

a specific constitutive equation, and to study in detail the effects that these properties have on the flow. Doing this, the importance of these isolated properties for the phenomenon of drag reduction can be estimated. However, in order to validate the predictions obtained using DNS, comparisons with experimental data must be made. Without this, DNS provides speculative predictions with no solid grounding. The main benefit of using DNS is that once validated experimentally, it can be reliably used to model the flow behaviour and provide a detailed picture of turbulent structure. Such a picture is difficult to obtain experimentally in optically clear laboratory fluids, and almost impossible to obtain in opaque, fine particle suspensions.

1.2.2 – Transitional pipe flow of Newtonian fluids

The study of transitional pipe flow has occupied many researchers since the time of Reynolds' experimental work (1883), so it is practically impossible to cite every paper on the subject. We will mention here some of the papers which are most relevant to the present investigation. A recent review of both numerical and experimental investigations, about transition from laminar to turbulent in pipe flow of Newtonian fluids, can be consulted for more detailed information (Eckhardt et al (2007)).

The pioneering study of transition to turbulence in a pipe flow was conducted by Reynolds (1883), who derived the law of similarity which now bears his name. Reynolds stated that there is a critical value of the dimensionless quantity

($\rho UD/\mu$), below which transition from laminar to turbulent flow does not occur regardless of the initial disturbance amplitude, commonly referred to as the critical Reynolds number (Re_C). Under favourable conditions, when the water in the supply tank had settled and the inflow was controlled with suitable funnels, Reynolds was able to maintain laminar flow until a Reynolds number (*Re*) of 12,000. On the other hand, with sufficiently strong perturbations, he was able to trigger transition near a Reynolds numbers of about 2000. Further investigations have shown that a pipe flow might remain laminar even at *Re* up to 100,000 (Hof et al (2003)), if the experiments are carried out under extremely careful conditions.

Stability experiments with disturbances introduced in the fully-developed region of the pipe were initially carried out by Leite (1959) using a hot-wire anemometer and a mechanical turbulence generator. He observed deviation of the velocity profile from axisymmetry for an air flow, the maximum velocity was found to be off the geometric axis. The cause of asymmetry was found to be thermal rather than geometrical and in order to combat distortions due to thermal effects, a heat source was used. By varying the heating, it was possible to fix the location of the maximum in the velocity profile. Another important conclusion was that transition to turbulent flow starts whenever the amplitude of a controlled disturbance exceeds a threshold value which decreases with increasing Reynolds number.

An important stability experiment with disturbances introduced in the inlet rather than in the fully-developed region was carried out by Wygnanski and Champagne (1973), using a hot-wire anemometer. They concluded that introducing disturbances into the inlet using various different obstructions alters the transitional Reynolds

number. Two different types of intermittently turbulent flow were discovered occurring naturally in a pipe flow, firstly, slugs which were caused by the instability of the flow to small disturbances in the inlet region of the pipe, and secondly puffs which were generated by large disturbances at the inlet around the critical Reynolds number. While slugs were associated with transition from laminar to turbulent flow, puffs represented an incomplete relaminarization process. Wygnanski et al (1975) investigated the structure of these puffs in some detail and found their structure to be very different from fully-developed turbulent pipe flow and essentially independent of the character of the disturbance which created them.

Darbyshire and Mullin (1995) used a constant mass flux system where the flow is pulled by a piston to fix the flow rate. The results obtained were consistent with those achieved with the pressure gradient driven systems used by Wygnanski and Champagne (1973), such that localised puffs and slugs were found at "low" Reynolds number (circa 2300) and fully-developed turbulence at larger flow rates.

Two studies from the same year using different working fluids in pipe flow, Draad and Nieuwstadt (1998) with water and Eliahou et al (1998) with air, observed asymmetric axial velocity profiles and suggested different causes for the observed distortions. Draad and Nieuwstadt (1998) attributed the cause of these distortions of the laminar velocity profiles to the Earth's rotation, suggesting the rotation of the Earth had a large effect on their setup. The effect of the Coriolis force due to the Earth's rotation in such a long pipe (~30 m) was due to the fact that the flow is governed by a force equilibrium between pressure forces and viscous forces, and inertia does not play a role once the flow is fully developed. As kinematic viscosity

is in general small, to balance even such a small force as the Coriolis force, a large deviation of the velocity profile is required. Numerical simulations were in good agreement with the experimental observations. According to Eliahou et al (1998), mean velocity distortion was in their case a consequence of the type of disturbance generated in the fully-developed flow, only observed when a high amplitude asymmetric perturbation was imposed. The transition to turbulence regime only occurred after the parabolic velocity profile (Hagen-Poiseuille profile) became distorted (asymmetric).

A new attempt to explain transition in pipe flow of Newtonian fluids has been made experimentally by Hof et al (2003) who concluded that the size (amplitude) of the perturbation required to cause transition scales as the inverse of the Reynolds number, the later numerical work of Mellibovsky and Meseguer (2006) agreed with this finding. Faist and Eckhardt (2004) and Peixinho and Mullin (2006) suggested that this relationship is not valid for small values of Reynolds number: below a critical value sustained turbulent flow cannot be created by introducing perturbations, no matter how large the amplitude of the perturbation. They also suggested that for Reynolds numbers exceeding that critical value the lifetime of turbulence becomes infinitely large, marking a change from transient to persistent turbulence. Recently Hof et al (2006) presented experimental data and numerical calculations contradicting that view showing that turbulence in pipe flow is only a transient event, contrary to the commonly held view, and the lifetime of turbulence does not diverge to infinity at finite critical Reynolds number but rather increases exponentially with Reynolds number. According to the authors if the pipe length is long enough and the

waiting time is sufficiently long the decay of turbulence would be detected and the flow would be relaminarized.

1.2.3 – Transitional pipe flow of non-Newtonian fluids

From the previous subsection it can be concluded that the transition mechanism from laminar to turbulent flow of Newtonian fluids in pipes, despite some considerable advances in the last two decades, is still a process not completely understood. For non-Newtonian fluids less is known, perhaps due to the additional complexity involved. Aside from a handful of papers, discussed below, there is virtually no data about the transitional flow of non-Newtonian fluids.

A few theoretical and numerical studies concerning the transition regime of non-Newtonian fluid flow, such as Metzner and Reed (1955), Ryan and Johnson (1959), Hanks (1962), Mishra and Tripathi (1971) and Slatter (1999), have been published. Comparing the different criteria used in those investigations (Nouar and Frigaard (2001)) to estimate the critical Reynolds number it is possible to find differences between them when the rheological behaviour departs significantly from Newtonian behaviour, leading to the conclusion that it is unclear under which circumstances transition of non-Newtonian pipe flow is different to transition for a Newtonian fluid.

As far as experimental investigations for the transitional flow regime are concerned, we will mention only the most relevant to the present investigation in chronological order.

Chung and Graebel (1972) used for the first time the laser Doppler anemometer (LDA) technique in non-Newtonian pipe flows. They showed a consistent delay in transition from laminar to turbulent regime with the addition of high-molecular-weight polymers to water. For tap water the critical Reynolds number for transition was found to be Re = 2395, but for fresh polymer solutions the range of critical Reynolds number varied between 6428 and 10570 depending on the concentrations and age of the solutions. Zakin et al (1977) also used LDA to measure the mean velocity and turbulence intensity of high-molecular-weight polymers, a Polyox coagulant and a polyacrylamide polymer, diluted in glycerine-water mixtures. Contradicting Chung and Graebel (1972), they observed that transition from laminar to turbulent flow occurs earlier for these polymer solutions than for the Newtonian liquids and is accompanied by a flattening of the mean velocity profile.

According to Park et al (1989), the transition region for slurries (suspensions of silica particles in oil) is much narrower than for Newtonian fluids and the mean velocity profile, as well the corresponding axial turbulent intensity profile, are similar to those obtained for a Newtonian liquid. However, far from the axis, the axial velocity fluctuations are higher for the slurry than for the Newtonian fluid. Slurries are shear-thinning fluids with "yield-stress", which can be defined as the stress below which the fluid does not yield, i.e. does not deform, only elastic behaviour is seen.

Pinho and Whitelaw (1990) and Escudier et al (1992) studied the delay in transition from laminar to turbulent flow for a series of shear-thinning solutions in pipe flow and confirmed that transition occurs at different Reynolds numbers for different

fluids. They also confirmed that Virk's maximum drag reduction asymptote is appropriate for these aqueous solutions.

A characteristic first identified by Escudier and Presti (1996) and a decade latter confirmed by Peixinho et al (2005) was that non-Newtonian yield-stress liquids in transitional pipe flow develop asymmetries of the axial velocity profiles not observed in either laminar or turbulent flows or for Newtonian liquids. This finding was the main source of motivation behind the present investigation; hence, the primary objective was to investigate further this mean velocity profile asymmetry phenomenon.

Perhaps the most extended experimental investigation of transition in pipe flow for non-Newtonian fluids was published by Draad et al (1998). The experimental measurements were conducted in a pipe 32 m in length with a diameter of 40 mm, using a LDA system. A periodic suction and injection of fluid was used to impose controlled disturbances to the water flow. With no disturbance they achieved a critical Reynolds number of approximately 60,000. This value could be obtained by avoiding and/or minimising all sources of flow disturbances during the design and construction of the pipe. For the non-Newtonian polymer solutions the critical Reynolds number was found to be in the range of $8000 \leq Re \leq 30{,}000$. Therefore, the main conclusion was that natural transition originating from disturbances present in the set up is strongly reduced by the addition of polymers (Paterson and Abernathy (1972) reported similar results). However, the exact cause of the reduction in natural transition by polymer additives remains unexplained.

Escudier et al (1999) used a very good method, initially suggested by Park et al (1989), to detect transition from laminar to turbulent flow by plotting the axial turbulence intensity (u'), measured at a fixed radial location (0.8 times the pipe radius), against the Reynolds number. This method (explained in detail in Chapter 4) provides a very clear region of transition, which can be practically indiscernible from the friction factor and Reynolds number data alone.

In 2005, three different groups of researchers, observed the velocity profile asymmetry phenomenon independently (reported jointly in Escudier et al (2005)). The paper reports mean velocity profile data for a wide rage of shear-thinning liquids, for laminar, transitional and turbulent flows in circular pipes. The main conclusion was that asymmetry, to varying degrees, is apparent at all stages of transition from laminar to turbulent flow. The fact that symmetrical velocity profiles were obtained for both laminar and turbulent flow of all the non-Newtonian liquids in three separate laboratories, in different countries (England, France and Australia), leads to the conclusion that the asymmetry must be a consequence of a fluid-dynamic mechanism, rather than geometrical imperfections in the flow facilities.

Recently, Esmael and Nouar (2008) published a paper which provides a three-dimensional description of the velocity profile asymmetries in transitional pipe flow of a yield-stress liquid. Axial velocity experimental measurements were conducted at different axial locations along the pipe and for different azimuthal angles of the cross section. The study confirmed the existence of axial velocity profile asymmetries in transitional flow of non-Newtonian liquids and highlighted the fact that the degree of asymmetry varies with the axial location and the azimuthal angle. They suggested the

existence of a robust nonlinear coherent structure characterised by two weakly modulated counter-rotating longitudinal vortices, mediating the transition between laminar and turbulent flow.

1.2.4 – Conclusions

From the literature review it can be concluded that even today, Reynolds' finding in 1883 has not been explained satisfactory by theory and we still know relatively little about the processes and mechanisms involved in the transition of Newtonian fluids in cylindrical pipe flow. This classical problem is to be considered as still open. But the scenario is worse for non-Newtonian fluids given the inherent additional complexity of different rheological behaviour involved. What is well known is, apart from the unexpected findings of Zakin et al (1977), that a delay in transition from laminar to turbulent flow occurs by addition of a trace percentage of certain polymers to the solvent and the delay is also influenced by polymer concentration. The best indicator of non-Newtonian transition is the axial velocity fluctuations (u'), measured near the wall, plotted against the Reynolds number.

The key point is that, for a range of different shear-thinning liquids, significant departures from axisymmetry in transitional pipe flow is observed. This asymmetry was not observed for either laminar or turbulent regimes. For the Newtonian case, apart from the special situation of the influence of the Coriolis acceleration due to the Earth's rotation, there is no evidence of mean-flow axisymmetry in fully-developed pipe flow for any of the three regimes. The present investigation aims to explore this

interesting effect and to provide a contribution in improving the knowledge of transition pipe flow of shear-thinning liquids.

1.3 – Thesis outline

The next chapter describes the rheology of the working fluids. A review of the relevant rheological concepts and models is presented, followed by a description of the rheological techniques that were applied to characterise the fluids used in this study. A description of fluid degradation that can occur with polymer solutions is also provided.

Chapter 3 presents the experimental arrangement and instrumentation used for the measurements of axial velocities, turbulence fluctuations, flow rate, and pressure difference. A description of the mixing procedure and information of the LDA system employed and associated uncertainties is also given in this chapter.

In Chapter 4 the relevant theoretical definitions and the description of the methodology used to detect the transitional regime for all fluids investigated are presented.

The experimental results obtained in this study are reported in Chapter 5 for laminar and turbulent flows and in Chapter 6 for transitional flow, whilst Chapter 7 presents the influence of changing conditions on the flow in the transitional regime.

Finally Chapter 8 summarises the contents of this work and gives some conclusions in an attempt to understand some general characteristics of non-Newtonian fluid flow within the transitional regime and makes suggestions for further investigation.

2 – Rheology

2.1 – Introduction

According to Barnes et al (1989) the term rheology was first accepted in 1929 when the American Society of Rheology was founded and defined as "*the study of the deformation and flow of matter*".

A flow with adjacent elements of the liquid moving relative to one another can be called either shear or extensional flow, depending upon whether the elements of the liquid flow over or past each other, or if the elements of the liquid flow toward or away from each other. Alternatively, if we visualise shear flow as the movement of hypothetical layers sliding over each other, the velocity of each layer increases or decreases with respect to its neighbour below. The gradient of velocity in the direction at right angles to the flow is called the shear rate ($\dot{\gamma}$) and the force per unit area produced by the flow is called the shear stress (τ). The shear viscosity (μ) is the ratio of shear stress to shear rate.

Just as the shear viscosity is a function of the shear rate, the extensional (or elongational) viscosity (μ_E) is a function of the extensional strain rate ($\dot{\varepsilon}$). However, the behaviour of the extensional viscosity (resistance of the fluid to extensional flow, stretch) is likely to be qualitatively different from that of the shear viscosity. For example, highly elastic polymer solutions that posses a viscosity that decreases with increasing shear rate (shear-thinning) often exhibit an extensional

viscosity that increases dramatically with increasing strain rate (tension-thickening). A fluid for which μ_E decreases with increasing $\dot{\epsilon}$ is said to be tension-thinning.

2.2 – Fluid classification

There are two categories of fluids, Newtonian and non-Newtonian fluids. Newtonian fluids are those whose behaviour, at constant pressure and temperature, has the following characteristics:

a) The shear viscosity is constant, does not vary with shear rate;

b) The only stress generated in a simple-shear flow is the shear stress;

c) The viscosity is constant with respect to the time of shearing and (for vanishing inertia, i.e. $Re \rightarrow 0$) the stress in the fluid falls to zero immediately the shearing is stopped; any reapplication of the shear will produce the same viscosity (Barnes et al (1989));

d) The viscosity measured in a uniaxial extensional flow is always three times greater than the viscosity measured in simple-shear flow.

Any fluid which deviates from the behaviour detailed above is classed as non-Newtonian. A Newtonian fluid is an idealisation, but in many cases it is a very good representation of a large number of liquids under everyday conditions, such as water and all gases. Non-Newtonian fluids are not all the same and they can exhibit a large range of different behaviours, therefore it is not sufficient to say that a fluid is non-Newtonian because they are likely to differ as much from each other as from a Newtonian fluid. Typical non-Newtonian characteristics are listed below (for more

detailed information see for example Ferry (1980), Bird et al (1996) or Barnes (2000)).

a) The shear viscosity is not necessarily constant, but usually varies with shear rate. For non-Newtonian fluids the shear viscosity is not constant but a function of shear rate, apart from the noticeable exception of the Boger fluid. A Boger fluid (Boger (1977)) is a highly viscoelastic fluid and is a dilute solution of a high-molecular-weight polymer in a normally viscous solvent. For this solution the decrease in viscosity is very small with increasing shear rate, and for all practical purposes can be taken as constant. The most common types of non-Newtonian fluids are shear-thinning (or pseudoplastics) which exhibit a decrease in shear viscosity with increasing shear rate. The general shape of the viscosity *versus* shear rate curve for a typical shear-thinning fluid is shown schematically in **Figure 2.1**. Two plateau of constant viscosity can usually be observed, at very low and very high shear rates, called the zero-shear viscosity and infinite-shear viscosity respectively. Some very shear-thinning liquids appear to have a so-called "yield stress" which is defined as the stress below which the liquid does not yield (i.e. no flow takes place) and only elastic behaviour is observed. The yield stress of a "solid-like" material is the point at which, when the applied stress is increased, the material first shows a "liquid-like" behaviour in that it continues to deform with no further increase in stress. Similarly, for a liquid, the yield stress is the point at which, when decreasing the applied stress, it first appears to show a "solid-like" behaviour in that it does not continue to deform. By implication, the viscosity of a yield-stress fluid is infinite at zero-shear rate and there is no question of a plateau at very low shear rate in this case.

b) Shear stress is not the only stress generated in a simple-shear flow, normal stresses can also occur. For a Newtonian fluid in a simple-shear flow the only stress is the shear stress $\tau_{xy} = \mu\dot{\gamma}_{xy}$, however, for viscoelastic fluids in a simple-shear flow, there are two additional normal stress, called the first and second normal-stress differences, N_1 and N_2, respectively. N_1 is always a positive function of the shear rate and in conjunction with the stress acting on a fluid can be used to determine the elasticity (Barnes et al (1989)). N_2 is of less practical significance and is always much smaller than N_1, and for a Borger fluid N_2 is virtually zero (Bird et al (1996)). These normal-stress differences are responsible for a number of interesting rheological effects. The most well known is the rod-climbing phenomenon usually referred to as the Weissenberg effect (Weissenberg (1949)). It is produced when a rotating rod is placed into a vessel containing a viscoelastic liquid. Whereas a Newtonian liquid will be forced towards the rim of the vessel by inertia, and thus have a free surface which is higher at the rim than near the rod, the viscoelastic liquid climbs the rotating rod and produces a free surface that is much higher near the rod. Another manifestation of large normal-stress differences is so-called die-swell (or more correctly extrudate swell). At low Reynolds number when a viscoelastic liquid is extruded from a die or flows from the exit of a tube, it usually swells to a much greater diameter than that of the hole.

c) The viscosity is not constant with respect to the time of shearing and the stress in the fluid does not immediately fall to zero upon cessation of the shearing even in the absence of inertia. The decrease of viscosity with shear rate shown in **Figure 2.1** must be distinguished from a decrease of viscosity with time of shearing which is called thixotropy. For viscoelastic liquids upon cessation of the shear stress

the stress throughout the liquid does not fall immediately to zero. The amount of deviation from purely viscous behaviour is characterised by the Deborah number:

$$De = \frac{\lambda}{T} \tag{2.1}$$

where T is the characteristic time of the deformation process being observed and λ is called the relaxation time of the liquid. The relaxation time is a characteristic of the fluid and for a Hookean solid it is infinite and for a Newtonian fluid is zero (i.e. in the absence of inertia effects Newtonian liquids instantaneously react when a stress is applied or removed). Clearly the greater the relaxation time the greater is the viscoelasticity in a given flow, although fluids with short relaxation times can also display significant elastic effects in flows with fast deformation process such as those encountered in micro-fabricated geometries for example (Rodd et al (2005)).

d) The viscosity measured in uniaxial extensional flow is not necessary three times greater than the viscosity measured in simple-shear flow and is not constant. The ratio of the uniaxial extensional viscosity and the shear viscosity is known as the Trouton ratio, and is always equal to three for Newtonian liquids. For non-Newtonian liquids the Trouton ratio starts at three for small deformation rates, and then, at some critical point, it can begin to rise (see for example Barnes et al (1989)). High values of Trouton ratio indicate high degrees of elasticity and fluids that have a ratio of around three show little elastic behaviour. A demonstration of high extensional viscosity behaviour is the easily reproduced situation when a polymer solution is transferred from one full container to a lower empty container. This open-syphon phenomenon can be directly attributed to the very high Trouton ratios exhibited by the polymer solution. Just as the shear viscosity is also a function of

shear rate the extensional viscosity is also a function of extensional rate. The obvious difference between the two kinds of viscosity is most marked in those cases where the extensional viscosity increases with increasing extensional rate, which even if the viscosity eventually begins to decrease at much higher extensional rates, still results in the extensional viscosity being very much larger then the shear viscosity.

2.3 – Modelling of inelastic non-Newtonian fluids

The simplest mathematical model for shear viscosity μ that can be used to characterise the behaviour displayed by an inelastic non-Newtonian fluid is the power-law model:

$$\mu = k\dot{\gamma}^{n-1} \tag{2.2}$$

where k is the power-law consistency index and n the power-law exponent. If n is equal to 1, the model describes a Newtonian fluid. The smaller the value of n (between 0 and 1), the greater the degree of shear-thinning shown by the fluid. If $n > 1$, that means the viscosity increases with shear rate and the fluid is called shear-thickening (or dilatant). Shear-thickening occurs when the act of deforming a material causes rearrangement of the microstructure of the fluid such that the resistance to flow increases with shear rate (Barnes et al (1989)). However, the behaviour of the majority of non-Newtonian fluids is far more complex than that which can be fitted using the power-law model. As already discussed a common trend in non-Newtonian fluids is for asymptotic behaviour to be observed at both low and high shear rates, resulting in two Newtonian plateaux (as shown in **Figure 2.1**).

The Cross model (Cross (1965)) provides a relationship which describes this behaviour (in log-log coordinates):

$$\frac{\mu-\mu_\infty}{\mu_0-\mu_\infty}=\frac{1}{1+(\lambda_C\dot{\gamma})^m} \tag{2.3}$$

where μ_0 is the viscosity at zero shear rate, μ_∞ the viscosity at infinite shear rate, λ_C the constant which represents the onset of shear-thinning and *m* the exponent. As Escudier et al (2002) demonstrated this model does not, in fact, contain plateau, it is the logarithmic plot that gives the impression of the asymptotic behaviour (μ_0 and μ_∞) and the power-law region.

A similar model to the Cross model is the Carreau-Yasuda model:

$$\frac{\mu-\mu_\infty}{\mu_0-\mu_\infty}=\frac{1}{\left[\left(1+(\lambda_{CY}\dot{\gamma})^a\right)\right]^{n/a}} \tag{2.4}$$

where λ_{CY} is a constant which represents the onset of shear-thinning, *n* is the power-law exponent and *a* is a constant introduced by Yasuda et al (1981). This model predicts the same shape of the general flow curve as the Cross model, but the transition between the zero shear viscosity and the power-law region is better captured because it has one more free parameter than the Cross model.

Additional models used to characterise the behaviour displayed by non-Newtonian fluids can be found in the work of Barnes (2000).

2.4 – Rheological tests

2.4.1 – Introduction

All rheological measurements reported here were carried out using a TA Instruments AR 1000N controlled stress rheometer, shown in **Figure 2.2**, equipped with a Peltier plate that allows the temperature to be controlled within ± 0.1 °C. All measurements were carried out at 20 °C. A solvent trap was employed to minimise any evaporation effects whilst the tests were conducted.

The rheological characterisation included measurements of the shear viscosity, the first normal-stress difference, and the storage and loss moduli (G' and G'', respectively, see definitions in subsection 2.4.3).

Density measurements of the fluids were obtained by employing a specific volume density bottle and Oertling RB153 electronic scales with a resolution of 0.001 gr in the range 0 – 150 gr and 0.01 gr in the range 150 – 1500 gr.

2.4.2 – Steady-shear tests

A steady-shear test consists of the application of a steady-shear stress to the liquid and the monitoring of the resulting shear rate, and can be used to measure the shear viscosity and the first normal-stress difference. Measurements of shear viscosity *versus* shear rate were carried out using three different geometries, shown

schematically in **Figure 2.3**, in order to obtain the widest rage of shear stresses possible. The double concentric cylinder, of mean diameter 41.2 mm, was used for lower shear stresses, the 60 mm diameter 2° acrylic cone for intermediate shear stresses, and the 40 mm diameter acrylic parallel plate for higher shear stresses. To obtain the first normal-stress difference the 60 mm acrylic cone was again used with the rheometer kept on for at least 72 hours prior the measurements to being taken to allow stabilisation of the normal-force transducers. The resolution of the rheometer allows measurements of forces between 0.01 N and 50 N (3.54 Pa < N_1 < 17680 Pa, for the 60 mm acrylic cone).

2.4.3 – Oscillatory-shear tests

Oscillatory shear tests consist of the application of an oscillatory stress or strain to the liquid and monitoring of the resulting oscillatory strain or stress output. The response of a viscoelastic liquid can be split into two components, the storage modulus G' and the loss modulus G'' (see for example Bird et al (1996)):

$$G' = \frac{\mu\lambda\omega^2}{1+(\lambda\omega)^2} \tag{2.5}$$

$$G'' = \frac{\mu\omega}{1+(\lambda\omega)^2} \tag{2.6}$$

where λ is the relaxation time of the liquid and ω the angular frequency. The ratio G'/G'' is proportional to λ and therefore it can be used to estimate the viscoelasticity of the liquid. For a Newtonian liquid (purely viscous response) $\lambda = 0$ and therefore $G' = 0$ and $G'' = \mu\omega$.

The oscillatory measurements were carried out with the acrylic cone (60 mm, 2°) geometry to minimise the unwanted effects of inertia. The instrument was "mapped" before oscillatory measurements to eliminate the very small variations in behaviour during one revolution of the shaft. A linearity check was initially conducted using a stress sweep at 0.1 Hz to determine the linear viscoelastic region, because this is the region within which all rheological parameters remain constant regardless of applied torque, i.e., the results in this mode are representative of the linear viscoelasticity of the solutions. All frequency sweeps were performed at a value well within the linear regime. Comparison with frequency-sweep data at higher oscillatory stress values, but still within the linear viscoelastic regime, always showed good agreement and confirmed that the viscoelastic properties observed were independent of the oscillatory stress value.

2.5 – Fluid degradation

Fluid degradation or deterioration of non-Newtonian liquids is due to mechanical stress or bacteriological influences. Mechanical stress causes irreversible changes in rheological properties because of the molecular breakage of the polymer solutions, as observed in the 1970's by Chung and Graebel (1972) and Zakin et al (1977). Bacteriological or biological degradation may occur because polymer solutions are generally organic, but can be reduced by adding a suitable amount of biocide (Shaver and Merrill (1959)).

Nakano and Minoura (1975) reported that mechanical degradation occurs in inverse proportion to concentration, however at high polymer concentrations, because of the reduction in local shear rates brought about by a more intense molecular interaction, the rate of degradation becomes independent of concentration. Reddy and Singh (1985) and Moussa and Tiu (1994) analysed the influence of the molecular environment on mechanical degradation, suggesting that degradation is also seen to be solvent-dependent with higher deterioration rates associated with poor solvent quality. According to Ernst (1966) for high-molecular-weight polymer solutions the deterioration occurs very quickly and should be closely controlled during experiments. From these studies the main conclusion is that degradation of polymer solutions in pipe flows is a complex process which depends on many variables, such as, molecular weight, polymer concentration, turbulent intensity, flow geometry and solvent quality.

The choice of the fluids was made considering all these characteristics so that they could have a good degree of resistance to mechanical degradation as the fluids were continually circulated for long periods of time. Frequent rheology tests of the fluid, before, during and after the measurements were made to check the degree of degradation. Over the experimental period the fluids were subjected to shearing which was dependent on the pump speed. By comparing the viscometric flow curves, mechanical degradation was considered to have occurred when the shear viscosity, at the lowest shear rate, decreased by more than 5% from its "fresh state".

2.6 – Working fluids

2.6.1 - Introduction

Tap water was used as the solvent for all fluids. The use of distilled water was impractical given the large volume of the flow loop, around 750 litres. A biocide, formaldehyde (40% w/w solution), was added at a concentration of 100 ppm to inhibit biological degradation. The Newtonian fluid used in this study was diluted glycerine (60% w/w) and the non-Newtonian fluids were two concentrations of a polyacrylamide, 0.03% and 0.125% w/w, and one concentration of a xanthan gum, 0.15% w/w.

An important feature of all the fluids used was that they should be optically clear, so that the LDA system could be used. The refractive indices of the working fluids, displayed in **Table 2.1**, were determined using an ABBE 60/ED high accuracy refractometer (type degree scale, ± 0.001%).

2.6.2 – Glycerine (Gly)

The use of a Newtonian fluid is always important because it provides a control to which the non-Newtonian fluids can be compared. Glycerine is a Newtonian fluid widely used in the pharmaceutical and food industries as a solvent, plasticizer, lubricant or emulsifying agent, in an assortment of products from cough medicines to antifreeze. Glycerine does not degrade biologically although at high concentrations it

absorbs moisture from the atmosphere. This effect was avoided as much as possible by pumping the glycerine with the tank closed, minimising the contact of the glycerine with the atmosphere. Checking the viscosity before and after the experiments allowed us to verify that this unwanted effect did not occur in our study. The properties of glycerine solutions have been widely reported and the work of Sheely (1932) was consulted before the solutions were prepared to obtain an indication of the viscosity and density for the required concentration.

A BP grade pure glycerine (vegetable based) supplied by Hays Chemicals Ltd was used for this study. Only one concentration, 60% (weight) of glycerine, was used which had a density (ρ) of 1140 kg/m^3 and a viscosity (μ) of 0.00858 Pa.s.

2.6.3 – Polyacrylamide (PAA)

Polyacrylamide (PAA) is a synthetic polyelectrolyte and has been widely used by researchers in the field (see for example Virk (1975), Ferguson and Walters (1990), den Toonder et al (1997), and Stokes et al (2001)), and its rheological properties discussed at some length by Argumedo et al (1978), Walters et al (1990), Tam and Tui (1993), and Ghannam and Esmail (1998).

PAA is extensively used as a thickening agent, suspending agent and as a turbulence drag-reduction agent (Argumedo et al (1978)). Some specific examples are: as a rheology modifier in liquid detergents, in hair care products, in cleaning products, in adhesives and as a flocculant in water-clarification plants. PAA is not widely used in

the food industry due to its high extensional viscosity and elasticity, having a negative consumer effect (Barnes (2000)). PAA has a very flexible molecular structure and gives solutions which are strongly viscoelastic (Walters et al (1990)) compared to other water-soluble polymers such as xanthan gum. It is known that the PAA molecules adopt, at rest, a randomly coiled spherical configuration but the application of a deformation causes the coil to straighten and to eventually become fully extended.

Choi et al (1992) suggested that PAA solutions are a good candidate for use in closed-loop systems, showing a good resistance to degradation. This study showed that dilute PAA solutions did not degrade completely under typical flow conditions, but maintained a plateau value of 25% friction reduction after an initial rapid degradation period.

The concentrations used for the experiments were 0.03% and 0.125% w/w supplied in a crystalline form as Separan AP273E by SNF UK limited, with a molecular weight of 1.9×10^6 g/mol (Poole (2002)). The rheological parameters for these solutions are shown in **Figures 2.4** to **2.7**, with the fitted Carreau-Yasuda model displayed. The model parameters, which are listed in **Table 2.2**, were determined using a program written in Fortran 77 language by Poole (2002) to fit any given rheological model to viscosity data. The program uses the least-squares-fitting procedure and consists in minimising the normalised error between the measured viscosity and the predicted viscosity by the model (see Escudier et al 2001)).

2.6.4 – Xanthan gum (XG)

Xanthan gum (XG) is a high-molecular-weight natural carbohydrate, a polysaccharide produced by a viscous fermentation process of bacterium *Xanthanoma Campestris*. For more analysis of the molecular structure of XG consult Jeanes et al (1961). The chemistry of XG may be found in Lapasin and Pricl (1995). XG is used as a stabiliser, thickener or gelling agent in the food industry, for example, in tomato ketchup or salad cream, and is also used in the pharmaceutical and personal care industries.

Aqueous solutions of XG are extremely shear-thinning and exhibit remarkable resistant to mechanical degradation. XG is usually classed as a semi-rigid polymer (Tam and Tui (1993)) which does not deform under the action of the flow; the molecules form a gel-like structure due to easy alignment and strong association of the rigid rods (Rochefort and Middleman (1987)).

The solution used for the experiments was 0.15% XG w/w, supplied in powder form as Keltrol TF by Nutrasweet-Kelco Ltd, with a molecular weight of 5.1×10^6 g/mol (Poole (2002)). Characteristic fluid parameters for these solutions are shown in **Figures 2.4**, **2.8** and **2.9**.

2.7 - Discussion of the rheological results

It can be seen from **Figure 2.4** that all the non-Newtonian liquids investigated are shear-thinning and that the 0.125% PAA and the 0.15% XG solutions have essentially similar degrees of shear-thinning with a slightly larger viscosity for the 0.125% PAA solution over the entire shear rate region. Such "matching" of the shear viscosity for the two solutions was chosen in an attempt to isolate elastic from shear-thinning effects. If shear-thinning is thought to be indicative of the breakdown of the polymer molecular structure, it would appear that 0.125% PAA shows a more significant change than 0.15% XG in the zero-shear and onset of power-law regions. At low shear rate the XG solution exhibits lower shear-thinning than the PAA solution, but has basically the same shear-thinning behaviour in the power-law region.

Comparing the two solutions of PAA (0.03% and 0.125%) it can be concluded that the degree of shear-thinning increases with concentration. None of the fluids show significant asymptotic behaviour either at high or low shear rates. A slight curvature at lower shear rates can be observed for the 0.125% PAA and 0.15% XG solutions and this curvature is more evident for the 0.03% PAA solution. At high shear rates the departure from power-law behaviour is only strongly evident for 0.03% PAA.

Figure 2.5 shows the first normal-stress difference for 0.125% PAA where N_1 increases with shear rate. The figure also includes a power-law fit equation of the $N_1(\tau)$ data. The higher the first normal-stress differences the higher the degree of elasticity of fluid. PAA is considered to be considerably more elastic than XG.

Unfortunately, the normal forces generated by the 0.03% PAA and 0.15% XG solutions were too low to be measured in our rheometer.

The results of the oscillatory shear tests, G' and G'', are shown respectively, in **Figures 2.6** and **2.8** for PAA and XG. The figures also include instrument limit lines which represent the limits of the measured data that can be trusted. These limits were obtained by measuring G' of water, knowing that should be zero, since water is inelastic. That the values are non-zero is purely a consequence of instrument inertia.

G' and G'' increase with increasing fluid concentration and the elastic component (G') is greater than the viscous component (G'') for the 0.125% PAA solution, but the opposite is observed for the 0.03% PAA solution. Despite G' for the 0.03% PAA solution being close to the instrument limit and therefore one cannot be 100% confident about the results, they suggest a more elastic response for the higher concentration of polyacrylamide in comparison with the viscous influence dominating the entire frequency range for the lower concentration. For 0.15% XG the contribution of the viscous properties are predominant in the fluid when compared with the elastic properties particularly at low frequencies.

Figures 2.7 and **2.9** provide an indication of agreement between steady shear and oscillatory shear tests, because in the lower limits of frequency and shear rate the following relationships between viscometric and linear viscoelastic functions must hold (Barnes et al (1989)):

$$\mu'(\omega)\big|_{\omega\to 0} = \mu(\dot{\gamma})\big|_{\dot{\gamma}\to 0} \tag{2.7}$$

$$\left.\frac{2G'(\omega)}{\omega^2}\right|_{\omega\to 0} = \Psi_1(\dot{\gamma})|_{\dot{\gamma}\to 0} \tag{2.8}$$

The data obtained with steady shear tests, the shear viscosity (μ) and the first normal-stress coefficient ($\Psi_1 = N_1/\dot{\gamma}^2$), are represented by hollow symbols (□, Δ) and the data obtained with oscillatory shear tests, the dynamic viscosity ($\mu' = G''/\omega$) and the dynamic rigidity ($2G'/\omega^2$), by filled symbols (■, ▲). The figures also include the Carreau-Yasuda fit to the viscosity data.

In our case the lack of available data for the lower limits of frequency and shear rate does not permit us to conclude that the steady shear and the oscillatory shear measurements are in complete agreement, but by extrapolation of the available data it is possible to predict an agreement within 5%.

Figure 2.10 illustrates the criteria used to define "dilute" and "concentrated" polymer solutions. The crossover of the lines, obtained by fitting power-law lines to the zero shear viscosity (μ_0) data over a range of polymer concentrations (c), indicates the critical overlap concentration (c^*). At this concentration the shape of zero shear viscosity *versus* concentration changes, and for concentrations greater than c^* the solution is considered to be "concentrated" while for concentration lower than c^* the solution can be said to be "dilute" (Rodd et al (2000)). The polymer solutions under investigation in the present study are "concentrated", apart from the 0.03% PAA solution which corresponds approximately to the critical overlap concentration (Keegan (2008) and Japper-Jaafar (2008)).

Table 2.1 - Refractive indices for all liquids investigated (at 20 °C)

Fluid	60% Gly	0.03% PAA	0.125% PAA	0.15% XG
Refractive index	1.407	1.332	1.333	1.334

Table 2.2 – Carreau-Yasuda parameters for all non-Newtonian liquids investigated

Fluid	μ_0 (Pa.s)	μ_∞ (Pa.s)	λ_{CY} (s)	n	a
0.03% PAA	0.1150	0.002210	10^{-6}	3.897	0.1730
0.125% PAA	4.220	0.003720	45.8	0.6600	1.250
0.15% XG	1.952	0.003815	0.01607	1.384	0.1979

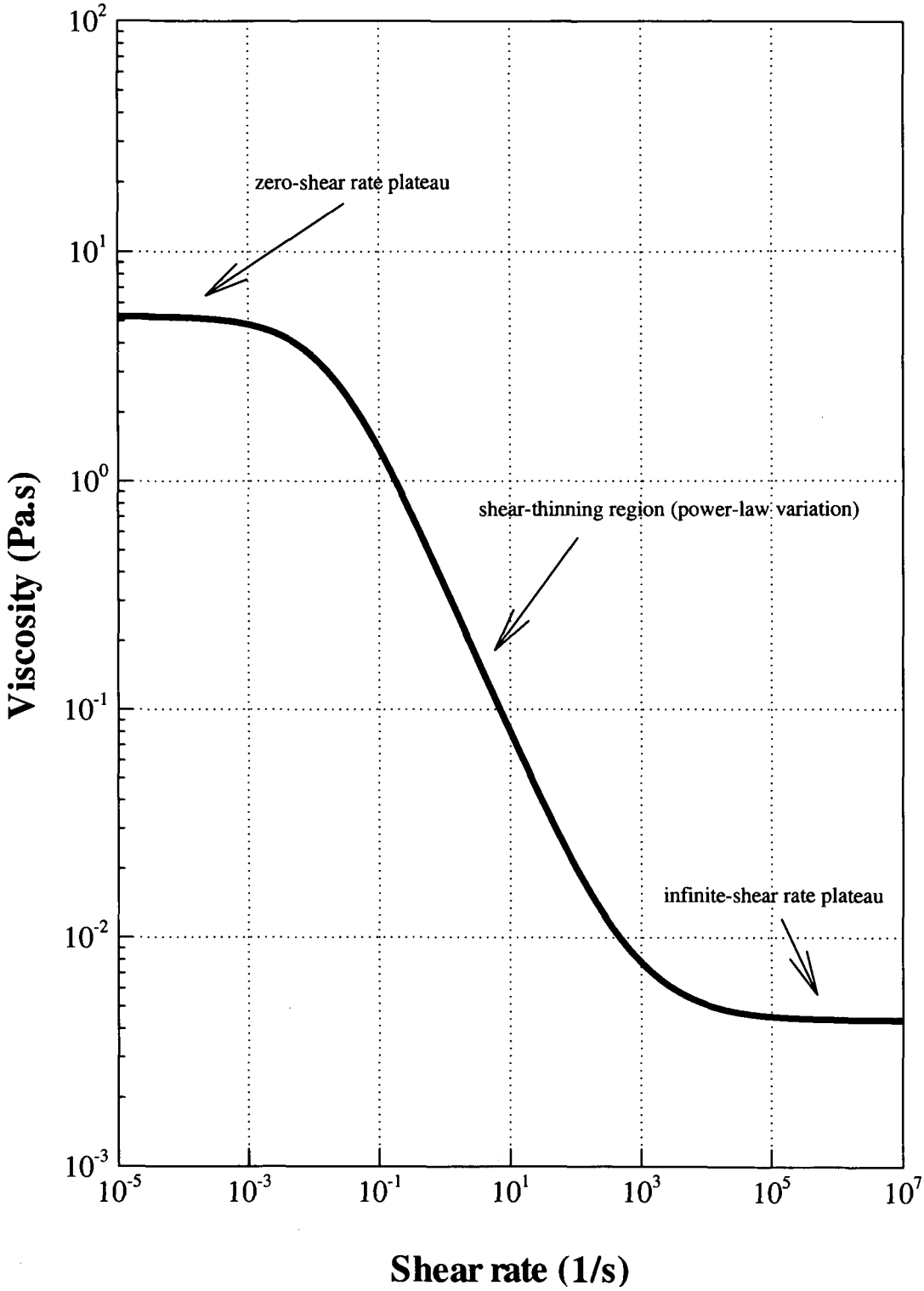

Figure 2.1 – General shape of a shear viscosity (μ) *versus* shear rate ($\dot{\gamma}$) plot for a shear-thinning liquid

Figure 2.2 – Photograph of the TA AR 1000N controlled stress rheometer

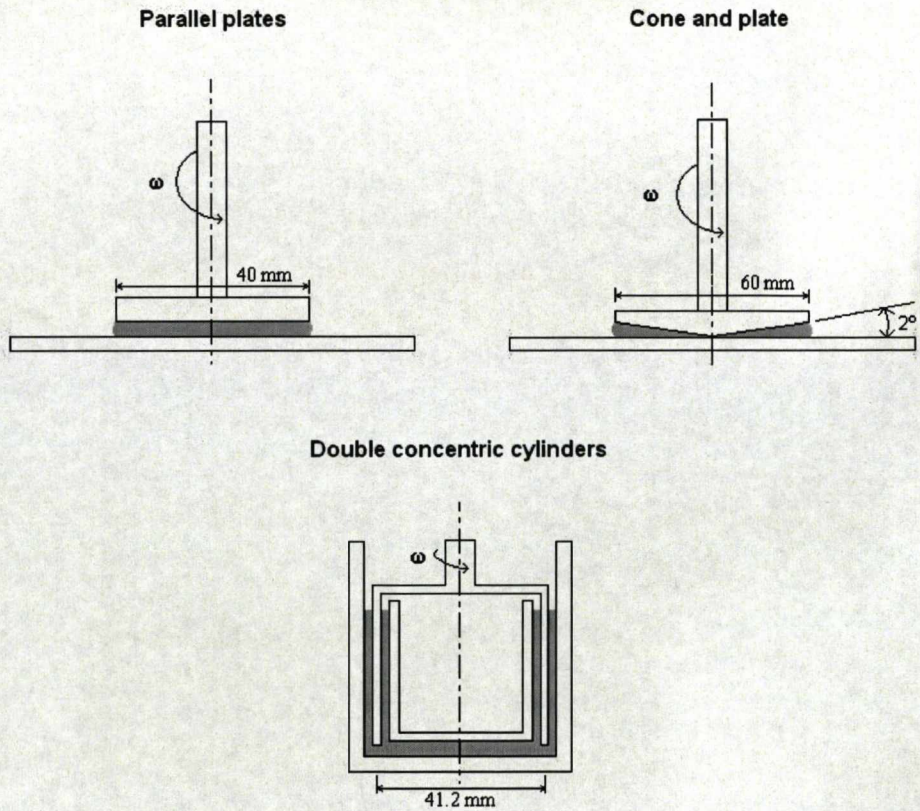

Figure 2.3 – Schematic diagrams of the rheometer geometries

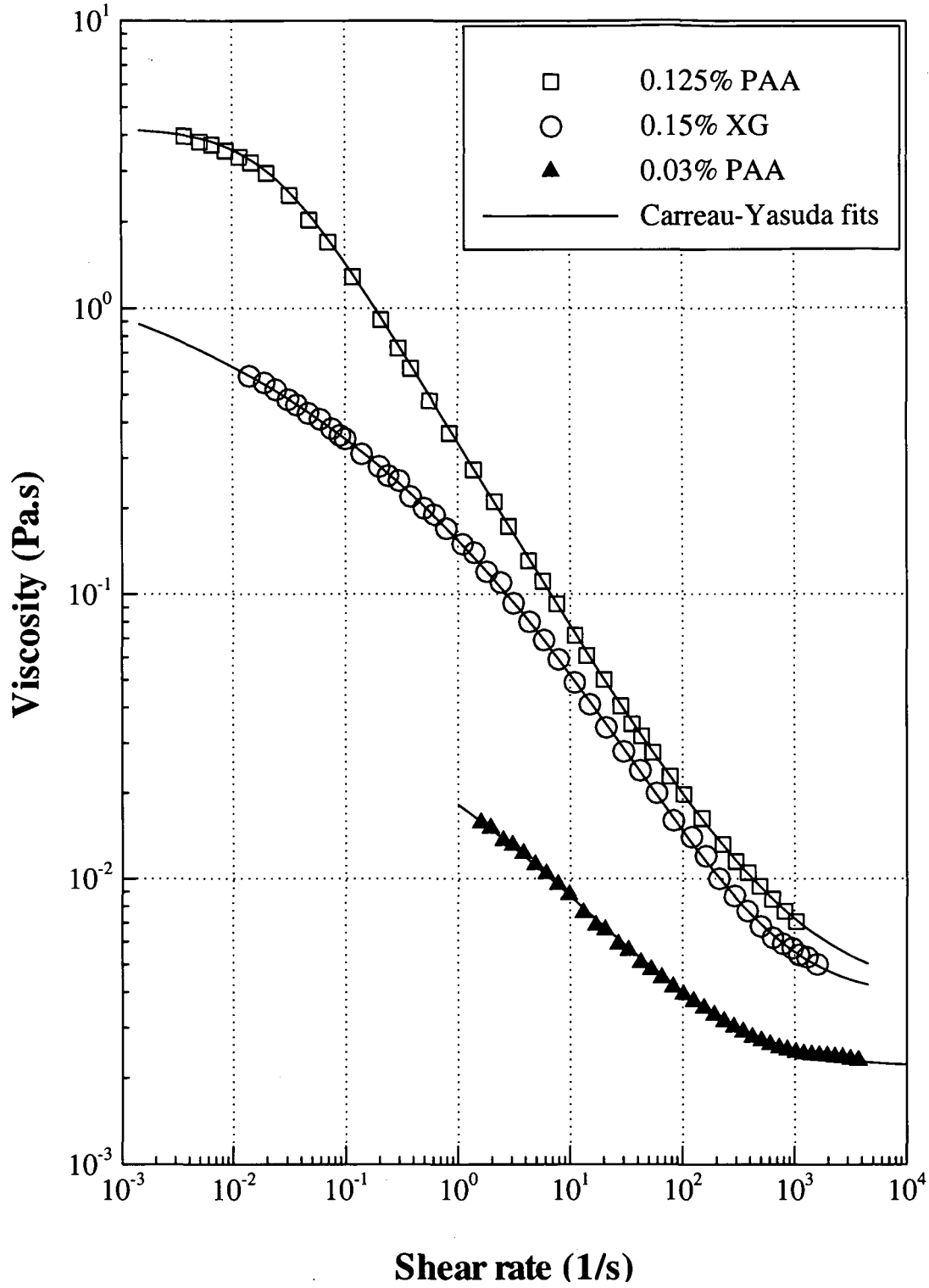

Figure 2.4 – Shear viscosity (μ) *versus* shear rate ($\dot{\gamma}$) for all non-Newtonian liquids investigated (Carreau-Yasuda parameters provided in **Table 2.2**)

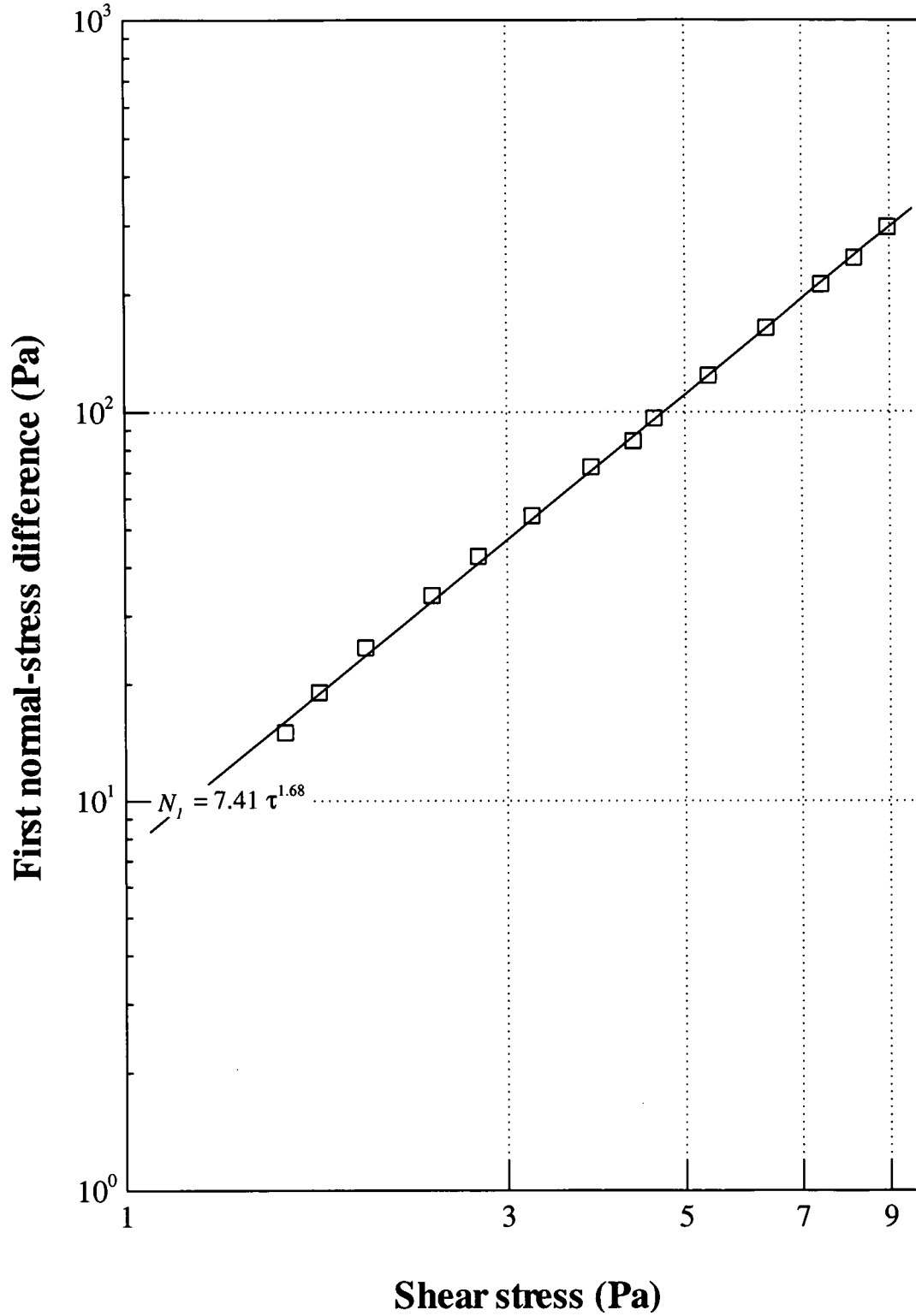

Figure 2.5 – First normal-stress difference (N_1) *versus* shear stress (τ) for 0.125% PAA, including a power-law fit

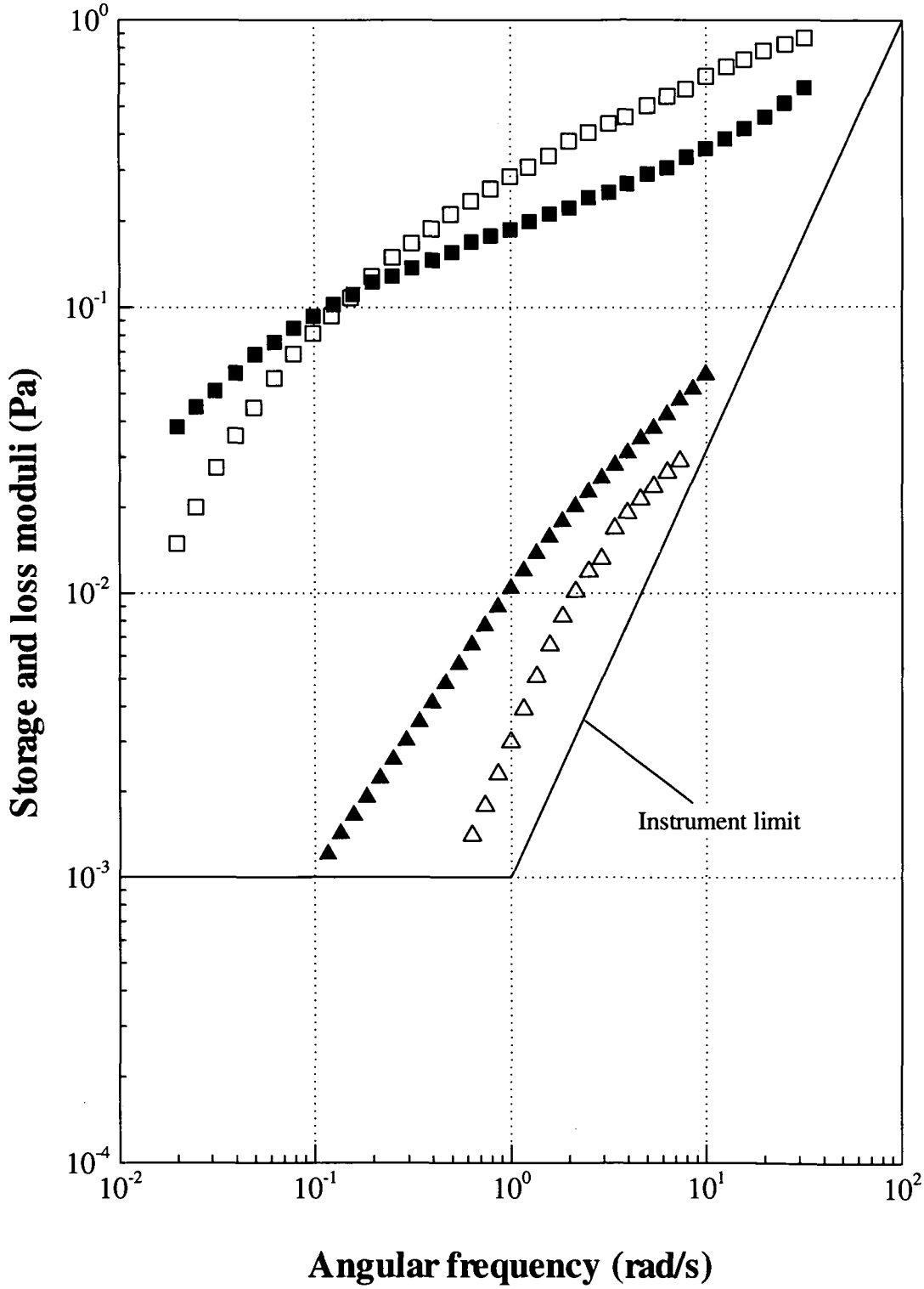

Figure 2.6 – Storage (G', open symbols) and loss (G'', filled symbols) moduli *versus* angular frequency (ω), for 0.125% PAA (□, ■) and 0.03% PAA (Δ, ▲)

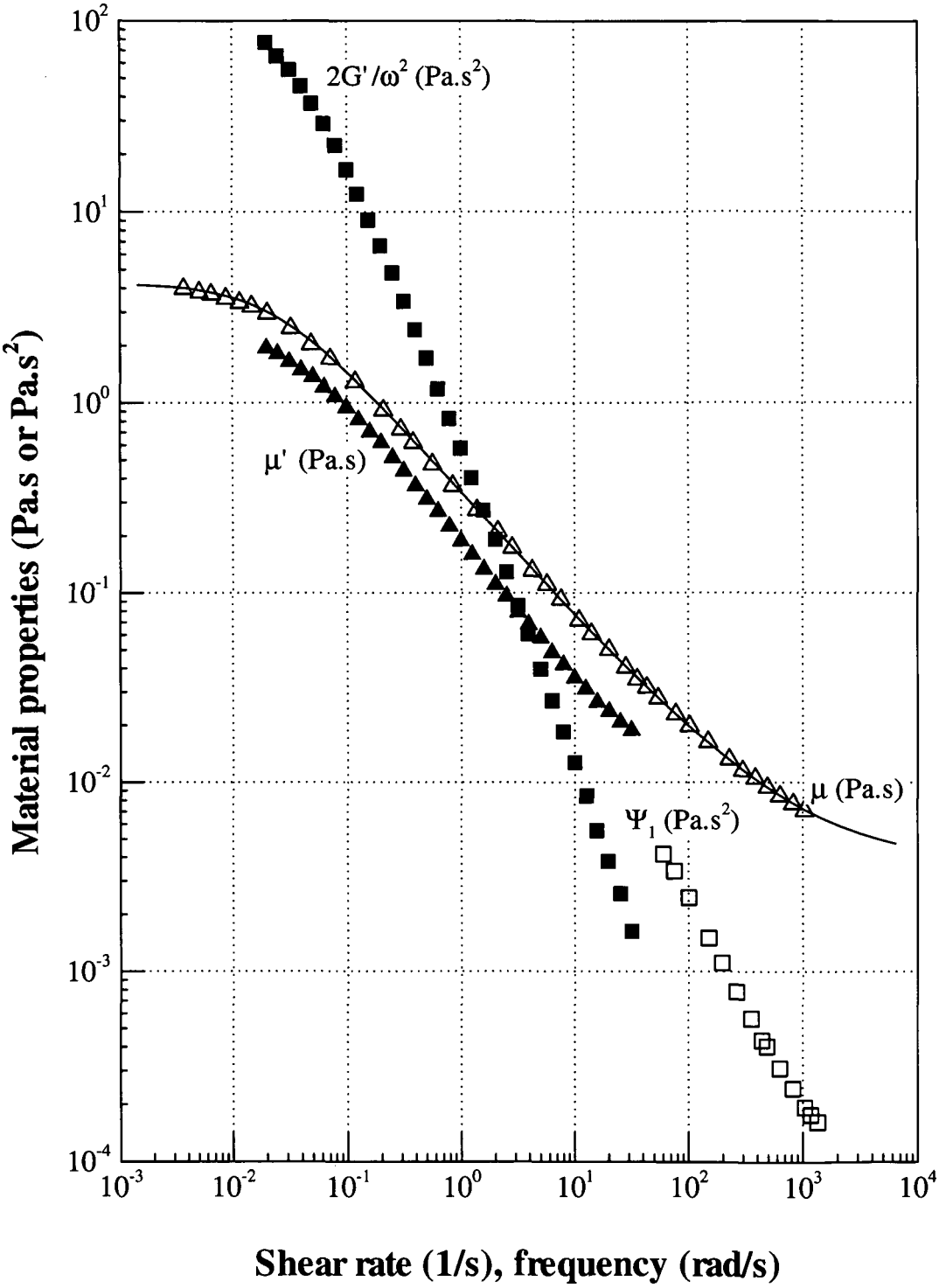

Figure 2.7 – Rheological properties of 0.125% PAA obtained from steady-shear flow (□, Δ) and small amplitude oscillatory-shear (■, ▲) tests, including Carreau-Yasuda fit (continuous line)

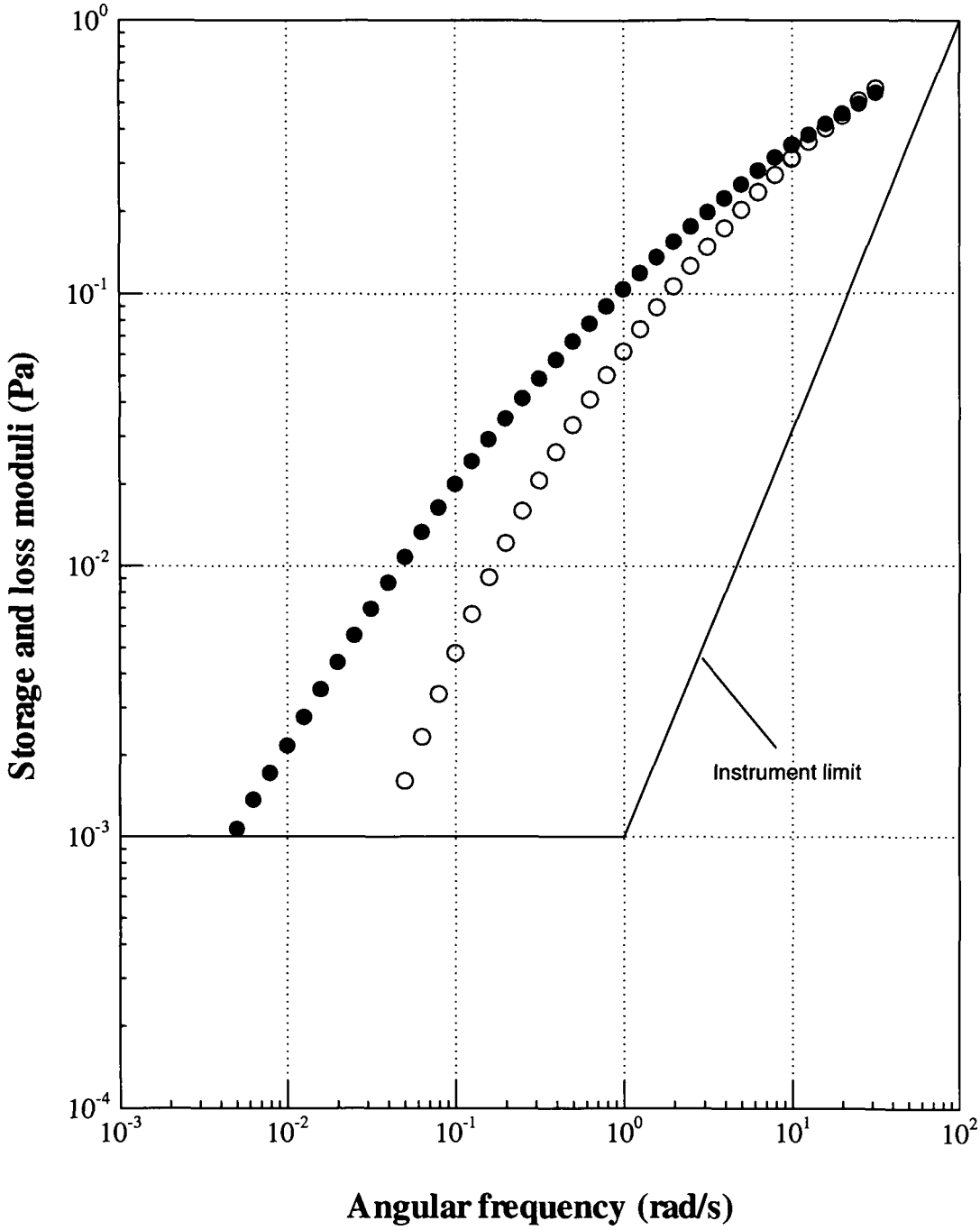

Figure 2.8 – Storage (G', open symbol) and loss (G'', filled symbol) moduli *versus* angular frequency (ω), for 0.15% XG

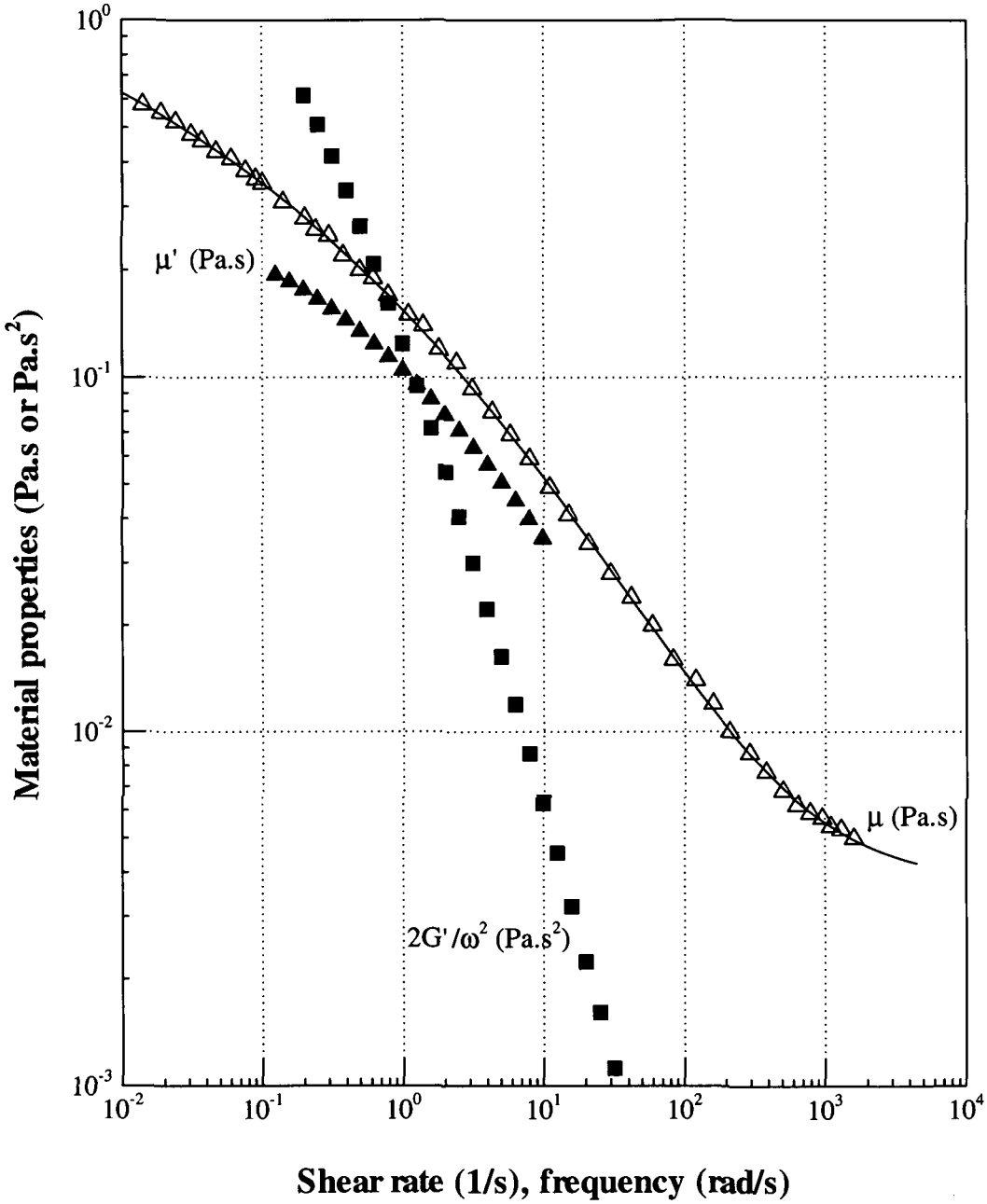

Figure 2.9 – Rheological properties of 0.15% XG obtained from steady-shear flow (Δ) and small amplitude oscillatory-shear (■, ▲) tests, including Carreau-Yasuda fit (continuous line)

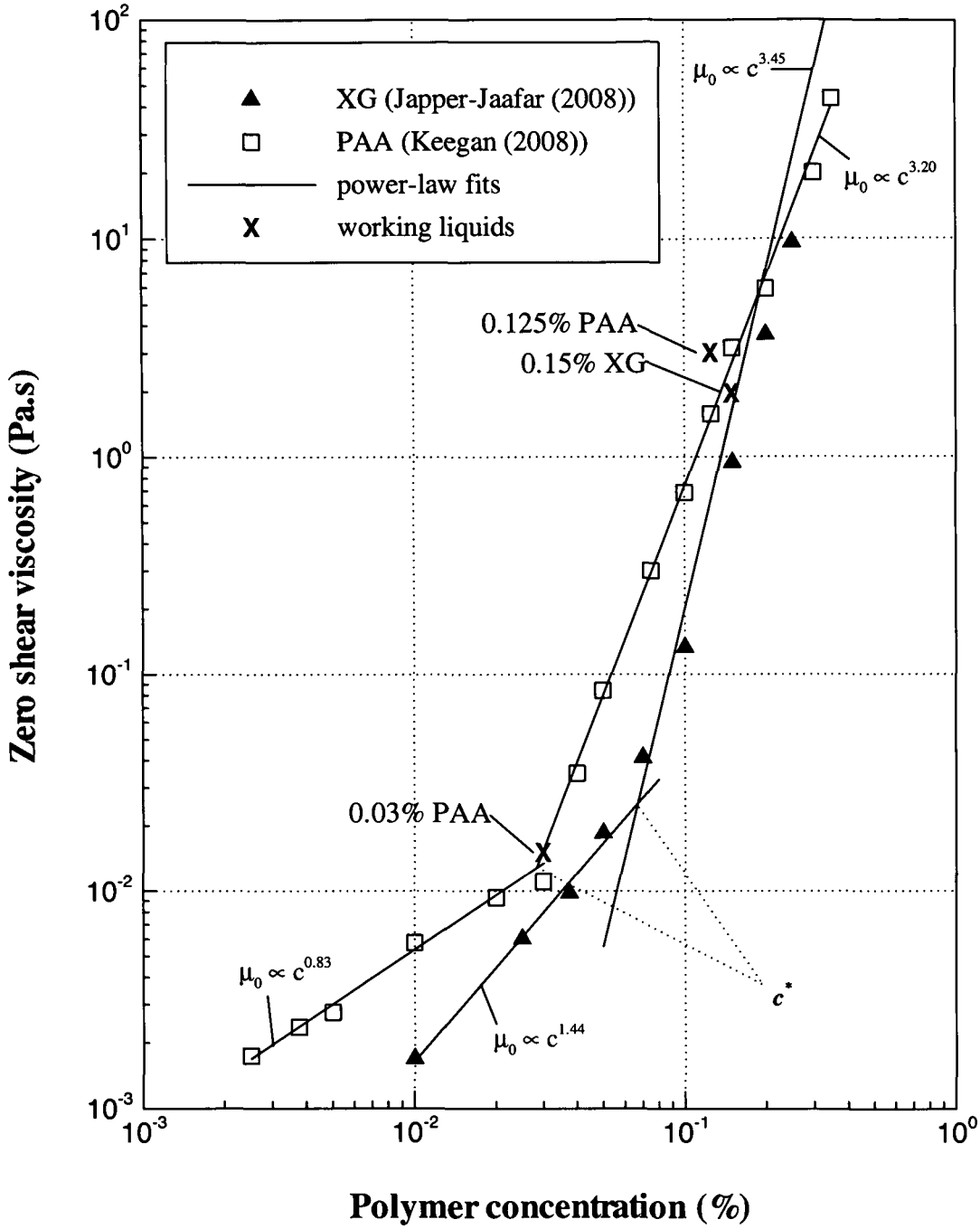

Figure 2.10 – Zero shear viscosity (μ_0) *versus* concentration (c) for PAA and XG, including critical overlap concentration (c^*)

3 - Experimental arrangement and instrumentation

3.1 – Introduction

This chapter describes the experimental apparatus and the experimental methods and attempts to estimate the uncertainties of the techniques used in the velocity and pressure-drop measurements of the pipe flow. Sections 3.2 and 3.3 provide details of the flow-loop configuration and the mixing procedure, respectively. Section 3.4 provides information about the laser Doppler anemometer (LDA) system employed and estimates the associated systematic and random errors.

3.2 – Flow-loop configuration

Figure 3.1 shows a schematic of the flow-loop used in the current study. Measurements were made in a horizontal glass pipe with 100.4±0.1 mm internal diameter (D). The total length of pipe was equal to 23.28 m and consisted of 22 precision-bore borosilicate glass tubes [7] (21 of length 1027 mm and a single pipe 656 mm in length) and one PVC plastic pipe at the test-section entrance 1060 mm in length. Each glass pipe was assembled into a module with matched male/female stainless steel flanges at alternate ends. The linear alignment of the glass pipe assemblies was carried out with a laser target arrangement. The laser device was positioned at the upstream end of the test section within the pipe and the target was manually placed in the other end of the pipe and the position of the pipe adjusted until the target was centred on the laser, this procedure enables the laser beam to

have its axis fixed along the entire length of the test section. After the first pipe alignment, subsequent pipe lengths were added by repeating the procedure. This procedure produced a linear alignment of the centreline of each pipe within ±0.1 mm of the first pipe. The maximum longitudinal curvature of the pipe (R_A) is estimated to be 10^6 m (see calculations in **Appendix**).

Immediately upstream of the pipe section a cylindrical plenum-chamber [6], approximately 70 litres in capacity, was installed in order to eliminate any swirl and suppress disturbances, with the intention of minimizing any asymmetry in the flow entering the test section, by providing a smooth uniform inflow to the test section. The plenum-chamber is shown schematically in **Figure 3.2**. Within the plenum-chamber is a disc of diameter equal to the inner diameter of the plenum-chamber, with a series of symmetrically-placed holes which combine to give an open area twice that of the plenum chamber exit (7.85×10^{-3} m^2). At the plenum-chamber inlet is a 90° bend within the plenum interior diverting flow to the rear wall of the chamber. A crossbeam flow straightener is located at the plenum-chamber outlet to suppress any residual swirling motion in the fluid entering the test section.

The fluid was pumped from a 500 litres steel reservoir tank [1] by a positive displacement progressive cavity pump [2] (Mono type E101) capable of delivering a flow rate of 0.025 m^3/s. The pump was driven by a 15 kW electric motor controlled by a frequency regulator which allows operation at controllable and constant speed.

Downstream of the pump, but upstream of the plenum-chamber, the flow passes through three dampers [4] designed to reduce flow pulsations and provide a constant flow rate. A constant flow rate is a very important requirement and highly desirable, especially for transition regime. Oscillation in the flow rate can occur when the flow is near transition, leading to a decrease in flow rate when the pressure drop remains constant. At this lower flow rate, relaminarization (Darbyshire and Mullin (1995)) may occur, accompanied by a lower pressure drop. Thus the flow rate increases again which in turn results in transition.

The bulk flow rate and the temperature were measured by a high-accuracy (uncertainty < 1%, based on results of Fyrippi et al (2004)) Coriolis mass flowmeter [5] (model Promass 63 manufactured by Endress + Hauser) incorporated in the flow-loop upstream of the test section, between the dampers and the plenum-chamber. It is important to note that the results form a Coriolis flowmeter are unaffected by the fluid rheology and therefore can be used for both, Newtonian and non-Newtonian liquids, as demonstrated by Fyrippi et al (2004).

Photographs of the experimental rig are shown in **Figure 3.3**. **Figure 3.3 (a)** shows the view of the entire pipe length looking downstream from the inlet end, with the plastic pipe (first) well visible. A view from the outlet end, with the traverse [10] placed 22 m from the inlet is shown in **Figure 3.3 (b)**.

The traverse system which moves the probe head was designed and built in-house and managed from a dedicated PC. It enables movements of the LDA control volume to an estimated inherent resolution of 15 μm. The traverse design permits

measurements not only along the horizontal and vertical radial planes, but also for every 15 degrees (see **Figure 3.4** with the azimuthal angle θ illustrated). The definition of the azimuthal angle is schematically presented in **Figure 3.5**, with the clockwise orientation adopted and $\theta = 0°$ corresponding to the vertical plane.

The effects of refraction in terms of control-volume position were compensated by traverse controller software written by Gouldson (1997), which enables the user to control the exact position of the control volume. Refraction occurs at the air-pipe interface due to the different refractive index of air and glass, and also at the pipe-fluid interface.

3.3 – Mixing procedure

All solutions of non-Newtonian fluids were prepared by first adding 700 litres of tap water to the flow-loop. Operation of the facility with water only was necessary to remove any dissolved air in the water. At this stage 37% (w/w) formaldehyde was added at 100 ppm to the water and then the mixing-loop [3] was closed off. The amount of polymer required was weighed out and then added gradually to the water with the pump turned on at a low speed. Once the entire amount of polymer had been added, the solution was pumped around the mixing loop for 12 hours until homogeneous. The mixing-loop was then opened and the fluid circulated around the whole flow-loop until mixed for a further 12 hours. The homogeneity of the working fluid was then checked before measurements were undertaken. This check was done

by comparison of the viscometric data of different fluid samples collected from the flow-loop every 30 minutes.

A solution of glycerine was prepared by calculating and adding to the rig the amount of water required and then glycerine (vegetable based) was added until the 700 litres capacity was achieved, formaldehyde at 100 ppm was then added to the solution. The solution was pumped around the whole flow-loop until homogeneous. Once again, the homogeneity was established by checking the consistency of the viscosity of the liquid before fluid-dynamic measurements were undertaken.

3.4 – Laser Doppler anemometer system

3.4.1 – General description

Measurements of the mean velocity and turbulence intensity were made using a laser Doppler anemometer (LDA) system, a technique which is now well established and documented in Durst et al (1981), Adrian (1983) and Tropea (1995) amongst others. Briefly, the LDA technique permits the measurement of the fluid velocity by means of a Doppler frequency shift caused in a monochromatic coherent light beam by scattering particles in a fluid. This Doppler-shifted frequency is linearly proportional to a component of the flow velocity at the point where light scattering occurs, allowing instantaneous measurements of the velocity components at the point. LDA was chosen because it is a non-intrusive technique (does not disturb the flow), as it is well known that intrusive probes are normally contaminated by the deposition of

polymer molecules as is often the case with hot-wire anemometry, see for example Rudd (1972). LDA was also chosen because it has high spatial resolution, allowing detailed near-wall measurements to be made.

The laser Doppler anemometer system used in this work was a Dantec Fibreflow system supplied by Dantec Electronics Ltd., UK. The laser used was an Argon-Ion (Model Stellar-Pro-CE) supplied by Laser Physics, UK, and manufactured in the USA by Modu-Laser, LLC. The maximum power of the laser is nominally 150 mW operating in TEMoo mode. Laser light was transmitted from the laser to the transmitting optics [9] (Dantec Fibreflow type, model 60x40) through optical fibres. The laser can provide three wavelengths of light but only green light (wavelength = 514.5 nm) was utilised here.

The front end of the LDA system comprised a Dantec 60x10 probe and a Dantec 55x12 beam expander in conjunction with a Dantec Burst Spectrum Analyzer (BSA) signal processor (model 57N25). The beam separation of the front lens was 40 mm and the focal length 160 mm which produces a measurement volume 0.02 mm in diameter and 0.21 mm in length.

Receiving optics [8] (Dantec model S055X0342) were used to permit the LDA system to operate in a forward-scatter mode to optimise the data rate as high data rates are preferable primarily because the signal-to-noise ratio is increased (van Maanen (1999)). To minimise statistical uncertainty (discussed in the following section), at each probe location 20,000 velocity samples were collected. Timiron seeding particles, with an average size of 5 μm and supplied by S. Blanck Ltd

(Supersilk MP-1005), were used to seed the flow when the natural contaminants present in the tap water were insufficient to obtain an acceptable data rate.

3.4.2 – Errors and uncertainties

The overall uncertainty of a measurement requires the analysis of the complete measuring system and the assessment of the uncertainties of each component. The uncertainties to be considered are; the velocity data given by the LDA system and the positional error of the measuring volume.

It is very difficult to estimate the accuracy of an LDA signal processor and be confident about velocity data because there are several sources of uncertainty; however, in this section we have attempted to estimate the accuracy of the velocity data obtained. The sources of uncertainty result in a wider probability density function of Doppler frequency than that of the true velocity data. The total Doppler frequency variance is equal to the sum of the velocity variance and broadening effects (Pinho (1990)).

Velocity bias is caused by a dependence of particle velocity on the arrival rate within the boundary of the control volume. When the particles arrive individually in the scattering volume the LDA provides velocity information averaged according to the occurrence of particles, thus the mean velocity is calculated from an ensemble average of data obtained to individual realisations. Therefore the distribution of velocity can be biased in favour of higher particle velocities because of the more

frequent arrival of faster particles in the fluid containing uniformly or randomly distributed scatters. Velocity-biasing effects can be significant, particularly in turbulent flow measurements because more high velocity particles cross the measuring volume than low velocity particles resulting in a skewing of the mean value to an average higher than the "true" time average. This phenomenon has been widely debated; see for example McLaughlin and Tiederman (1973), and Herrin and Dutton (1993). To try to eliminate the effect of biasing, transit-time weighting was used to correct the velocity measurements as proposed by Dimotakis (1976):

$$u = \frac{\sum u_i \Delta t_i}{\sum \Delta t_i} \tag{3.1}$$

$$u' = \sqrt{\frac{\sum (u_i - u)^2 \Delta t_i}{\sum \Delta t_i}} \tag{3.2}$$

where u_i is the individual velocity and t_i the transit time. Δt_i represents the duration of the Doppler signal when its amplitude varies from the maximum to half of the maximum.

The software used to process the raw velocity data and correct the effects of velocity bias was Burstware 3.21 supplied by Dantec Elektronik.

The relative statistical error of a sample of finite size on both mean velocity (u) and turbulence intensity (u') can be estimated, assuming a Gaussian velocity probability, by:

$$Error_u = Z_C \frac{\frac{S_S}{P_S}}{\sqrt{N_S}} \tag{3.3}$$

$$Error_{u'} = Z_C \frac{1}{\sqrt{2N_S}} \tag{3.4}$$

where N_S is the number of data points in a samples (sample size), P_S and S_S are the average and standard deviation, respectively. Z_C represents the confidence coefficient, which is 1.98 for a 95% confidence level with a sample size bigger than 50 (Yanta and Smith (1973)). In our case, collecting 20,000 velocity samples per point, the maximum relative statistical error, assuming $S_S / P_S = (u'/U_b)_{max}$, was approximately 0.3% in the mean velocity and 1% in the turbulence intensity.

Broadening can be caused by mean velocity gradients, turbulence and finite transit-time. Mean velocity gradients across the measuring volume lead to a broadening of the probability density function across the measuring volume, but due to the small size of the measuring volume in the current study this effect can be neglected (see for example Presti (2000) or Smith (2000)). This assumption can be also applied to the error introduced by velocity fluctuation effects (turbulence).

For time-domain signal processing systems, broadening due to transit-time effects is zero, provided the validation circuits prevent information influenced by the presence of more than one particle in the scattering volume from being measured, and consequently inherent noise becomes the main source of error.

The major inaccuracy in positioning resulted from the zero location of the measurement control volume at the inner-wall. This positional error was minimised by observing a distinct change in slope of the velocity profile, plotting the mean

velocity against the position near the wall. Therefore by linear extrapolation of the velocity distribution measurements, prior to change in the slope, the zero velocity point was found which was taken to be the wall location (see **Figure 3.6**). This method of locating the control volume inside both sides of the pipe led to an uncertainty of about 0.1 mm in radial location.

From the estimated uncertainty and the reproducibility of data it is estimated that the maximum experimental uncertainty of the velocity data in this work is less then 3% for the mean velocity and less than 6% for the turbulence intensities.

3.5 – Pressure-drop measurements

Wall-pressure measurements over a segment of pipe were obtained using a Druck differential pressure transducer (model LPX9381), for which full scale corresponds to a pressure drop of 50 mbar. The values given by the differential transducer were periodically checked against a MKS Baratron high accuracy (0.01% of reading) differential pressure transducer (1000 torr fsd) manufactured by MKS Instruments Inc., USA. The zero reading, under no flow conditions, was made at the beginning and at the end of each flow experiment to account for any drifts of pressure readings. Connections between pressure tappings and transducer were provided by clear vinyl tubing filled with de-ionised water to eliminate corrections due to different specific gravities.

The pressure difference was measured over a pipe length (L) of 7.02 m in order to minimise the relative error and the beginning of the measuring section was located 14.04 m (140 pipe diameters) after the entrance of the pipe to allow a constant pressure gradient over the entire segment. The wall shear stress (τ_w) is then given by:

$$\tau_w = \left(\frac{\Delta p}{L}\right)\left(\frac{D}{4}\right) \tag{3.5}$$

where Δp represents the pressure drop over the length L of the test pipe with an internal diameter D.

Special care was taken with the pressure tappings to avoid disturbing the flow, generating an error in the measurements that can be minimised by resorting to the smallest possible holes. However, the quality of the hole entrance, specially for small dimensions, is critical because they can introduce large errors if the hole has burrs, rounded edges or other imperfections (Franklin and Wallace (1970)). Consequently, all pressure tappings were 1 mm in diameter and were surface polished and therefore the pressure-drop errors have been ignored in this study.

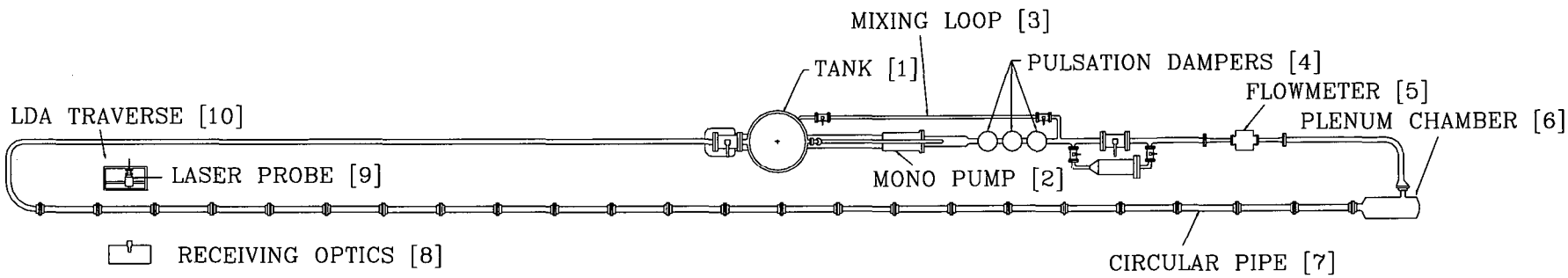

Figure 3.1 – Schematic of the flow-loop

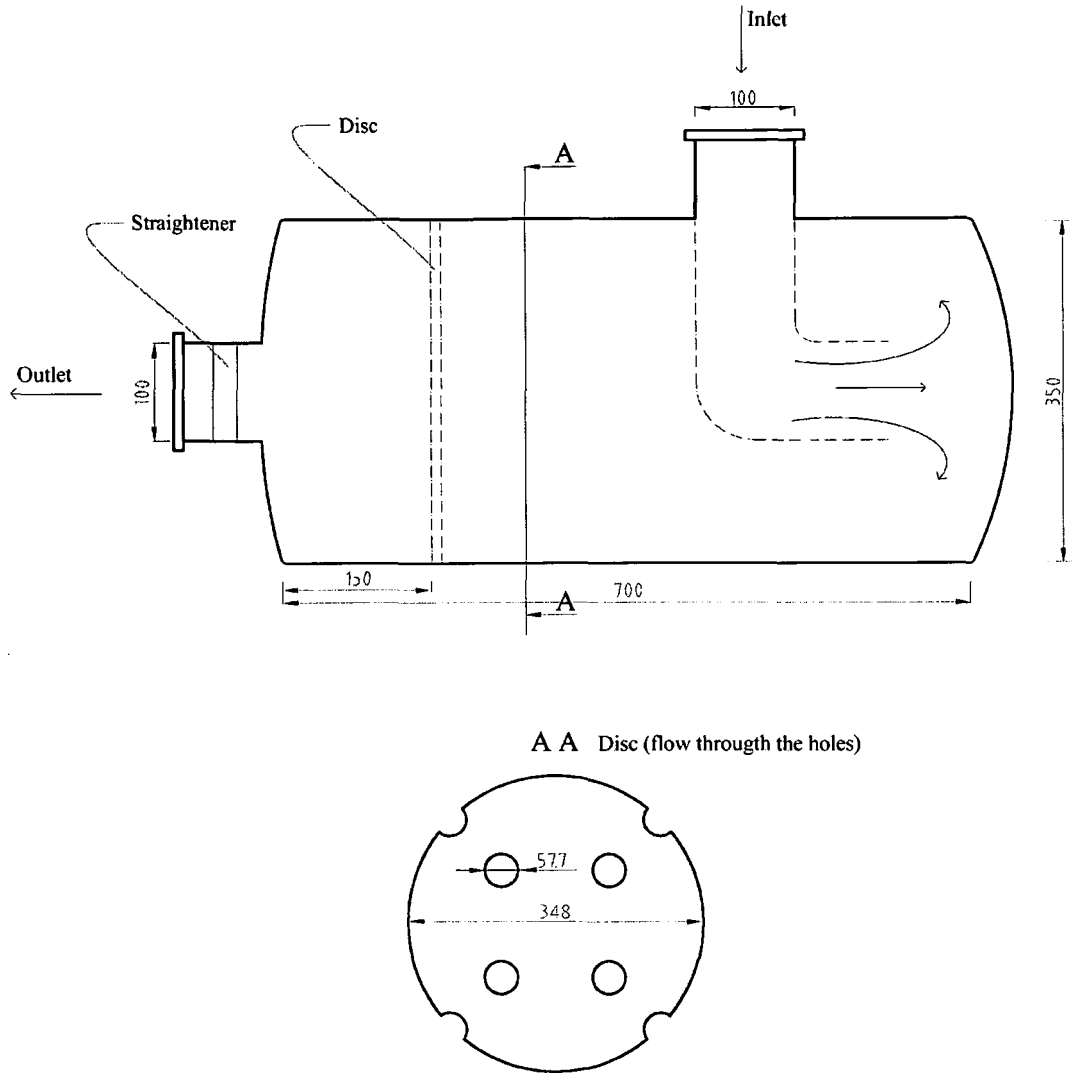

Figure 3.2- Schematic of the plenum-chamber (values in mm)

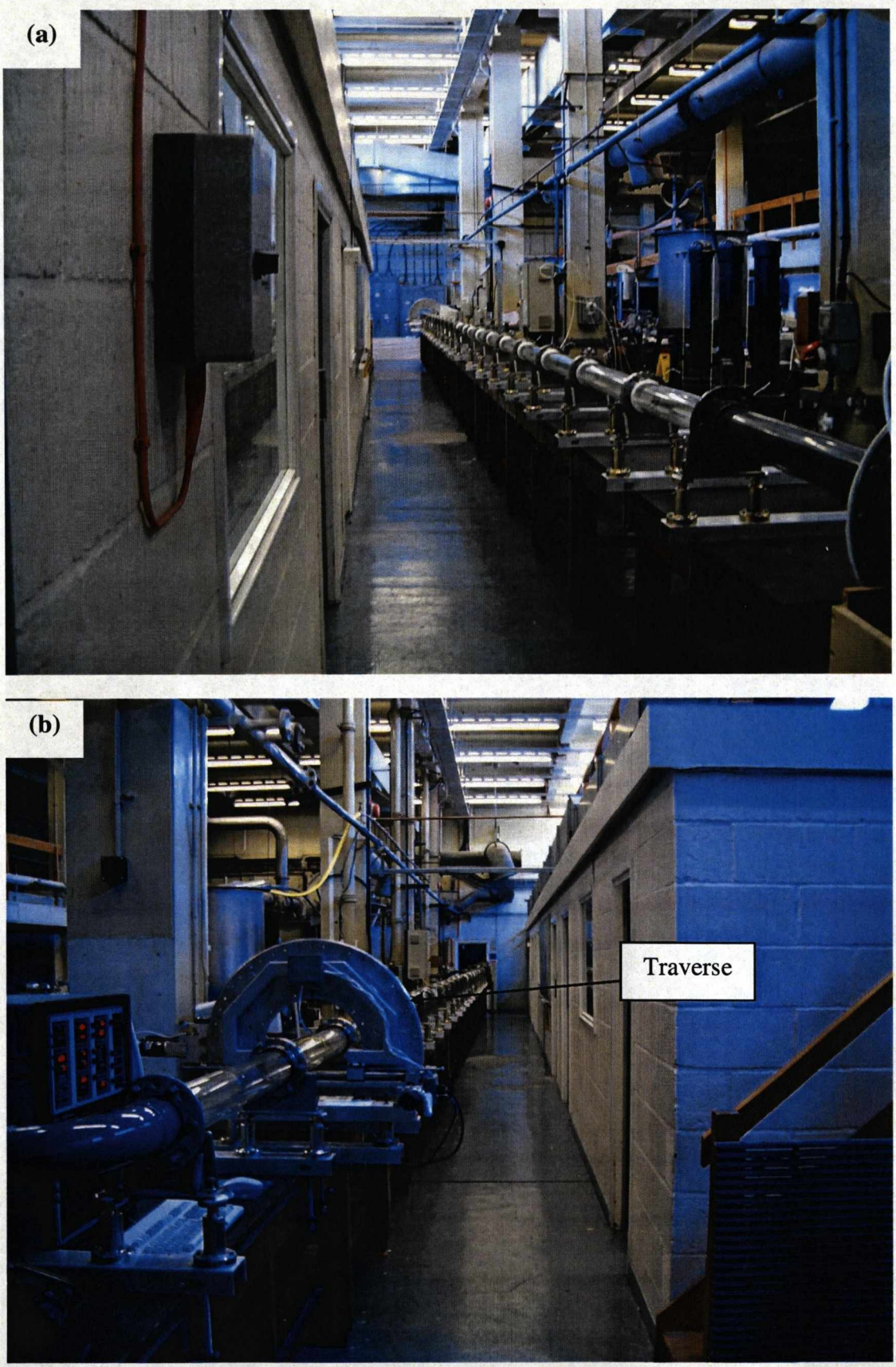

Figure 3.3 – Photographs of the flow facility;

(a) Inlet end looking downstream, (b) Outlet end looking upstream

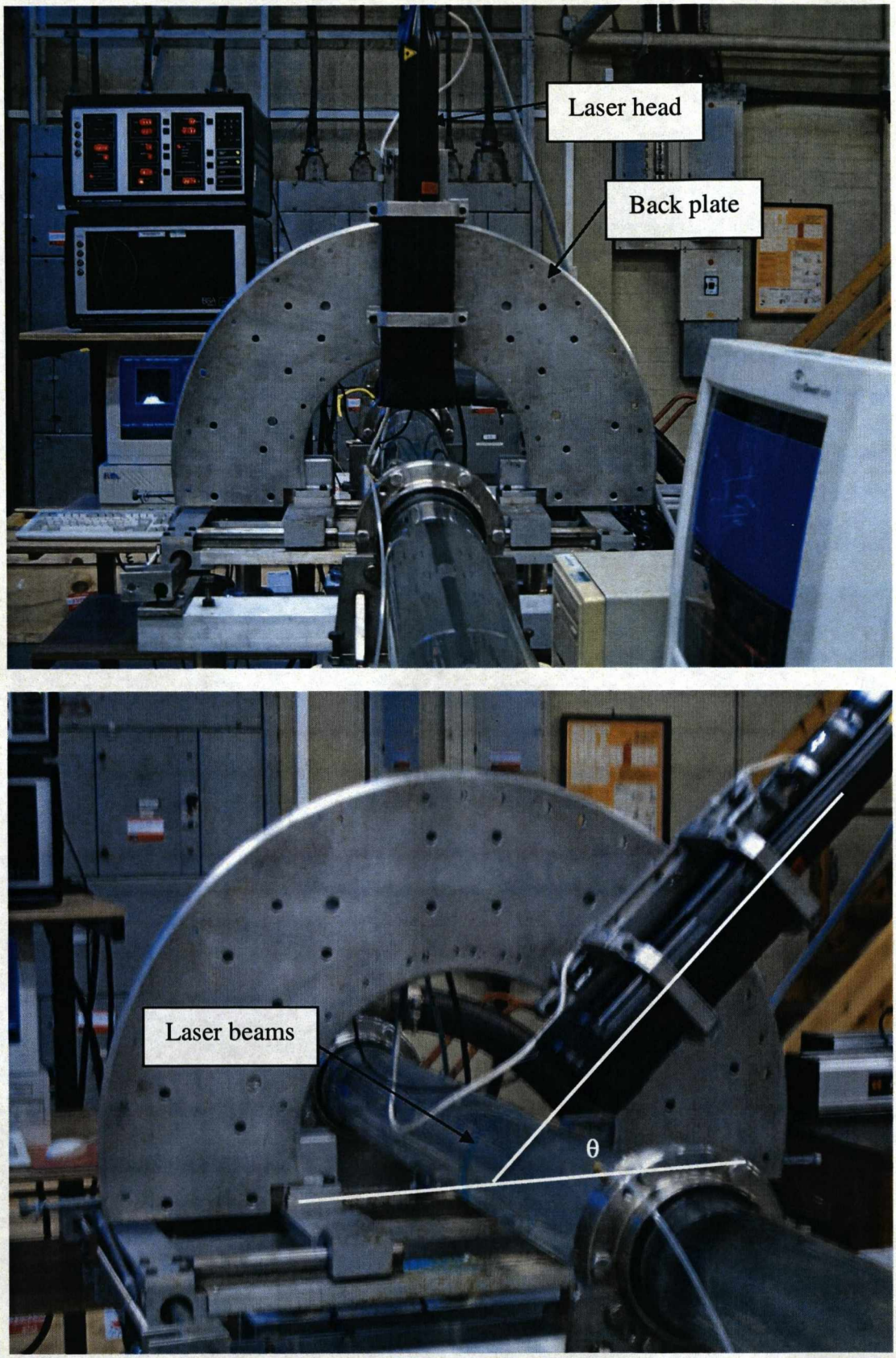

Figure 3.4 – Photographs of the LDA traverse

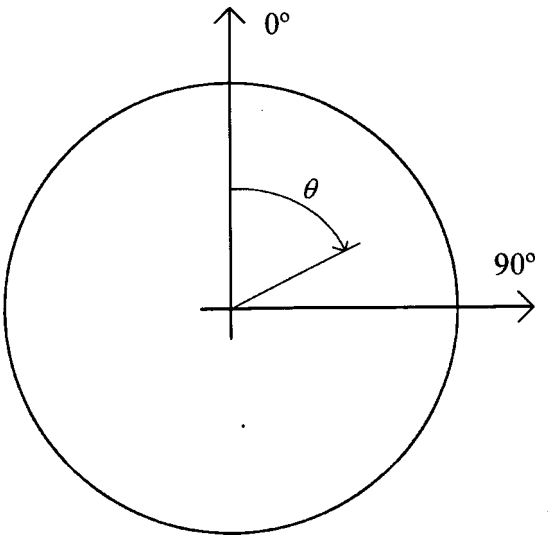

Figure 3.5 – Definition of the azimuthal angle θ (flow into the page)

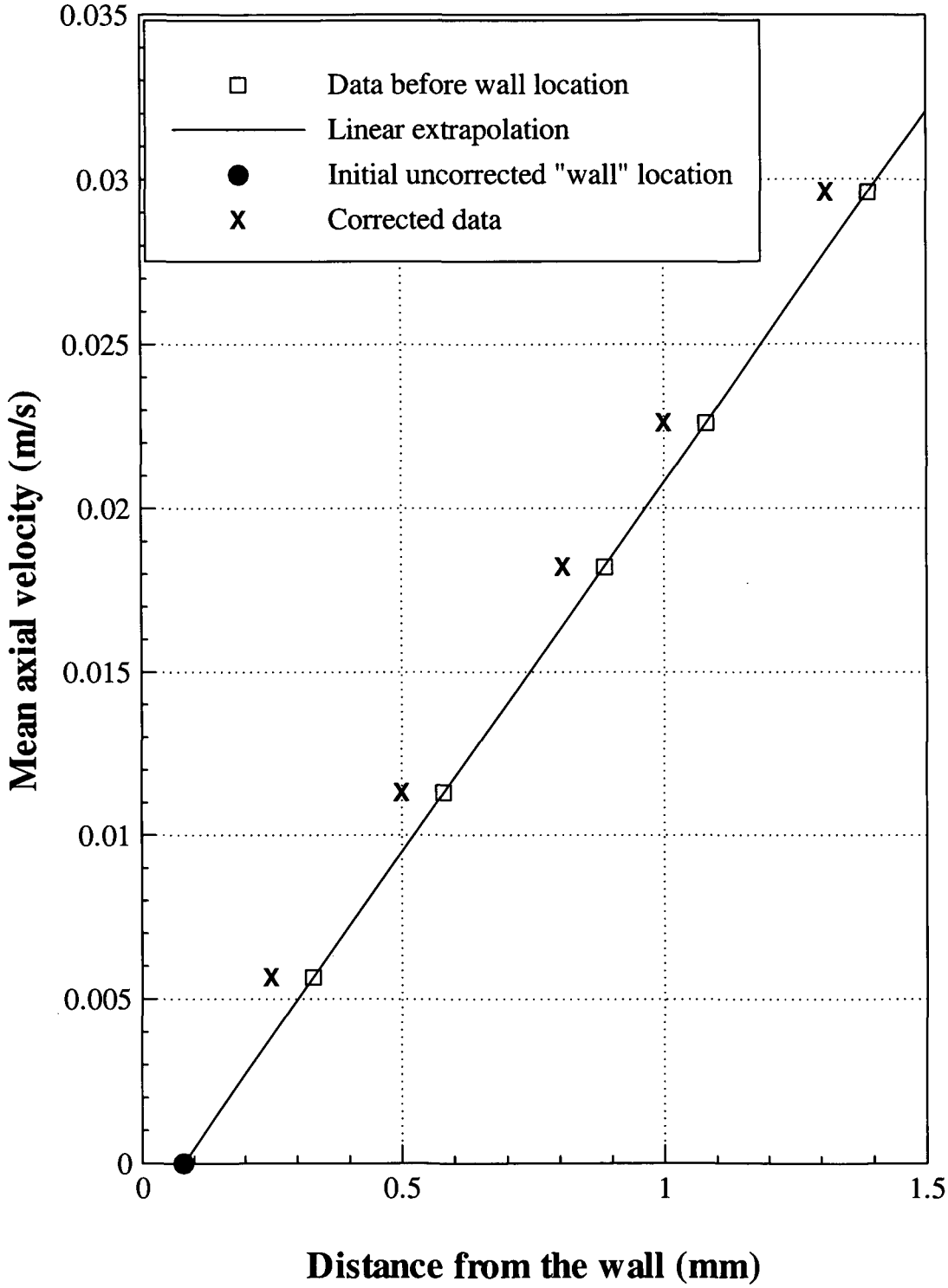

Figure 3.6 – Axial velocity profile near the wall, for 0.03% PAA

4 – Definitions and methodologies

4.1 – Introduction

This chapter presents the definitions and methodologies used in the experimental work, including the adopted definitions, so that the results can be correctly analysed and compared. The Reynolds number is defined in Section 4.2, the friction factor concept is introduced and the explanation of the calculation procedure used to obtain all flow parameters in Section 4.3, followed by a description of the methodology used to detect the transitional regime in Section 4.4. Section 4.5 presents theoretical and empirical equations for the axial velocity profiles that can be used for comparison with the experimental velocity profiles. A coefficient of asymmetry is defined to allow the quantification of the degree of asymmetry of the mean velocity profiles. Virk's three-zone flow model mentioned in Chapter 1 is also presented in this section. The chapter ends with the definition of the Ekman number (Section 4.6) which allows us to evaluate the contribution of the Earth's rotation to the asymmetry of the axial velocity profiles in laminar flow.

4.2 – Reynolds number

As usual the Reynolds number is given by:

$$Re = \frac{\rho U_b D}{\mu} \tag{4.1}$$

with U_b the mean bulk velocity in the pipe, ρ the density of the fluid and μ the viscometric shear viscosity of the fluid.

For Newtonian fluids the viscosity is constant and therefore the Reynolds number is obtained directly from Equation 4.1, for non-Newtonian fluids the viscosity is not constant and depends upon the shear rate, in turn the shear rate depends on the location in the pipe, becoming zero in the centre of the pipe and maximum at the wall. As Chhabra and Richardson (1999) pointed out, one of the intrinsic difficulties with analysing flows of non-Newtonian fluids is in the correct definition of the Reynolds number, where the viscosity must be adequately defined for the flow in consideration. The most straightforward Reynolds number is that based on a characteristic shear rate $\dot{\gamma} = U_b / D$, which can be called the Collins-Schowalter Reynolds number (Collins and Schowalter (1963)):

$$Re_{CS} = \frac{\rho U_b^{\,2-n} D^n}{k} \tag{4.2}$$

where n is the power-law index and k the consistency index of the power-law model. This Reynolds number was obtained by substituting the characteristic shear rate $\dot{\gamma} = U_b / D$ in the power-law model equation ($\mu = k\dot{\gamma}^{n-1}$) and then substituting the resultant viscosity in Equation 4.1.

In spite of the appealing simplicity of the Re_{CS} definition it is well known that it is not always the most appropriate. In 1955, Metzner and Reed (1955) defined a generalised Reynolds number as:

$$Re_{MR} = \frac{\rho U_b^{2-n} D^n}{k} \cdot 8\left(\frac{n}{6n+2}\right)^n \tag{4.3}$$

This Re_{MR} was defined on the basis of laminar pipe flow considerations to ensure that for laminar pipe flow of a power-law fluid the friction equation $f \cdot Re = 16$ is recovered, where f is the Fanning friction factor (see below). It is worth noting that these formulations are inter-related thus:

$$Re_{MR} = 8\left(\frac{n}{6n+2}\right)^n \cdot Re_{CS} \tag{4.4}$$

These definitions of the Reynolds number use the power-law model, thus they do not take into account the entire shear rate range. Therefore, these definitions are not always appropriate, for example, in flows where a yield stress is present it is necessary to use a Reynolds number definition that considers a different rheological model. Several researchers, such as Pinho and Whitelaw (1990), Draad (1996), Ptasinski et al (2001), Poole and Escudier (2004), Escudier et al (2005) and Peixinho et al (2005) have used a Reynolds number definition based on the wall viscosity (μ_W) which consists in substituting μ of Equation 4.1 by μ_W. The shear viscosity at the pipe wall is by definition:

$$\mu_W = \frac{\tau_W}{\dot{\gamma}_W} \tag{4.5}$$

where τ_W and $\dot{\gamma}_W$ are the wall shear stress and the wall shear rate, respectively. This "wall Reynolds number" (Re_W) definition was also chosen for this thesis as a Reynolds number based on the wall viscosity gives a better representation of

transitional and turbulent flows because it is in the wall region that viscous stress plays a dominant role. An advantage of using Re_W lies in the fact that it can be used for any rheological model at any flow regime since it requires only the viscosity at the wall.

For an experimental measurement, the wall viscosity and consequently the wall Reynolds number are calculated as follows: for a given value of the wall shear stress, which is known from the pressure-drop measurements (Equation 3.5), the wall viscosity and the wall shear rate are obtained by solving together Equation 4.5 and the Carreau-Yasuda rheological model adopted with the mean bulk velocity obtained from the flow rate measurements, using the equation:

$$\dot{m} = \rho U_b \pi R^2 \tag{4.6}$$

The ranges of wall shear rate where the experiments were conducted are shown in **Figure 4.1** for all non-Newtonian liquids investigated.

4.3 – Friction factor

The wall shear stress (τ_W) is given by the Equation 3.5 and is valid for fully-developed flows of Newtonian and non-Newtonian fluids, for all three regimes. The wall shear stress can be expressed in terms of the Fanning friction factor (f) as:

$$f = \frac{\tau_W}{\frac{1}{2}\rho U_b^{\,2}} \tag{4.7}$$

For a Newtonian fluid the relationships between the friction factor and the Reynolds number, for laminar and fully-turbulent pipe flows are given by:

$$\text{Laminar,} \qquad f = \frac{16}{Re} \tag{4.8}$$

$$\text{Turbulent,} \qquad \frac{1}{\sqrt{f}} = 4.0 log\left(Re\sqrt{f}\right) - 0.4 \tag{4.9}$$

These relationships are known respectively as the Hagen-Poiseuille law (theoretical) and the Prandtl-Karman law (empirical), respectively. In turbulent flow of polymeric non-Newtonian fluids the friction factor deviates from Equation 4.9, and is dependent on several variables, for example, type of polymer, type of solvent, polymer concentration and pipe diameter. That deviation is limited by an asymptote, given by an empirical relation proposed by Virk (1975) and known as, "Virk's maximum drag reduction asymptote":

$$\frac{1}{\sqrt{f}} = 19.0 log\left(Re_w \sqrt{f}\right) - 32.4 \tag{4.10}$$

Figure 4.2 shows the results of the measurements carried out to obtain the Fanning friction factor for a range of Reynolds number, for all working fluids. The behaviour of the glycerine solution in both the laminar and turbulent regimes follows the relationships given above with a clear demarcation at transition.

For the non-Newtonian working solutions in the laminar regime the experimental data also follow the theoretical relationship for a power-law fluid ($f = 16/Re_w$). However in the turbulent regime the drag-reduction phenomenon is evident and dependent on fluid type and Reynolds number. The transition from laminar flow to

turbulent flow can be very smooth in contrast to the abrupt change in data observed for the Newtonian case, therefore, detect transition for non-Newtonian liquids using the $f - Re_W$ plot is difficult. We have used a different methodology do detect transition which will be presented in the following section.

Different levels of drag reduction for each polymer solution in the turbulent flow regime are illustrated in the **Figure 4.2**. At high Reynolds number the drag reduction ranking is: 0.03% PAA, 0.15% XG and 0.125% PAA. At lower Reynolds number the curve of 0.15% XG and 0.125% PAA cross over. These results are consistent with those obtained by Escudier et al (1999).

The results of the flow parameters obtained during the experiments are shown in **Table 4.1** for all working liquids. The table gives the results of the mass flow rate ($\dot{m}$), the pressure gradient ($\Delta p / L$), the mean bulk velocity (U_b), the wall shear stress (τ_W), the wall shear rate ($\dot{\gamma}_W$), the viscosity at the wall (μ_W), the wall Reynolds number (Re_W) and the Fanning friction factor (f).

4.4 – Transition detection

As already discussed in the previous section from the friction factor *versus* Reynolds number behaviour, for Newtonian fluids, a demarcation of the transition from the laminar to the turbulent regime is well identified as illustrated in **Figure 4.2**. However, for the non-Newtonian case, transition can be very smooth and $f - Re_W$ data do not provide a clear indication of transition, in contrast to the abrupt change

for a Newtonian fluid. As a consequence it is frequently impossible to detect the Reynolds number corresponding to transition from laminar to turbulent flow for non-Newtonian fluids using a $f - Re_W$ curve.

It has been suggested that the turbulence intensity (or velocity fluctuation) measured near the wall is the best indicator of transition from laminar to turbulent flow of non-Newtonian fluids as Zakin et al (1977), amongst other researchers, discussed. For this study, the method initially suggested by Park et al (1989) and used by Escudier et al (1999), Presti (2000) and Esmael and Nouar (2008) amongst others, has been used. In this method the turbulence intensities in a vicinity "close" to the wall are plotted against the wall Reynolds number. This representation of data gives a clear indication of onset and offset of transition.

From **Figure 4.3**, for a representative non-Newtonian fluid (0.125% PAA), transition is more easily detected from the $u'/U_b - Re_W$ curve than from the $f - Re_W$ curve. The turbulence intensity measurements were taken at 10 mm from the wall for the azimuthal angle (θ) of 270° with respect to the vertical "looking downstream", i.e. horizontal plane (see **Figure 3.5**).

Re_1 and Re_2 in **Figure 4.3** represent the limits of transition, i.e. the transition regime corresponds to the region with Reynolds numbers between Re_1 and Re_2. The first, Re_1, is used to identify the onset of transition seen as noticeable change in turbulence activity (u'/U_b). The subsequent peak in u'/U_b data represents the offset of transition (or onset of fully-turbulent flow) and is denoted as Re_2.

Figure 4.4 shows the axial velocity fluctuations levels at 10 mm from the wall (r/R = - 0.8) obtained for all fluids investigated: 60% Gly, 0.03% PAA, 0.125% PAA and 0.15% XG. The velocity fluctuations observed in the laminar region are essentially a consequence of noise in the LDA signal. **Table 4.2** summarises the data in terms of the two Reynolds numbers (Re_1 and Re_2), identifying the transitional region for each working fluid.

Transition to turbulence, for the Newtonian case (60% Gly), occurs at $Re \approx 2100$ which agrees with widely accepted values of transition for Newtonian pipe flows. Although, for the non-Newtonian cases, it appears that the flow remains laminar up to higher Reynolds numbers and the delay in transition increases with increasing in concentration by comparison of Re_1 for the two polyacrylamide solutions (0.03% PAA and 0.125% PAA). The results of Re_2 for the two concentrations of polyacrylamide also suggest that polymer addition also delays the onset of turbulent flow to higher Reynolds numbers than for Newtonian liquids, in agreement with the previous studies of Draad et al (1998), Presti (2000) and Escudier et al (2005).

4.5 – Velocity distributions

4.5.1 – Mean velocity profiles

The theoretical profile for a Newtonian fluid in fully-developed laminar flow is given by:

$$u = u_0\left(1-\left(\frac{r}{R}\right)^2\right) \tag{4.11}$$

where u_0 is the maximum velocity, the velocity at the centreline of the pipe, which is equal to twice the bulk velocity in pipe flow ($u_0 = 2U_b$). This parabolic profile is called the Hagen-Poiseuille profile to commemorate the experimental work of G. Hagen in 1839 and J. L. Poiseuille in 1840, both of whom established the pressure-drop law (Equation 3.5).

The analytical solution for fully-developed pipe flow of a power-law fluid in laminar regime is also well known (see for example Bird et al (1996)) and given by:

$$u = u_0\left(1-\left(\frac{r}{R}\right)^{\frac{n+1}{n}}\right) \tag{4.12}$$

where n is the power-law index and u_0 is the velocity at the centreline of the pipe, which is related to the bulk velocity U_b through:

$$u_0 = U_b\left(\frac{3n+1}{n+1}\right) \tag{4.13}$$

The theoretical velocity profiles are very useful in allowing us to compare the experimental velocity profiles and indicate the degree of asymmetry of the experimental velocity profiles. **Figure 4.5** shows an axial velocity profile in the transitional regime (Re_W = 11560) for 0.125% PAA, including a reference curve corresponding to the average of the velocity data on both sides of the centreline of

the pipe, which can be used to evaluate the degree of asymmetry of the velocity profile. A slight asymmetry can be seen in this figure.

In order to quantify the degree of asymmetry we have defined a coefficient of asymmetry α (%), such that:

$$\alpha \equiv \frac{\int_0^R (u - u_m) r \cdot dr}{\int_0^R u_m r \cdot dr} \cdot 100 \tag{4.14}$$

where u is the measured mean axial velocity at a location r and u_m is the arithmetic average of the velocity data on either side of the centreline at the same location r. It should be noted that α varies with the azimuthal angle θ and therefore it is calculated for each side of the centreline (half velocity profile). For a symmetric profile $u = u_m$ and $\alpha = 0$.

The bulk velocity obtained from the Coriolis flowmeter could be checked by numerical integration of the average velocity profiles, using the equation:

$$U_b = \frac{2}{R^2} \cdot \int_0^R u_m r \cdot dr \tag{4.15}$$

The deviation of the bulk velocity between the flowmeter readings and the velocity profile integrations obtained during the experiments was less then 2%.

4.5.2 – Virk's three-zone model

In order to clarify the wall structure of drag reduction in turbulent fluid flow, Virk et al (1970) proposed the three-zone flow model to describe the mean velocity profiles. The model comprises three distinct regions: a viscous zone, an interactive zone and a Newtonian turbulent zone. Virk's three-zone model scheme is illustrated in wall coordinates, u^+ *versus* $\log y^+$, in **Figure 4.6**.

The non-dimensional velocity (u^+) and the non-dimensional distance from the pipe wall (y^+) are defined in "wall" coordinates as:

$$u^+ = \frac{u}{u_\tau} \tag{4.16}$$

$$y^+ = \frac{\rho u_\tau}{\mu_W} y \tag{4.17}$$

where u_τ represents the friction velocity:

$$u_\tau \equiv \sqrt{\frac{\tau_W}{\rho}} \tag{4.18}$$

It should be noted that the values quoted for y^+ to classify the various zones vary from one source to another in literature, reflecting the difficulty in establishing precisely the criteria for the boundary between each zone as clearly pointed out by some investigators (see for example Patel and Head (1969)). However, the following values of y^+ are commonly accepted as a reference for the three distinct zones:

$0 < y^+ < 5$ for the viscous sublayer, $5 < y^+ < 30$ for the transition and $y^+ > 30$ for the turbulent zone.

In the viscous zone the velocity distribution is represented by the linear law:

$$u^+ = y^+ \tag{4.19}$$

In the turbulent zone the velocity distribution of Newtonian fluids is represented by the Newtonian law of the wall:

$$u^+ = 2.5 ln\, y^+ + 5.5 \tag{4.20}$$

For non-Newtonian fluids the maximum possible drag reduction occurs when the interactive zone extends over the entire cross-section of the pipe, which is represented by the ultimate profile:

$$u^+ = 11.7 ln\, y^+ - 17 \tag{4.21}$$

The interactive zone, also called the elastic sublayer, is characteristic of drag reduction. It is the region between the viscous sublayer and the Newtonian plug where the mean velocity of drag-reducing polymers increases to above the Newtonian law of the wall. From the pipe axis inward, the velocity profiles are parallel-shifted upward from the Newtonian law (effective upshift).

Mean velocity profiles plotted in law-of-the-wall coordinates can be very useful, they can yield significant changes that are not immediately evident from their corresponding u/U_b *versus* r/R plot. **Figure 4.7** represents in law-of-the-wall coordinates (u^+ *versus* y^+) half of the velocity profile (corresponding to $r/R > 0$) for

0.125% PAA in transitional flow regime shown previously in **Figure 4.5** in u/U_b *versus* r/R coordinates.

4.6 – Ekman number

As mentioned in the Introduction (Chapter 1), according to Draad and Nieuwstadt (1998), in fully-developed laminar pipe flow through a straight circular pipe, the streamlines are parallel, viscous forces are balanced by pressure forces, the fluid inertia is unchanging and so plays no role in the fluid-dynamics. The influence of the Coriolis acceleration due to the combined effects of the Earth's rotation and the parallel flow is to generate a component of acceleration perpendicular to the pipe axis which leads to a distortion of the velocity profile. This rotational influence of the Earth can be evaluated by the Ekman number:

$$Ek = \frac{\mu_W}{2\Omega\rho D^2 \sin\beta} \tag{4.22}$$

where Ω is the angular velocity of the Earth (7.272×10^{-5} rad/s) and β the angle between the pipe axis and the rotation axis of the Earth, which is 52° for our case.

The lower the value of *Ek*, the more important rotational effects becomes compared with viscous forces (Escudier et al (2005)). Draad and Nieuwstadt (1998) have shown that for a laminar flow with an Ekman number of 5.23 the parabolic profile was significantly affected especially at higher Reynolds numbers. **Table 4.3** lists the Ekman number for all flows investigated, from where it is reasonable to conclude

that, for 60% Gly and 0.03% PAA in the laminar regime, the Earth's rotation may well be responsible for eventual velocity profile asymmetries.

Table 4.1 – Flow parameters for all liquids investigated

Fluid	$\dot{m}$ kg/s	$\Delta p / L$ Pa/m	U_b m/s	τ_w Pa	$\dot{\gamma}_w$ 1/s	μ_w Pa.s	Re_w	f
60% Gly ρ = 1140 kg/m^3	0.452	1.35	0.051	0.0338	0.000290	0.00858	670	0.0233
	0.533	1.54	0.060	0.0385	0.000330		790	0.0191
	0.681	1.92	0.076	0.0481	0.000413		1010	0.0146
	0.93	2.68	0.104	0.0670	0.000574		1380	0.0109
	1.04	3.13	0.116	0.0783	0.000672		1540	0.0103
	1.42	4.27	0.158	0.107	0.000917		2110	0.00747
	1.61	5.34	0.180	0.134	0.00115		2400	0.00722
	2.21	10.3	0.247	0.256	0.00220		3280	0.00738
	2.27	12.8	0.253	0.321	0.00275		3360	0.00878
	2.76	19.9	0.308	0.499	0.00428		4090	0.00923
	3.17	26.6	0.354	0.666	0.00571		4710	0.00931
	3.77	37.2	0.421	0.929	0.00798		5600	0.00920
	4.51	50.1	0.504	1.25	0.0108		6700	0.00866
	5.19	63.8	0.580	1.60	0.0137		7710	0.00832
	6.17	87.6	0.689	2.19	0.0188		9160	0.00809
	7.27	115	0.812	2.88	0.0248		10780	0.00768
	8.59	155	0.959	3.88	0.0333		12750	0.00740
0.03% PAA ρ = 998 kg/m^3	0.940	3.56	0.120	0.089	10.6	0.00836	1430	0.0124
	1.44	4.70	0.184	0.118	16.3	0.00721	2540	0.00698
	1.94	6.41	0.248	0.160	26.2	0.00611	4040	0.00524
	2.43	8.26	0.310	0.207	38.6	0.00536	5780	0.00431
	2.93	10.4	0.374	0.260	54.4	0.00478	7800	0.00373
	3.42	12.8	0.436	0.321	73.9	0.00434	10030	0.00337
	3.91	15.7	0.499	0.392	98.4	0.00398	12510	0.00315
	4.41	18.7	0.563	0.467	126	0.00371	15120	0.00295
	4.89	22.1	0.624	0.552	158	0.00349	17820	0.00284
	5.39	25.6	0.688	0.641	193	0.00332	20650	0.00272
	5.88	29.9	0.750	0.748	236	0.00317	23610	0.00266
	6.87	38.9	0.876	0.972	329	0.00296	29580	0.00254
	7.85	49.9	1.00	1.25	446	0.00280	35760	0.00249
	8.82	62.0	1.13	1.55	577	0.00268	41850	0.00245
	9.79	75.5	1.25	1.89	726	0.00260	47950	0.00242
	10.8	91.2	1.37	2.28	900	0.00253	54110	0.00242
0.125% PAA ρ = 998 kg/m^3 (cont.)	0.943	30.9	0.120	0.773	9.88	0.0782	150	0.107
	1.95	40.6	0.248	1.01	20.3	0.0501	500	0.0330
	2.94	47.7	0.375	1.19	30.5	0.0391	1000	0.0170
	3.89	54.1	0.496	1.35	41.5	0.0326	1520	0.0110
	4.86	62.7	0.620	1.57	58.6	0.0267	2320	0.00817

(cont.)

Table 4.1 (continuation)

Fluid	$\dot{m}$ kg/s	$\Delta p / L$ Pa/m	U_b m/s	τ_w Pa	$\dot{\gamma}_w$ 1/s	μ_w Pa.s	Re_w	f
0.125% PAA ρ = 998 kg/m^3	5.41	67.2	0.690	1.68	68.9	0.0244	2820	0.00708
	5.87	71.9	0.749	1.80	80.2	0.0224	3330	0.00643
	6.78	81.8	0.865	2.04	106	0.0193	4480	0.00547
	7.27	84.5	0.928	2.11	114	0.0186	4980	0.00492
	7.74	87.3	0.987	2.18	122	0.0179	5500	0.00449
	8.22	90.4	1.05	2.26	131	0.0172	6070	0.00412
	8.77	93.6	1.12	2.34	141	0.0166	6710	0.00375
	9.18	97.2	1.17	2.43	152	0.0160	7310	0.00355
	9.65	106	1.23	2.65	181	0.0146	8390	0.00351
	10.1	113	1.29	2.82	204	0.0138	9320	0.00338
	10.7	116	1.36	2.91	217	0.0134	10140	0.00313
	11.1	117	1.41	2.91	217	0.0134	10650	0.00297
	11.5	117	1.47	2.92	218	0.0134	11270	0.00278
	12.2	118	1.55	2.95	223	0.0132	11560	0.00243
	12.6	120	1.60	3.01	230	0.0130	11930	0.00236
	13.0	129	1.65	3.22	263	0.0123	13460	0.00231
	13.4	136	1.72	3.39	288	0.0118	14550	0.00228
	13.9	140	1.78	3.51	306	0.0114	15490	0.00223
	14.4	144	1.84	3.60	322	0.0112	16390	0.00214
	14.9	149	1.90	3.72	340	0.0109	17360	0.00206
	15.4	154	1.96	3.84	360	0.0107	18370	0.00200
0.15% XG ρ = 998 kg/m^3 (cont.)	0.938	20.7	0.120	0.516	9.82	0.0526	230	0.0722
	1.45	24.9	0.184	0.623	14.7	0.0424	430	0.0367
	1.95	28.6	0.249	0.716	19.9	0.0359	690	0.0232
	2.45	31.5	0.313	0.787	24.6	0.0320	980	0.0161
	2.95	34.8	0.377	0.869	30.7	0.0283	1330	0.0123
	3.45	37.3	0.440	0.933	36.1	0.0258	1700	0.00964
	3.94	40.5	0.503	1.01	43.3	0.0233	2150	0.00800
	4.44	42.7	0.567	1.07	49.1	0.0218	2600	0.00666
	4.94	45.9	0.630	1.15	57.6	0.0199	3150	0.00580
	5.44	49.1	0.694	1.23	67.2	0.0183	3780	0.00512
	5.94	52.7	0.757	1.32	78.5	0.0168	4500	0.00460
	6.43	56.7	0.821	1.42	92.1	0.0154	5320	0.00421
	6.93	59.8	0.884	1.50	103	0.0145	6100	0.00384
	7.42	64.5	0.947	1.61	122	0.0133	7120	0.00360
	7.91	68.4	1.01	1.71	137	0.0125	8080	0.00336
	8.40	72.6	1.07	1.82	155	0.0117	9150	0.00317
	8.88	76.9	1.13	1.92	174	0.0110	10260	0.00300
	9.38	79.8	1.20	1.99	187	0.0106	11220	0.00279
	9.86	86.7	1.26	2.17	220	0.00984	12750	0.00275

(cont.)

Table 4.1 (continuation)

Fluid	$\dot{m}$ kg/s	$\Delta p / L$ Pa/m	U_b m/s	τ_w Pa	$\dot{\gamma}_w$ 1/s	μ_w Pa.s	Re_w	f
0.15% XG $\rho = 998$ kg/m^3	10.4	94.9	1.32	2.37	261	0.00909	14490	0.00273
	10.8	101.4	1.38	2.54	295	0.00861	16020	0.00266
	11.3	111	1.44	2.77	344	0.00805	17910	0.00266
	11.8	118	1.51	2.95	383	0.00769	19530	0.00261
	12.3	124	1.57	3.09	414	0.00745	20980	0.00252
	12.8	127	1.63	3.18	435	0.00731	22230	0.00240
	13.2	136	1.69	3.39	483	0.00702	24010	0.00238
	13.7	141	1.75	3.52	513	0.00686	25440	0.00231
	14.2	150	1.81	3.75	567	0.00662	27310	0.00229
	14.7	157	1.87	3.93	608	0.00646	28930	0.00225

Table 4.2 – Onset of transition and turbulent flow (data from **Figure 4.4**)

Fluid	Re_1	Re_2
60% Gly	2110	3360
0.03% PAA	4040	10030
0.125% PAA	4480	11930
0.15% XG	3150	12750

Table 4.3 – Ekman numbers for all liquids investigated

60% Gly								
Re	670	790	1010	1380	1540	**2110**	2400	3280
Ek	6.6							
0.03% PAA								
Re_W	1430	2540	**4040**	5780	7800	10030	12510	15120
Ek	7.3	6.3	5.3	4.7	4.2	3.8	3.5	3.2

0.125% PAA								
Re_W	150	500	1000	1520	2320	2820	3330	**4480**
Ek	68	44	34	29	23	21	20	17
0.15% XG								
Re_W	230	430	980	1330	1700	2150	2600	**3150**
Ek	46	37	28	25	23	20	19	17

Numbers in bold correspond to Re_1

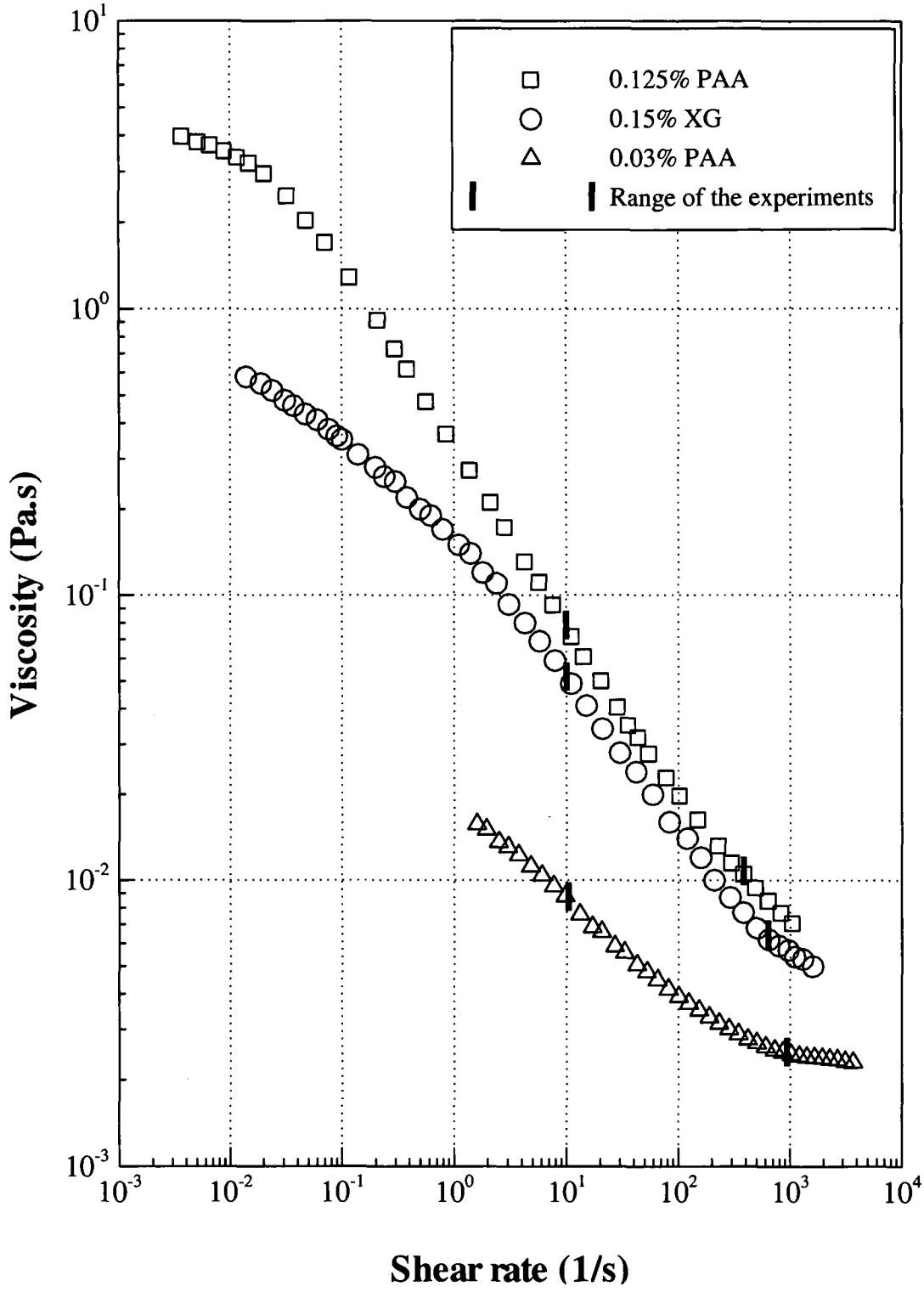

Figure 4.1 – Ranges of wall shear rate ($\dot{\gamma}_w$) used during experiments, for all non-Newtonian liquids investigated

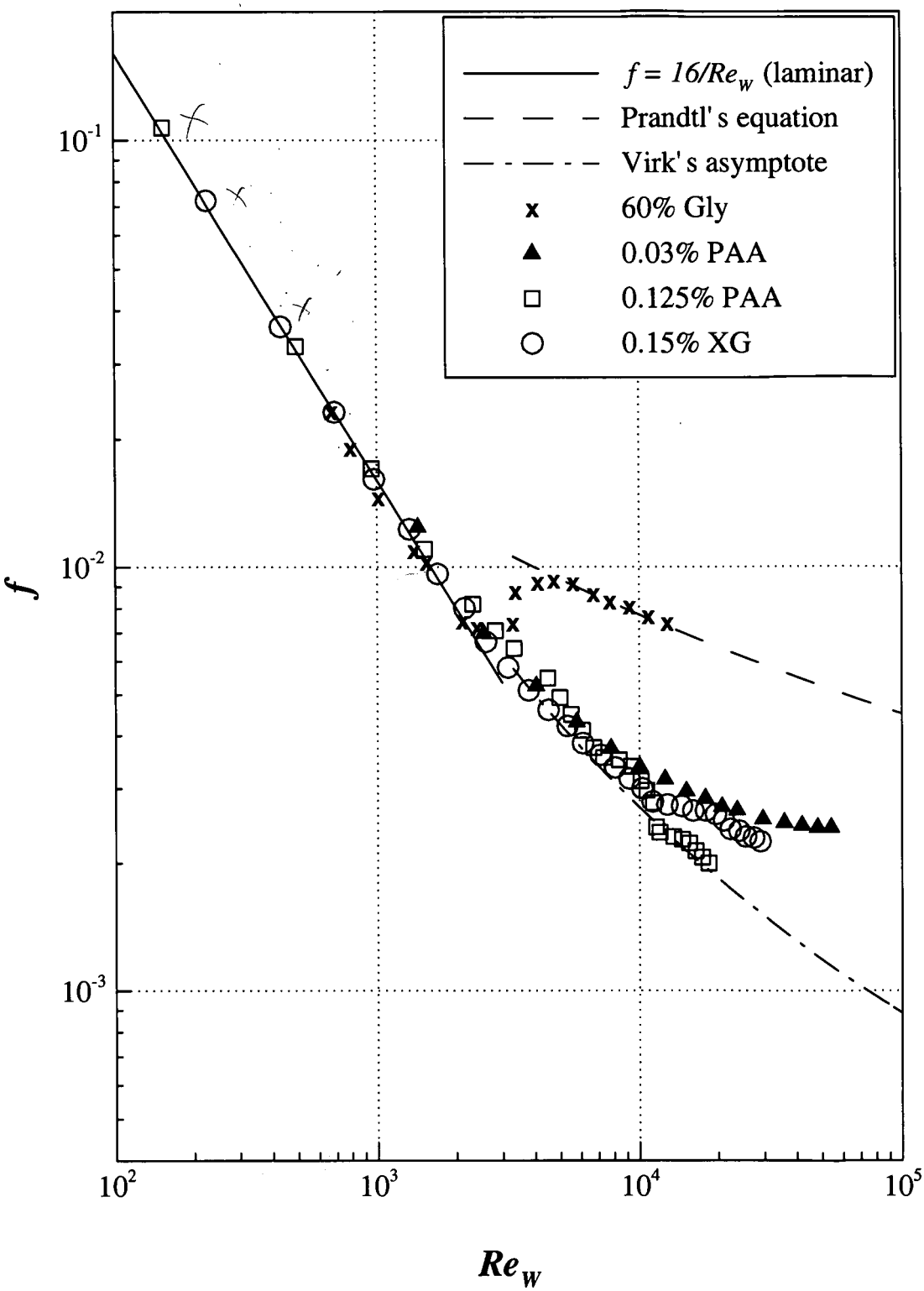

Figure 4.2 – Fanning friction factor (f) *versus* Reynolds number (Re_w), for all liquids investigated

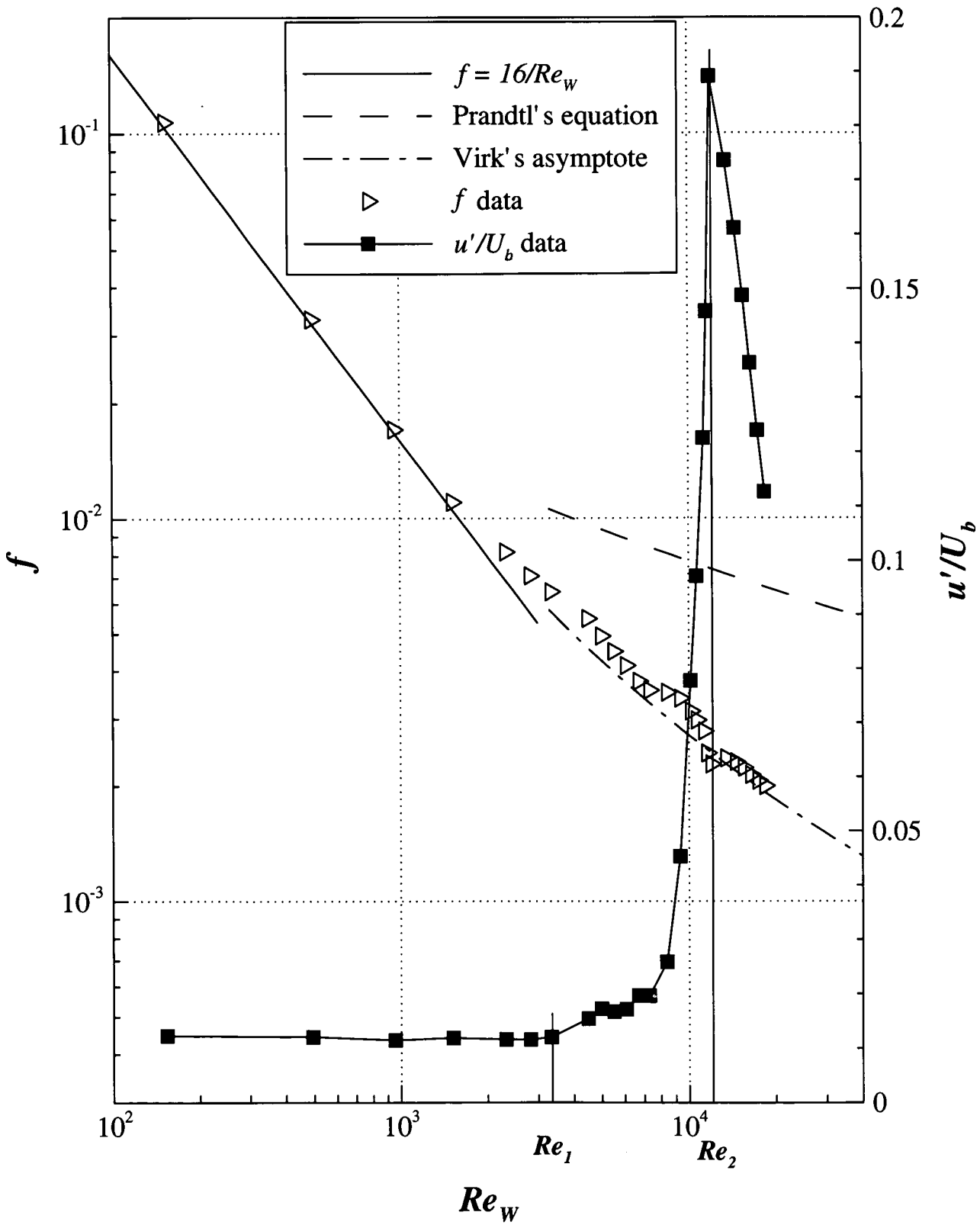

Figure 4.3 – Fanning friction factor (f) and velocity fluctuations (u'/U_b) *versus* Reynolds number (Re_W) at r/R = - 0.8, for 0.125% PAA

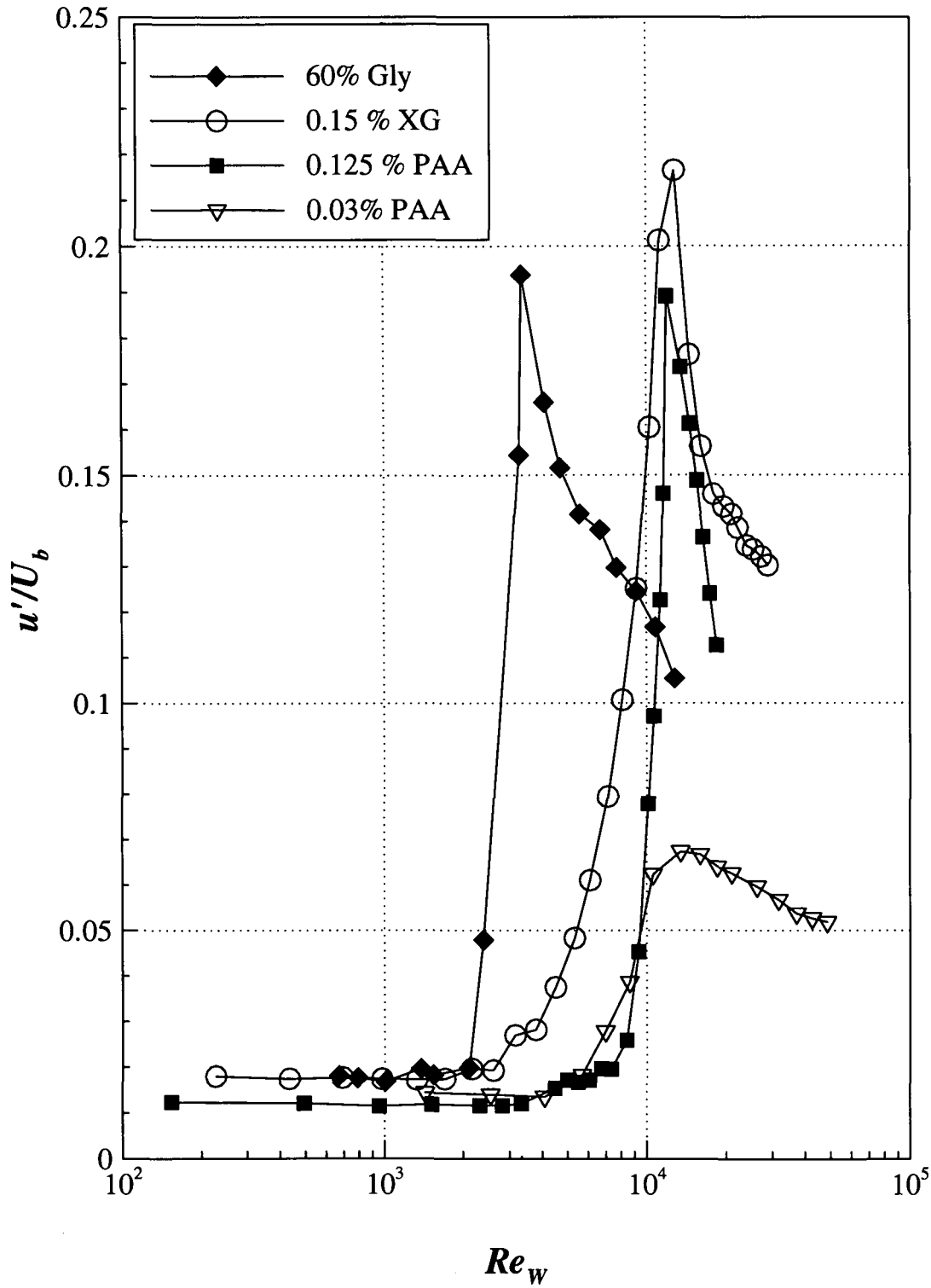

Figure 4.4 – Velocity fluctuations (u'/U_b) *versus* Reynolds number (Re_W) at r/R = - 0.8, for all liquids investigated

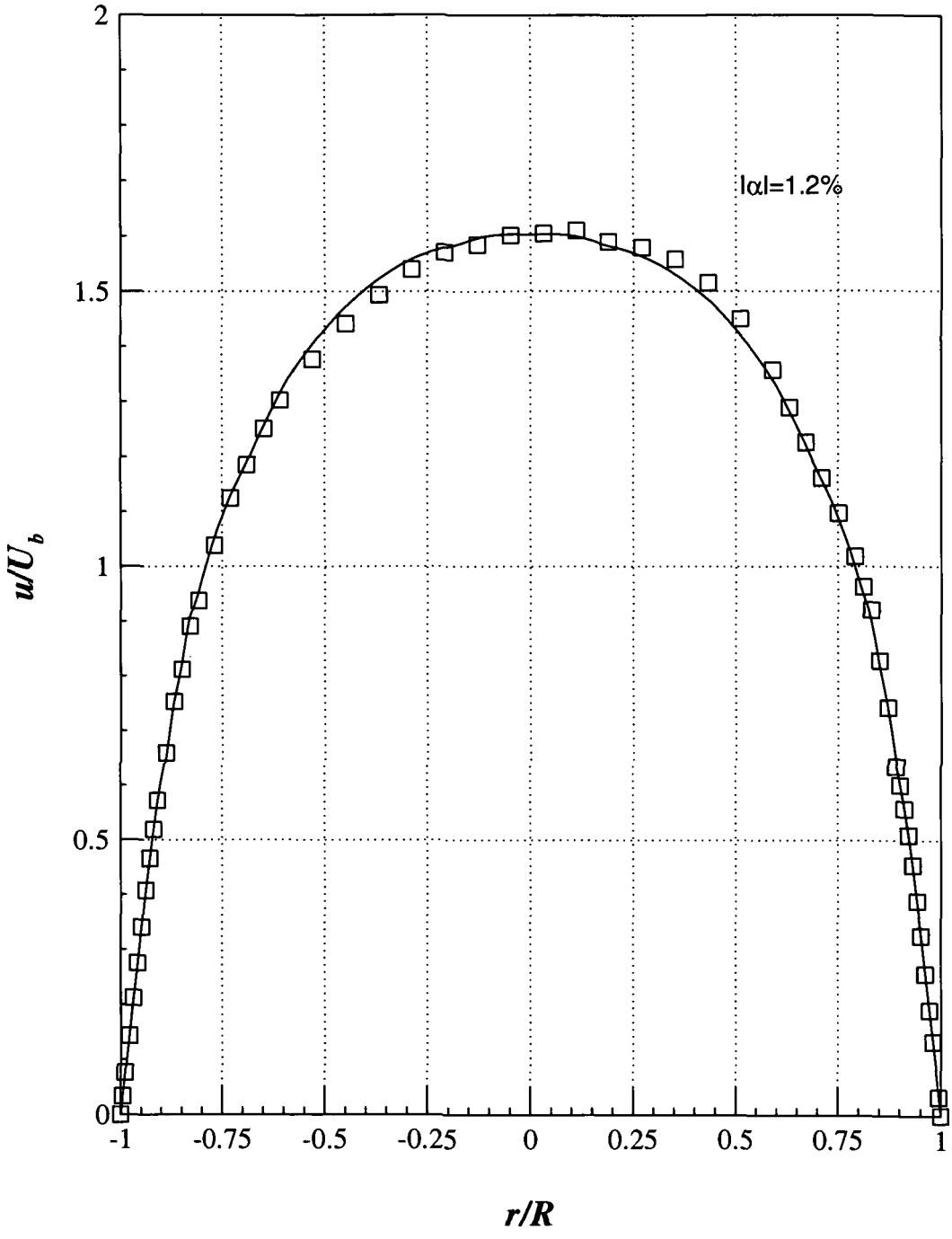

Figure 4.5 – Horizontal (θ = 90°, 270°) velocity profile at Re_w = 11560 and x/D = 220, including average (continuous line), for 0.125% PAA

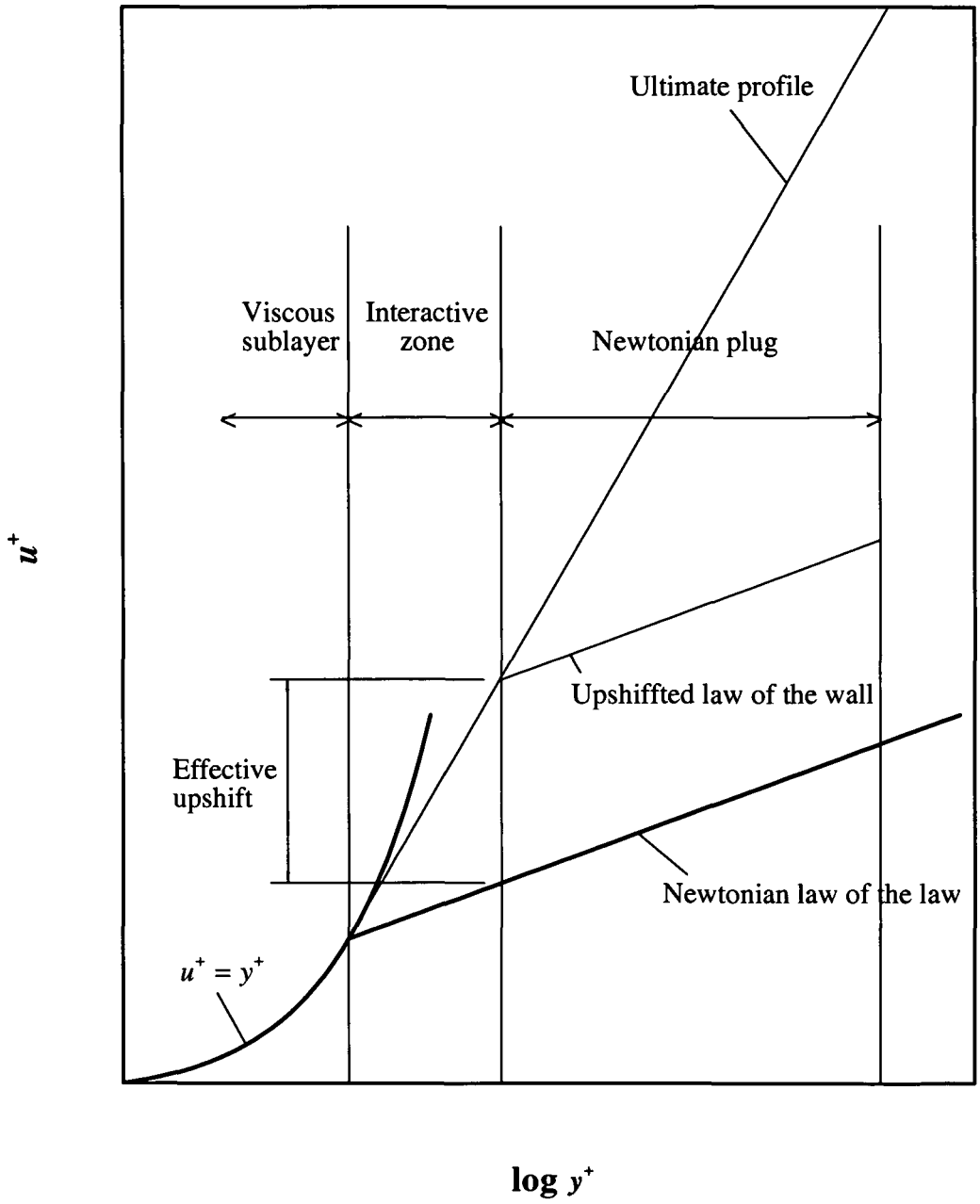

Figure 4.6 – Schematic of the three-zone mean flow model (Virk et al (1970))

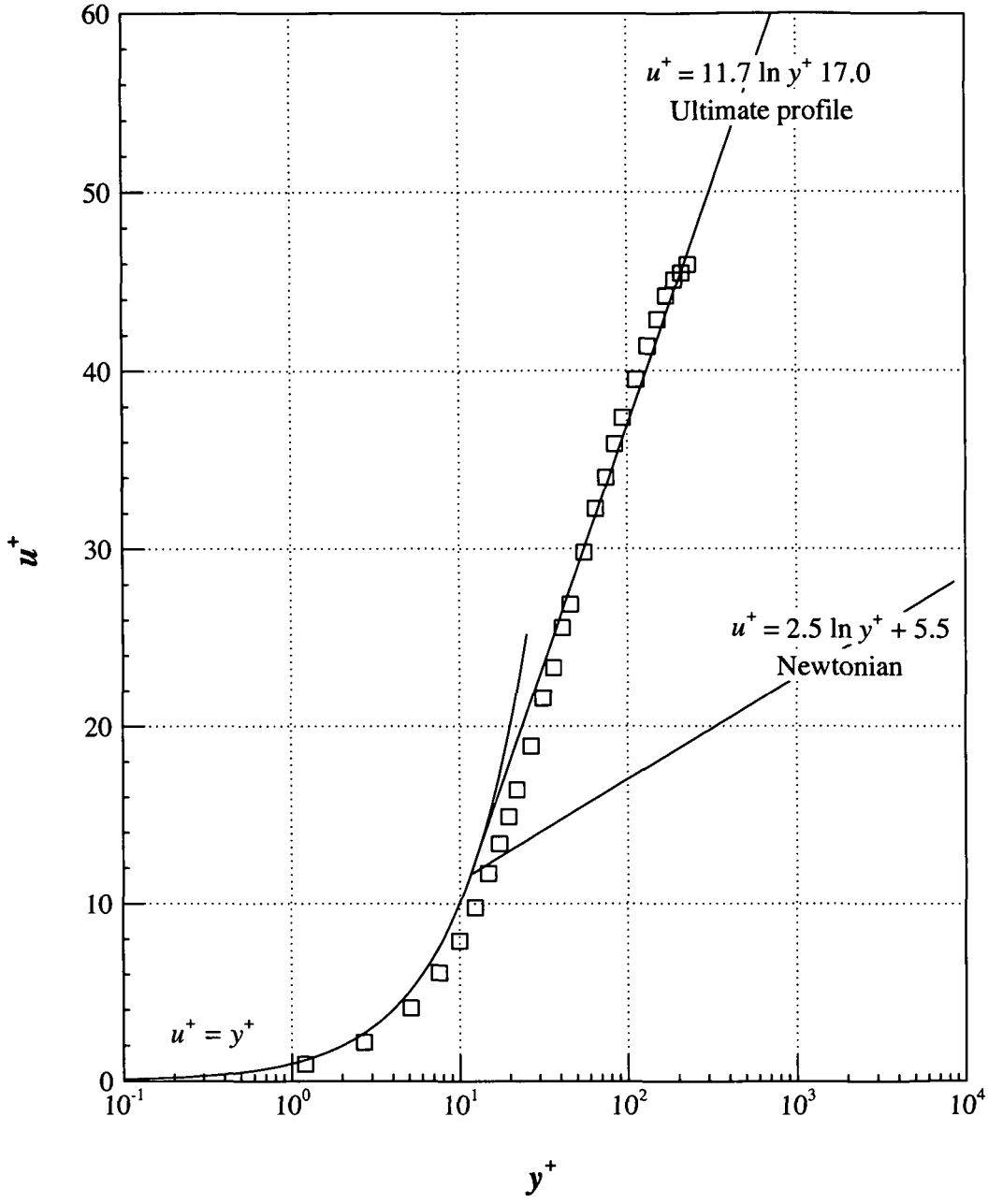

Figure 4.7 – Half horizontal (θ = 90°) velocity profile in law-of-the-wall coordinates at Re_W = 11560 and x/D = 220, for 0.125% PAA

5 – Laminar and turbulent flows

5.1 – Introduction

In this chapter we present the results of experiments carried out within the laminar and turbulent flow regimes. The next section presents experimental results of the mean axial velocities under laminar flow conditions, followed by Section 5.3 with results of the mean axial velocities and the turbulence intensities for the turbulent regime. The experimental results are in good agreement with the literature and therefore represent a "validation" of the experimental arrangements and instrumentation used in this work.

All the results reported in this chapter were obtained for a single "cut" through the flow field, the horizontal plane (θ = 90°, 270°), at a particular position (x) along the pipe, 22 m from the entrance (x/D = 220).

5.2 – Laminar flow

5.2.1 – Newtonian fluid

Figure 5.1 shows the axial velocity profiles of the Newtonian fluid, 60% Gly, for two different Reynolds numbers. The shape of each velocity profile is in good agreement with the theoretical profile of Hagen-Poiseuille (Equation 4.11). At Re = 790 and Re = 1380 the velocity ratio of the centreline measurement from the

LDA to the average velocity from the flowmeter (u_0/U_b) is 1.97 and 2.01 respectively, compared to the theoretical value of 2.00.

The figure also shows that in laminar flow the axial velocity profiles are basically symmetric, despite a slight asymmetry observed for the lower Reynolds number. The coefficient of asymmetry (α) calculated from Equation 4.14, is 0.05% for the velocity profile corresponding to Re = 1380 and 1.7% for that corresponding to Re = 790. These values are small and because they are within the uncertainty of the results it is not possible to say with total confidence that these two velocity profiles are not axisymmetric.

At this stage it is useful to set a reference level for the coefficient of asymmetry below which we can say the velocity profile is essentially axisymmetric. Considering the uncertainty and the reproducibility of the experimental results, a value of 2% seems reasonable. This reference level should be kept in mind in the discussion which follows.

As Draad and Nieuwstadt (1998) have shown, the Earth's rotation can be responsible for the distortion of the velocity profiles in laminar flow. The presence of Coriolis force due to the Earth's rotation was the explanation for the parabolic velocity profile distortion observed in their investigation with water. They used the Ekman number to evaluate the influence of the Earth's rotation, which represents the ratio of the viscous to the Coriolis force (see Equation 4.22). In our study, for the 60% Gly solution the Ekman number is constant and 6.6 (see **Table 4.3**), which is sufficiently low to admit with reasonable confidence that the Earth's rotation may play a role in

the axial velocity asymmetry observed for Re = 790 ($|\alpha|$ = 1.7%). However the value is lower than the reference level of 2% (within the uncertainly of the results) and inconsistent with the work of Draad and Nieuwstadt (1998) where the velocity profile asymmetry increases with the Reynolds number. It is also important to note that our Reynolds numbers are much lower than those obtained by Draad and Nieuwstadt (1998), our highest Reynolds number within laminar flow conditions was 1380, and the lowest Reynolds number published by them was 2500 with an estimated α of 4%.

5.2.2 – Non-Newtonian fluids

For the 0.03% PAA solution the axial velocity profile in laminar flow (Re_W = 2540) is represented in **Figure 5.2** which includes the analytical solution for fully-developed pipe flow of a power-law fluid (Equation 4.12) with n = 0.64 for comparison. As expected the velocity ratio of the centreline to the average velocity (u_0 / U_b = 1.78) is lower than the theoretical value for Newtonian fluids ($u_0 / U_b = 2$).

As observed for the Newtonian case a small degree of asymmetry also exists for this polymer solution. In this case the coefficient of asymmetry (α) is 1.9% for a Reynolds number of 2540. Here the Ekman number is 6.3, which is basically the same as for the 60% Gly solution, so could suggested that the Earth's rotation influences the velocity profile asymmetry, however this value is, as for the 60% Gly,

lower than the reference level of 2% and therefore the flow for the 0.03% PAA solution in laminar flow is also considered essentially axisymmetric.

For the 0.125% PAA solution we have carried out measurements of the axial velocity within the laminar regime for three different Reynolds numbers. The velocity profiles are represented in **Figure 5.3** which includes power-law profiles with $n = 0.47$. The lower value of n indicates that this fluid is more shear-thinning than the 0.03% PAA solution. The velocity profiles are in good agreement with the power-law profile, especially at the lowest Reynolds number. As the Reynolds number increases the corresponding profile becomes progressively flatter and diverge from the power-law fit, but are still in acceptable agreement. The ratio of the centreline to the average velocity (u_0 / U_b) is lower than that for the 0.03% PAA: 1.64 for 0.125% PAA and 1.78 for 0.03% PAA. From the figure it is also possible to conclude that in laminar flow the axial velocity profiles for the 0.125% PAA solution are symmetric as would be expected as the lowest Ekman number is equal to 21, and so too high for Coriolis effects to play a role in these flows.

Figure 5.4 shows the axial velocity profile for the 0.15% XG solution at $Re_W = 1330$ (laminar flow), including a power-law profile ($n = 0.48$). In this case $Ek = 25$ and the velocity profile is symmetric ($|\alpha| = 0.07\%$). The velocity ratio of the centreline to the average velocity (u_0 / U_b) is equal to 1.65, which is very close to that observed for the 0.125% PAA solution (1.64) and lower than that found for the 0.03% PAA solution (1.78), confirming that the 0.15% XG and the 0.125% PAA solutions have about the same degree of shear-thinning but higher than the 0.03% PAA solution.

This is confirmed by values of the exponent n, which are: 0.47 for 0.125% PAA, 0.48 for 0.15% XG and 0.64 for 0.03% PAA.

5.3 – Turbulent flow

This section presents the experimental results of the mean axial velocities and the turbulence intensities for the Newtonian fluid (60% Gly) and three non-Newtonian fluids (0.03% PAA, 0.125% PAA and 0.15% XG), under turbulent-flow conditions.

5.3.1 – Newtonian fluid

Figure 5.5 shows the axial velocity profiles in the horizontal plane, (θ = 90° and 270°) for the 60% Gly solution, for three different Reynolds numbers: 3360, 4090 and 12750. The shape of the velocity profiles is in agreement with what should be expected for turbulent flow, displaying steeper velocity gradients near the wall and a flatter variation in the central region of the pipe than the parabolic profile of laminar flow. This behaviour can be seen in this figure with progressively flatter profiles towards the centre of the pipe as the Reynolds number increases with a resultant increase in velocity gradient near the wall. The results of the ratio of the maximum to the mean velocity (u_0 / U_b) are in good agreement with previous experimental works (for example, Laufer (1954), Pinho (1990) and Presti (2000)) (see **Table 5.1**). The results of u_0 / U_b also provide an indication of how turbulent the flow is.

Figure 5.5 includes average curves corresponding to the velocity data on both sides of the centreline highlighting that all three velocity profiles, covering a range of turbulent flow conditions, are perfectly symmetric.

The corresponding turbulence intensities normalised by U_b are plotted in **Figure 5.6**, showing higher levels of velocity fluctuations in the region $0.75 < |r/R| < 0.95$ and lower in the central region. The data corresponding to Reynolds numbers of 3360 and 4090 is characterised by higher levels of velocity fluctuation in comparison with the Reynolds number of 12750. As the Reynolds number increases, the flow develops from transitional to fully turbulent flow, the peak value of u'/U_b decreases and shifts nearer towards the wall.

5.3.2 – Non-Newtonian fluids

Figures 5.7, **5.8** and **5.9** represent the axial horizontal velocity profiles for 0.03% PAA, 0.125% PAA and 0.15% XG solutions, respectively. The averages of the velocity data highlight the symmetric shape of the velocity profiles in the turbulent flow regime. The corresponding mean velocity profiles in law-of-the-wall coordinates are shown in **Figures 5.10**, **5.11** and **5.12**. The experimental data represented in these figures corresponds to one side of the centreline of the pipe, $r/R > 0$. For $y^+ < 10$ the experimental results for all polymer solutions are in excellent agreement with the linear law $u^+ = y^+$. For $y^+ > 10$ the results are in good agreement with Virk's asymptote.

In **Figures 5.13**, **5.14** and **5.15** the corresponding axial velocity fluctuations (or turbulence intensities) are plotted. The peak values of the turbulence intensity normalised by the bulk velocity in the region near the wall are similar for the three polymer solutions, 0.18 for 0.125% PAA, 0.15 for 0.03% PAA and 0.16 for 0.15% XG. It is also evident from the figures that these peaks decrease progressively and move closer to the wall as the Reynolds number increases.

5.4 – Conclusions

Under laminar-flow conditions the velocity profiles are well represented by the Hagen-Poiseuille profile for the Newtonian liquid and by the power-law fits for the non-Newtonian liquids. The velocity ratio of the centreline to the average velocity (u_0 / U_b) was found to decrease with the degree of shear-thinning. Measurements of the axial velocity in turbulent flow indicate progressively flatter distributions of velocity towards the centre of the pipe as the Reynolds number increases with a resultant increase of the velocity gradient near the pipe wall. All liquids investigated do not exhibit any considerable velocity profile asymmetry within laminar and turbulent flow conditions.

Velocity profiles plotted in law-of-the-wall coordinates for the non-Newtonian liquids investigated confirm that in the viscous zone the experimental data faithfully follows the linear law $u^+ = y^+$, and for the transitional and turbulent zones ($y^+ > 5$) the velocity profiles are in reasonable agreement with Virk's asymptote.

The velocity fluctuations normalised against the bulk velocity indicate peak values in the region near the wall which occur over larger distances and further away from the wall for non-Newtonian fluids than for the Newtonian. The peak axial velocity fluctuation reduces progressively as the Reynolds number increases and the peak moves closer to the wall for all fluids.

Table 5.1 – Velocity characteristics in turbulent pipe flow of Newtonian fluids

Reference	Fluid	Re	u_0 / U_b
This Work	60% Gly	3660	1.39
This Work	60% Gly	4460	1.35
This Work	60% Gly	13860	1.25
Presti (2000)	60% Gly	8000	1.28
Presti (2000)	60% Gly	36000	1.22
Presti (2000)	60% Gly	61000	1.20
Pinho (1990)	Water	32000	1.27
Pinho (1990)	Water	62000	1.23
Laufer (1954)	Air	40000	1.25

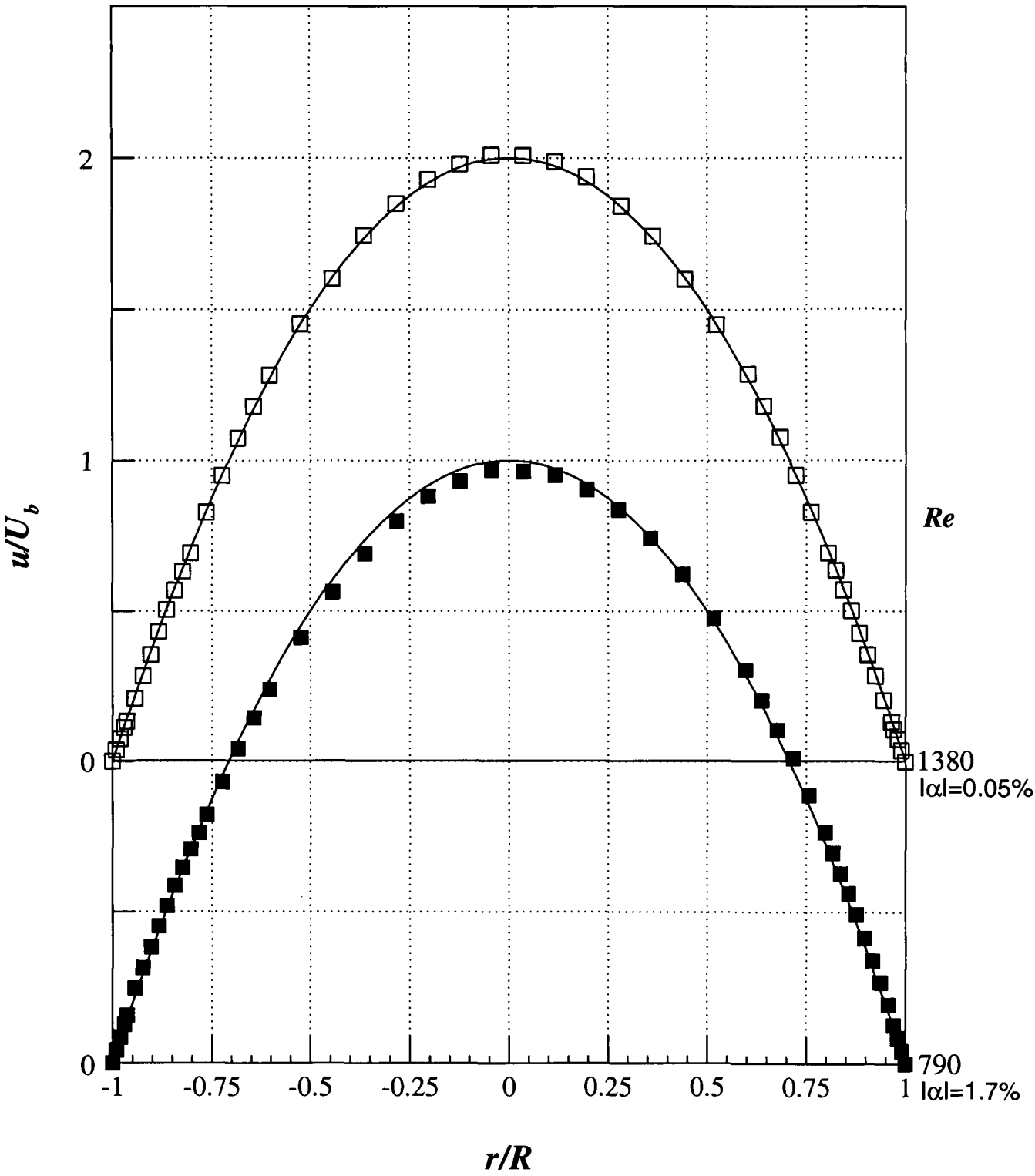

Figure 5.1 – Horizontal (θ = 90°, 270°) velocity profiles for two different Reynolds numbers within laminar regime at x/D = 220, including Hagen-Poiseuille profile (continuous lines), for 60% Gly

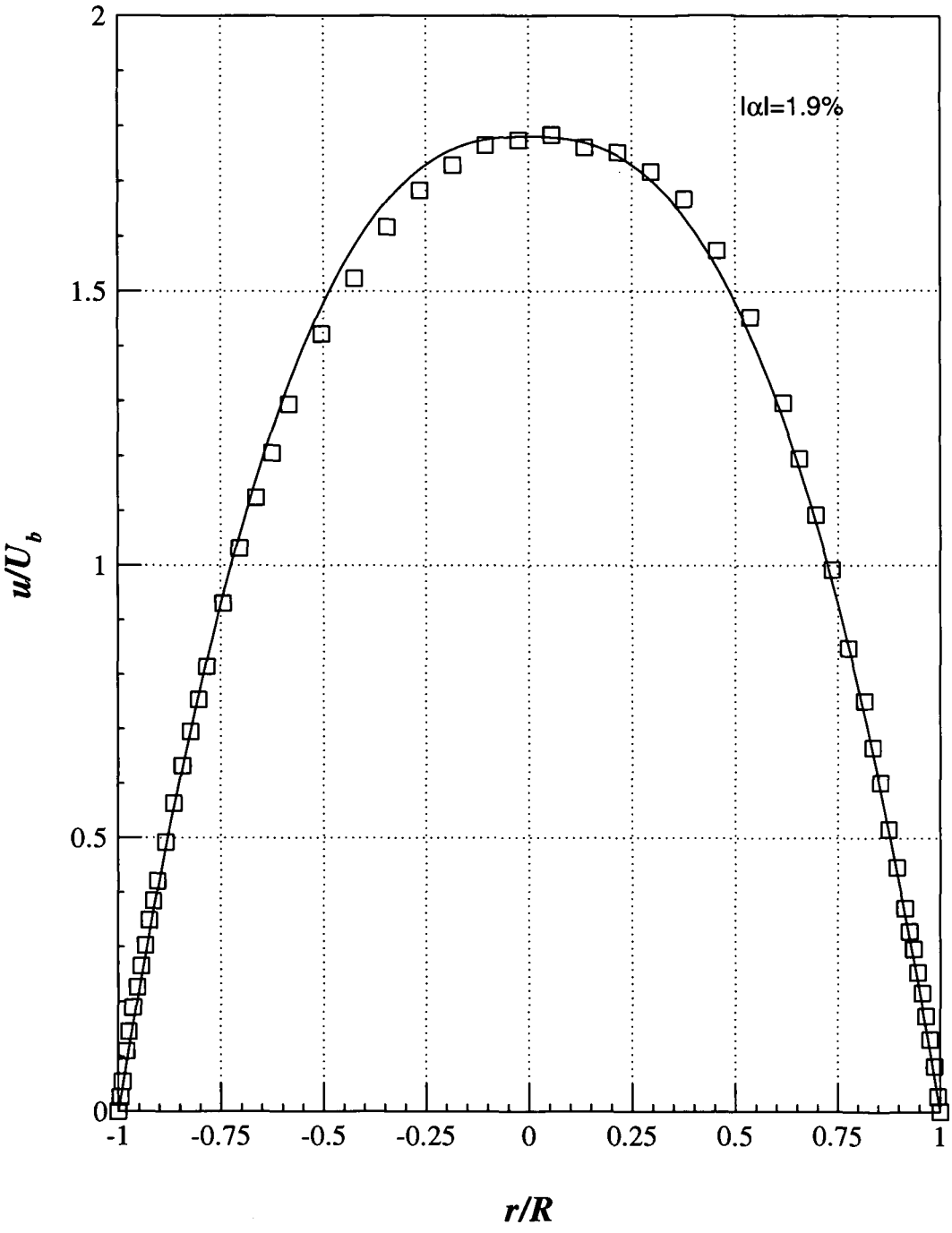

Figure 5.2 – Horizontal (θ = 90°, 270°) velocity profile within laminar regime (Re_w = 2540) at x/D = 220, including power-law profile with n = 0.64 (continuous line), for 0.03% PAA

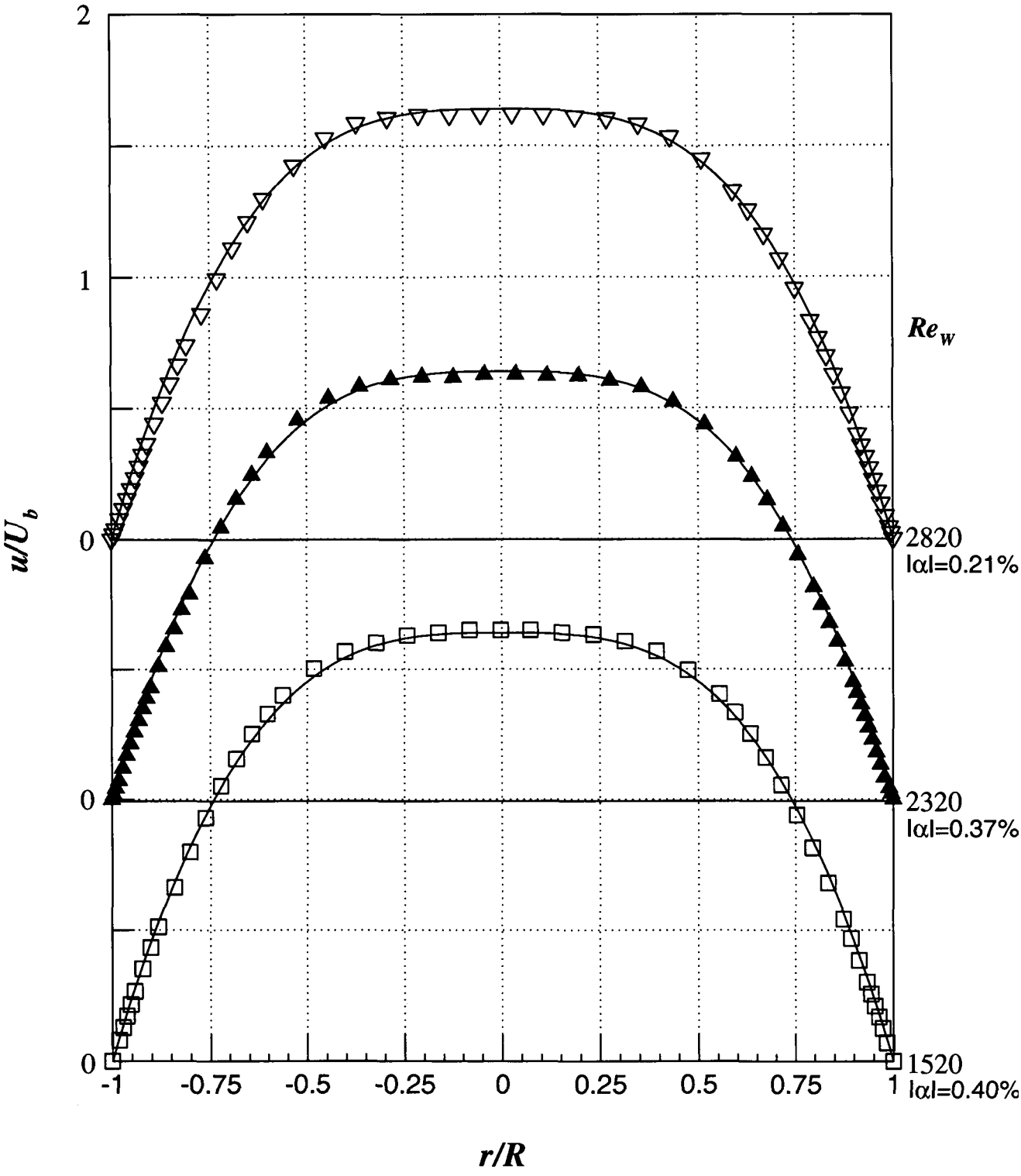

Figure 5.3 – Horizontal (θ = 90°, 270°) velocity profiles for three different Reynolds numbers within laminar regime at x/D = 220, including power-law profile with n = 0.47 (continuous lines), for 0.125% PAA

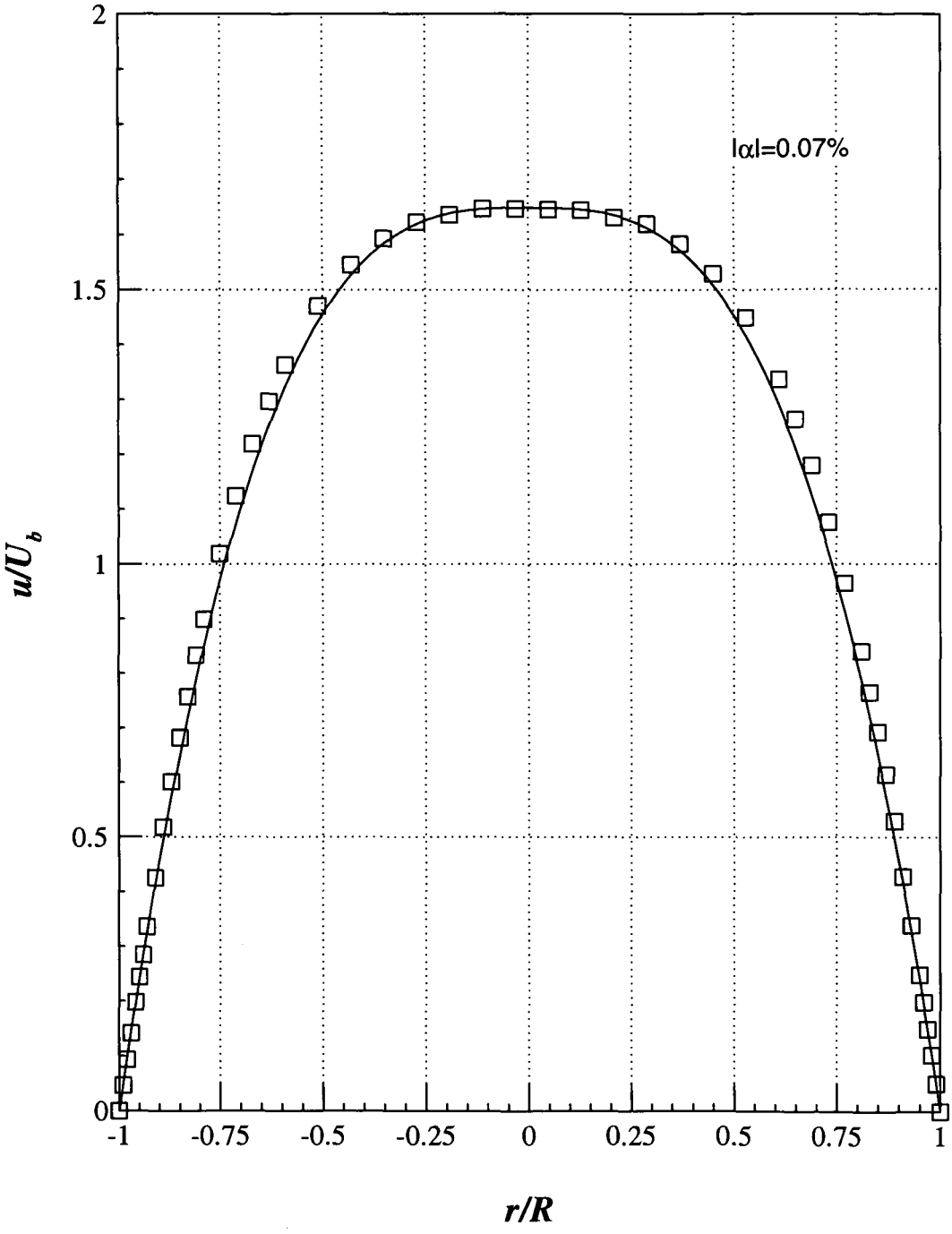

Figure 5.4 – Horizontal (θ = 90°, 270°) velocity profile in laminar regime (Re_w = 1330) at x/D = 220, including power-law profile with n = 0.48 (continuous line), for 0.15% XG

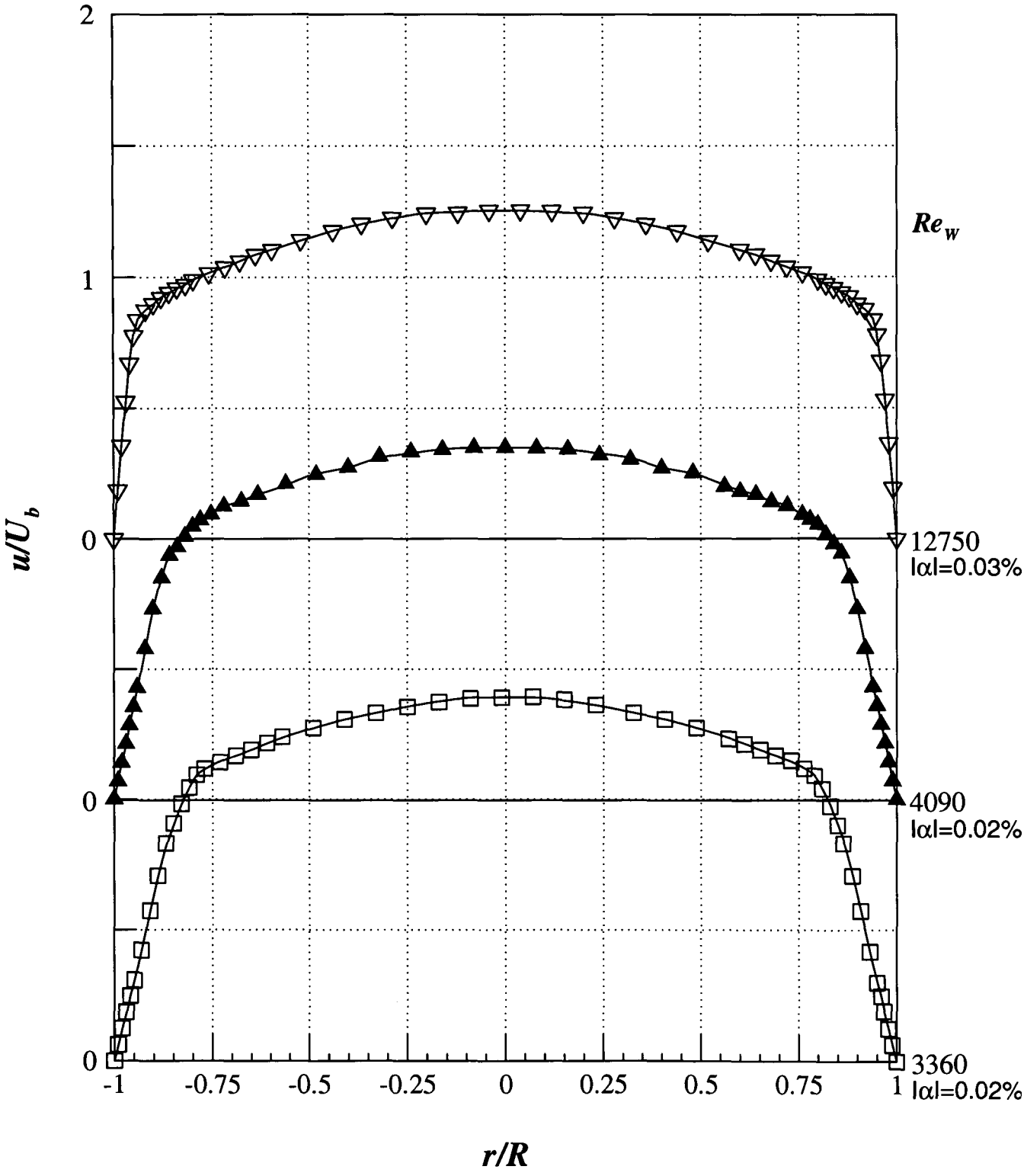

Figure 5.5 – Horizontal (θ = 90°, 270°) velocity profiles for three different Reynolds numbers within turbulent regime at x/D = 220, including averages (continuous lines), for 60% Gly

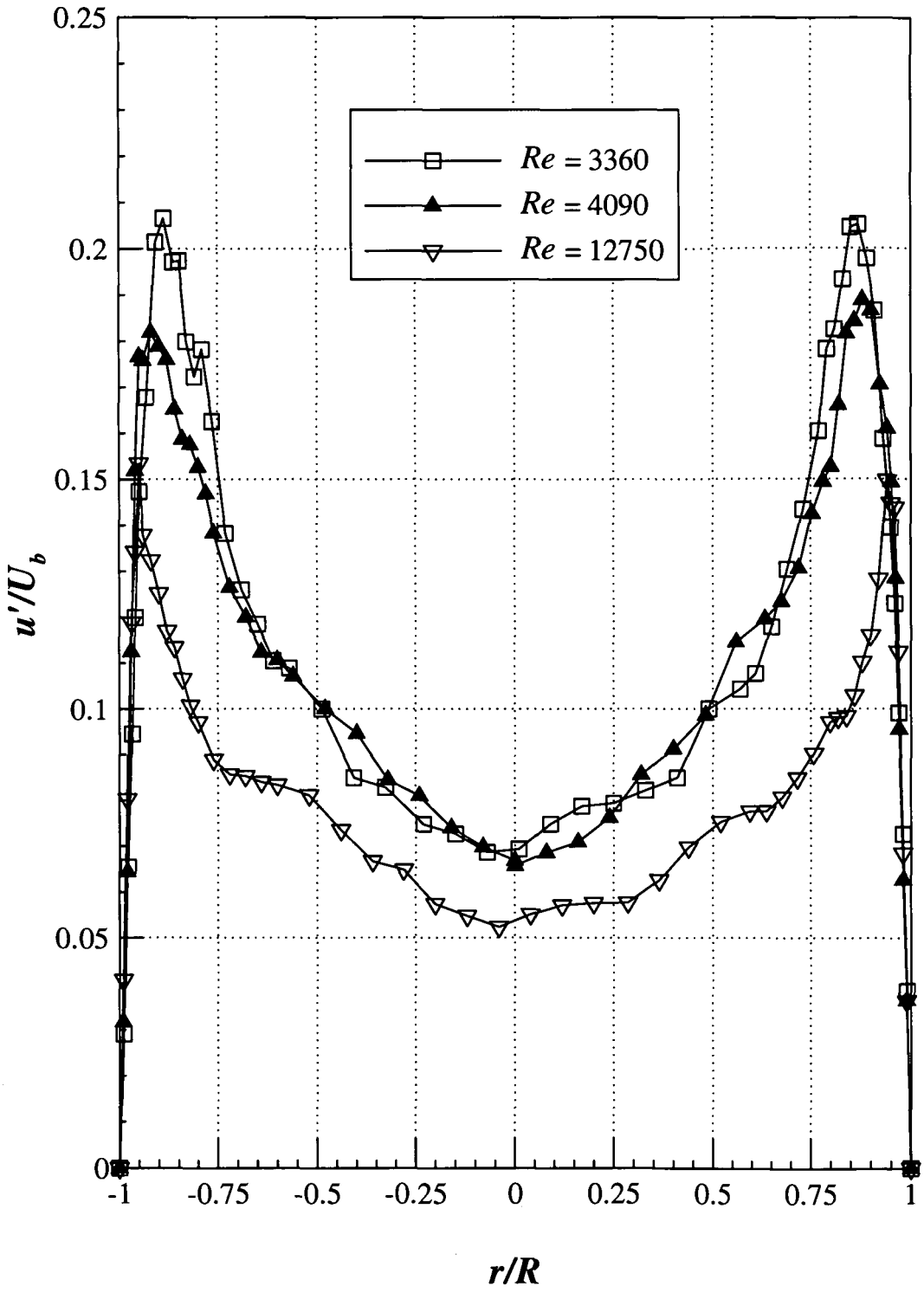

Figure 5.6 – Horizontal (θ = 90°, 270°) velocity fluctuations for three different Reynolds numbers within turbulent regime at x/D = 220, for 60% Gly

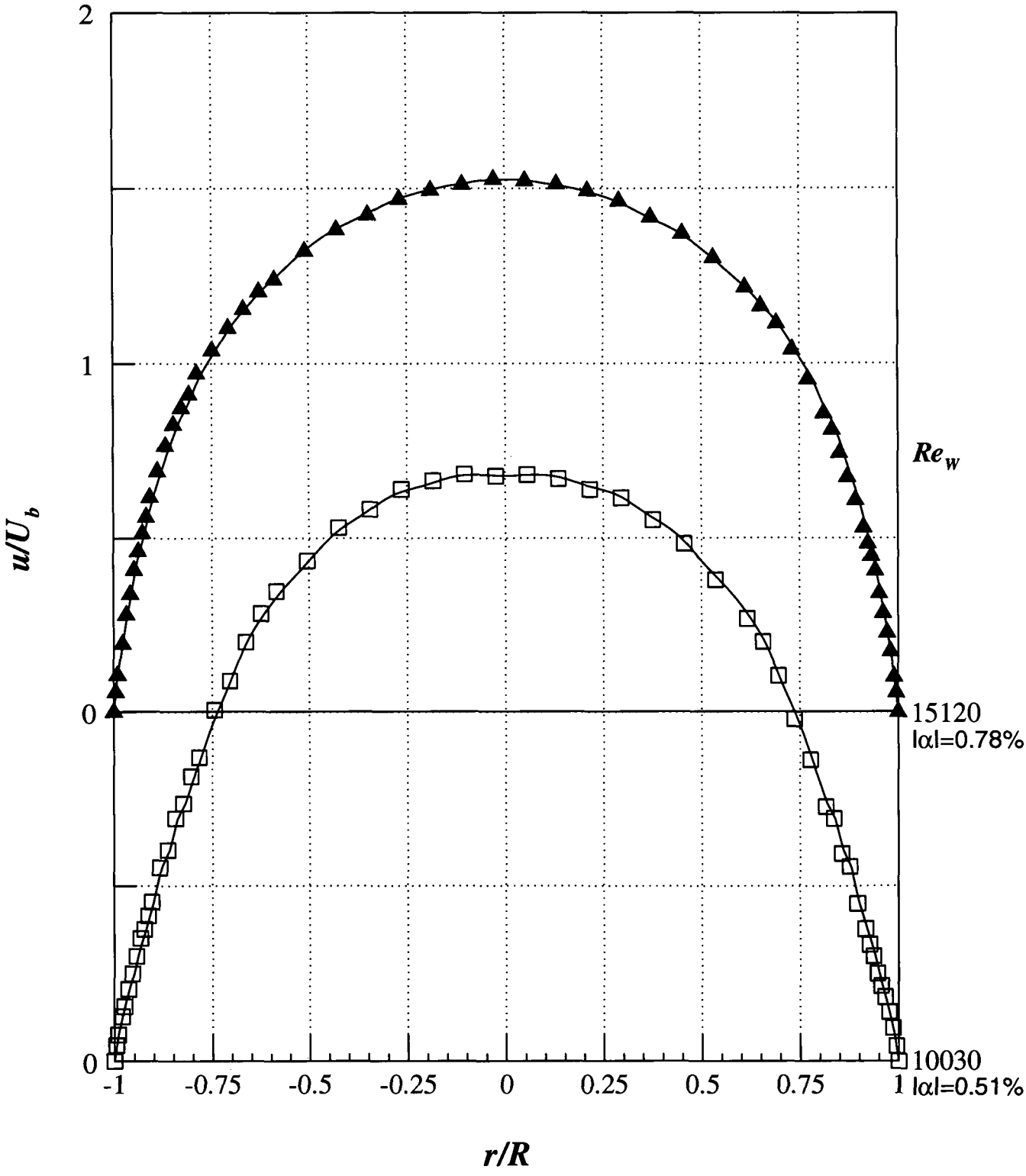

Figure 5.7 – Horizontal (θ = 90°, 270°) velocity profiles for two different Reynolds numbers within turbulent regime at x/D = 220, including averages (continuous lines), for 0.03% PAA

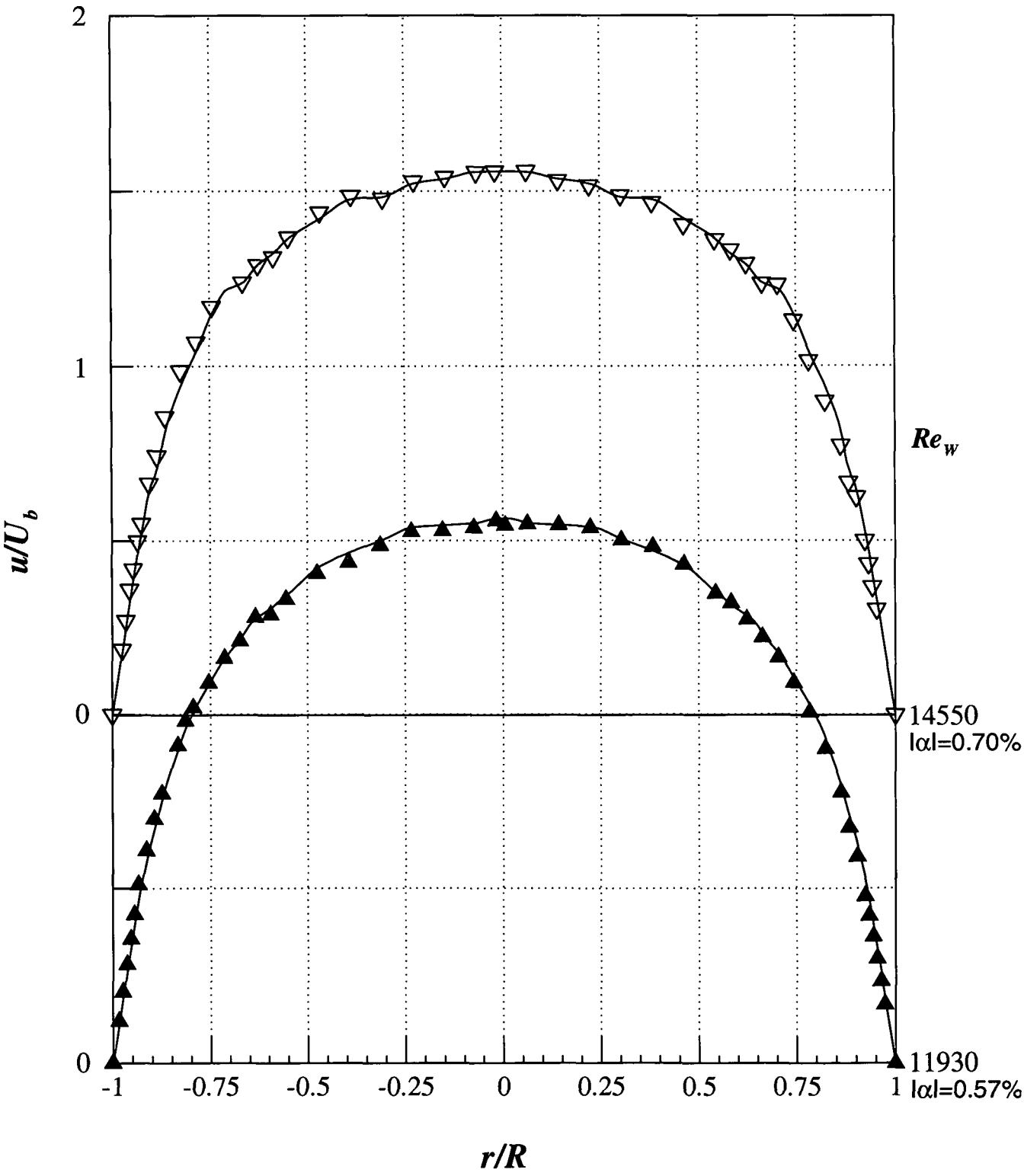

Figure 5.8 – Horizontal (θ = 90°, 270°) velocity profiles for two different Reynolds numbers within turbulent regime at x/D = 220, including averages (continuous lines), for 0.125% PAA

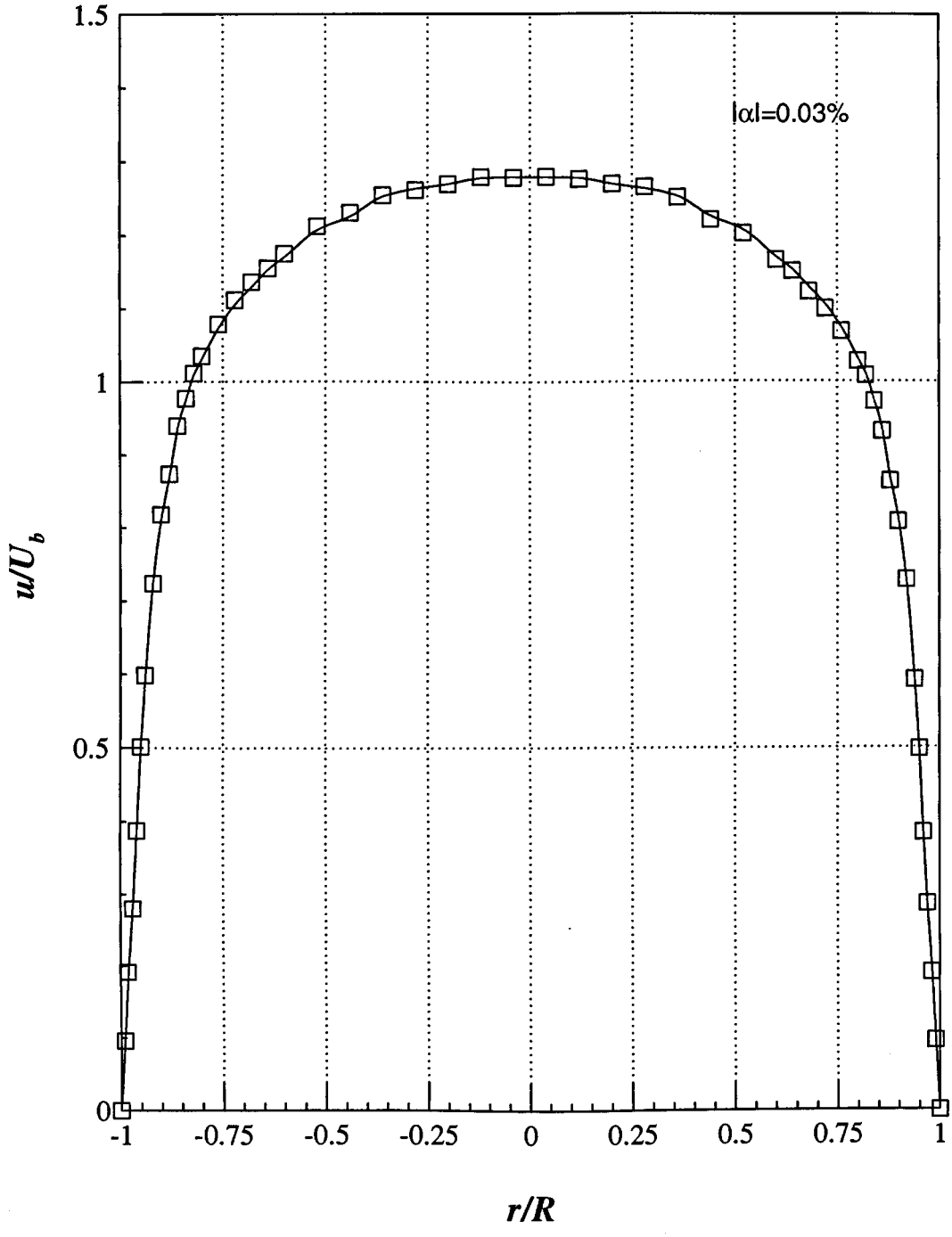

Figure 5.9 – Horizontal (θ = 90°, 270°) velocity profile within turbulent regime (Re_w = 16020) at x/D = 220, including average (continuous line), for 0.15% XG

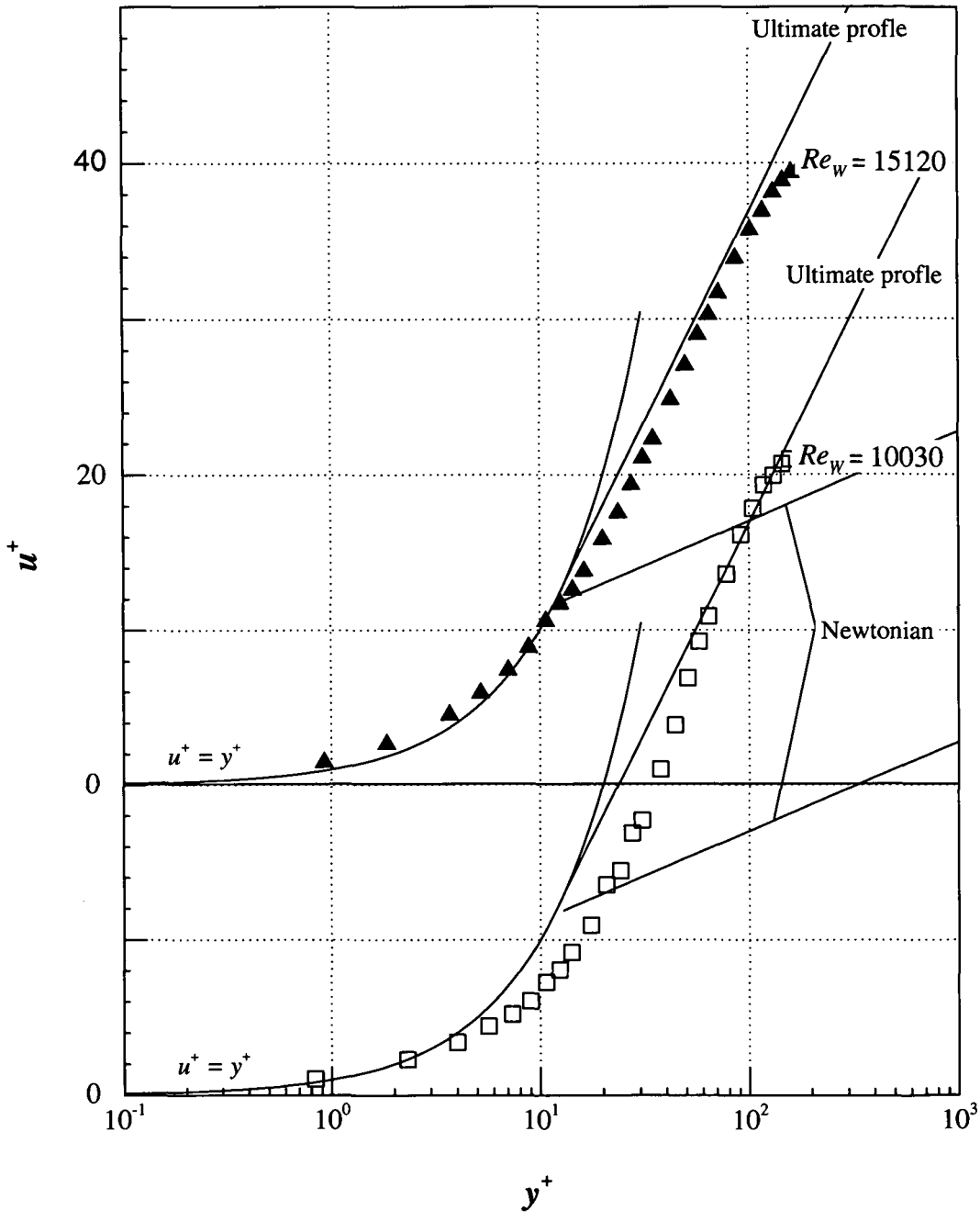

Figure 5.10 – Half horizontal (θ = 90°) velocity profiles in law-of-the-wall coordinates for two different Reynolds numbers within turbulent regime at x/D = 220, for 0.03% PAA

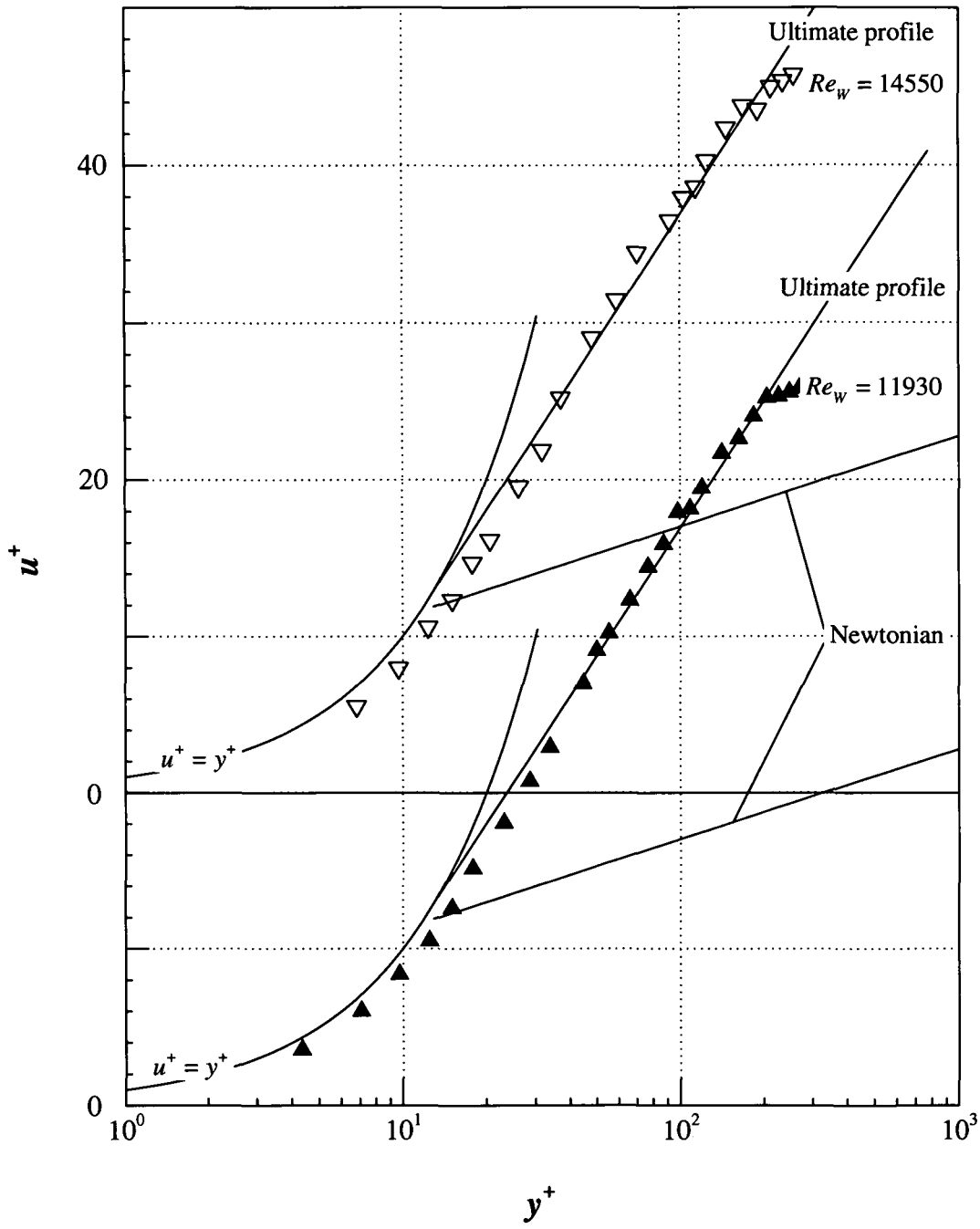

Figure 5.11 – Half horizontal (θ = 90°) velocity profiles in law-of-the-wall coordinates for two different Reynolds numbers within turbulent regime at x/D = 220, for 0.125% PAA

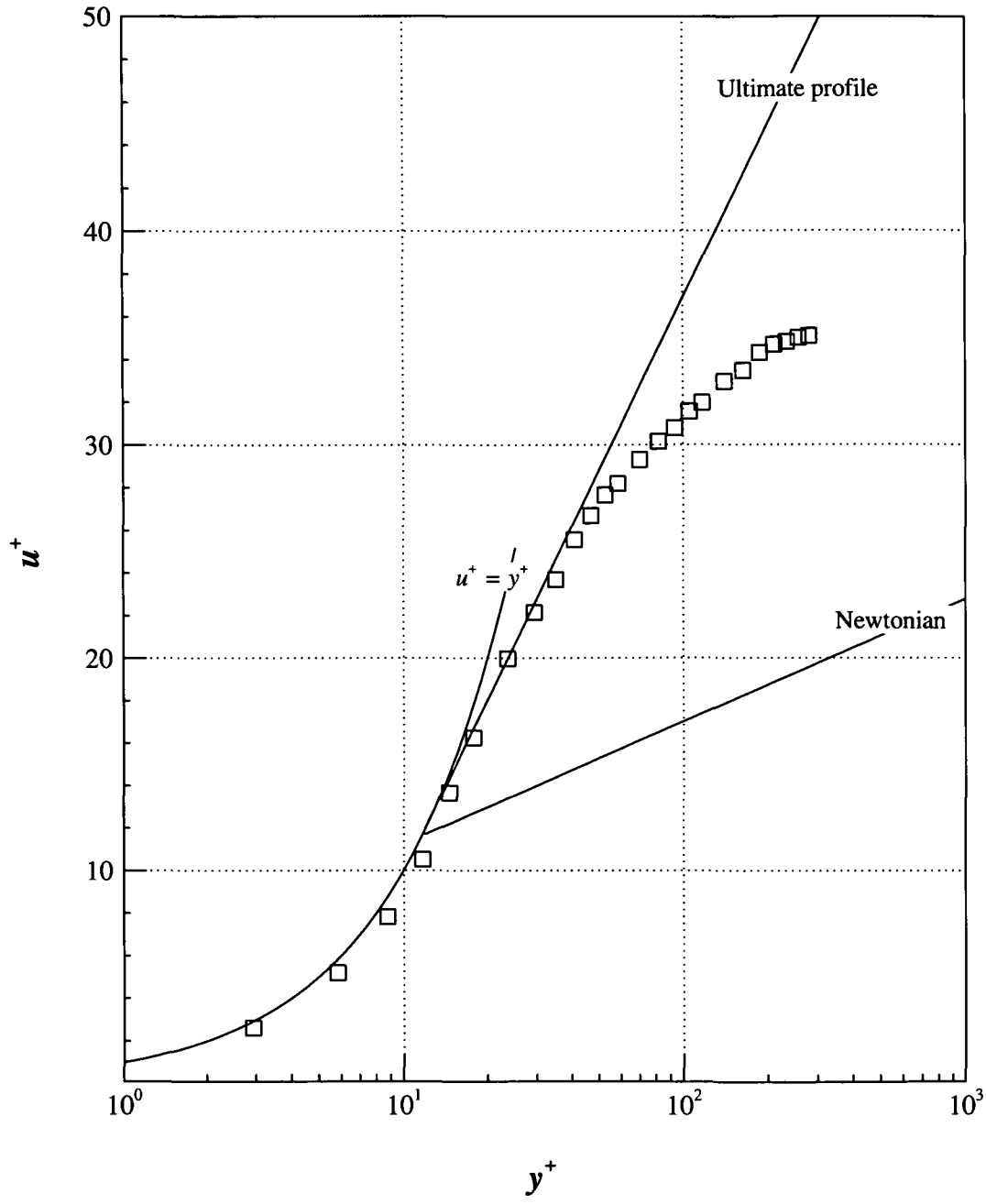

Figure 5.12 – Half horizontal (θ = 90°) velocity profile in law-of-the-wall coordinates within turbulent regime (Re_W = 16020) at x/D = 220, for 0.15% XG

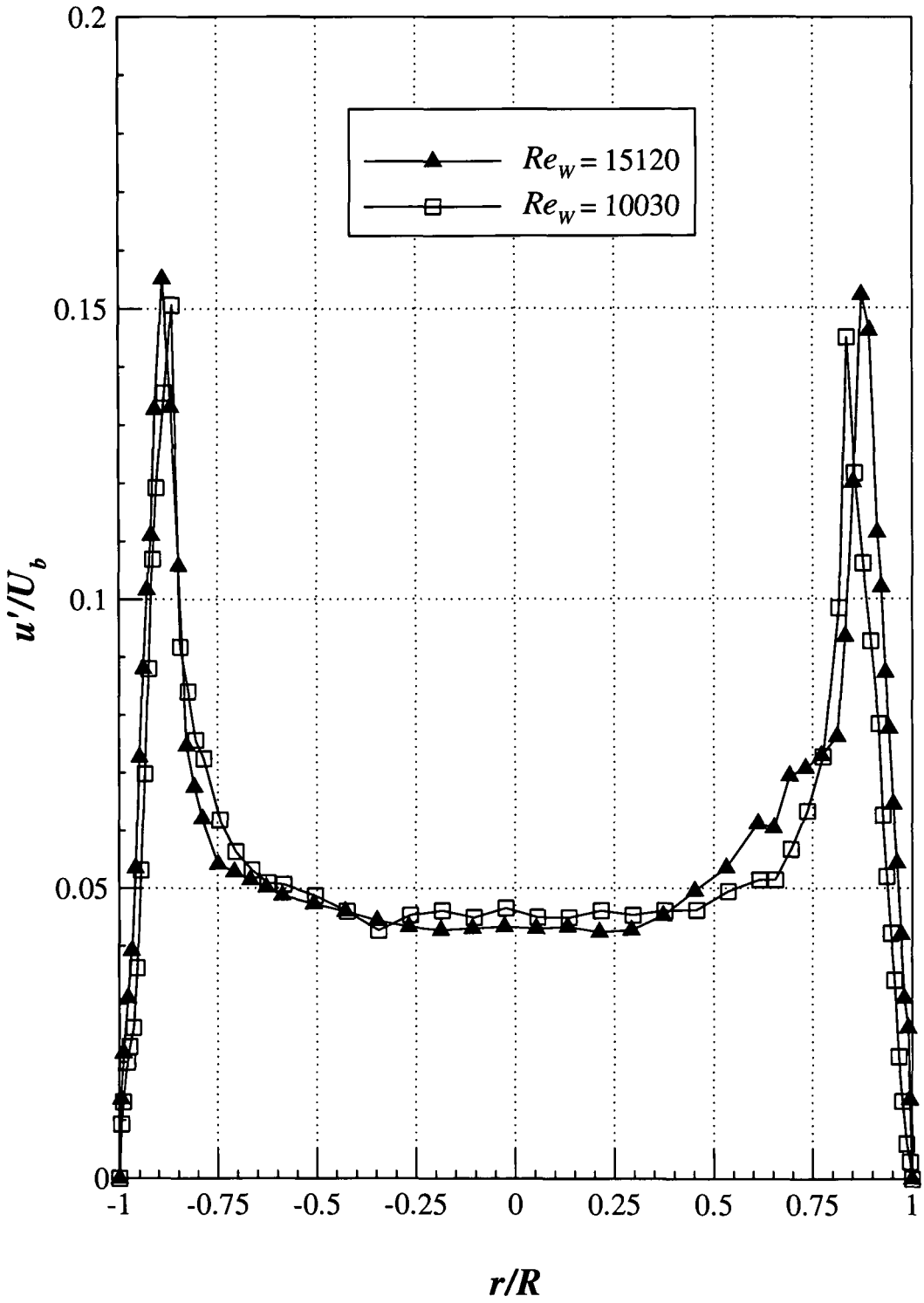

Figure 5.13 – Horizontal (θ = 90°, 270°) velocity fluctuations for two different Reynolds numbers within turbulent regime at x/D = 220, for 0.03% PAA

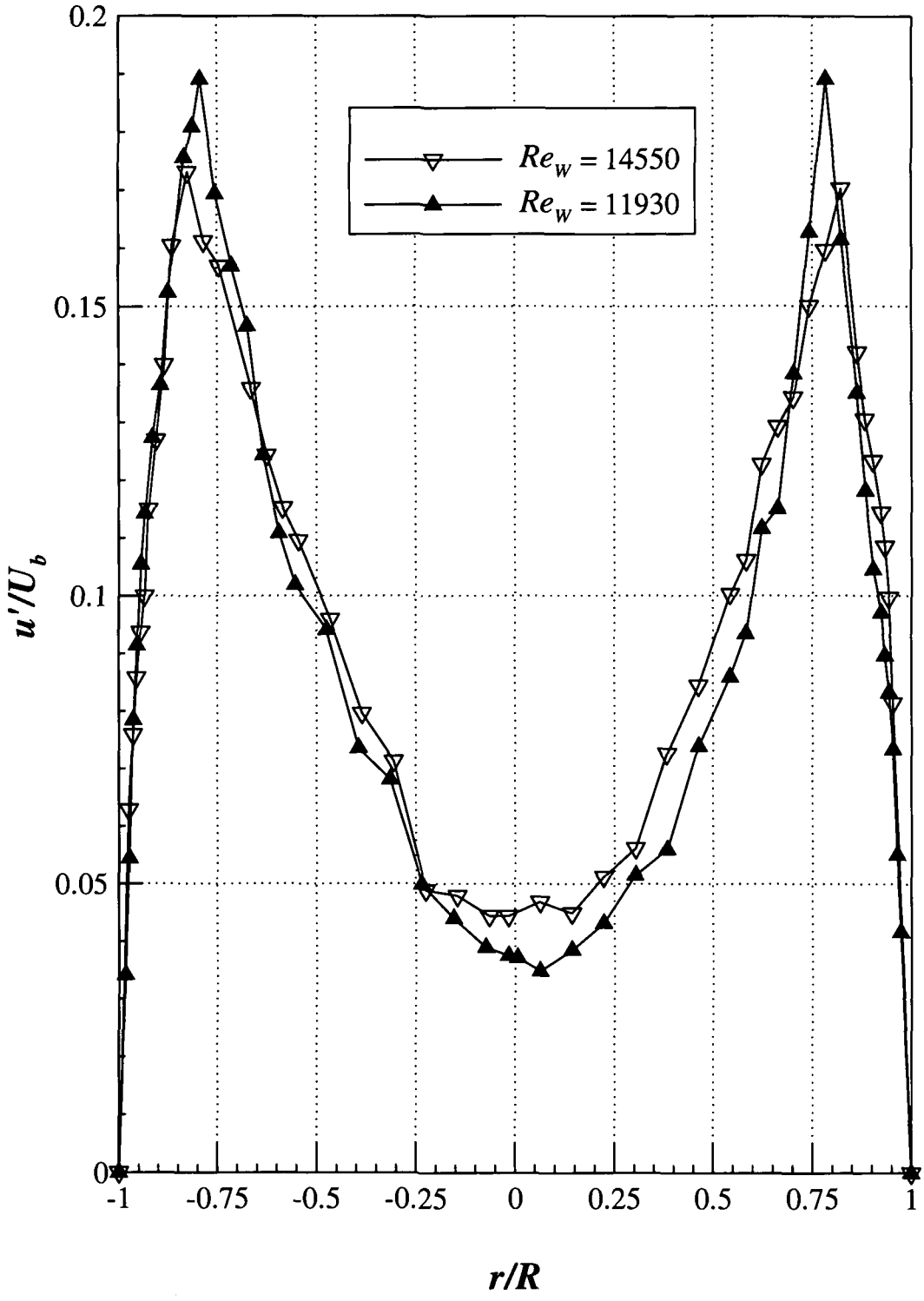

Figure 5.14 – Horizontal (θ = 90°, 270°) velocity fluctuations for two different Reynolds numbers within turbulent regime at x/D = 220, for 0.125% PAA

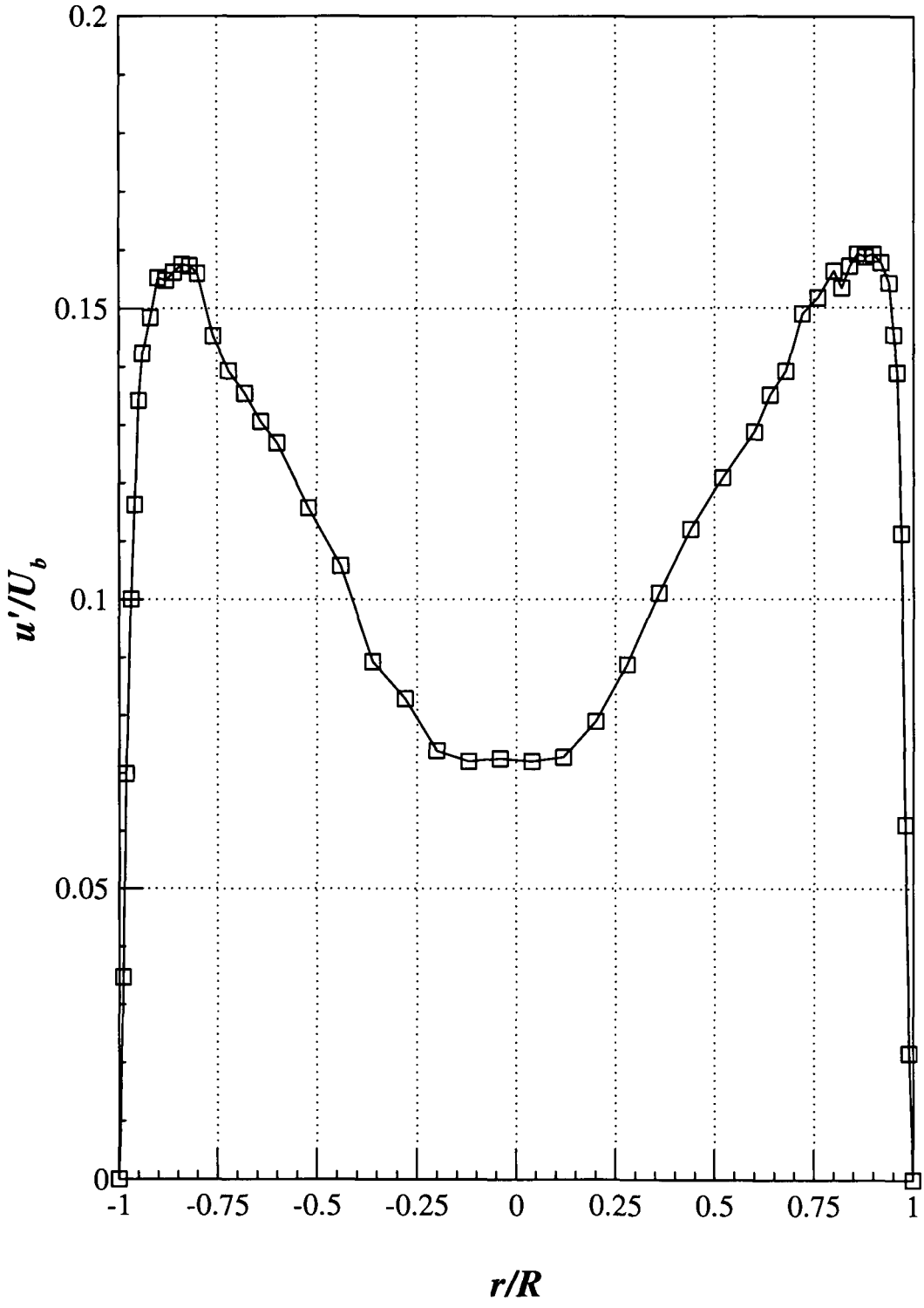

Figure 5.15 – Horizontal (θ = 90°, 270°) velocity fluctuations within turbulent regime (Re_w = 16020) at x/D = 220, for 0.15% XG

6 – Transitional flow

6.1 – Introduction

While the experiments carried out within the laminar and turbulent regimes are in good agreement with the literature, the experiments carried out under transitional-flow conditions resulted in significant new observations of the phenomenon first observed in Escudier and Presti (1996) and Peixinho et al (2005). In this chapter we present profiles of mean axial velocity and the associated turbulence intensity for different "cuts" through the flow field (corresponding to various azimuthal angles), at different axial locations along the pipe, for all liquids investigated within the transitional regime. We present the results for the Newtonian liquid (60% Gly) followed by the three non-Newtonian liquids investigated in the following order; 0.125% PAA, 0.03% PAA and 0.15% XG. This sequence of presenting the experimental results for the non-Newtonian liquids coincides with the sequence of the experiments and was chosen because the experiments carried out with the 0.125% PAA solution produced more detailed data.

6.2 – 60% Gly

The axial velocity profiles are shown in **Figure 6.1** for the horizontal plane (θ = 90°, 270°), 22 m downstream from the entrance (x/D = 220). The figure also includes the theoretical parabolic profile for fully-developed laminar flow and a "power-law" profile (White (1994)) for fully-turbulent flow (n = 1/7) for comparison As expected

from the literature (for example Patel and Head (1969)), with increasing Reynolds number the velocity profile progressively changes from the parabolic profile and becomes flatter towards the centre of the pipe with a resultant increase of the velocity gradient near the pipe wall.

That these velocity profiles are perfectly symmetric (α < 0.04%) can be seen in **Figure 6.2** which includes the average curves corresponding to the velocity data on both sides of the centreline. This observation is in agreement with the idea put forward in Draad and Nieuwstadt (1998) that, once inertia forces begin to play a role as in transitional flow conditions, the Rossby number (ratio of inertia to Coriolis forces) is the key dimensionless group to determine Coriolis effects and their influence is much diminished (as opposed to fully-developed laminar flow where inertia plays no role and the Ekman number is the relevant dimensionless group).

The corresponding axial velocity fluctuations are represented in **Figure 6.3**. For the lowest Reynolds number (Re = 2110) the maximum level of fluctuation is located in the centre of the pipe and is always less then 5% when normalised by U_b. The Reynolds number corresponds exactly to the onset of transition or the offset of laminar flow ((Re_1 = 2110) see **Figure 4.4**), thus the "turbulence intensity" (velocity fluctuation) remains at the same level as observed in the laminar flows which are essentially a consequence of noise in the LDA signal. It is also worth noting that, as $u = 2U_b$ on the centreline, when normalised by the local velocity u the fluctuation would be just 2.5%. For the higher Reynolds number the figure shows a peak value of u'/U_b in the region 0.75 < |r/R| < 0.95 and lower values in the centre of the pipe, behaviour typical of transitional flow and consistent with previous experimental

works (for example Pinho (1990) and Presti (2000)), which is characterised by higher levels of u'/U_b and closer to the centre of the pipe than for fully-turbulent flow.

In order to investigate in further detail the velocity distribution under transitional-flow conditions we have carried out measurements at five different axial locations along the pipe at Re = 2400 (i.e. only just within the transitional regime) and for each location both the vertical (θ = 0°, 180°) and the horizontal (θ = 90°, 270°) planes were measured. The velocity profiles as they evolve along the pipe, from x/D = 15 until x/D = 220, shown in **Figures 6.4** and **6.5** for the horizontal and the vertical planes respectively, again indicate a high level of symmetry and similar profile shapes of both "cuts" through the flow field. An exception is the vertical profile at x/D = 65 which is slightly asymmetric ($|\alpha|$ = 1.9 %) but still lower than the reference level of 2% (within the uncertainly of the results).

At a finite axial distance from the entrance of a duct with constant cross-sectional area, called the "entrance length" (L_e), the axial velocity no longer changes with the axial distance x and is said to be fully developed. Downstream of $x = L_e$ the velocity profile is constant, the wall shear stress constant and the pressure drops linearly with the distance x. This entrance length is given by:

Laminar (Durst et al (2005)), $$\frac{L_e}{D} \approx \left[0.619^{1.6} + (0.0567\,Re)^{1.6}\right]^{1/1.6} \qquad (6.1)$$

Turbulent (White 1994), $$\frac{L_e}{D} \approx 4.4\,Re^{1/6} \qquad (6.2)$$

From the evolution of the velocity profiles in **Figures 6.4** and **6.5** it can be concluded that the entrance effect can essentially be neglected after x/D = 160 which is in agreement with Equation 6.1: with Re = 2400 the predicted normalised entrance length L_e / D is 136.

6.3 – 0.125% PAA

Figure 6.6 shows the horizontal axial velocity profiles at x/D = 220 for different Reynolds numbers within the transitional flow regime for 0.125% PAA, including the averages of the velocity data on both sides of the centreline. The figure indicates that the velocity profiles initially exhibit an increasing degree of asymmetry with increasing Reynolds number until returning to symmetry at the highest Reynolds numbers. These asymmetries can also be observed in **Figure 6.7** which represents the velocity profiles in law-of-the-wall coordinates for both sides of the centreline of the pipe, where the experimental velocity data for the two sides of the centreline ($r/R < 0$ and $r/R > 0$) do not agree except for the highest Reynolds numbers.

As shown in Chapter 5, for laminar and turbulent flows the velocity profiles for the 0.125% PAA solution are symmetric (see **Figures 5.5** for the laminar data and **5.13** for the turbulent data). Plotting the data of all three flow regimes in a single figure (**Figure 6.8**) we easily conclude that as the Reynolds number increases from laminar conditions, a progressive asymmetry develops under transitional flow and a return to symmetric flow is observed at turbulent flow, in agreement with previous observations by Escudier and Presti (1996), Peixinho et al (2005), Escudier et al

(2005) and Esmael and Nouar (2008). These asymmetries have not yet been explained and the reason why they appear in transitional flow is not yet understood, therefore this work aims to study in detail these asymmetries.

In **Figure 6.9** the axial velocity fluctuations in the horizontal plane are plotted for different Reynolds numbers at x/D = 220, showing that much as for the mean axial velocity the associated velocity fluctuations, normalised by the bulk velocity U_b, also exhibit asymmetry within the transitional flow regime, which was not seen for turbulent flow (see the highest Re_W data in this figure and **Figure 5.16**). For Re_W = 8390, 10140 and 11270 they are clearly asymmetric (differences in peak values of up to 23%) and for the highest Reynolds number (Re_W = 11560) the velocity fluctuation profile returns to symmetric, following the same evolution as that observed for the mean axial velocity profiles. However, if we normalise the velocity fluctuations by the local velocity u (see **Figure 6.10**) this link is no longer evident. For Re_W = 10140 the highest peak value is even shifted to the opposite side of the centreline. Therefore, care should be taken when interpreting the fluctuation data, as a consequence in what follows we include figures showing both normalisations.

Figure 6.11 shows the axial velocity profiles at the same axial position of the pipe flow (x/D = 220), for different Reynolds numbers under transitional-flow conditions, but for a different azimuthal "cut" than the horizontal plane, in this case for the plane corresponding to an angle of 45° (and 225°). From **Figures 6.6** and **6.11** it is evident that the most asymmetric velocity profile (with the highest degree of asymmetry) is

observed for Re_W = 10140. It is also evident that the degree of asymmetry varies with the azimuthal angle, considering the same Reynolds number of 10140, the velocity profile for θ = 45° (and 225°) is more asymmetric than for θ = 90° (and 270°). This figure also highlights the danger of assuming axisymmetry based on measurements in a single plane; for example, for Re_W = 11560 in **Figure 6.6** (horizontal plane) the flow appears to be almost axisymmetric, however from **Figure 6.11** (45° plane) it is clear that it is not.

To highlight the three-dimensional structure of the flow we have plotted the radial distributions of the mean axial velocity for various azimuthal angles θ in **Figures 6.12**, **6.13** and **6.14**, for three Reynolds numbers, 6710, 10140 and 11560, respectively, all within transitional-flow conditions at x/D = 220. For all three Reynolds numbers, the "peak" velocity is shifted to the upper right quadrant of the pipe (i.e. between 0° and 90°), with a corresponding maximum negative shift in the velocity profile in the bottom left quadrant (i.e. between 180° and 270°). This variation of the coefficient of asymmetry with the azimuthal angle is represented in **Figure 6.15**. The degree of asymmetry varies in a similar manner for all Reynolds numbers and also varies smoothly with the azimuthal angle - with the profiles at 135° and 315° being practically symmetric - and the asymmetry greatest at approximately 45° and 225°.

In **Figures 6.16** to **6.19**, each figure corresponding to one of four different axial locations, the axial velocity profiles for different azimuthal angles at Re_W = 10140 are shown. This Reynolds number was chosen because it is the "most transitional", with the highest degree of asymmetry. The farthest upstream location (near the

entrance) x/D = 15 (**Figure 6.16**), exhibits a deficit in the velocity profiles detected in the centre of the pipe. This deficit was not seen for the Newtonian case (60% Gly) and must be a direct consequence of the disc within the plenum chamber immediately upstream of the inlet to the test section. At this concentration PAA is highly elastic and so this deficit is essentially a "memory" effect of the fluid. As we move downstream and the flow develops this effect disappears (see **Figures 6.17**, **6.18** and **6.19**). The velocity profiles become progressively more "parabolic", with higher values of u/U_b at the centreline of the pipe and a clear increase of asymmetry appears after $x/D > 160$.

The evolution of the velocity profiles along the pipe at Re_W = 10140 is shown in **Figures 6.20**, **6.21** and **6.22**, for θ = 90° (270°), θ = 0° (180°) and θ = 45° (225°), respectively. The profiles from the entrance until x/D = 160 are far from an idealized "developed" profile. From Equation 6.1 with Re_W = 4480 (offset of laminar flow or onset of transition (**Table 4.2**)), L_e/D = 254. However, the flow is not laminar but transitional and the liquid is not Newtonian, therefore Equation 6.1 can give just a rough guide. Using Equation 6.2, which is for turbulent flow of Newtonian fluids, with Re_W = 11930 (offset of transition or onset of turbulent flow (**Table 4.2**)) the entrance length is an order-of-magnitude shorter, L_e/D = 21. Nevertheless, as **Figure 6.23** shows, from the entrance until x/D = 160 the flow is not strongly asymmetric and slight asymmetries vary with the azimuthal angle in a different way than for axial locations greater than x/D = 160. Therefore, the asymmetry is not a consequence of the entrance conditions. From x/D = 160 to x/D = 220 the velocity

profiles only change so far as the magnitude of the asymmetry is concerned with the maximum α coefficient increasing up to 20%.

So to reiterate it appears that the velocity profiles although initially complex, due to a combination of the disc in the plenum chamber and the fluid's viscoelasticity, develop approximately axisymmetrically before the asymmetry manifests at some downstream location (for Re_W = 10140, x/D > 160).

6.4 – 0.03% PAA

In order to evaluate how the shear-thinning behaviour affects the velocity profile asymmetry we have carried out a series of experiments using the same polymer (PAA) but with a different concentration (0.03%), which has a much lower degree of shear-thinning. Although much lower in concentration it is well known that at this concentration level this fluid is still an excellent "drag reducer" in turbulent flow, confirmed by our friction factor data shown in **Figure 4.2**. The experiments were conducted in a way that would make it possible to compare the experimental results under similar situations for the higher concentration, i.e. for the same azimuthal angles and for the same axial locations along the pipe.

The axial velocity profile in the horizontal plane for the 0.03% PAA solution in the transitional regime (Re_W = 5780), 22 m downstream of the entrance (x/D = 220) is shown in **Figure 6.24**, which is asymmetric ($|\alpha|$ = 5.2%). As much as for the 0.125% PAA solution discussed in the previous sub-section, from the associated

velocity fluctuations normalised by U_b (**Figure 6.25**) it could be concluded that they also exhibit an asymmetric profile, but when normalised by the local velocity (u) the velocity fluctuations are basically symmetric (see **Figure 6.26**).

To see the evolution of the degree of asymmetry with Reynolds number we plot the axial velocity data for the three regimes in **Figure 6.27**. Again, as the Reynolds number increases form laminar to transition the velocity profile asymmetry increases and then when fully-turbulent flow is reached the velocity profile returns to symmetry.

Figure 6.28 shows the axial velocity profiles for different azimuthal angles at Re_W = 5780 (transition) with the corresponding coefficients of asymmetry displayed in **Figure 6.29**, which include data for the higher PAA concentration for comparison. The figure represents the asymmetry associated with the Reynolds numbers that exhibits the highest degree of asymmetry, 5780 for 0.03% PAA and 10140 for 0.125% PAA, at the same axial location x/D = 220. The asymmetry of the velocity profiles for the 0.03% PAA solution follow the same pattern as for the 0.125% PAA solution with the higher asymmetries in the region around 45° (and 225°), and being practically symmetric at 135° (and 315°). The 0.03% PAA solution presents lower values of asymmetry, suggesting that the asymmetry is shear-thinning dependent and increases with shear-thinning. However the elasticity also differs with PAA concentration and therefore concluding that the degree of asymmetry is just shear-thinning dependent is not possible just from these data sets. In the next section we isolate the elasticity effect in order to evaluate its influence on the degree of asymmetry and, in so doing, confirm the shear-thinning dependence.

The axial velocity profile evolution along the pipe at Re_W = 5780 is shown in **Figures 6.30** and **6.31** for the horizontal and vertical planes, respectively. The velocity profiles "develop" earlier then for the 0.125% concentration, at *x/D* = 160 the profiles are not yet "developed" for the 0.125% concentration, but for the 0.03% concentration they are already "developed", therefore the entrance length L_e is shorter for the 0.03% PAA. Close to the entrance at *x/D* = 15, the velocity profile exhibits a defect in the centre of the pipe smaller than for the 0.125% PAA solution which was attributed to the disc shape within the plenum chamber and elasticity, but not seen for the Newtonian liquid (60% Gly).

Figure 6.32 shows the asymmetry coefficient *versus* angle for different locations along the pipe flow at Re_W = 5670, for the 0.03% PAA solution. As was also observed for the 0.125% PAA solution, from the entrance until a certain axial location (*x/D* > 65) the velocity profiles are essentially symmetric ($\alpha < 2\%$), but from that location downstream the degree of asymmetry suddenly increases following the same "pattern" of asymmetry in agreement with the work of Esmael and Nouar (2008). An exception to this "pattern" is the evolution observed for *x/D* = 65 which inexplicably exhibits a consistent asymmetry in the "opposite" sense, but with values of α lower than 3% (essentially symmetric when compared with downstream locations).

6.5 – 0.15% XG

A series of steady-shear tests with xanthan gum were performed in an attempt to select a concentration with a viscometric flow curve "matching" as far as possible the data for the 0.125% PAA solution, this was found to be a concentration of about 0.15%. By doing so we were attempting to isolate elastic from shear-thinning effects, by comparing the experimental results obtained with two non-Newtonian liquids with similar shear-thinning behaviour but with very different elastic characteristics.

According to Barnes et al (1989) a recoverable shear (i.e. $N_1 / 2\tau_w$) greater than 0.5 indicates a highly elastic state. This condition is represented in **Table 6.1** for different Reynolds numbers for the 0.125% PAA solution, from where we conclude that 0.125% PAA is highly elastic. The data of N_1 as a function of the wall shear stress τ_w was obtained from the power-law fit displayed in **Figures 2.5**. As already mentioned in Chapter 2, for the 0.03% PAA and 0.15% XG solutions it was not possible to obtain values of N_1 because the values produced were below the resolution of the rheometer even at the highest shear stresses.

The velocity profile and associated velocity fluctuations in the horizontal plane for Reynolds numbers within the transitional-flow regime (Re_w = 10260) at x/D = 220, are shown in **Figures 6.33** and **6.34**, respectively. As observed for the 0.125% PAA solution, the mean velocity profile is also strongly asymmetric under transitional-flow conditions. Looking to the velocity fluctuations, despite the asymmetry observed when the velocity fluctuations are normalised by the bulk velocity (**Figure 6.34**), it is clear that, when normalised by the local velocity (**Figures 6.35**),

the velocity fluctuations exhibit a different profile, and in this case the peak value is shifted to the other side of the centreline.

Figure 6.36 shows that for the 0.15% XG solution the asymmetry varies with the azimuthal angle in a similar manner as for the PAA solutions, with higher asymmetry in the region around 45° (225°). This can be more easily discerned from **Figure 6.37**, which compares the coefficient of asymmetry between all three non-Newtonian liquids investigated, each one for a different Reynolds number corresponding to the most transitional flow, with the highest degree of asymmetry in each. That the much more elastic behaviour of 0.125% PAA produces essentially the same degree of asymmetry as 0.15% XG is a strong indication that elasticity is not the underlying cause for the asymmetry.

The evolution of the velocity profiles along the pipe, represented in **Figures 6.38** to **6.40** show that the profiles remain symmetric until somewhere between 6.5 m and 16 m downstream of the entrance (between x/D = 65 and x/D = 160) and then the asymmetry suddenly increases with axial distance, as observed for the other polymer solutions investigated.

6.6 - Conclusions

The main conclusion of this chapter is that the mean axial velocity profiles of non-Newtonian liquids are asymmetric under transitional-flow conditions but axisymmetric for Newtonian liquids. As the Reynolds number increases from the

laminar flow region entering the transitional regime the velocity profile asymmetry progressively increases and then as the flow leaves the transitional regime approaching fully-turbulent flow conditions, the asymmetry progressively decreases. In fully-turbulent flow the profiles are again axisymmetric.

The coefficient of asymmetry varies with the azimuthal angle for all non-Newtonian liquids investigated with the same "pattern" of asymmetry (greatest α at 45° and practically symmetric at 135°). It is possible to draw iso-(u/U_b) lines at each axial location studied, as done in **Figure 6.41** for 0.125% PAA at *x/D* = 220 (most asymmetric flow). The result of this procedure clearly shows the regions where the flow is faster, shifted from the centre of the pipe to the right quadrant of the pipe. Plotting the same data using iso-($(u-u_m)/U_b$) lines (**Figure 6.42**) we can observe the two modulated vortices identified by Esmael and Nouar (2008).

The degree of asymmetry depends on the polymer concentration, 0.125% PAA presents higher degree of asymmetry than 0.03% PAA, but does not depend on the elasticity of the flow, 0.125% PAA and 0.15% XG have similar viscosity yet drastically different elasticity but exhibit the same degree of asymmetry.

Observing the evolution along the pipe of the velocity profile, for all three non-Newtonian liquids investigated, it can be concluded that form the entrance until a certain axial location (*x/D* > 65) the velocity profile is essentially axisymmetric but once this entrance length is achieved the asymmetry suddenly appears.

So far we have observed the asymmetry, and its evolution with the angle and axial location, but have not been able to identify the cause of the asymmetry. In the next chapter we will present the experimental results obtained after making some modifications to the upstream and downstream geometry of the pipe facility. Our aim there is to be able to study the influence of each particular change on the axial velocity profiles and with this hopefully better understand the mechanism which leads to this asymmetry in the transitional flow regime of non-Newtonian liquids.

Table 6.1 – Rheological and flow parameters for 0.125% PAA

Fluid	Re_w	τ_w Pa	$\dot{\gamma}_w$ 1/s	μ_w Pa.s	N_1* Pa	$N_1 / 2\tau_w$
0.125% PAA	4480	2.04	106	0.0193	25.5	6.25
	4980	2.11	114	0.0186	27.1	6.42
	5500	2.18	122	0.0179	28.7	6.57
	6070	2.26	131	0.0172	30.4	6.72
	6710	2.34	141	0.0166	32.3	6.89
	7310	2.43	152	0.016	34.3	7.06
	8390	2.65	181	0.0146	39.6	7.47
	9320	2.82	204	0.0138	43.8	7.76
	10140	2.91	217	0.0134	46.1	7.93
	10650	2.91	217	0.0134	46.1	7.93
	11270	2.92	218	0.0134	46.3	7.93
	11560	2.95	223	0.0132	47.2	8.01
	11930	3.01	230	0.013	48.5	8.06

* $N_1 = 7.41\tau_w^{1.69}$ (from **Figure 2.5**)

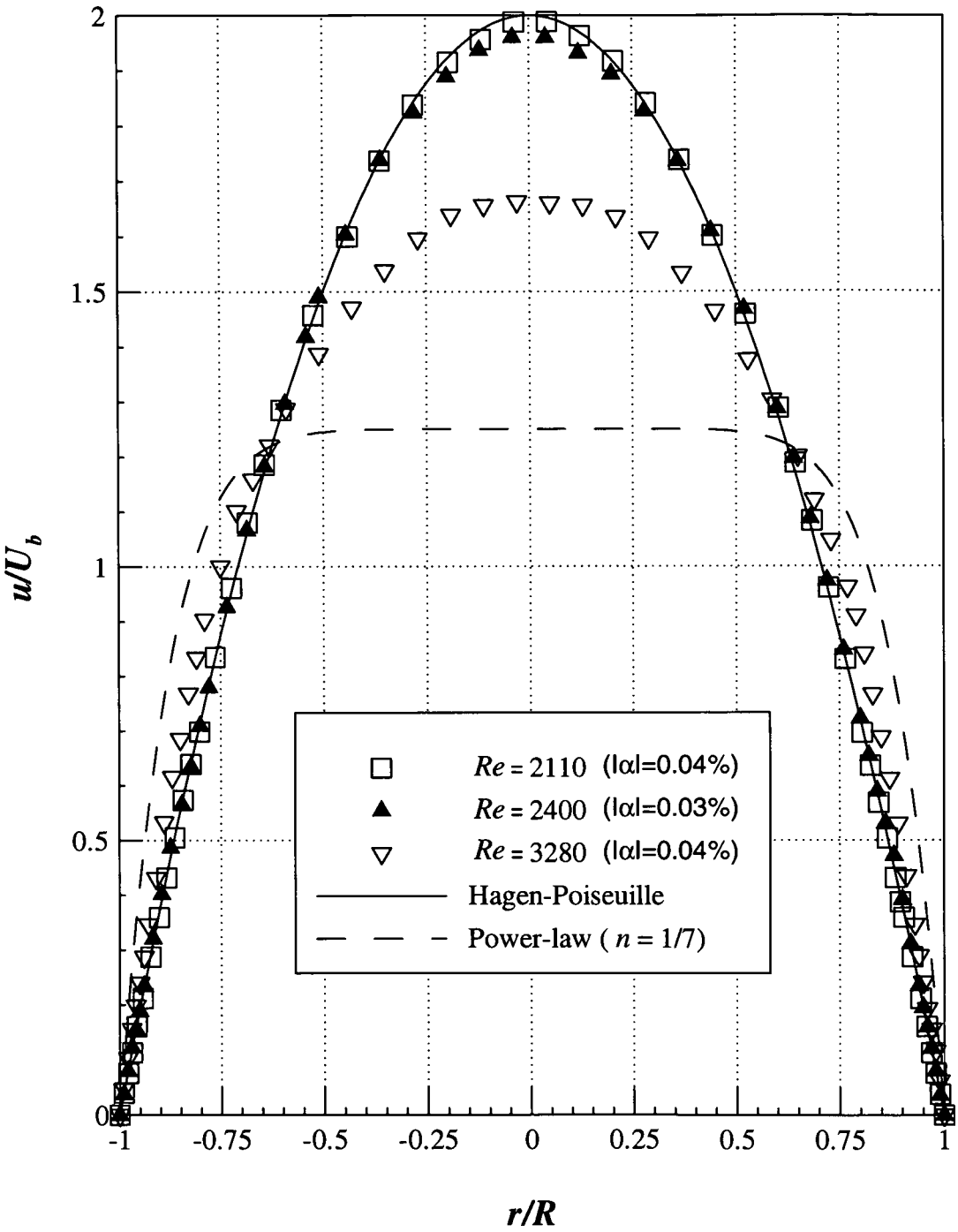

Figure 6.1 – Horizontal (θ = 90°, 270°) velocity profiles for three different Reynolds numbers within transitional regime at x/D = 220, including the Hagen-Poiseuille and the power-law profiles, for 60% Gly

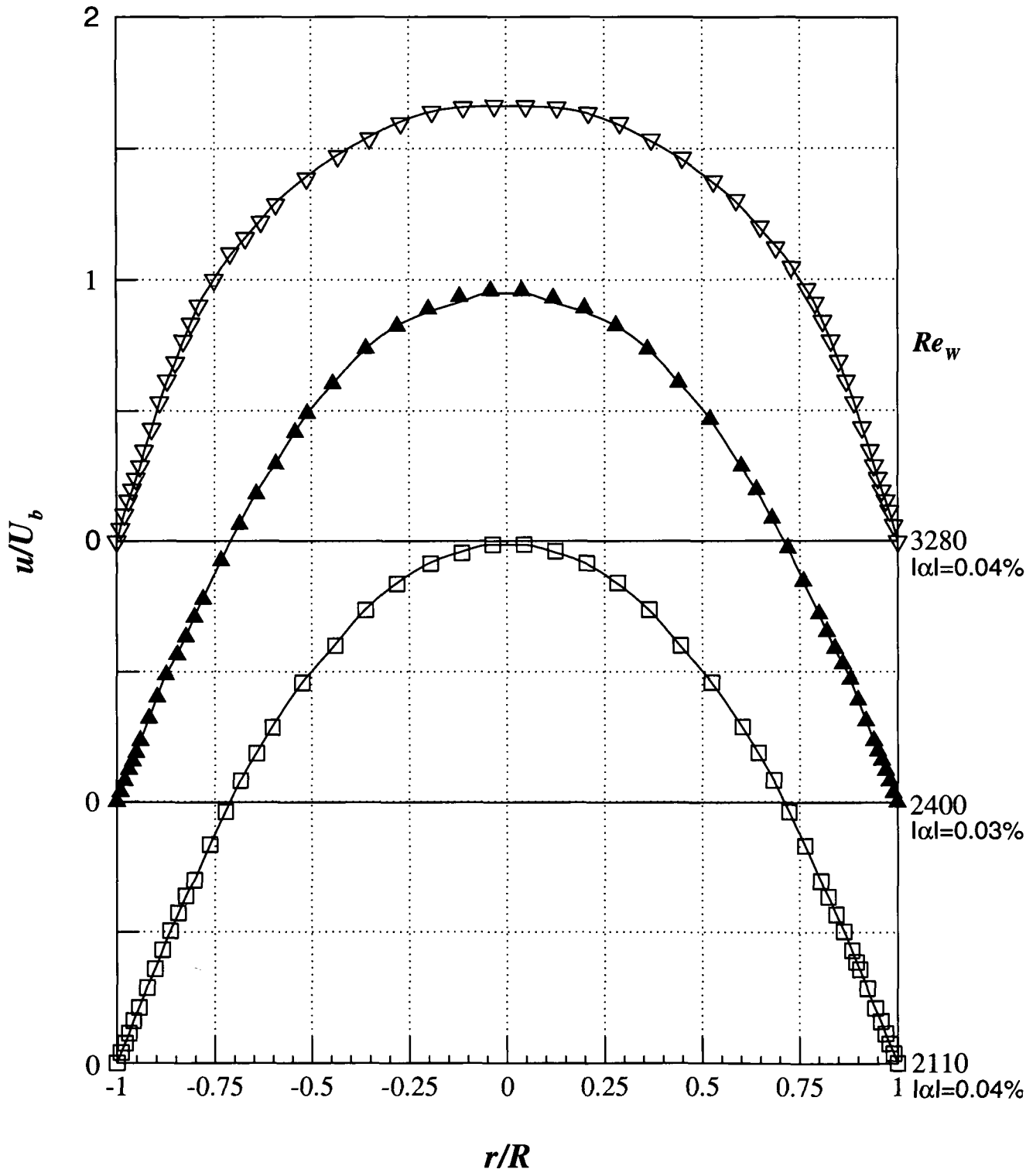

Figure 6.2 – Horizontal (θ = 90°, 270°) velocity profiles for three different Reynolds numbers within transitional regime at x/D = 220, including averages (continuous lines), for 60% Gly

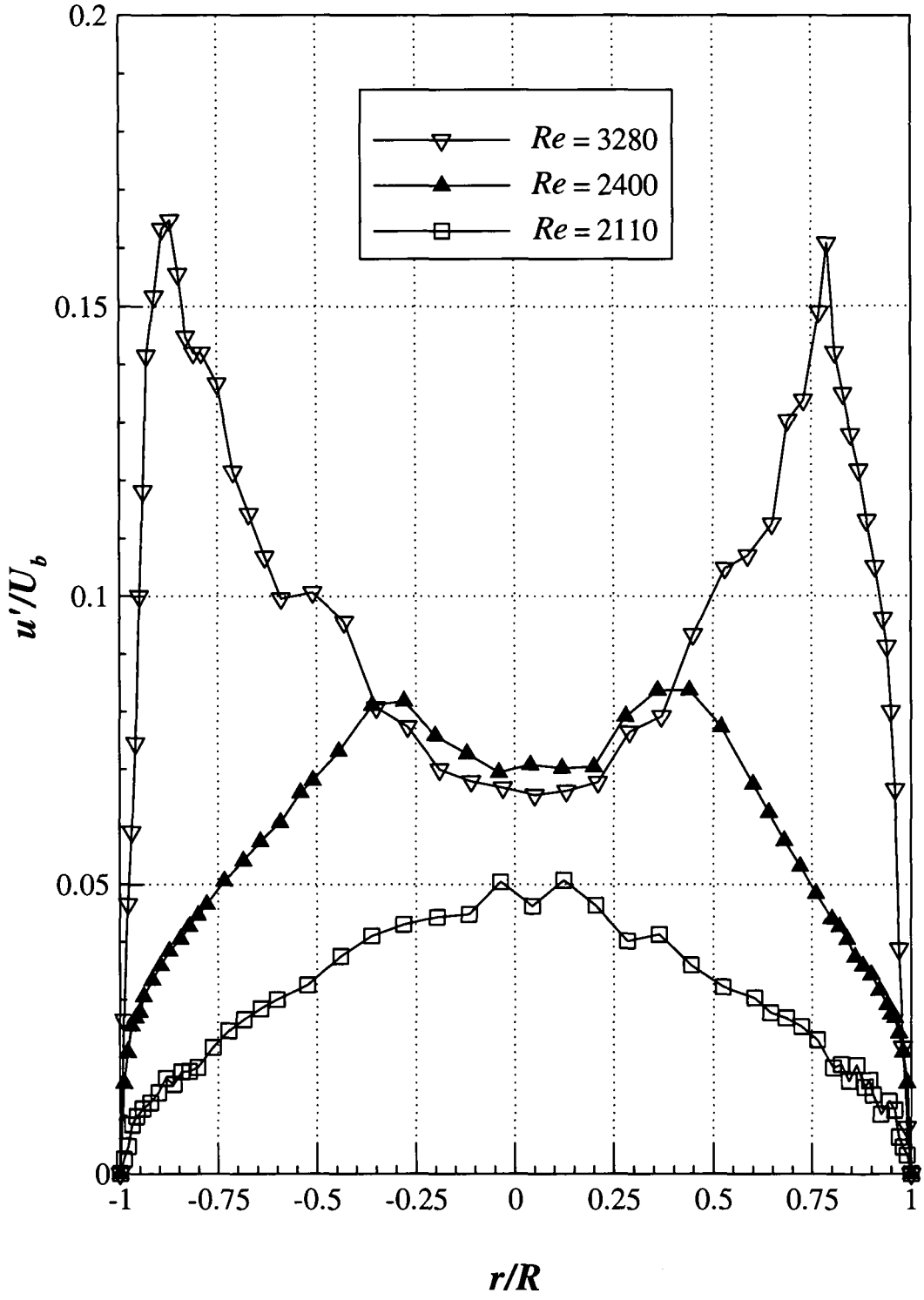

Figure 6.3 - Horizontal (θ = 90°, 270°) velocity fluctuations for three different Reynolds numbers within transitional regime at x/D = 220, for 60% Gly

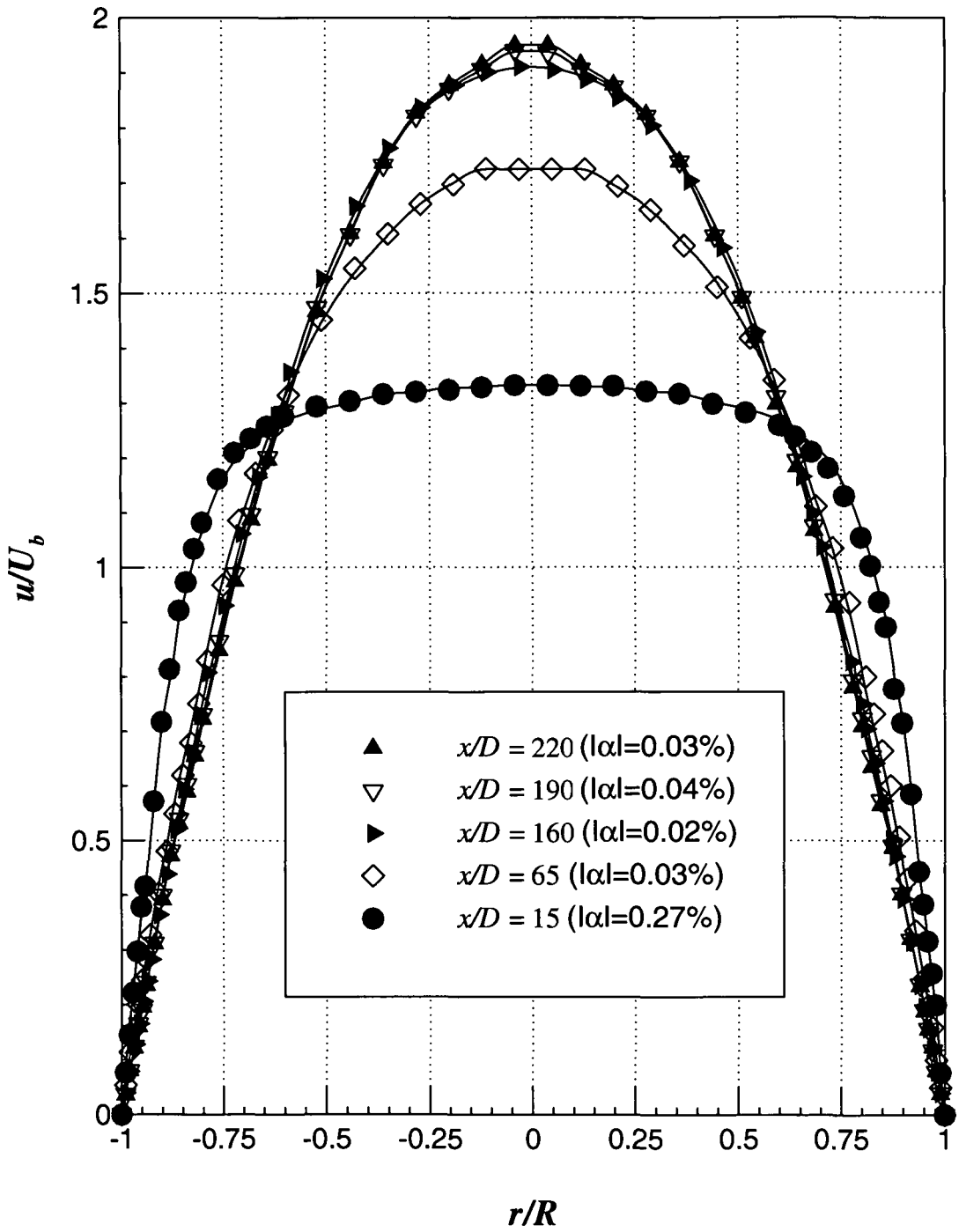

Figure 6.4 - Horizontal (θ = 90°, 270°) velocity profiles for different axial locations (x) at Re = 2400, including averages (continuous lines), for 60% Gly

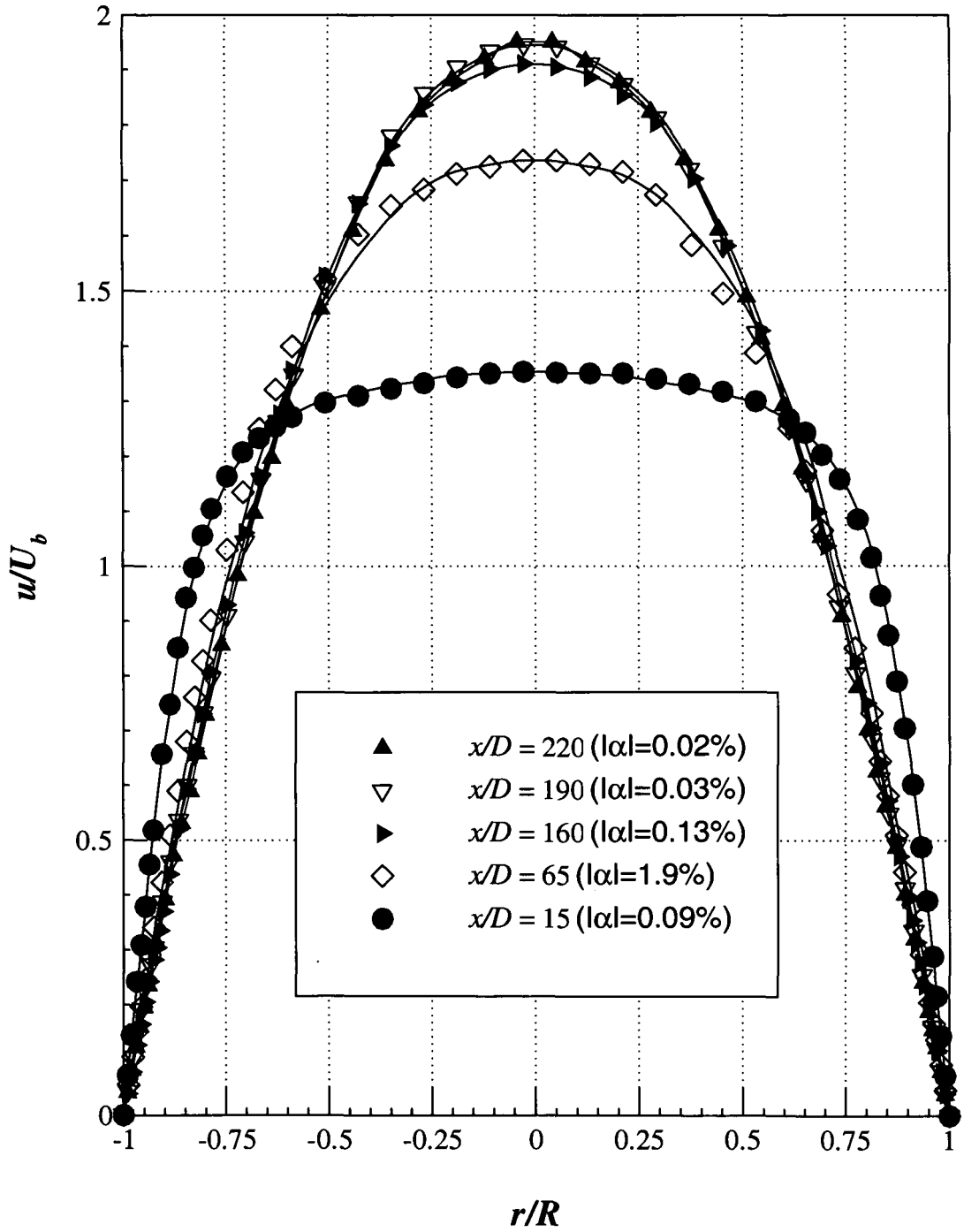

Figure 6.5 - Vertical (θ = 0°, 180°) velocity profiles for different axial locations (x) at Re = 2400, including averages (continuous lines), for 60% Gly

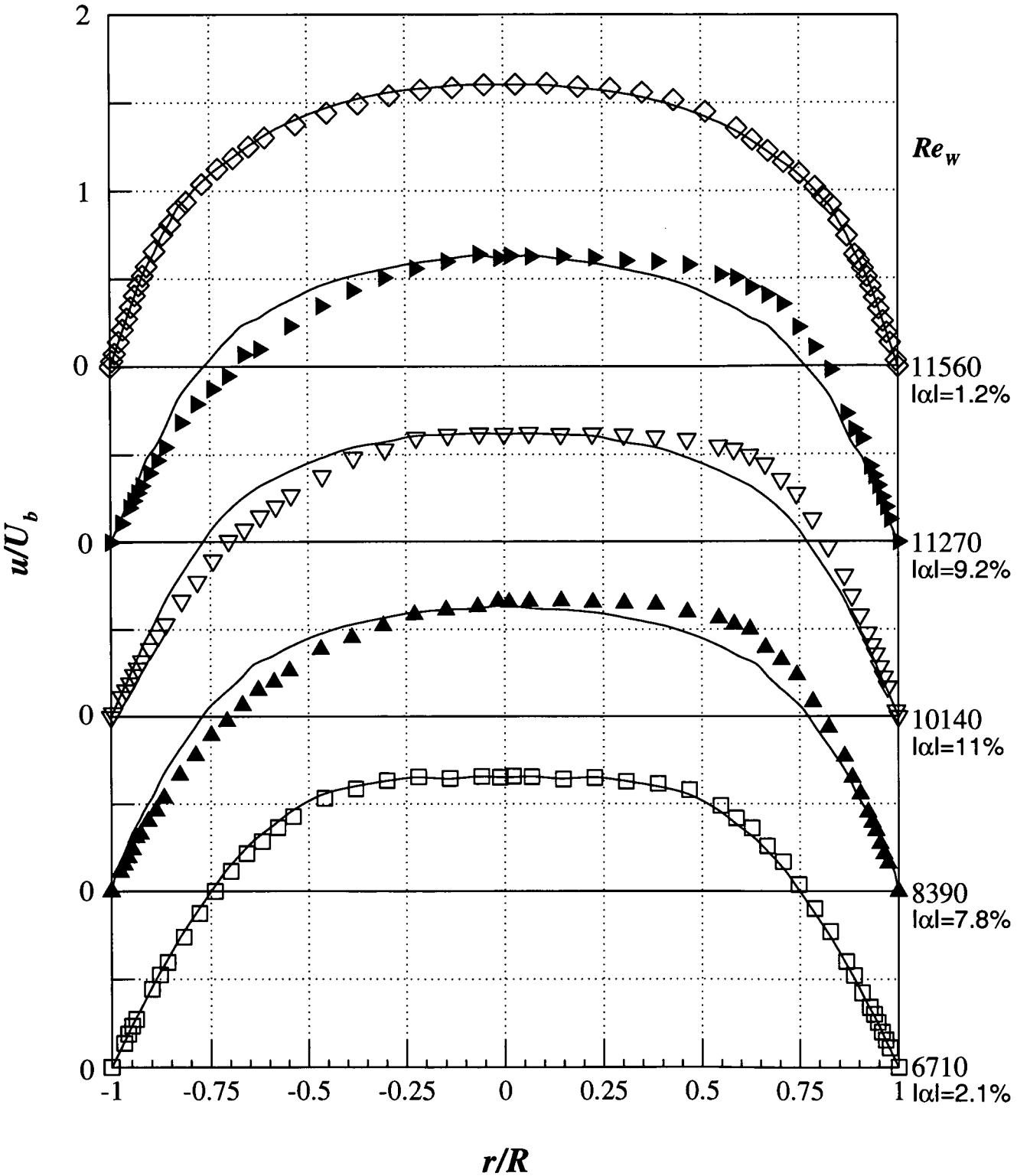

Figure 6.6 - Horizontal (θ = 90°, 270°) velocity profiles for different Reynolds numbers within transitional regime at x/D = 220, including averages (continuous lines), for 0.125% PAA

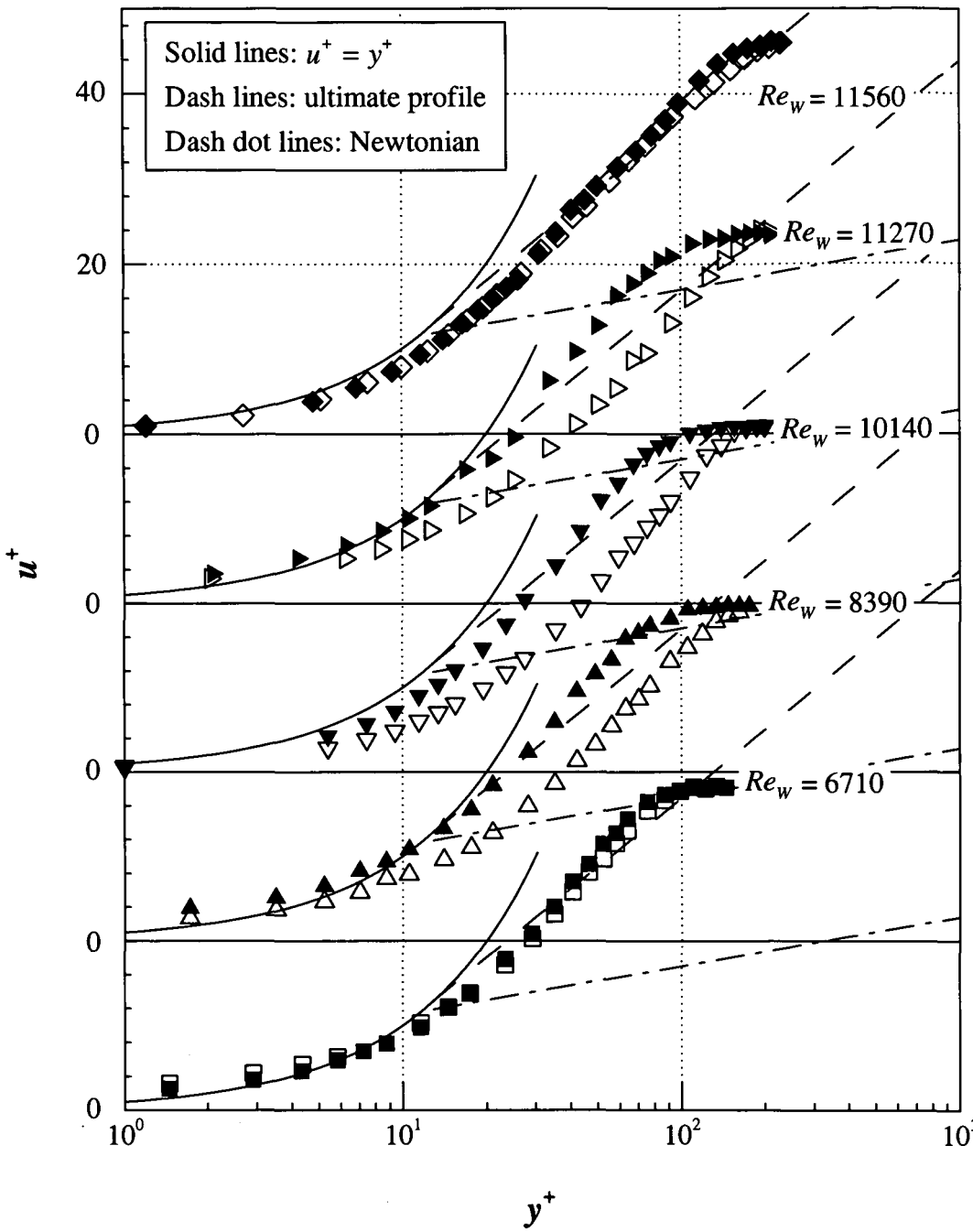

Figure 6.7 - Horizontal velocity profiles in law-of-the-wall coordinates (θ = 270°: open symbols; θ = 90°: filled symbols) for different Reynolds numbers within transitional regime at x/D = 220, for 0.125% PAA

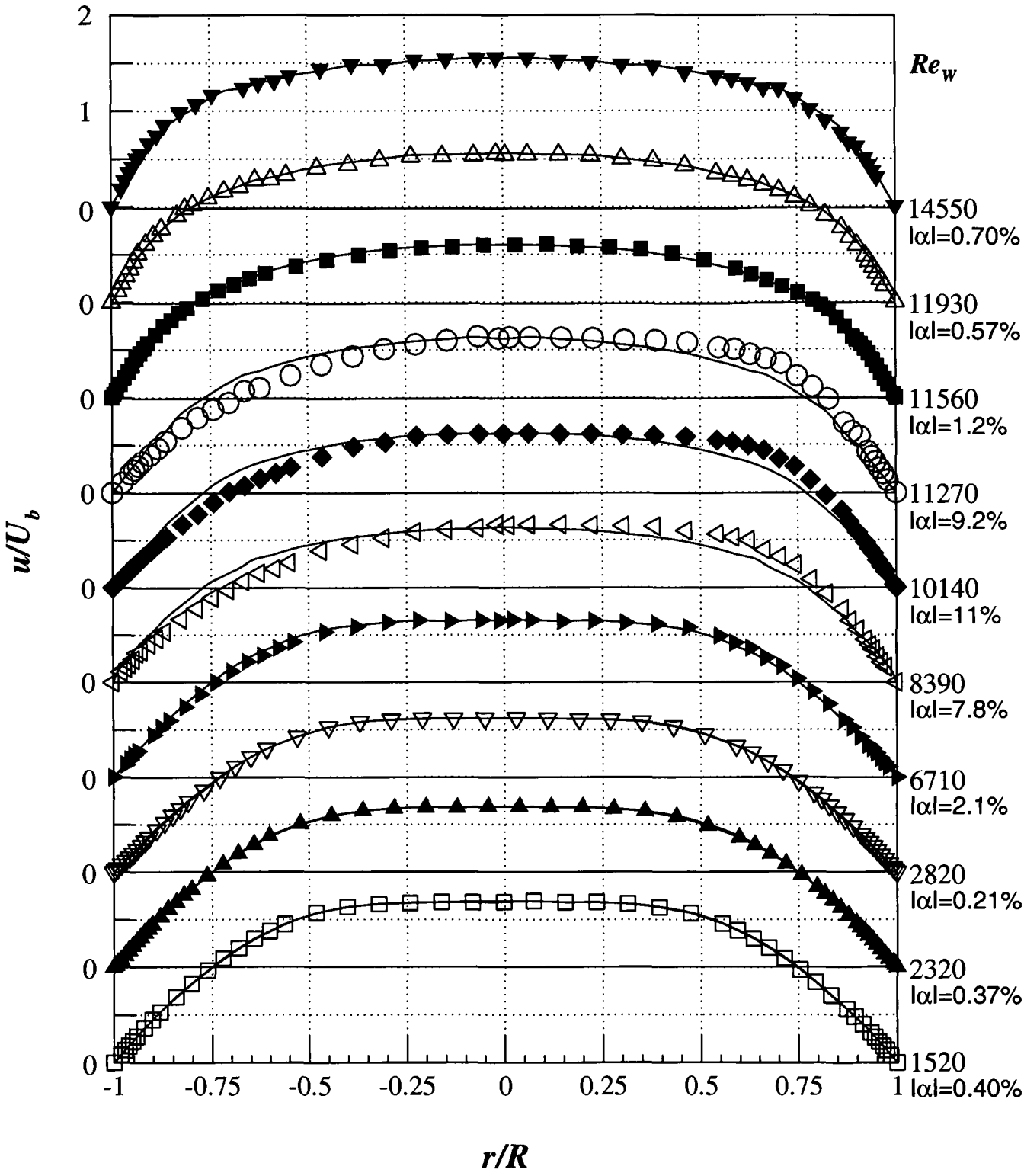

Figure 6.8 - Horizontal (θ = 90°, 270°) velocity profiles for different Reynolds numbers (all regimes) at x/D = 220, including averages (continuous lines), for 0.125% PAA

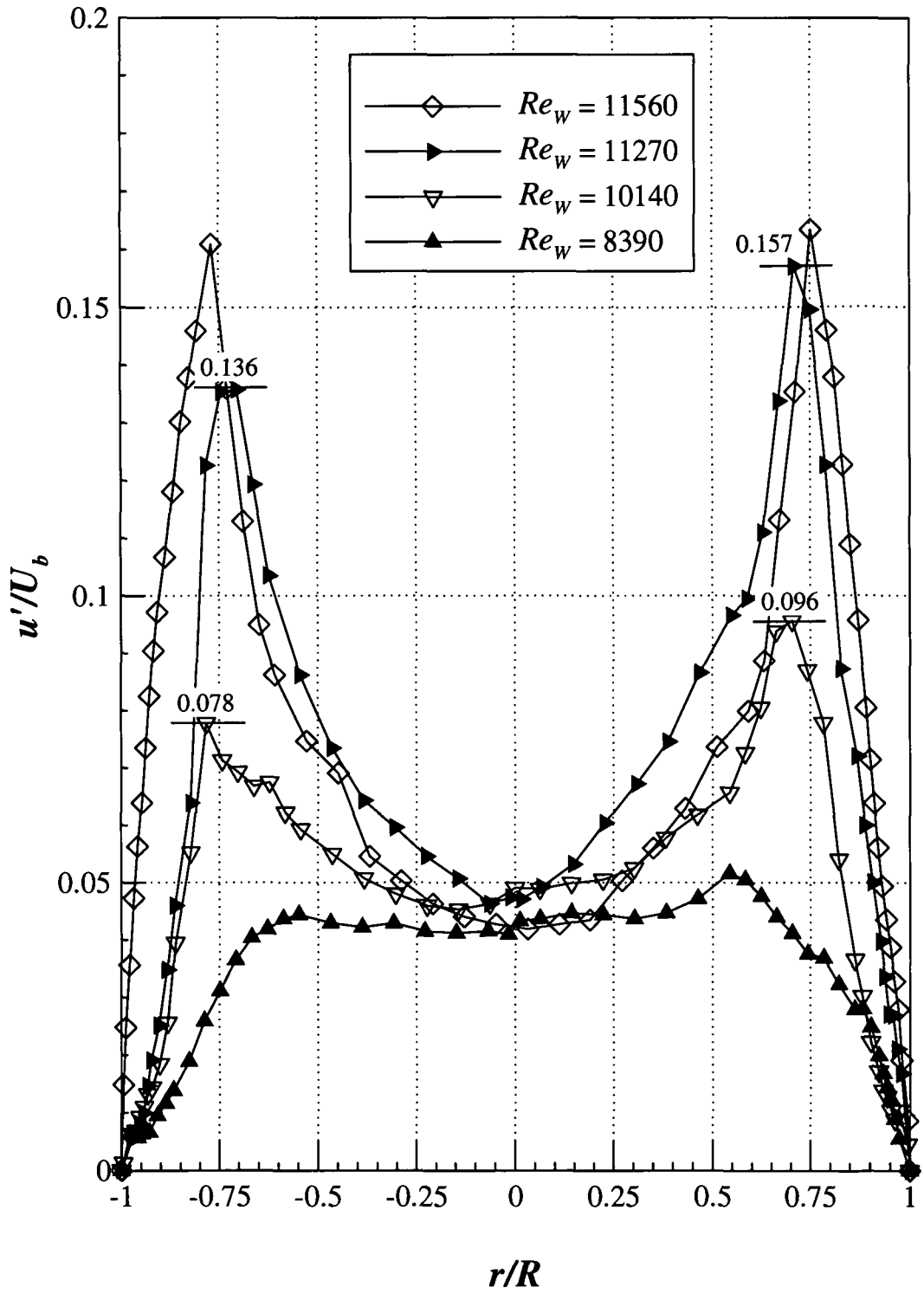

Figure 6.9 - Horizontal (θ = 90°, 270°) velocity fluctuations (u'/U_b) for different Reynolds numbers within transitional regime at x/D = 220, for 0.125% PAA

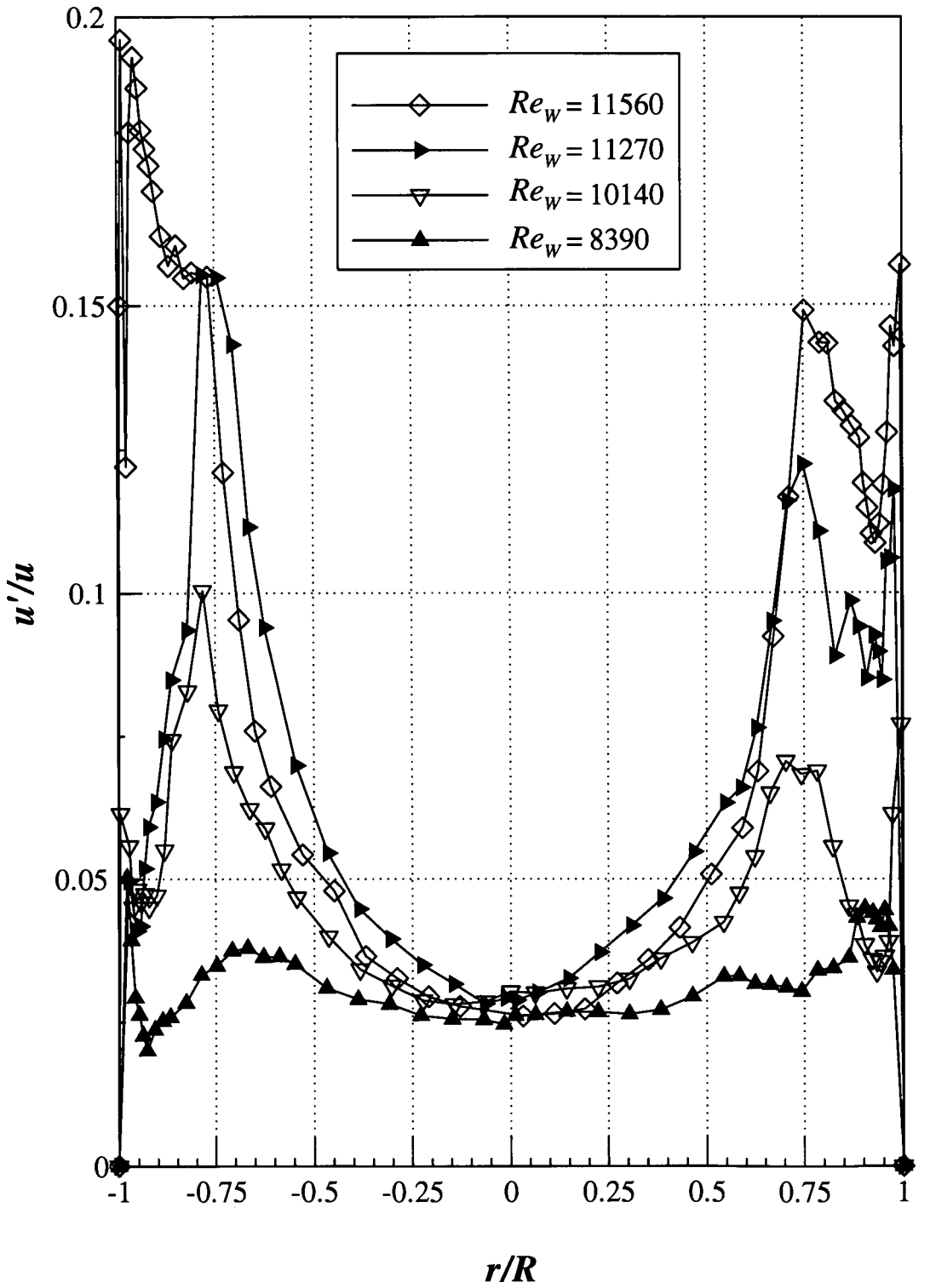

Figure 6.10 - Horizontal (θ = 90°, 270°) velocity fluctuations (u'/u) for different Reynolds numbers within transitional regime at x/D = 220, for 0.125% PAA

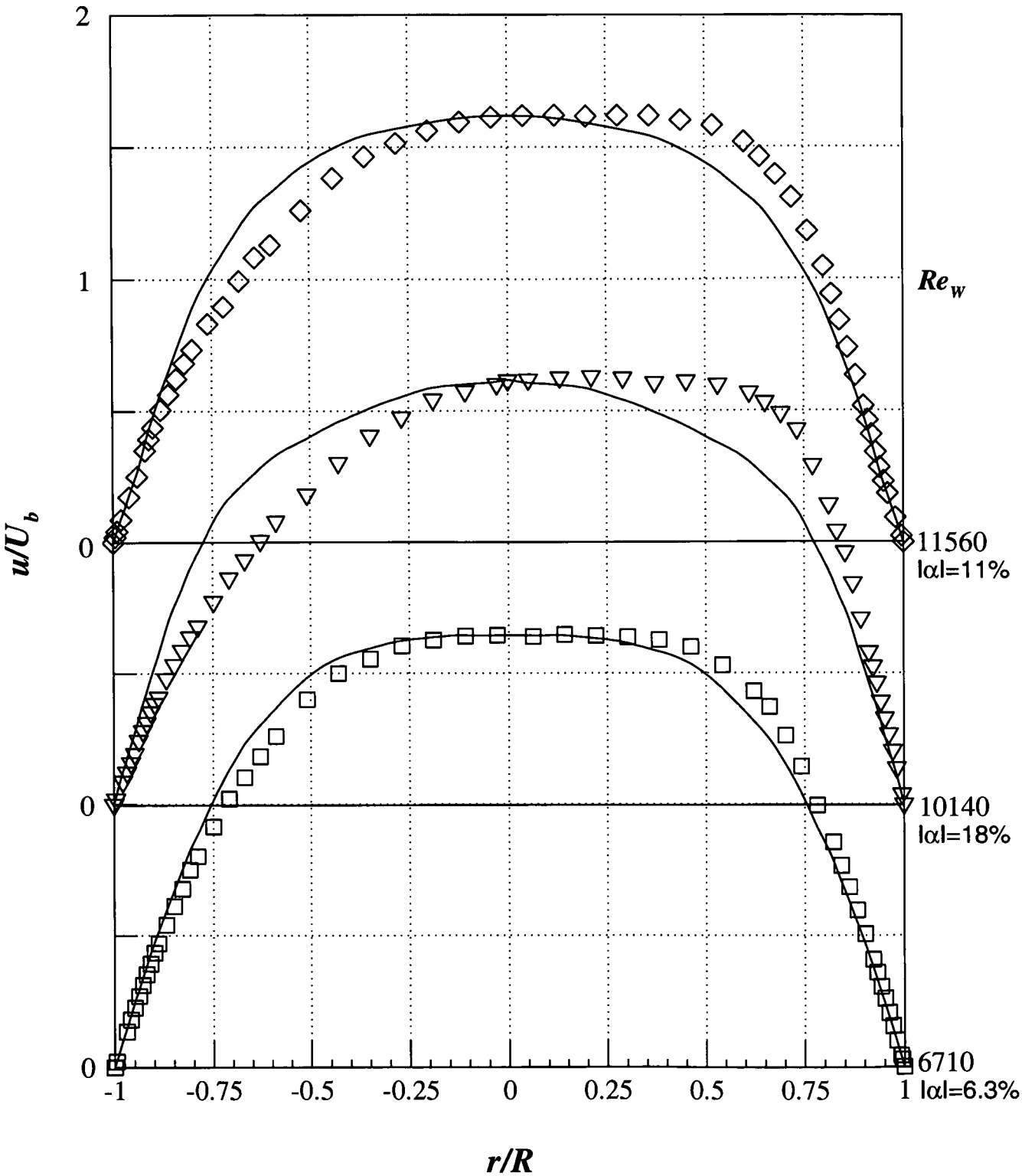

Figure 6.11 - Velocity profiles for the θ = 45° (and 225°) plane, for different Reynolds numbers within transitional regime at x/D = 220, including averages (continuous lines), for 0.125% PAA

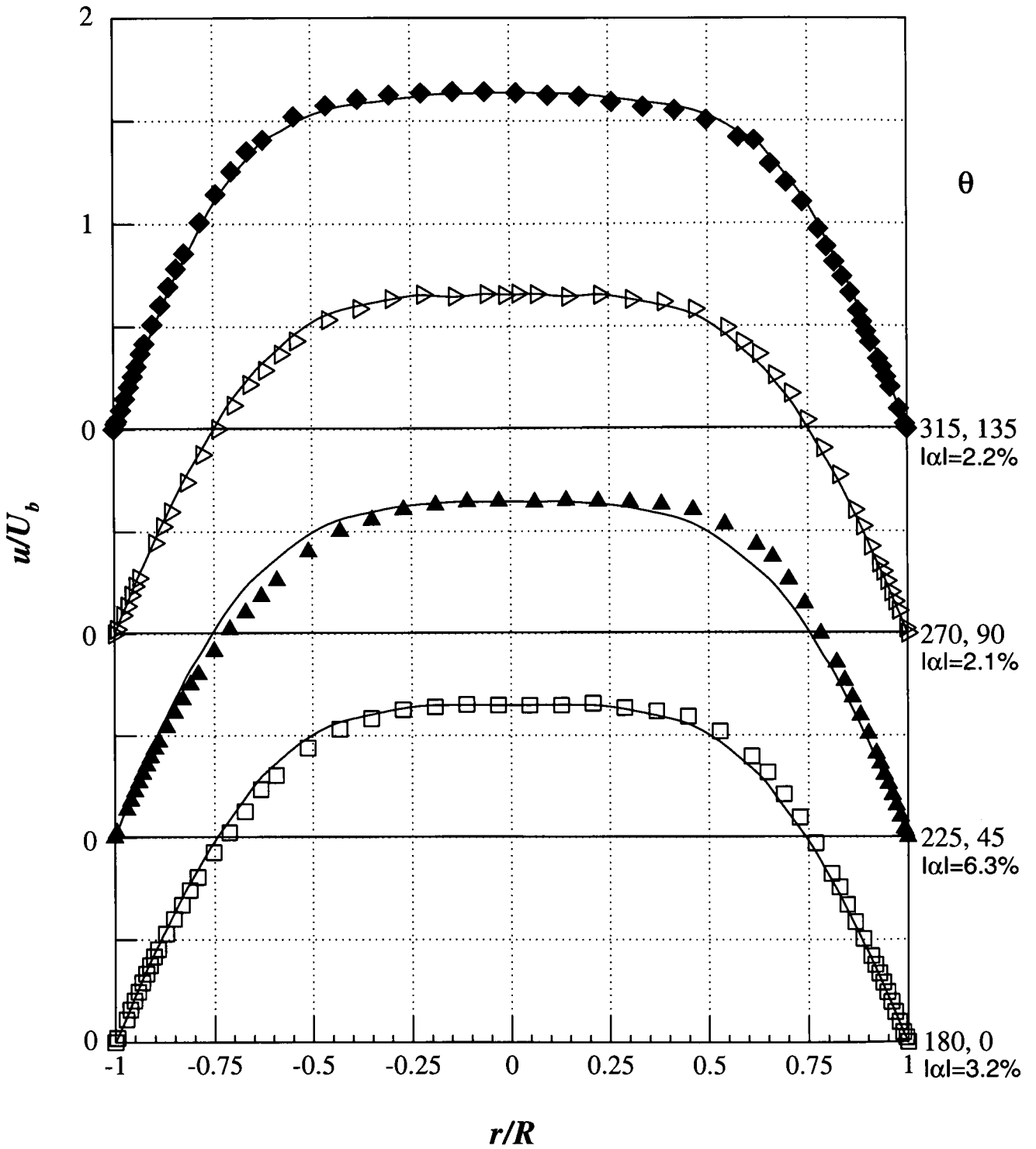

Figure 6.12 – Velocity profiles for different angles (θ) at Re_W = 6710 and x/D = 220, including averages (continuous lines), for 0.125% PAA

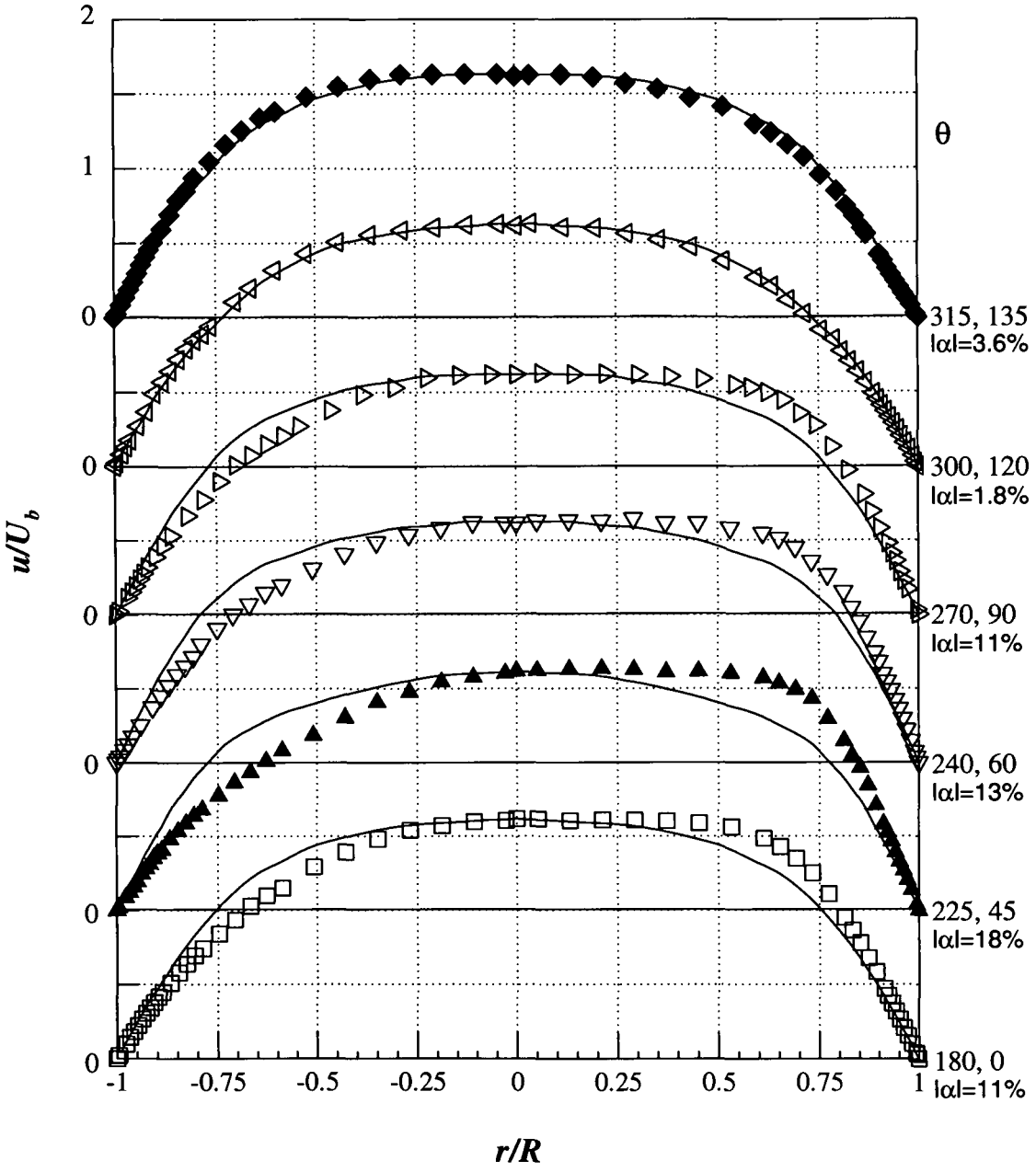

Figure 6.13 – Velocity profiles for different angles θ at Re_w = 10140 and x/D = 220, including averages (continuous lines), for 0.125% PAA

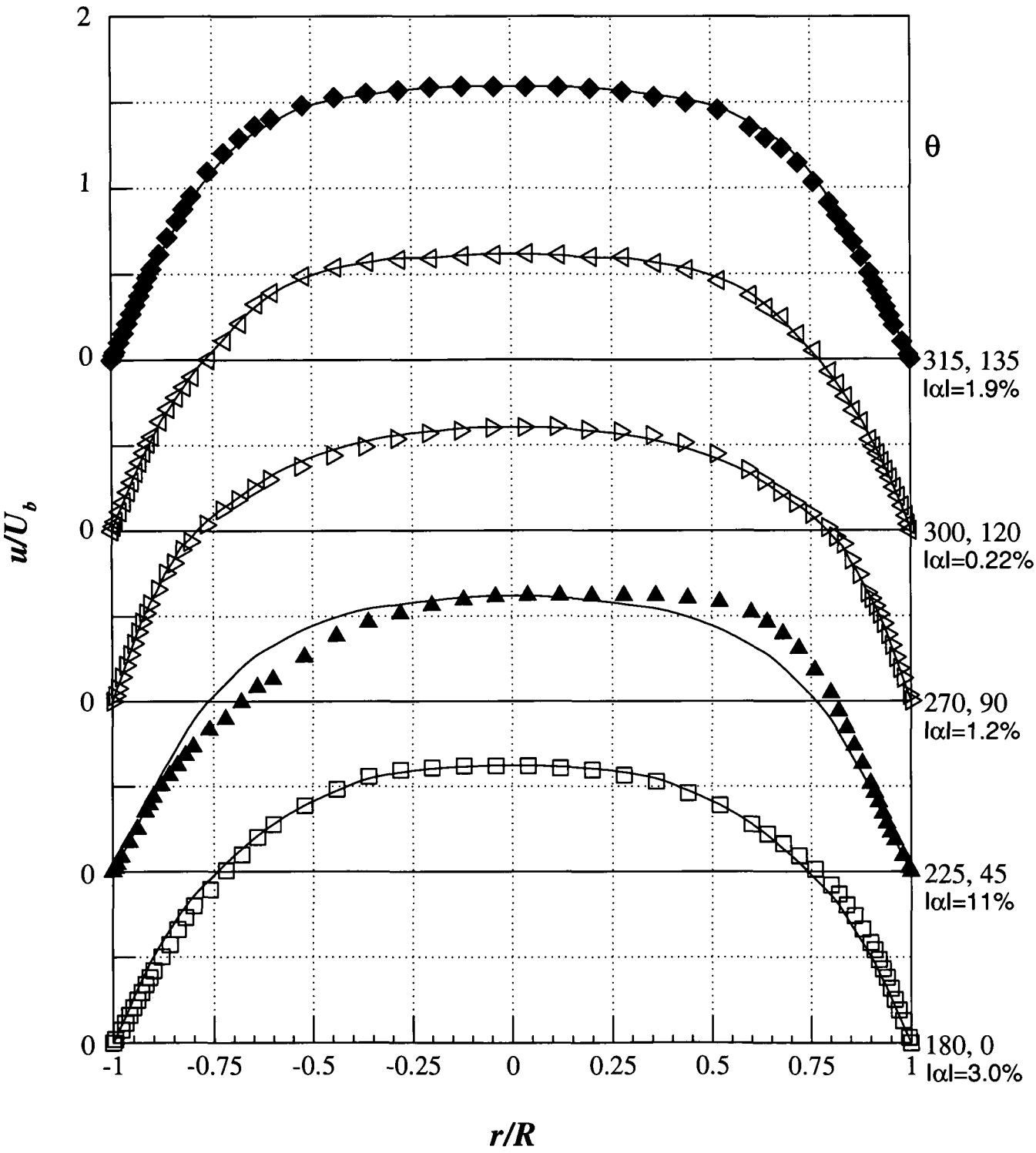

Figure 6.14 – Velocity profiles for different angles (θ) at Re_w = 11560 and x/D = 220, including averages (continuous lines), for 0.125% PAA

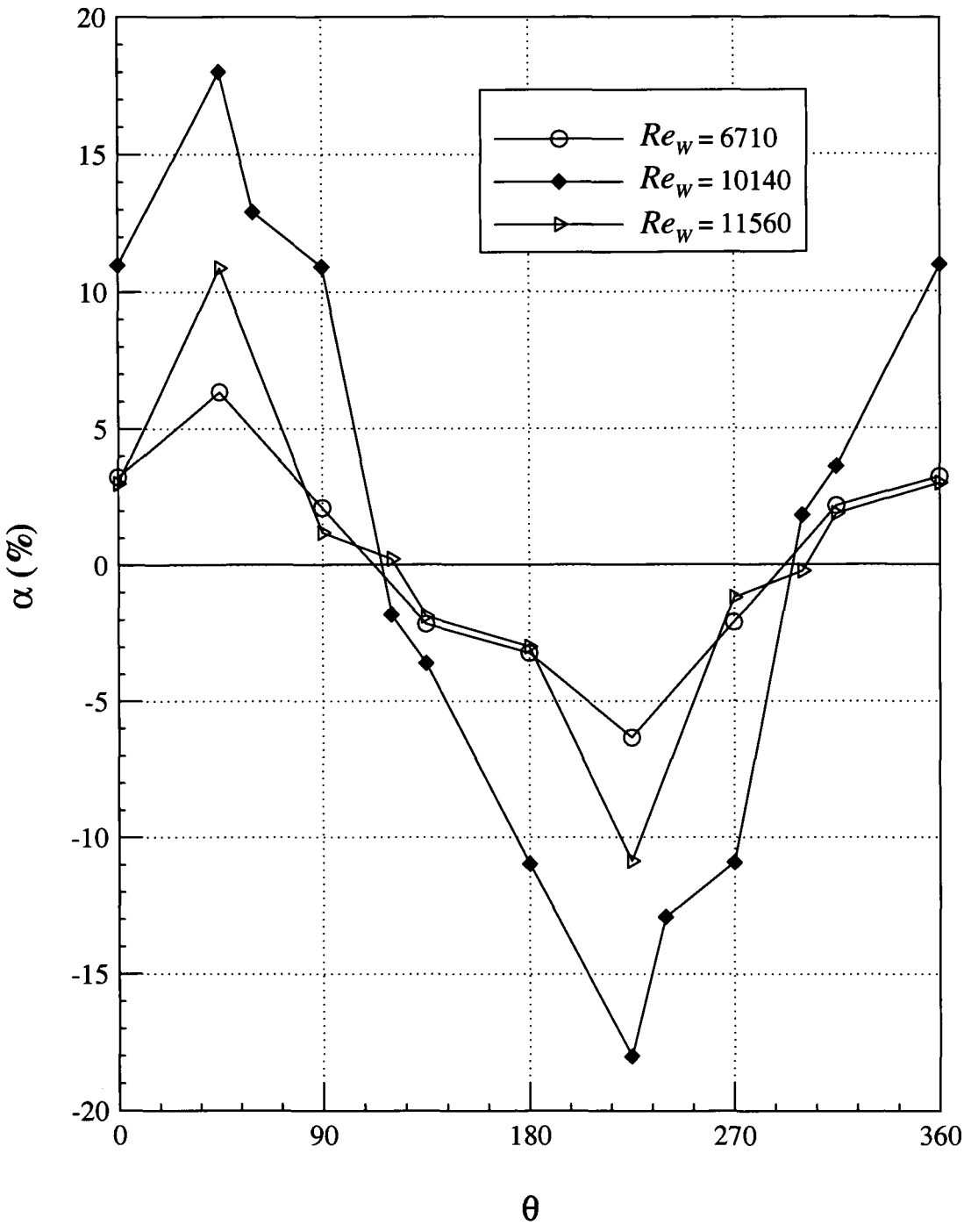

Figure 6.15 – Asymmetry for different Reynolds numbers at x/D = 220, for 0.125% PAA

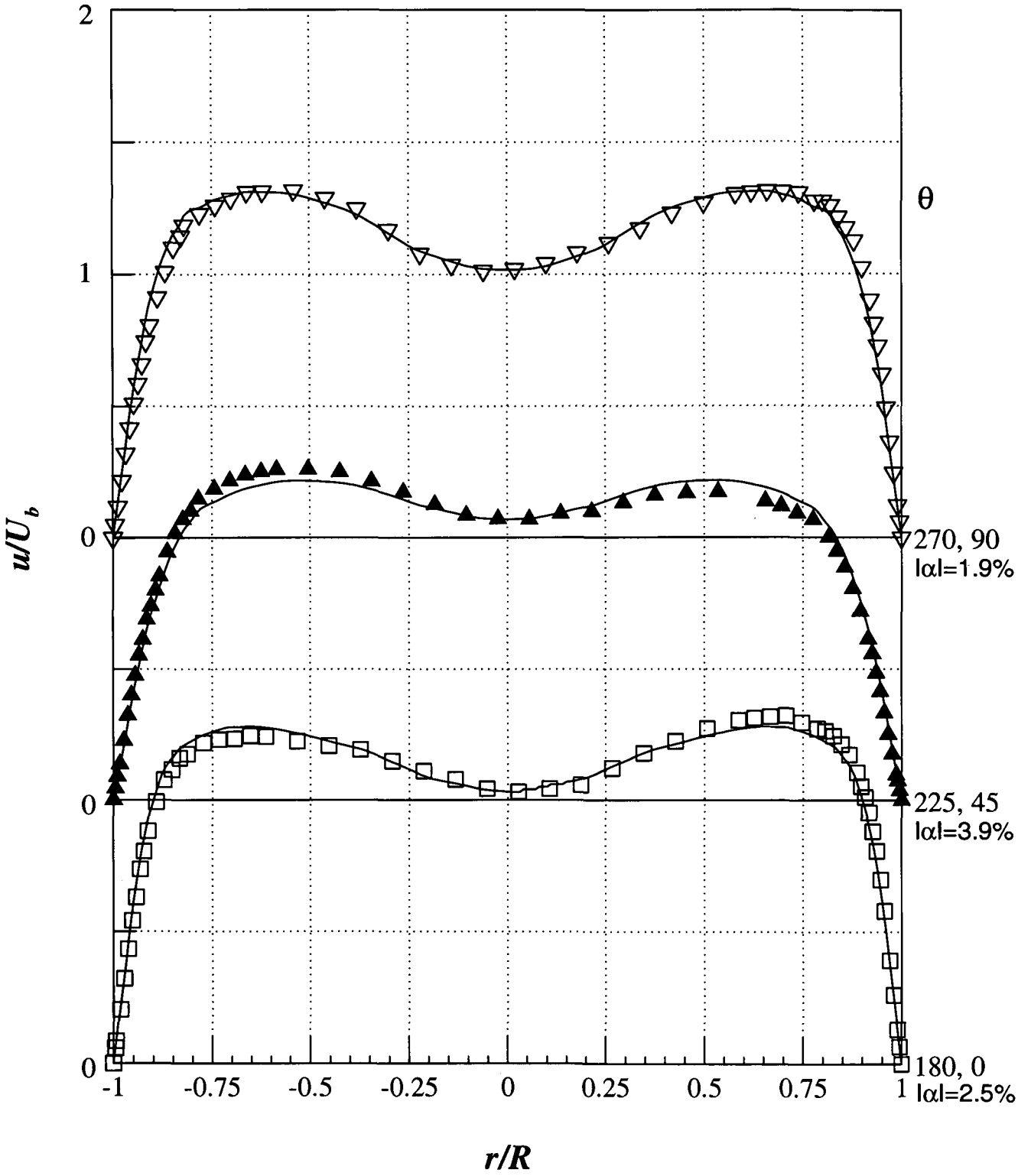

Figure 6.16 – Velocity profiles for different angles (θ) at x/D = 15 and Re_W = 10140, including averages (continuous lines), for 0.125% PAA

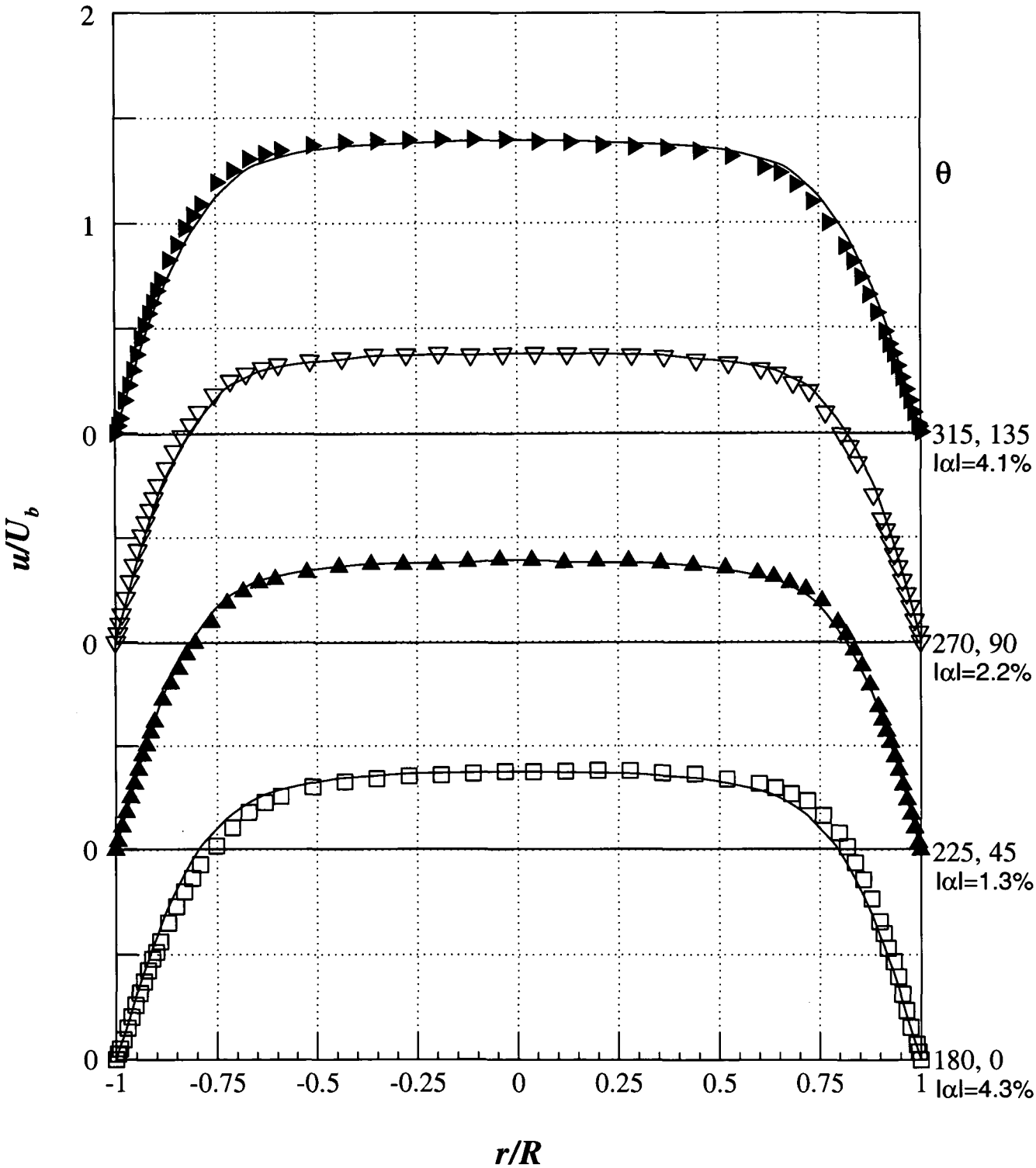

Figure 6.17 – Velocity profiles for different angles (θ) at x/D = 65 and Re_w = 10140, including averages (continuous lines), for 0.125% PAA

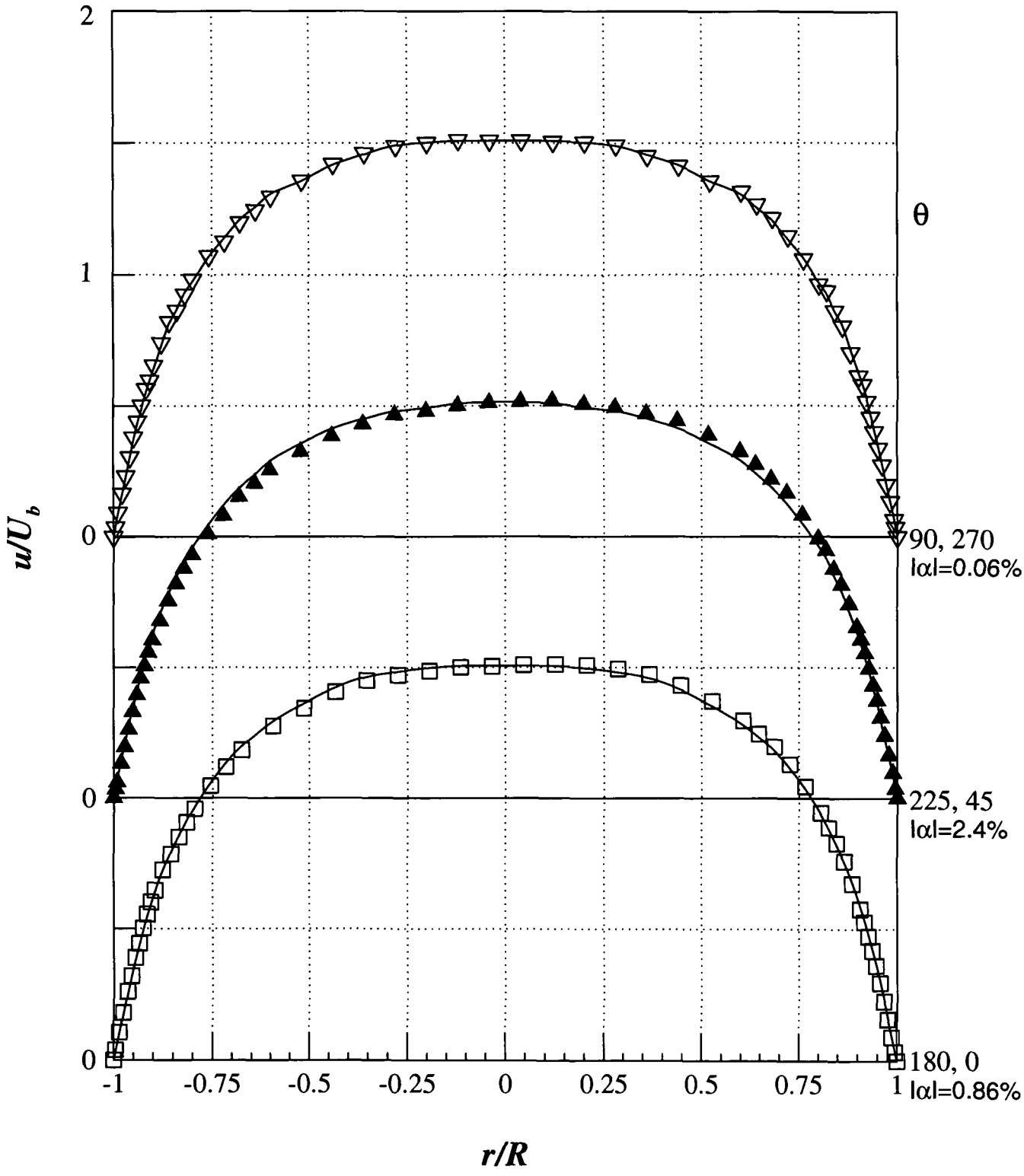

Figure 6.18 – Velocity profiles for different (θ) at x/D = 160 and Re_w = 10140, including averages (continuous lines), for 0.125% PAA

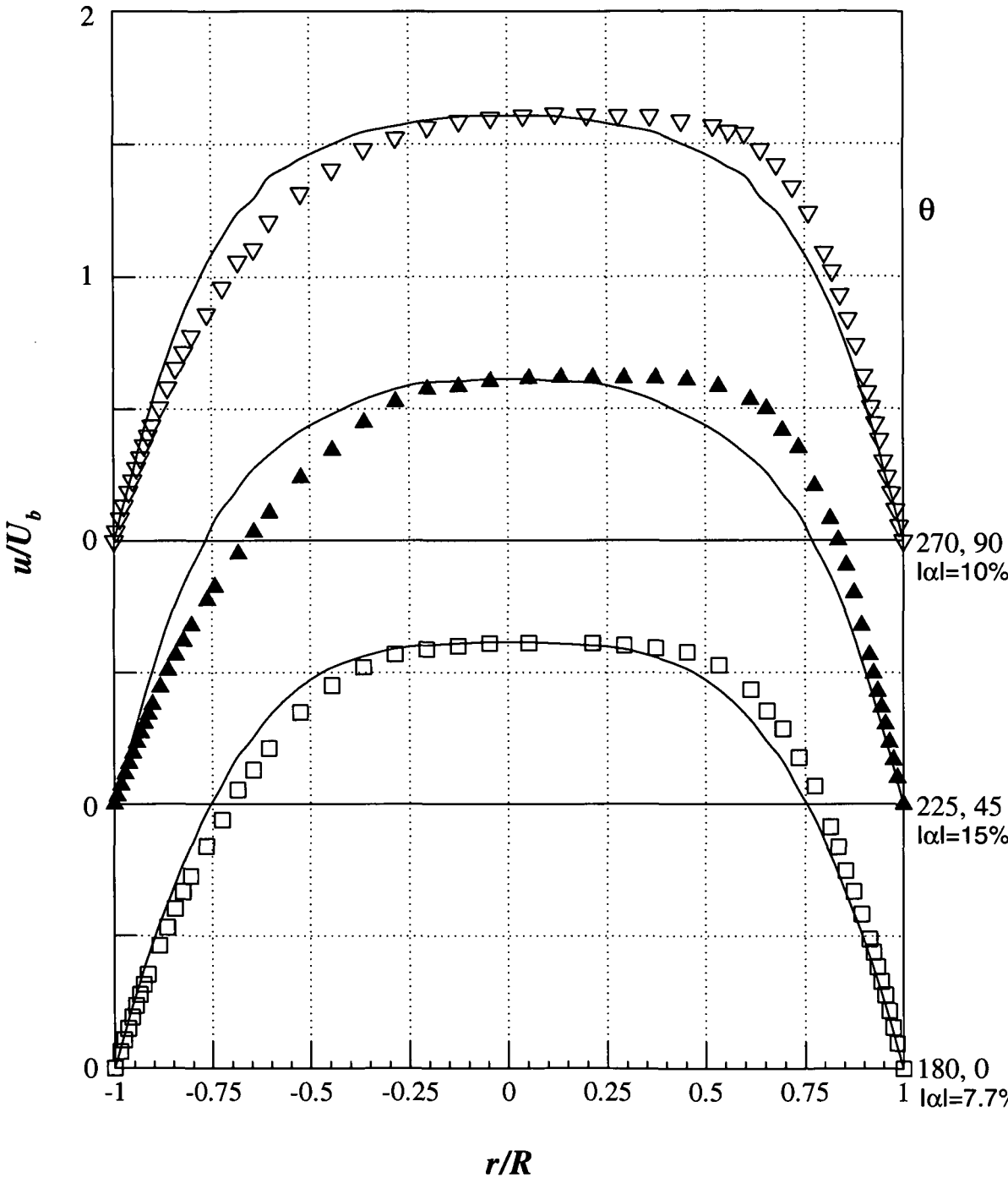

Figure 6.19 – Velocity profiles for different angles (θ) at x/D = 200 and Re_W = 10140, including averages (continuous lines), for 0.125% PAA

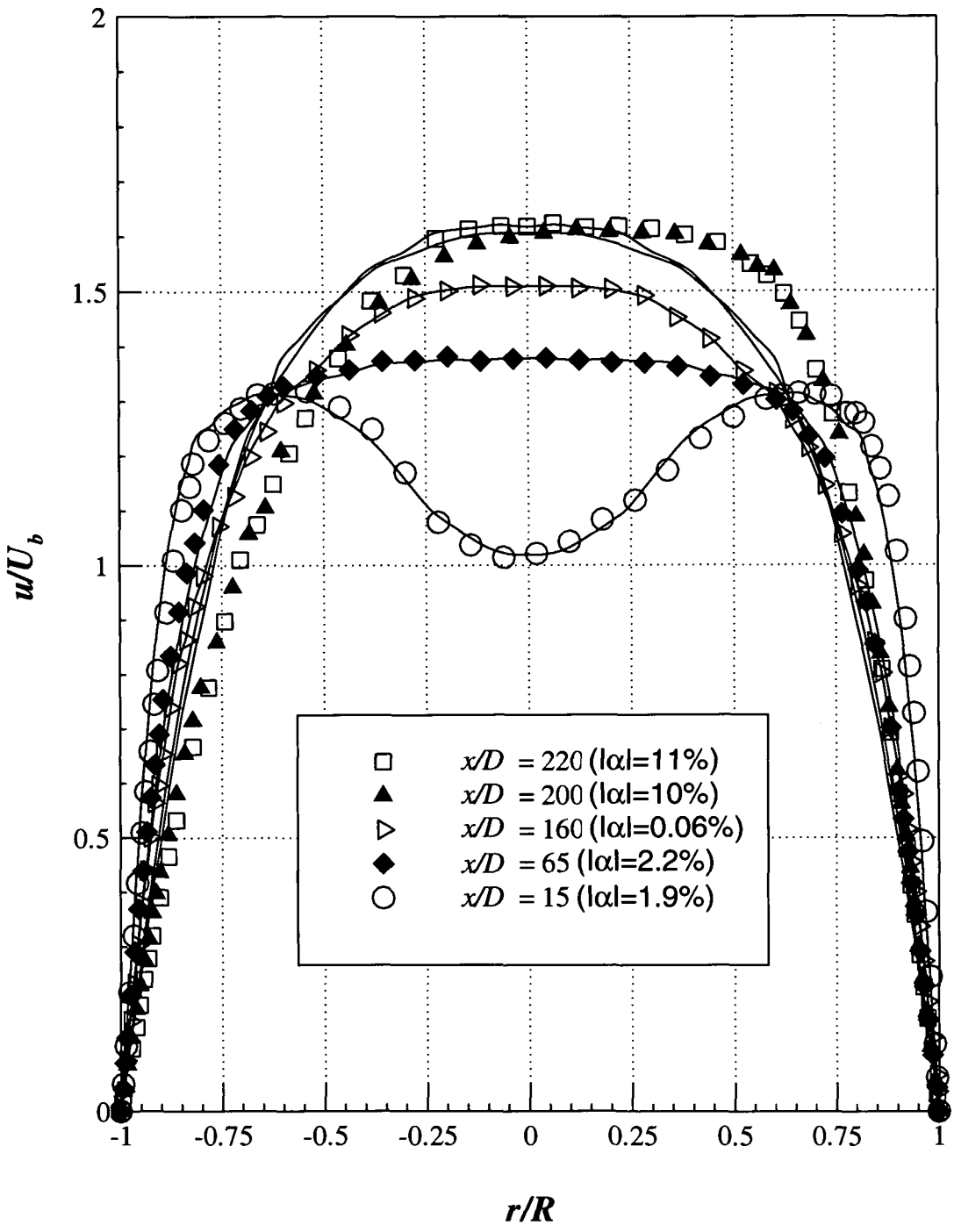

Figure 6.20 – Horizontal (θ = 90°, 270°) velocity profiles for different axial locations (x) at Re_w = 10140, including averages (continuous lines), for 0.125% PAA

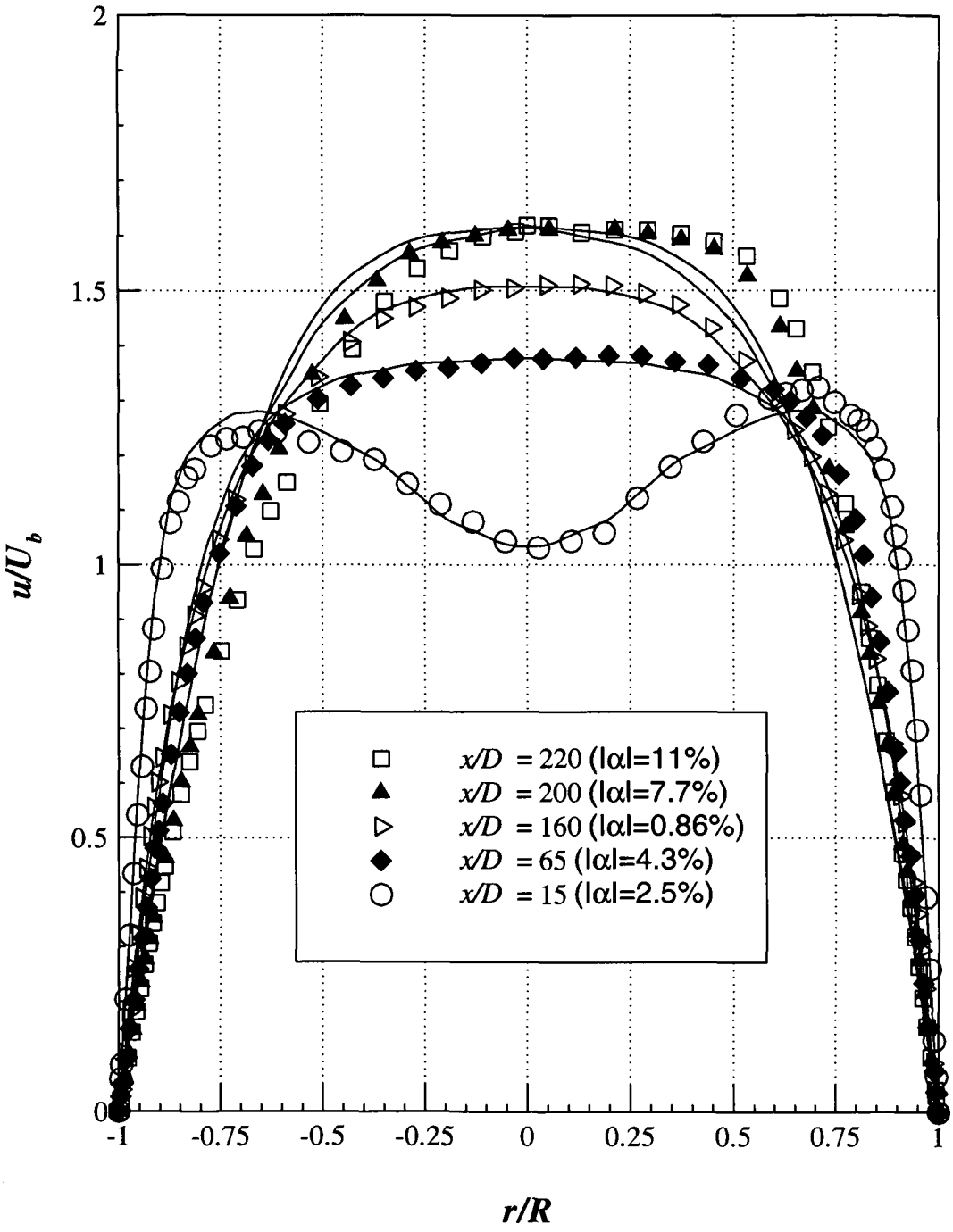

Figure 6.21 – Vertical (θ = 0°, 180°) velocity profiles for different axial locations (x) at Re_w = 10140, including averages (continuous lines), for 0.125% PAA

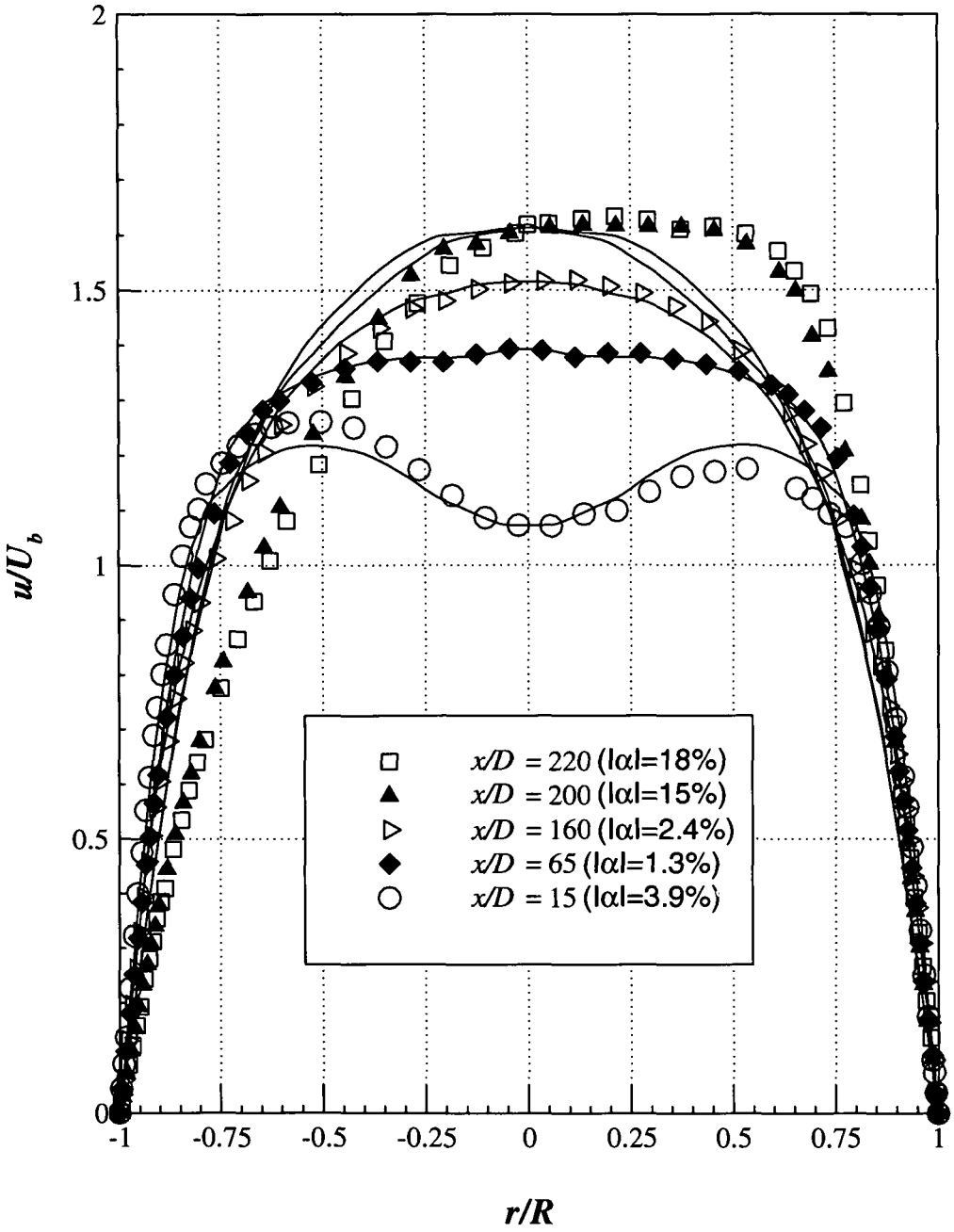

Figure 6.22 – Velocity profiles for the 45° (225°) plane, for different axial locations (x) at Re_w = 10140, including averages (continuous lines), for 0.125% PAA

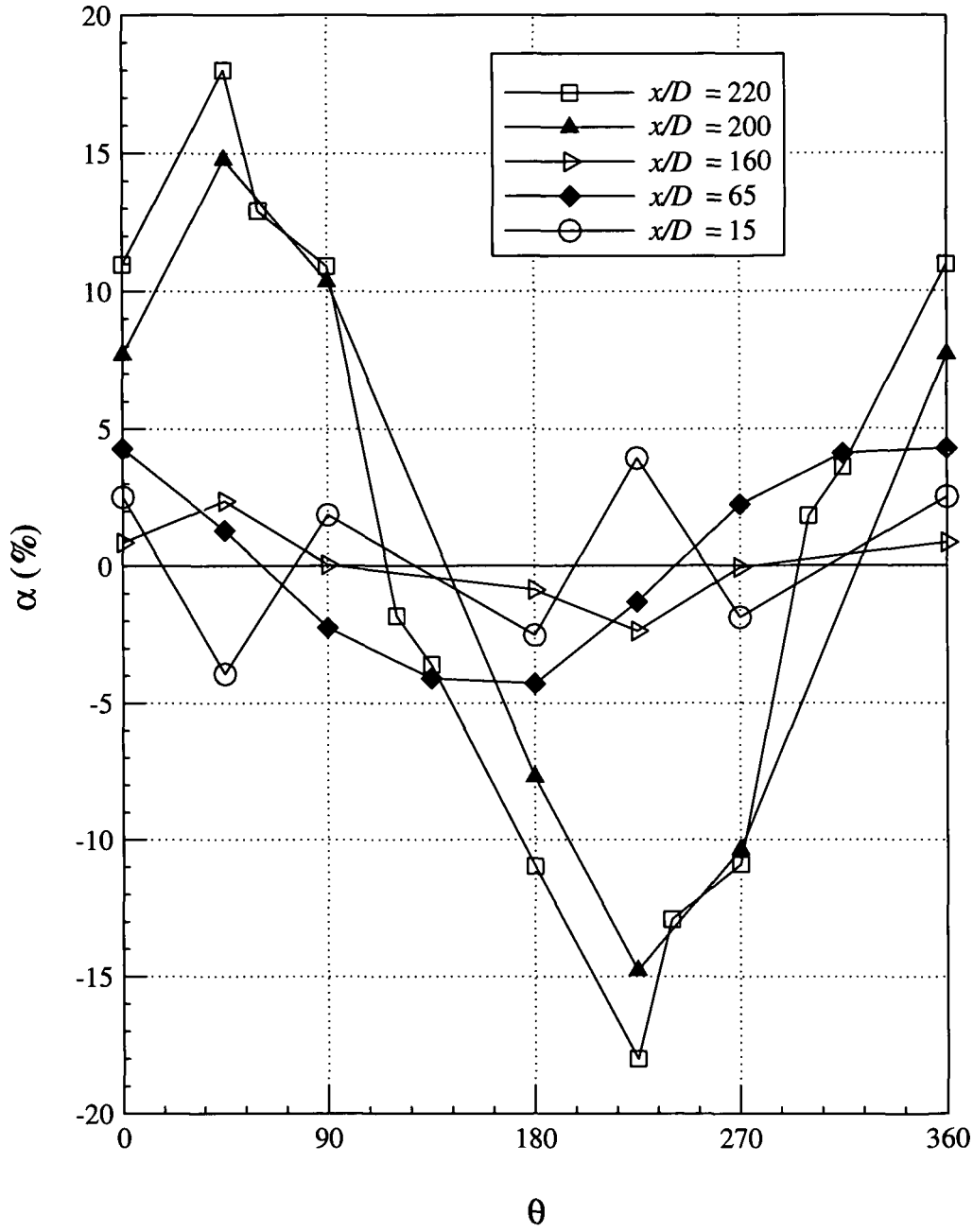

Figure 6.23 – Asymmetry for different axial locations (x) at Re_w = 10140, for 0.125% PAA

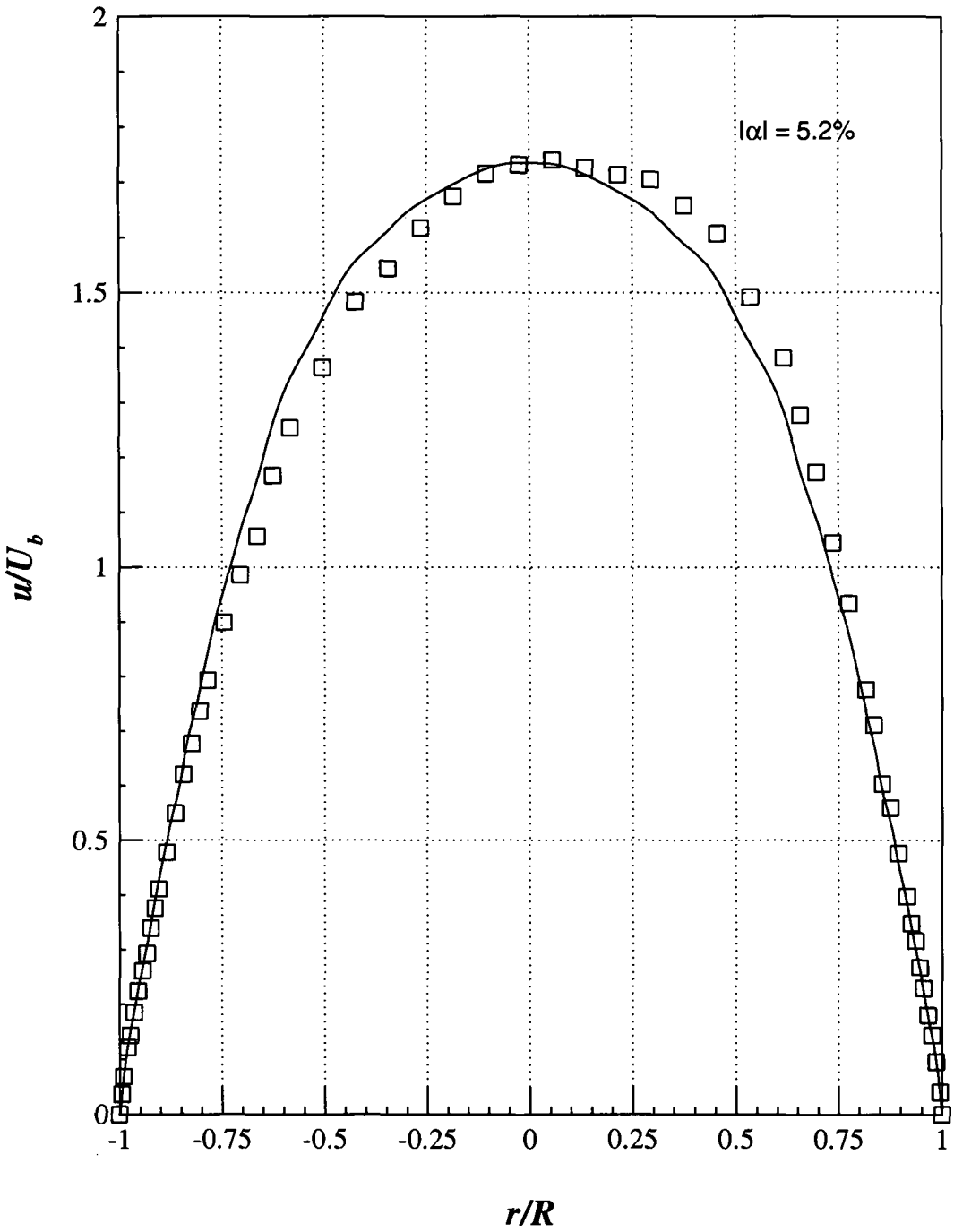

Figure 6.24 - Horizontal (θ = 90°, 270°) velocity profiles at Re_w = 5780 and x/D = 220, including average (continuous line), for 0.03% PAA

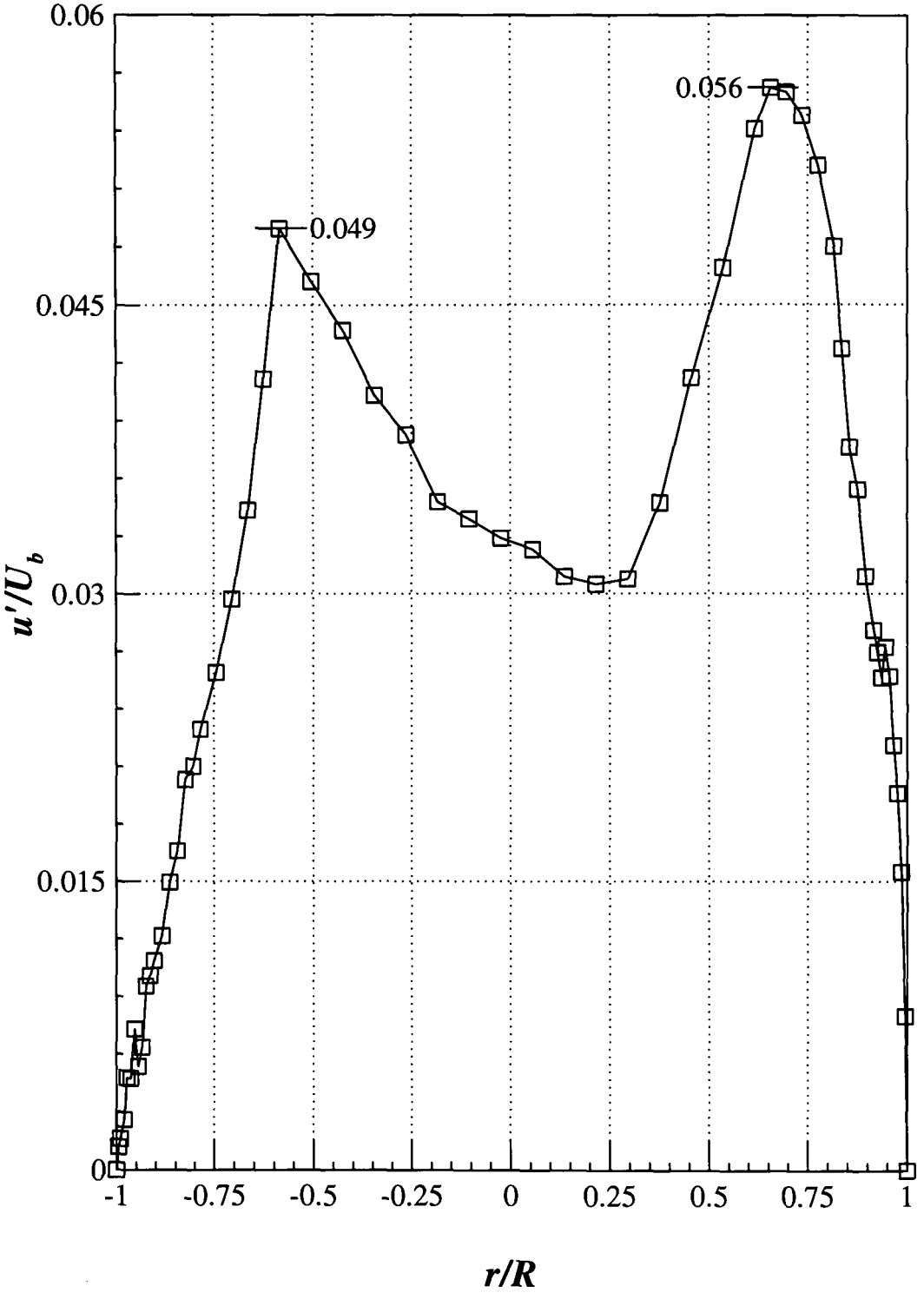

Figure 6.25 - Horizontal (θ = 90°, 270°) velocity fluctuations (u'/U_b) at Re_w = 5780 and x/D = 220, for 0.03% PAA

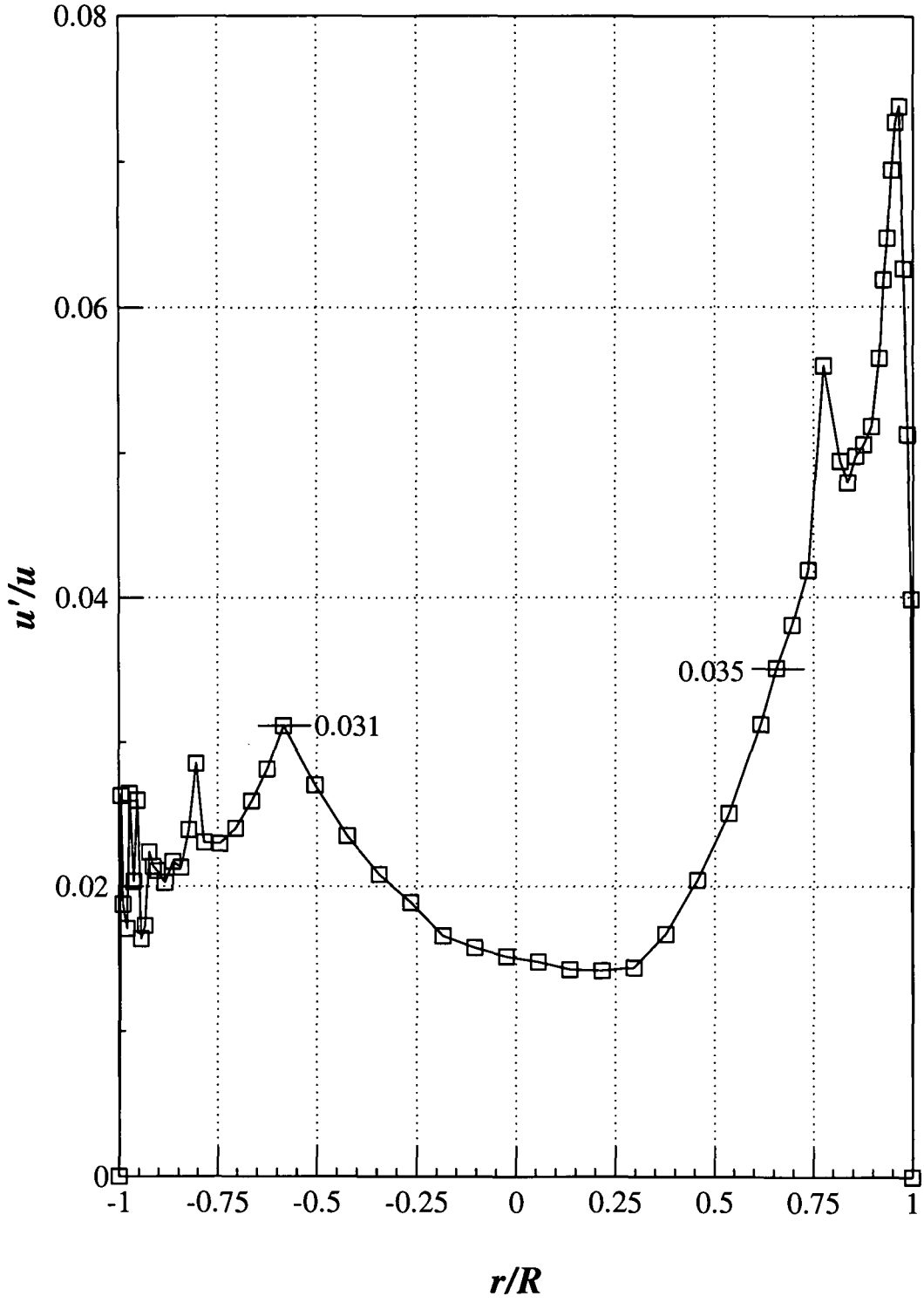

Figure 6.26 - Horizontal (θ = 90°, 270°) velocity fluctuations (u'/u) at Re_w = 5780 and x/D = 220, for 0.03% PAA

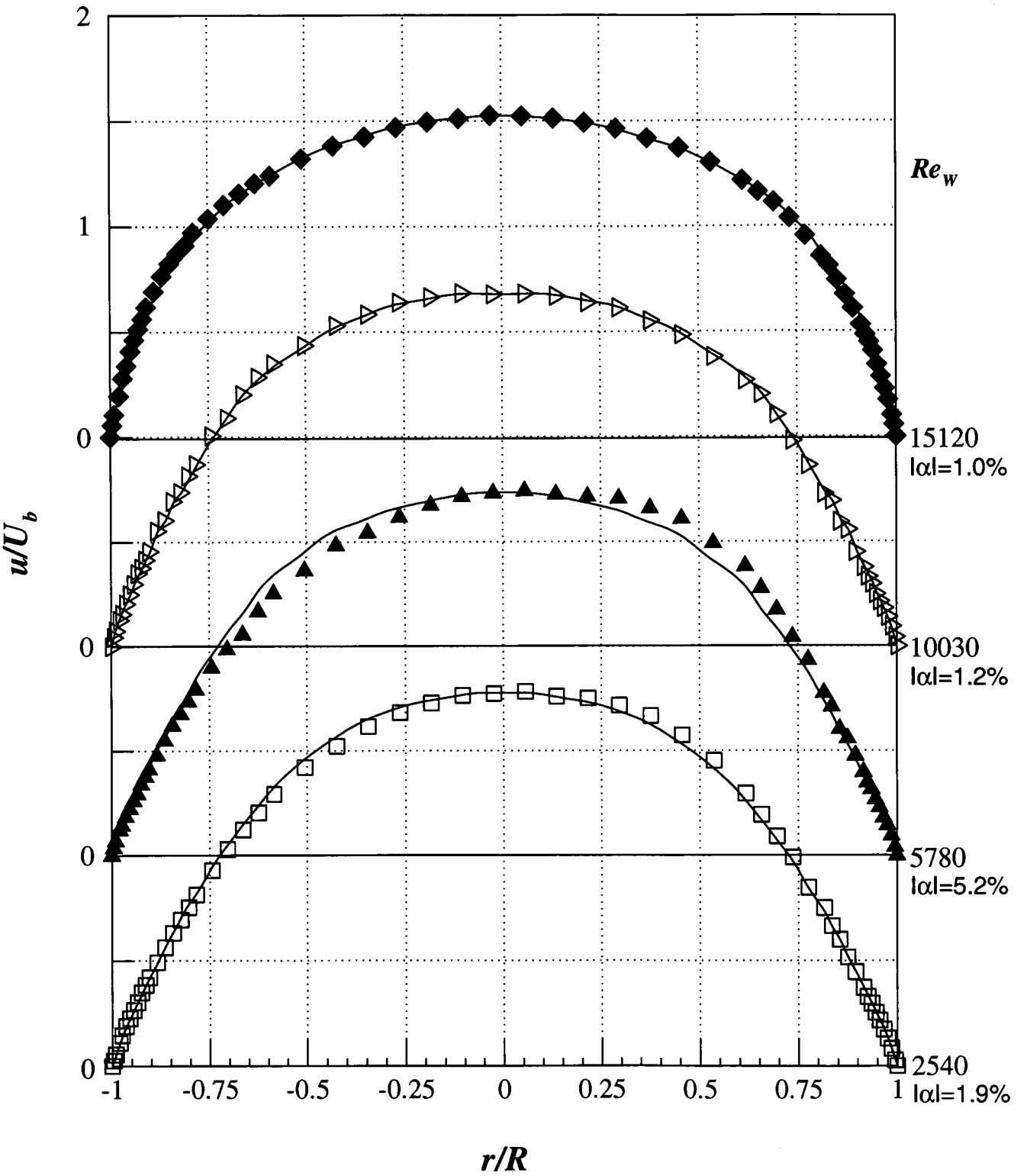

Figure 6.27 - Horizontal (θ = 90°, 270°) velocity profiles for different Reynolds numbers (all regimes) at x/D = 220, including averages (continuous lines), for 0.03% PAA

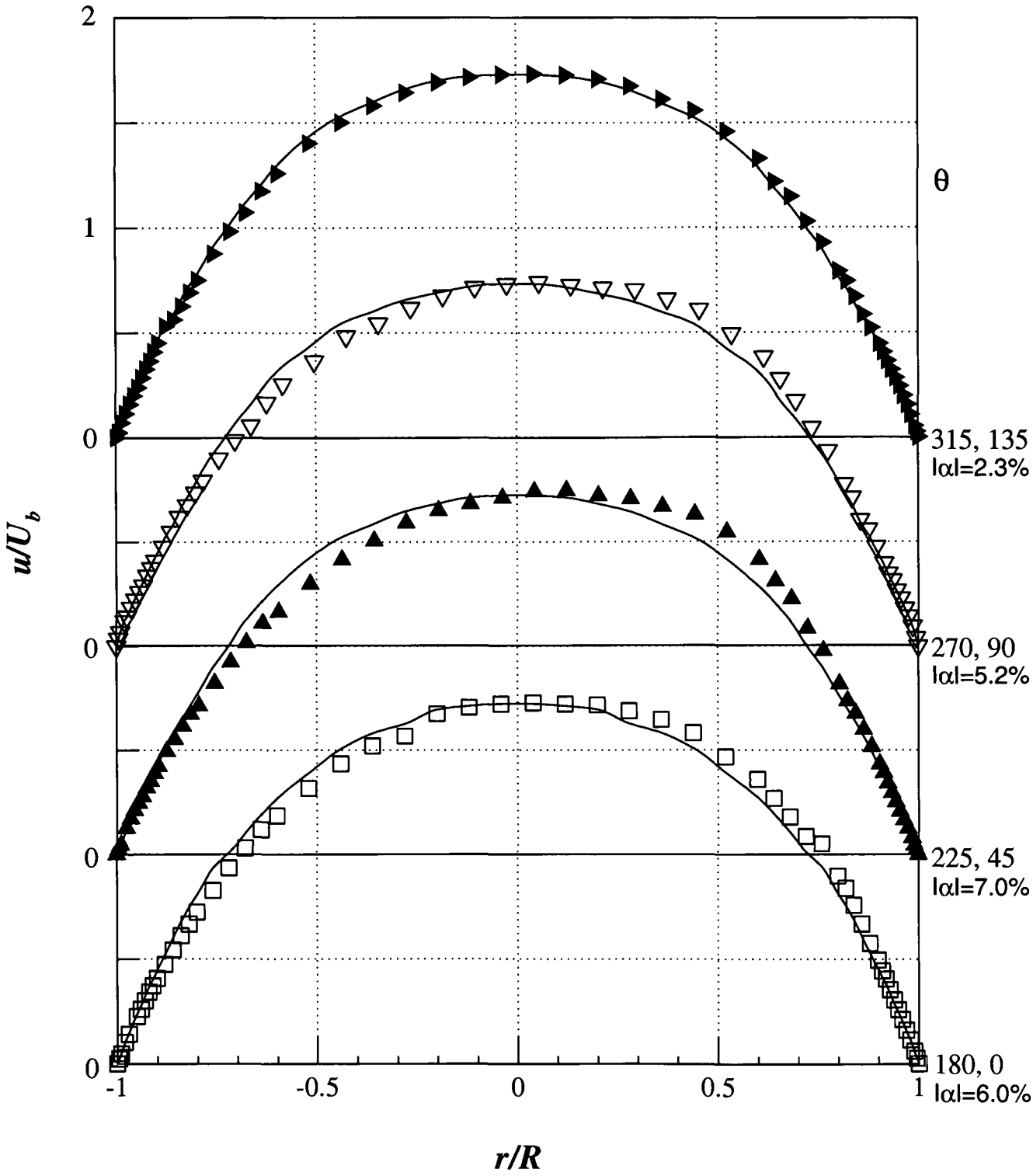

Figure 6.28 - Velocity profiles for different angles (θ) at Re_w = 5780 and x/D = 220, including averages (continuous lines), for 0.03% PAA

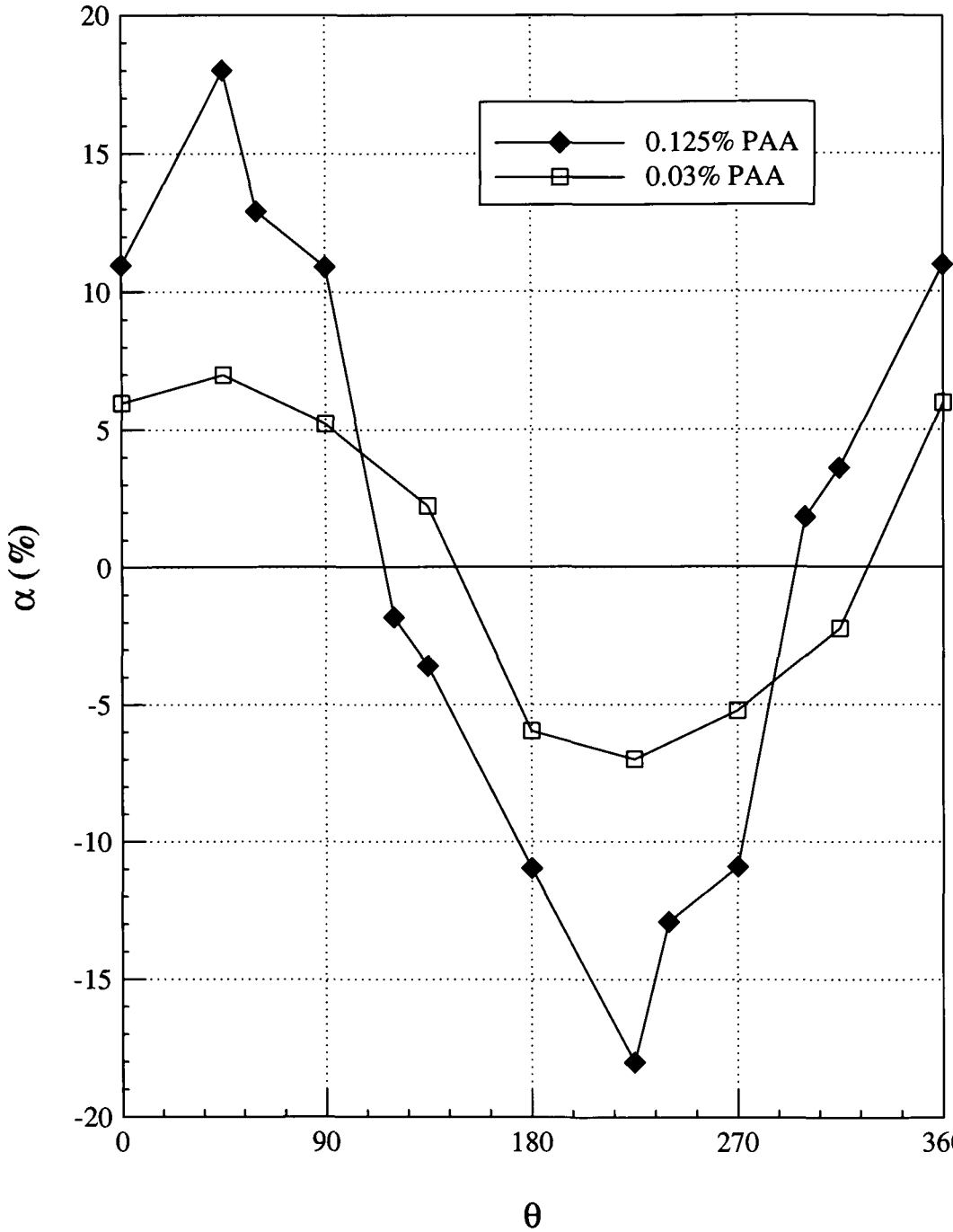

Figure 6.29 – Asymmetry comparison between 0.03% PAA (Re_w = 5780) and 0.125% PAA (Re_w = 10140) at x/D = 220

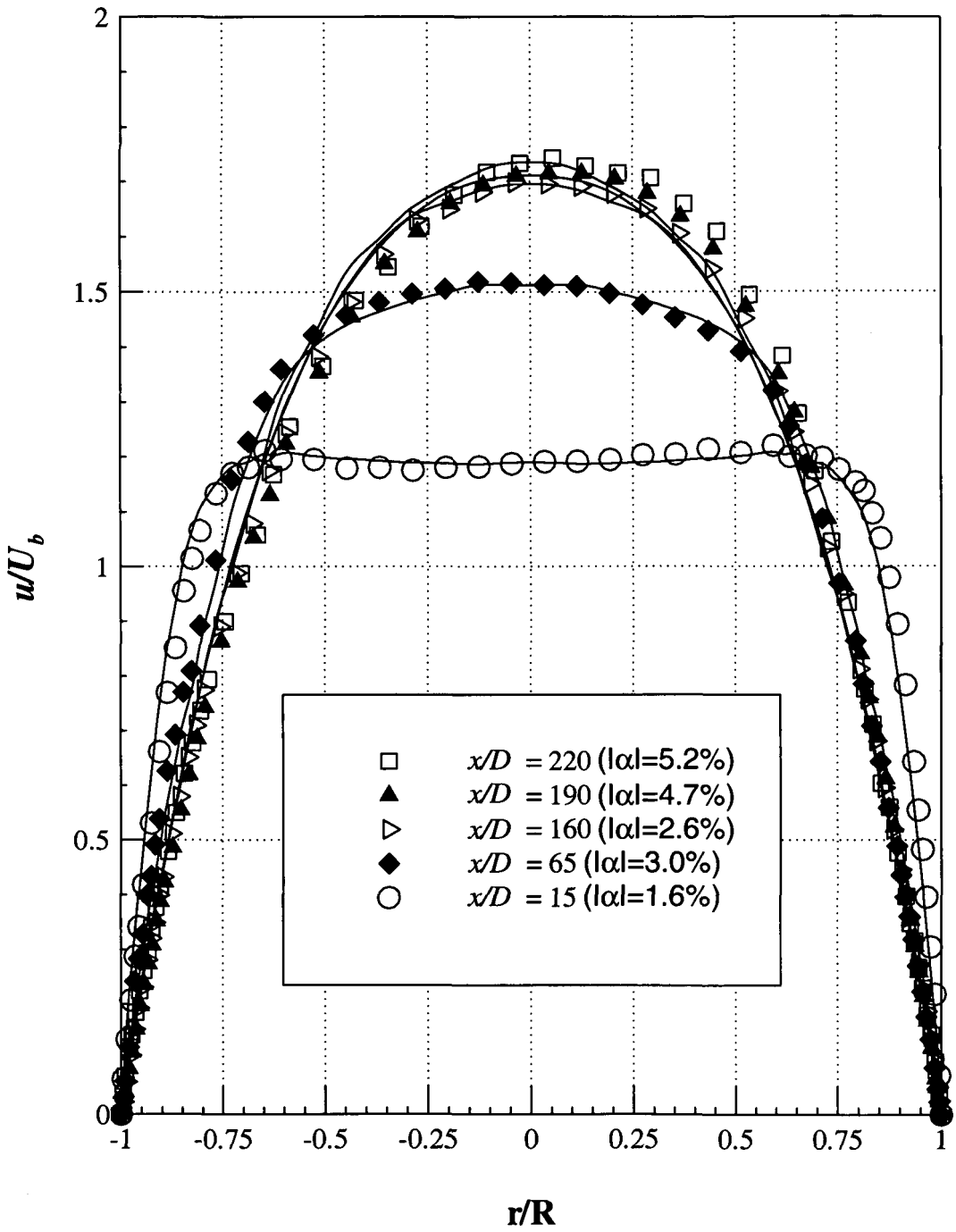

Figure 6.30 – Horizontal (θ = 90°, 270°) velocity profiles for different axial locations (x) at Re_w = 5780, including averages (continuous lines), for 0.03% PAA

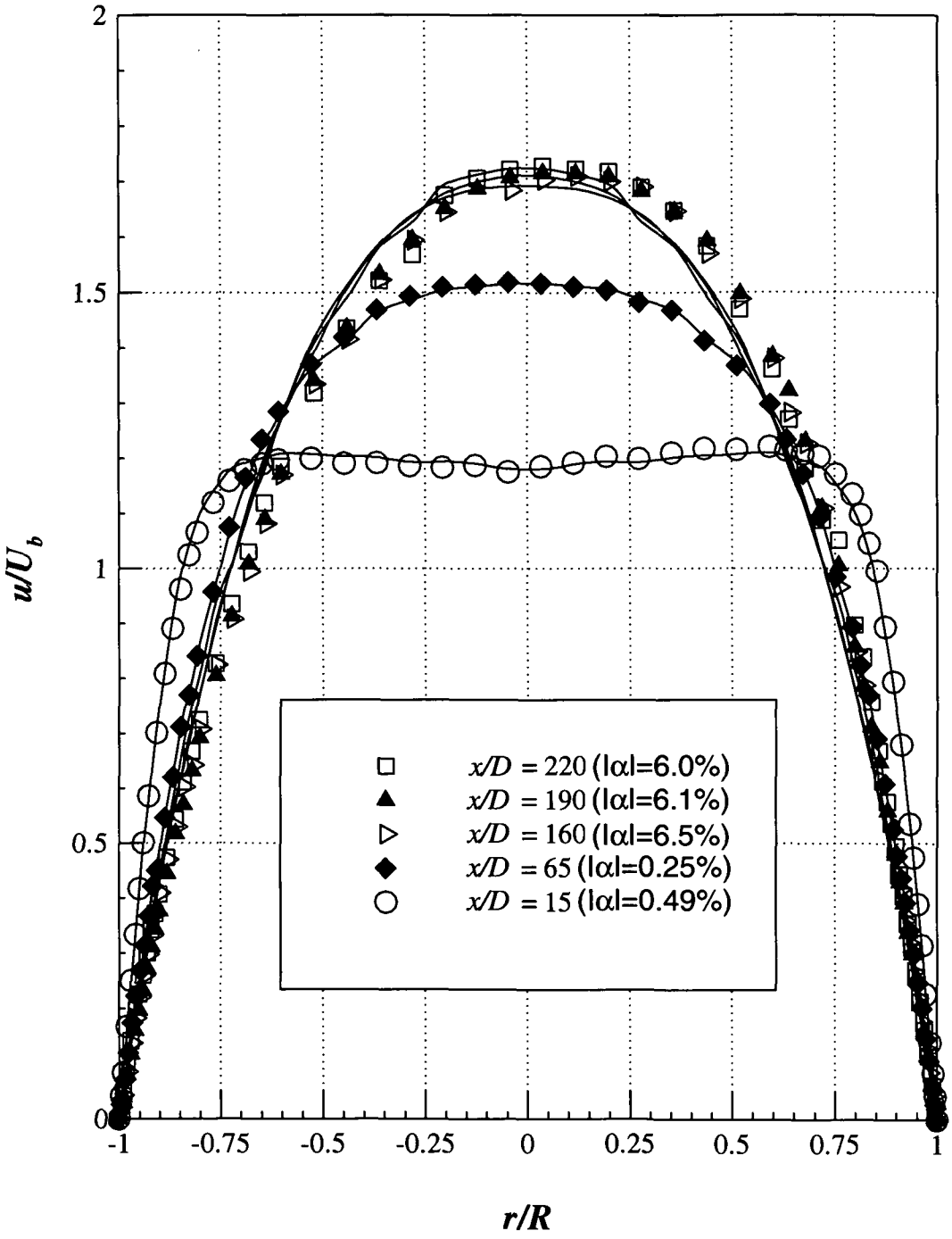

Figure 6.31 – Vertical (θ = 0°, 180°) velocity profiles for different axial locations (x) at Re_w = 5780, including averages (continuous lines), for 0.03% PAA

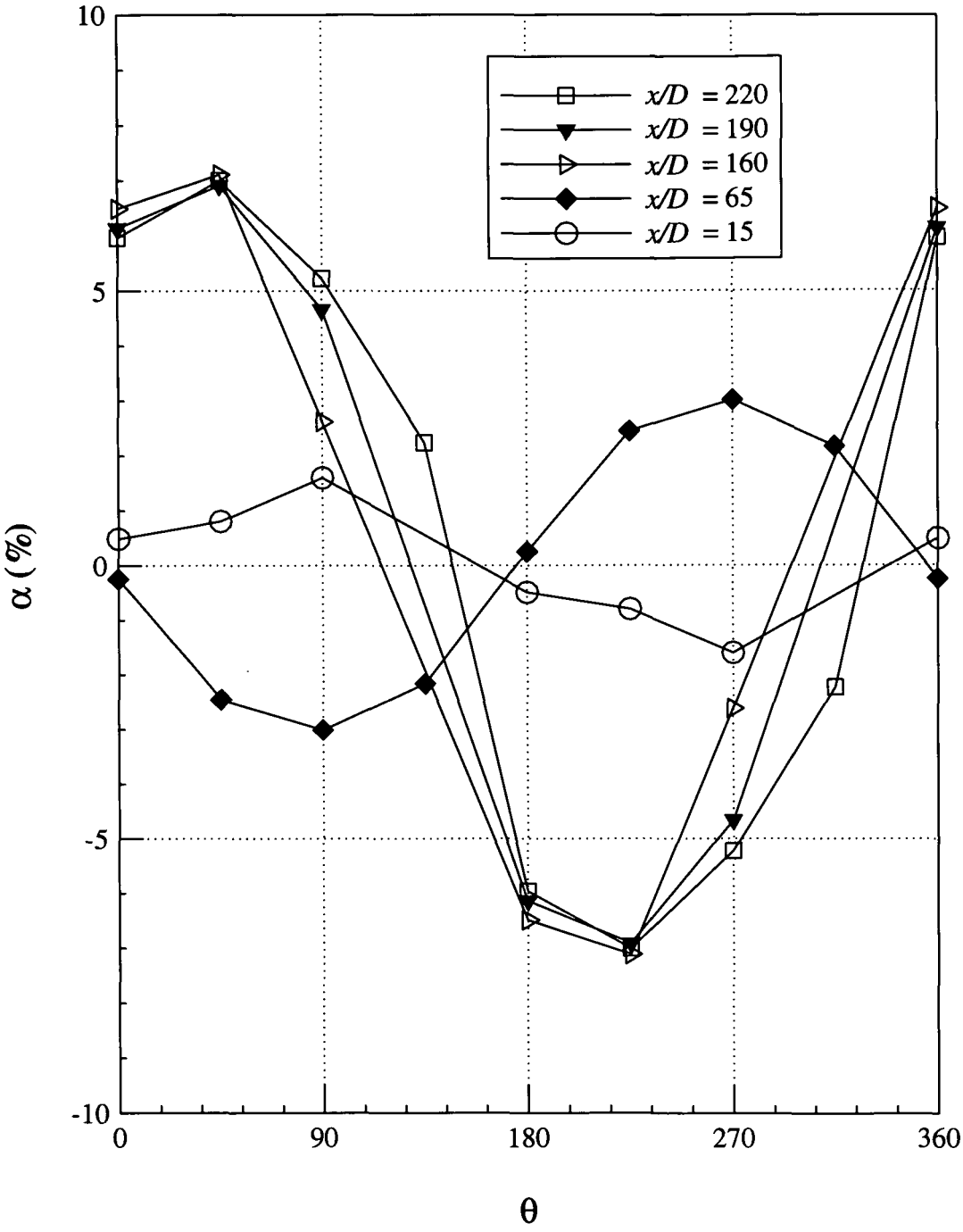

Figure 6.32 – Asymmetry for different axial locations (x) at Re_w = 5780, for 0.03 PAA%

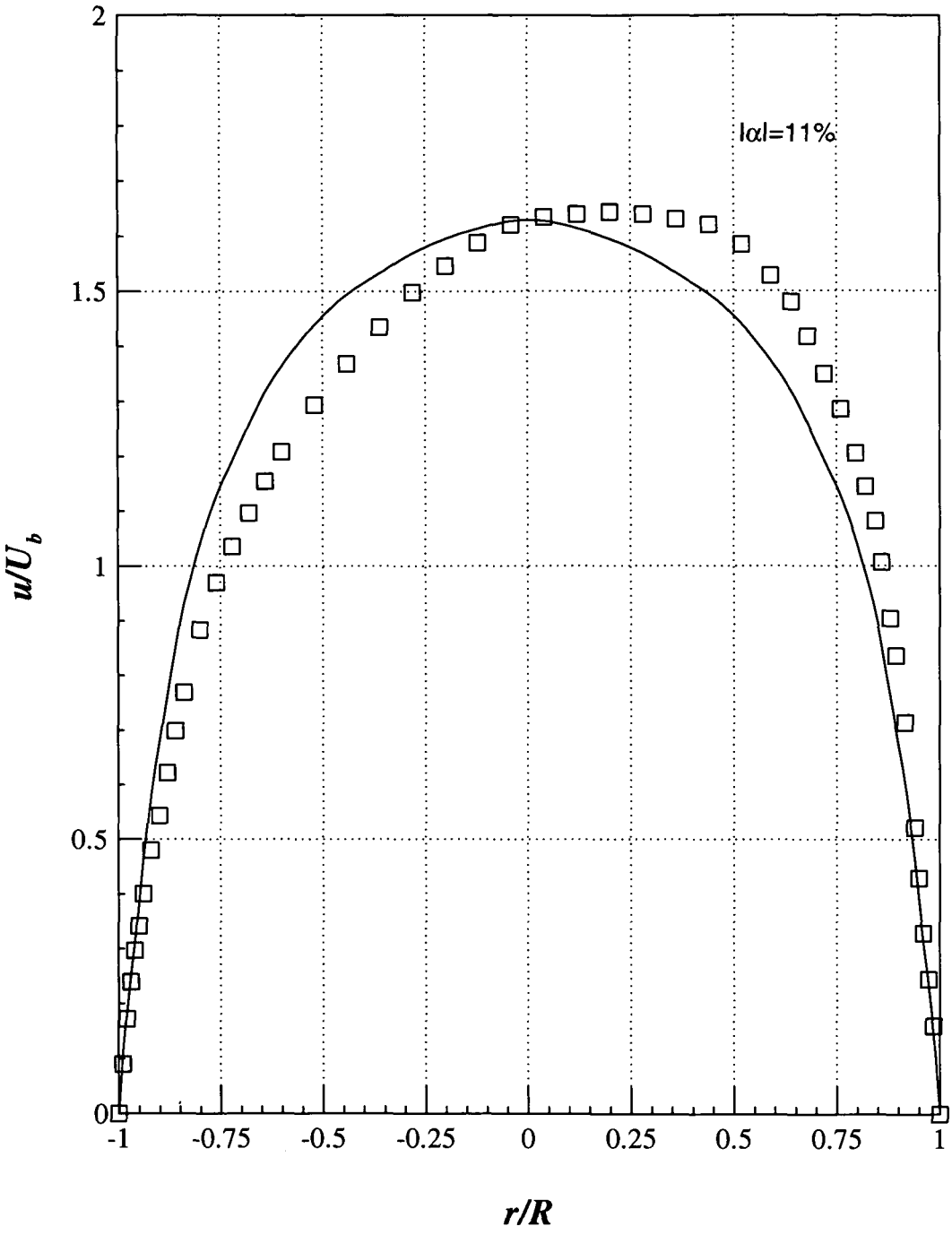

Figure 6.33 - Horizontal (θ = 90°, 270°) velocity profile at Re_w = 10260 and x/D = 220, including average (continuous line), for 0.15% XG

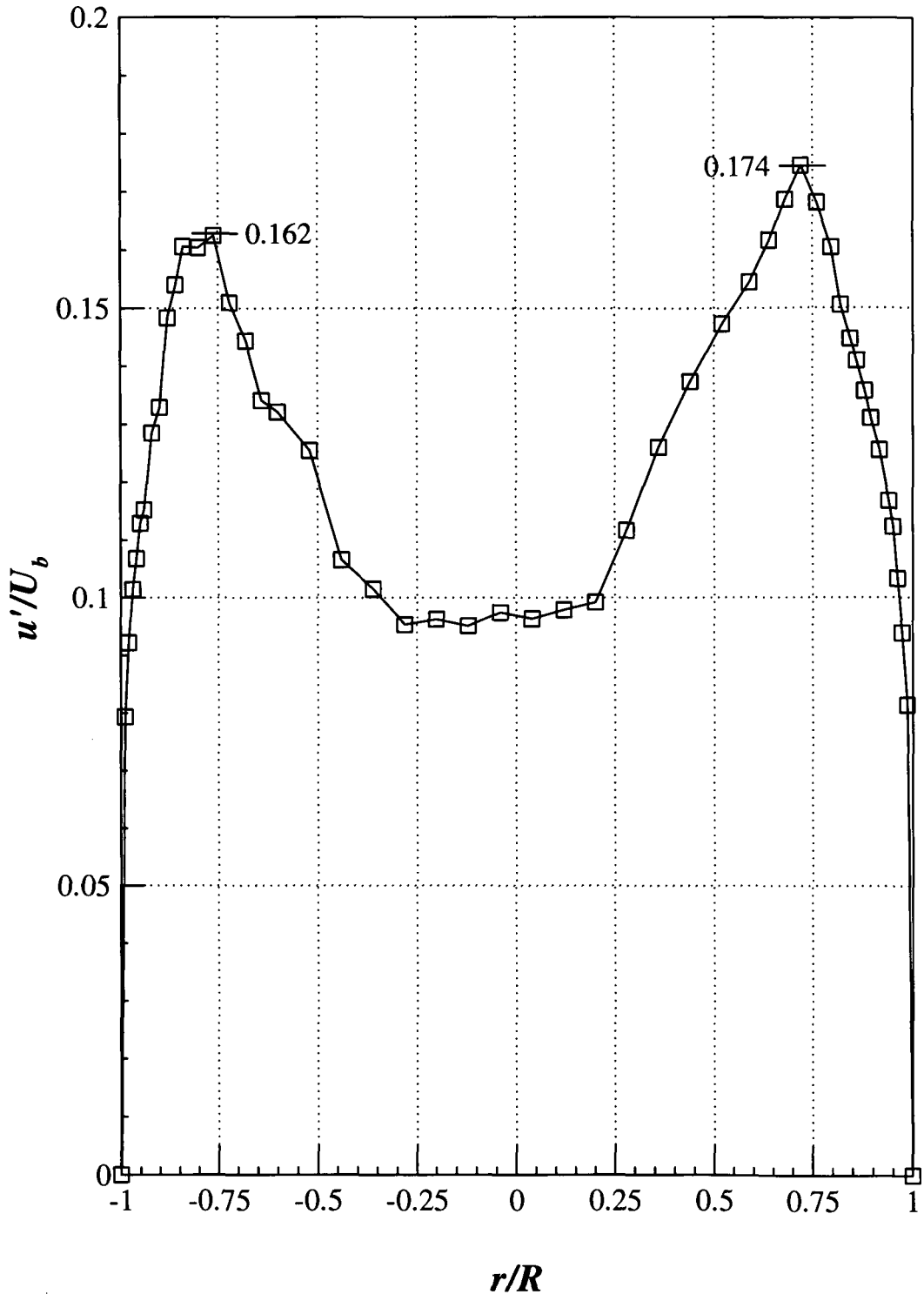

Figure 6.34 - Horizontal (θ = 90°, 270°) velocity fluctuations (u'/U_b) at Re_W = 10260 and x/D = 220, for 0.15% XG

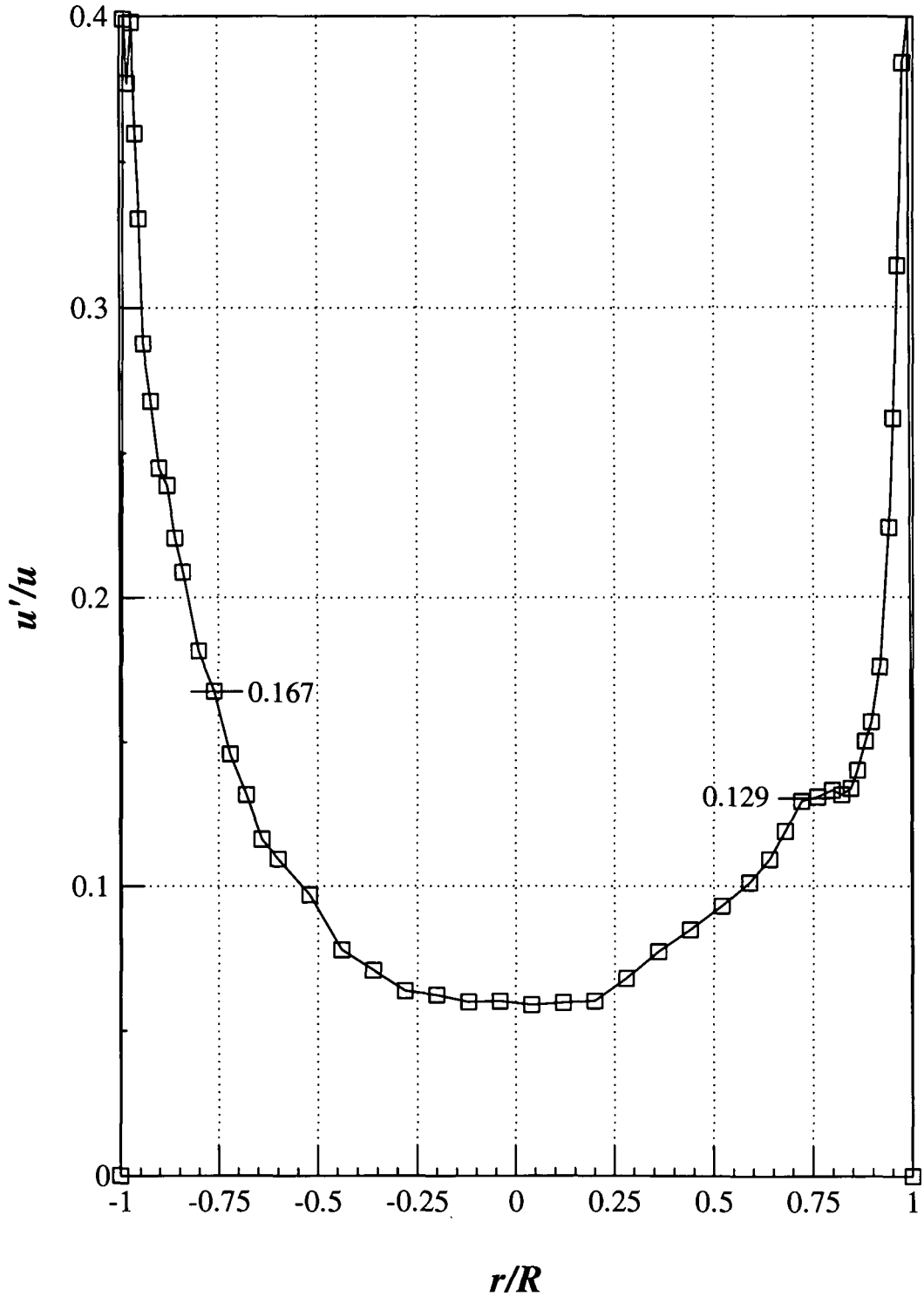

Figure 6.35 - Horizontal (θ = 90°, 270°) velocity fluctuations (u'/u) at Re_w = 10260 and x/D = 220, for 0.15% XG

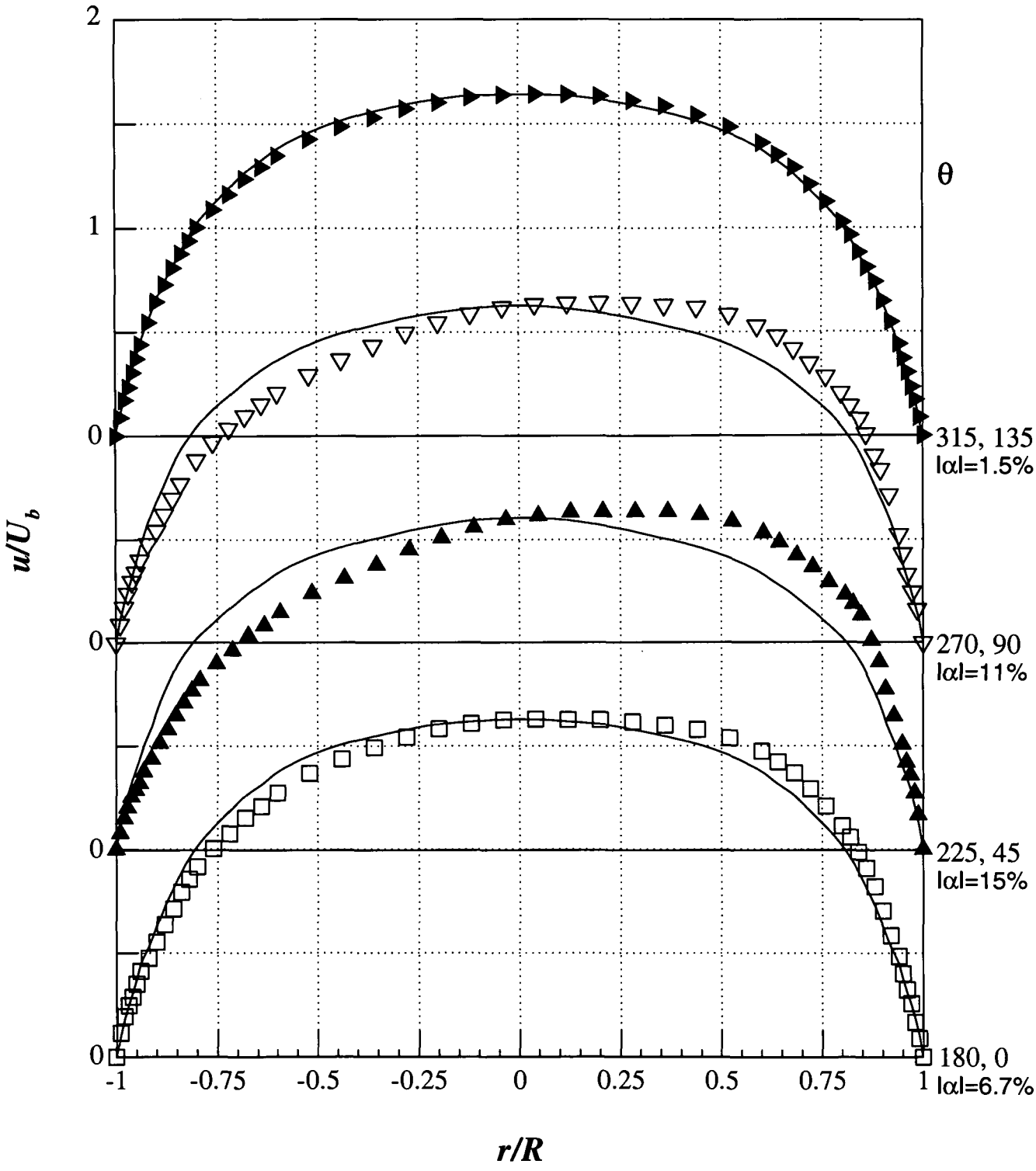

Figure 6.36 – Velocity profiles for different angles θ at Re_w = 10260 and x/D = 220, including averages (continuous lines), for 0.15% XG

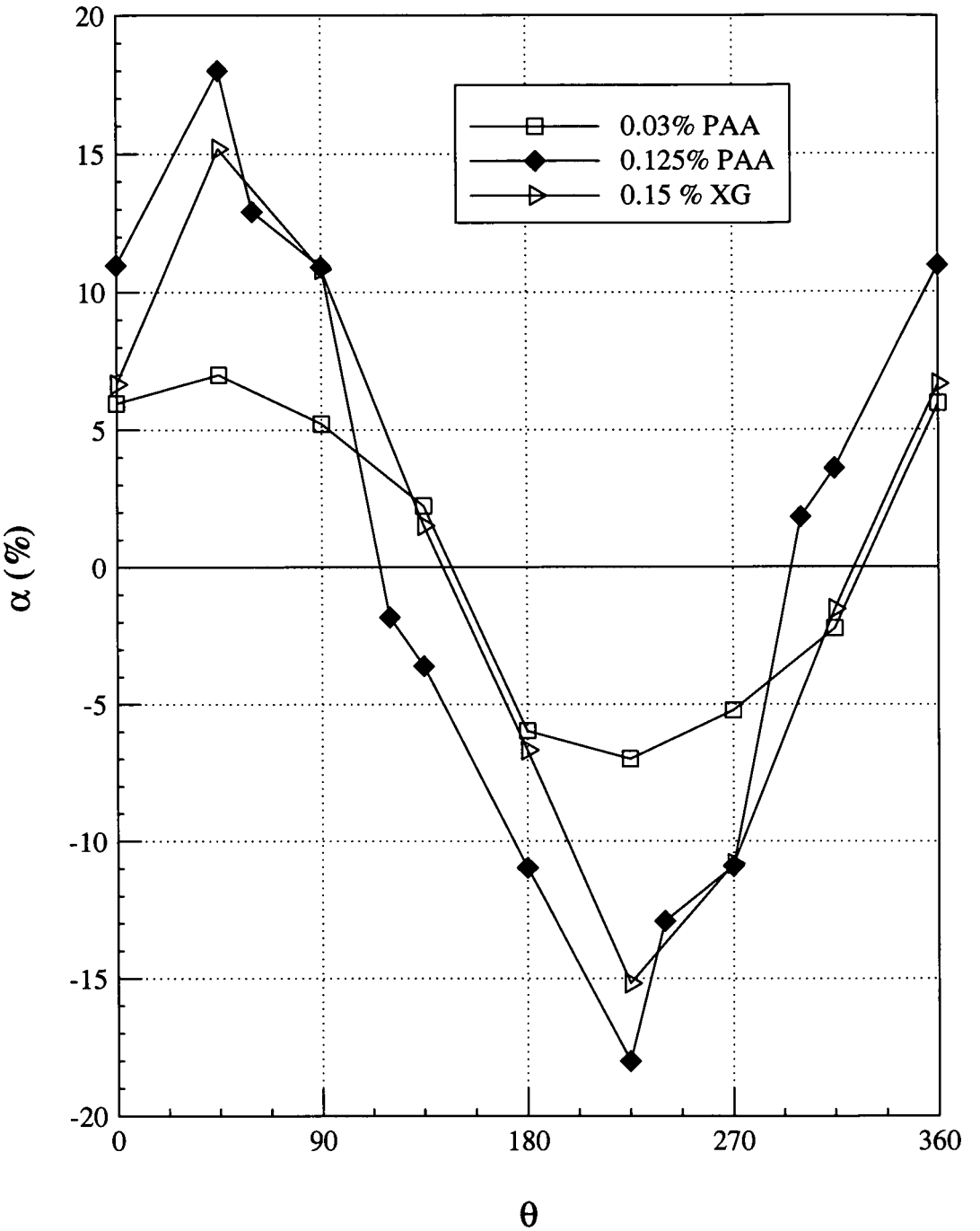

Figure 6.37 – Asymmetry comparison between 0.03% PAA (Re_w = 5780), 0.125% PAA (Re_w = 10140), and 0.15% XG (Re_w = 10260), at x/D = 220

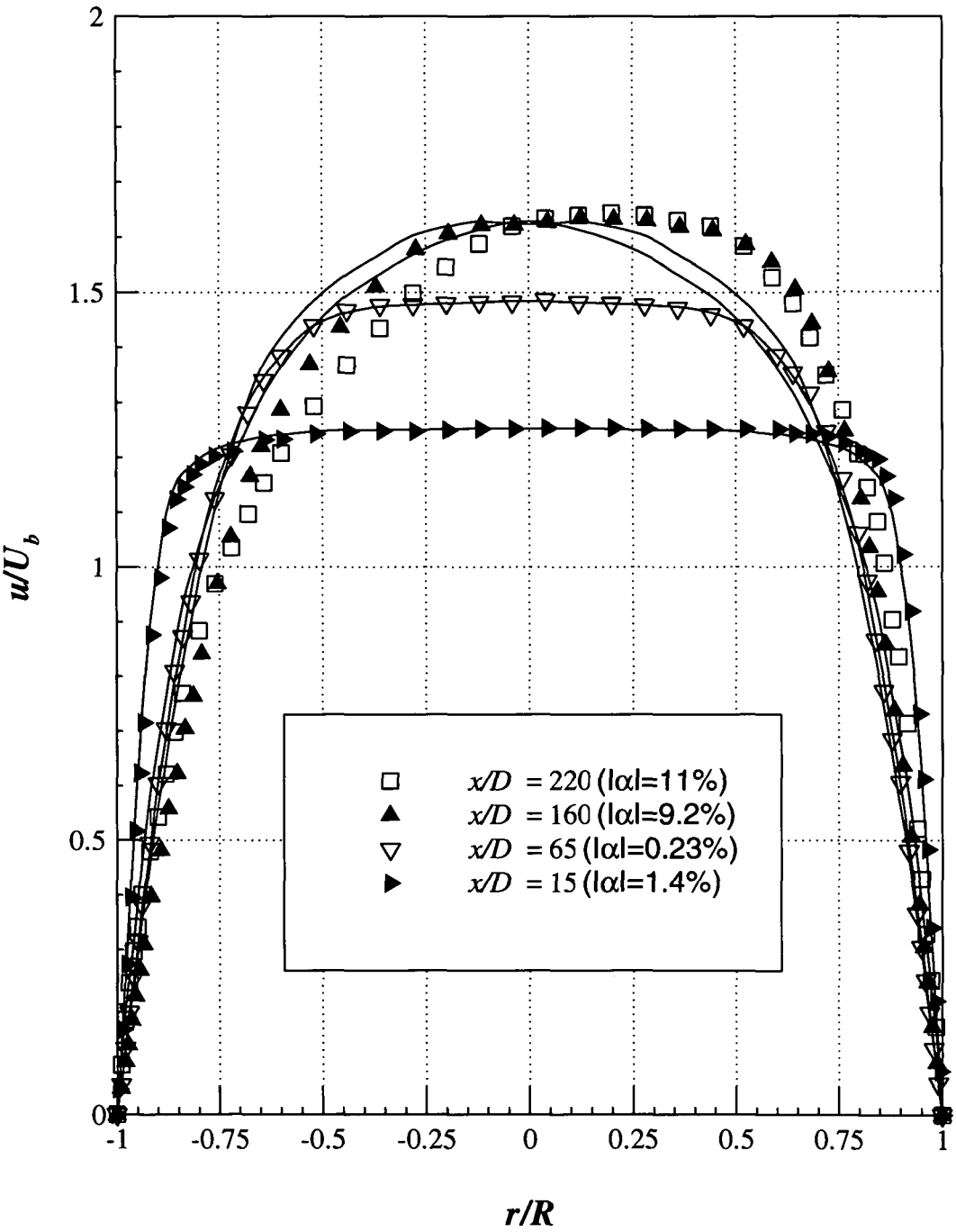

Figure 6.38 – Horizontal (θ = 90°, 270°) velocity profiles for different axial locations (x) at Re_w = 10260, including averages (continuous lines), for 0.15% XG

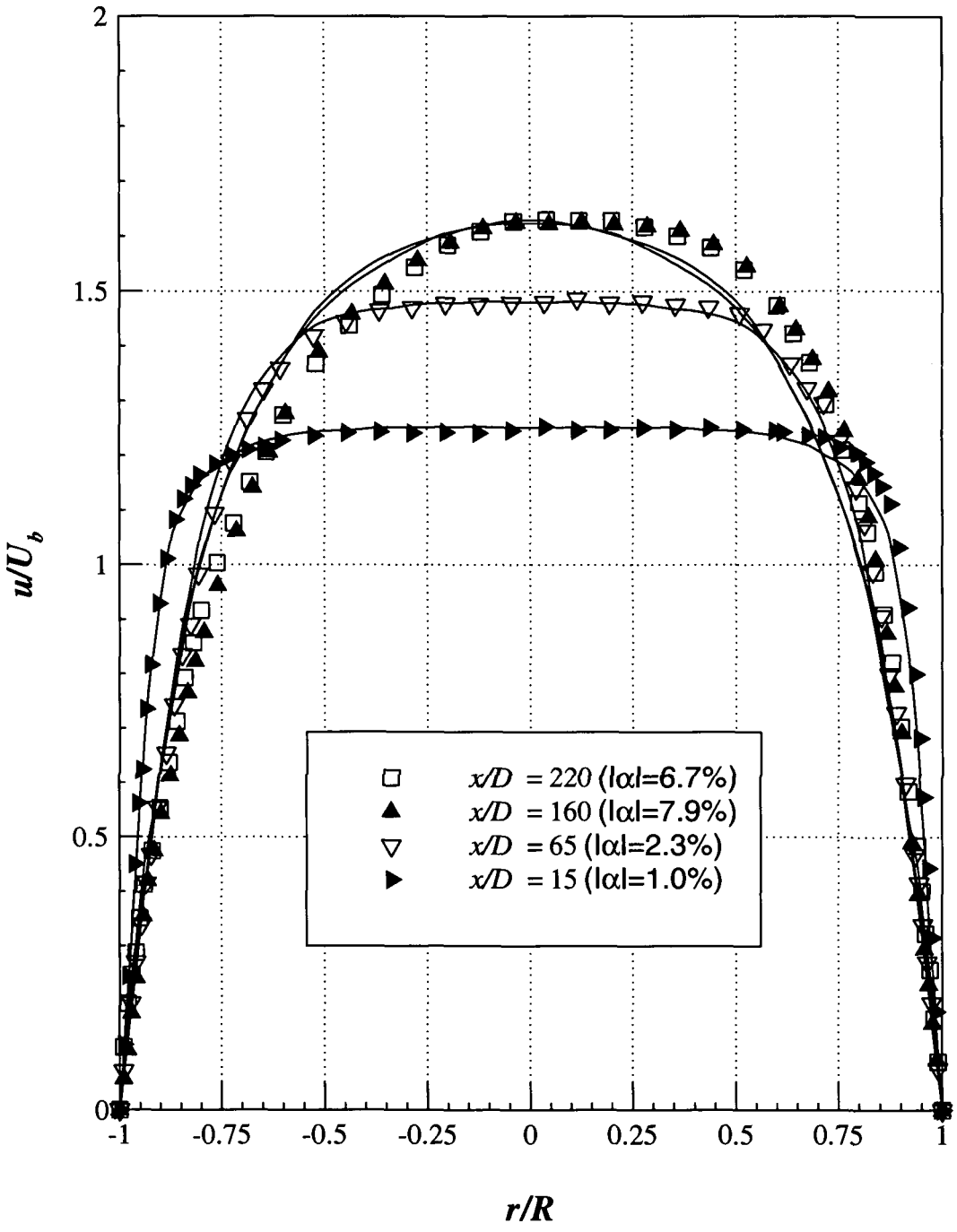

Figure 6.39 – Vertical (θ = 0°, 180°) velocity profiles for different axial locations (x) at Re_w = 10260, including averages (continuous lines), for 0.15% XG

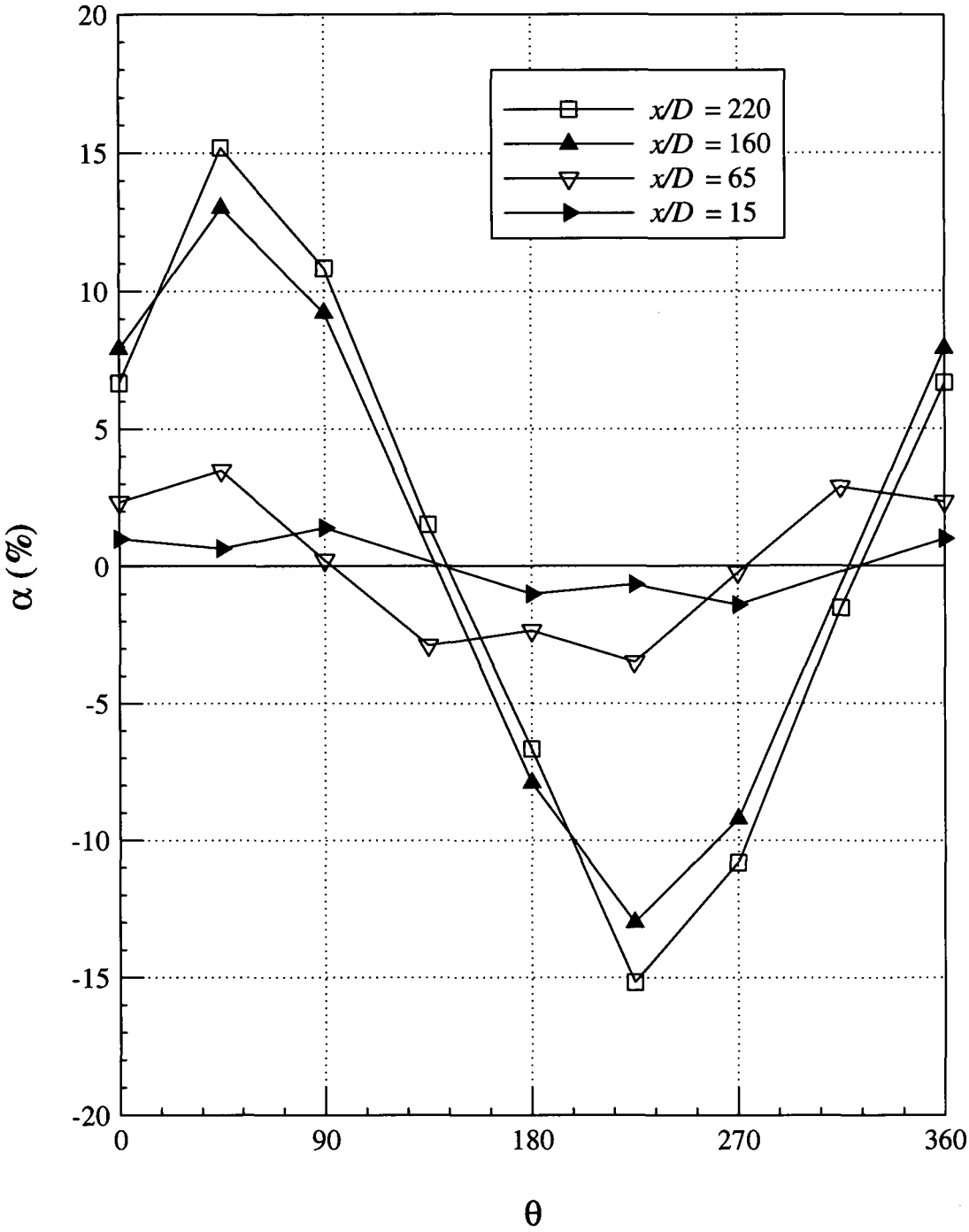

Figure 6.40 – Asymmetry for different axial locations (x) at Re_w = 10260, for 0.15% XG

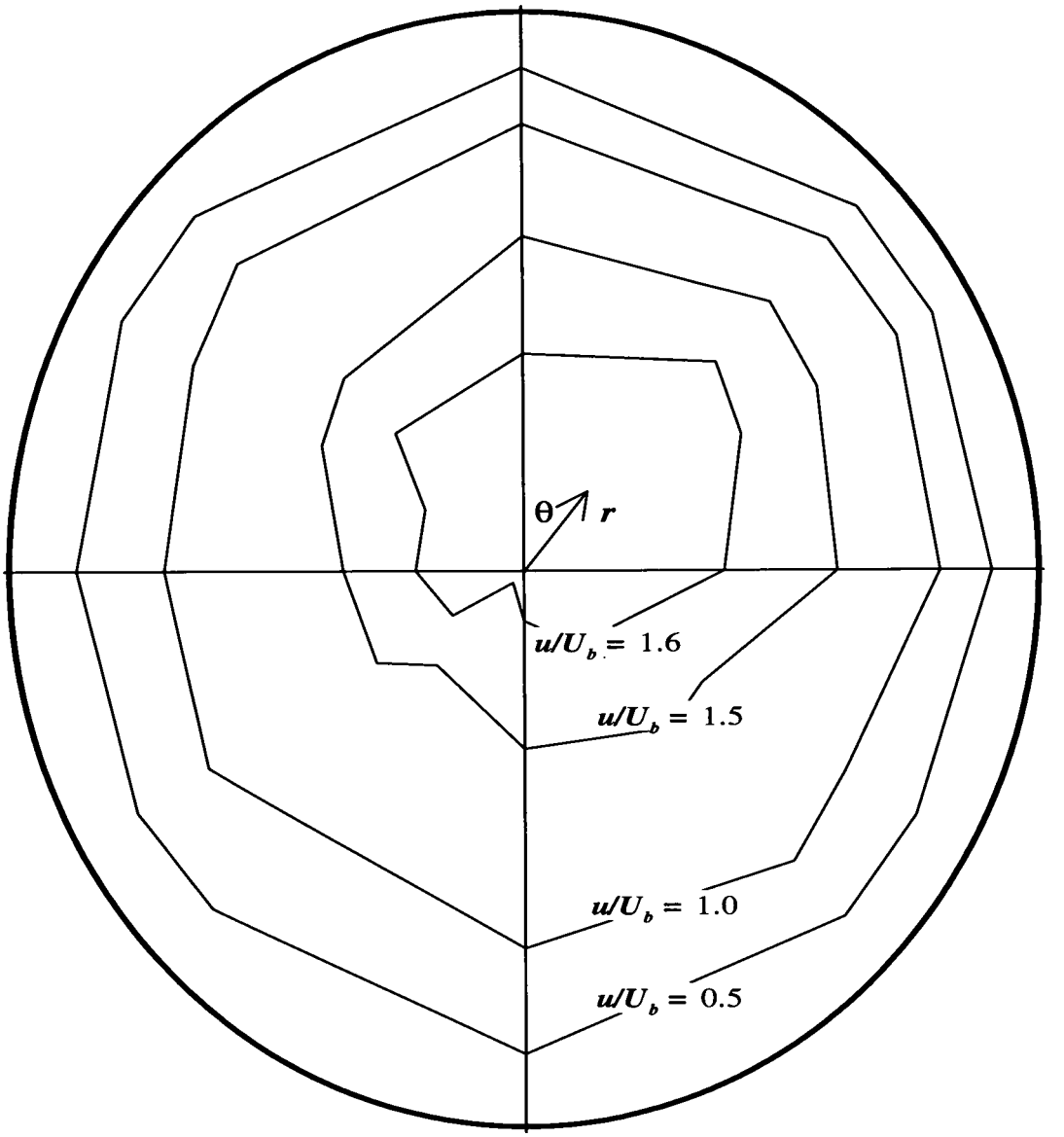

Figure 6.41 – Iso–(u / U_b) lines at Re = 10140 and x/D = 220, for 0.125% PAA

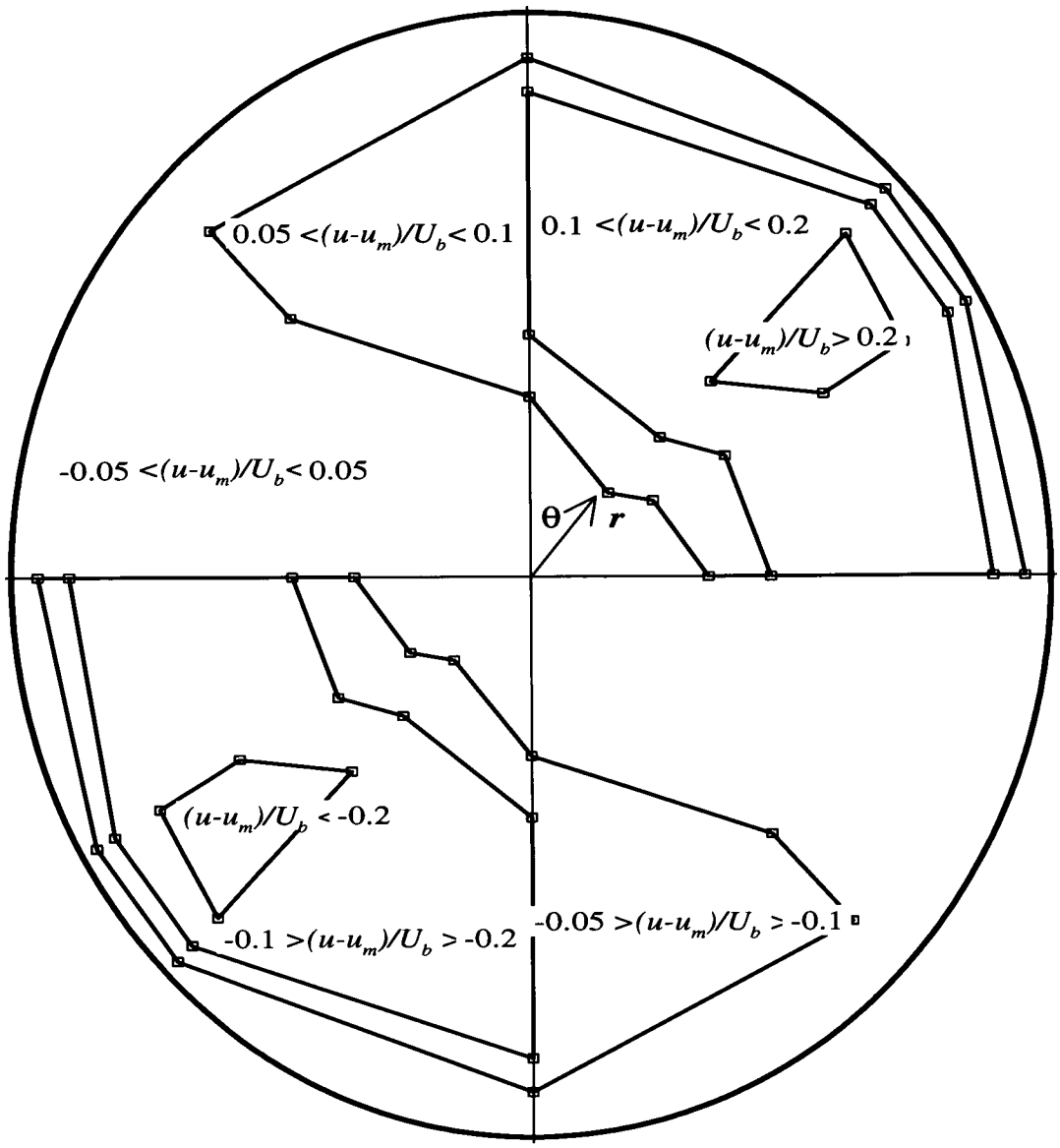

Figure 6.42 – Iso–$((u-u_m)/U_b)$ lines at Re = 10140 and x/D = 220, for 0.125% PAA

7 - Effect of changes to upstream and downstream conditions

7.1 – Introduction

This chapter is concerned with how changes in the flow conditions affected the asymmetry of the velocity profiles. The objective of these investigations was to better understand why the asymmetry appears and how the asymmetry evolves when the inlet and outlet conditions are changed. For simplicity, and its enhanced resistance to mechanical degradation, all of the results presented in this chapter are for the 0.15% XG solution.

7.2 – Outlet conditions

It is known that, due to the viscoelastic effect of liquids, changes in the outlet-flow conditions may affect the flow upstream, so we decided to make a change in the downstream geometry of the pipe facility, which consisted in rotating the pipe exit 90° in the anticlockwise direction. After making this change we started the experiments by detecting transition, which once again consisted in plotting u'/U_b, taken in the horizontal plane at r/R = - 0.8, against Re_W, as described in Section 4.4. **Figure 7.1** compares the results before and after rotation of the pipe exit and shows that changing the outlet does not influence the transition from laminar for turbulent flow. The small differences between the turbulence intensity levels are consistent with repetition of nominally identical conditions. Therefore, the following

measurements were carried out for the same transitional Reynolds number (Re_W = 10260) as in Chapter 6.

Figure 7.2 compares the velocity profiles for the two different outlet conditions. The profiles correspond to Re_W = 10260 (transitional regime) for different angles and were obtained at x/D = 220. From this figure and also from **Figure 7.3**, which compares the coefficient of asymmetry, we see that the velocity profiles have essentially the same asymmetry for both outlet flow conditions, and therefore conclude that the asymmetries are due to other flow or fluid characteristics rather than the outlet condition.

7.3 – Inlet conditions

The change in the entrance flow conditions consisted of placing an obstruction inside the plenum-chamber (**Figure 3.2**) in order to obstruct the flow in half of the pipe region between θ = 315° and θ = 135°, which is the region corresponding to the location of maximum velocity for the asymmetric profiles. For that propose we used a half-disc schematically shown in **Figure 7.4**. With this procedure it was possible to test the hypothesis of upstream disturbances affecting the velocity profiles.

An unwanted side affect of the obstruction was the change in the critical Reynolds number at which transition initiates. As pipe flow is linearly stable and therefore it is possible to delay transition to very large *Re*, it is well known that inlet effects can have a profound change on the critical Reynolds number for transition and that is

what we observed here. **Figure 7.5** shows how the location of the transitional regime was altered in terms of the Reynolds number range. As might be expected the transition from laminar to turbulent flow occurs earlier when the obstruction is placed in the chamber than without the obstruction. This conclusion can be reinforced by comparing the horizontal velocity profiles for the two inlet situations at the same Reynolds number (Re_W = 10260) as in **Figure 7.6**, which shows a velocity profile for the situation "with obstruction" with more a "turbulent-like" shape, flatter in the centre of the pipe, indicating earlier turbulent flow.

We have carried out measurements at Re_W = 10260 and x/D = 220 for different azimuthal angles and present the corresponding coefficient of asymmetry in **Figure 7.7** to compare with the previous measurements without the inlet obstruction. This figure also indicates that the "most transitional" Reynolds number is now lower than 10260. However it must be realised this figure is highlighting the change in critical Reynolds number not the effect of inlet conditions.

Figure 7.8 represents the velocity profiles in the horizontal plane for different Reynolds numbers at x/D = 220 with the obstruction in place. For this case (with obstruction) the most asymmetric profile is observed for Re_W = 7120, lower than Re_W = 10260 observed for the previous case (without obstruction). In spite of different degrees of asymmetry for these two different Reynolds numbers, the pattern of asymmetry remains the same. **Figure 7.9** shows the velocity profiles for the "maximum transition" Reynolds number for different azimuthal angles and **Figure 7.10** compares the corresponding coefficient of asymmetry with the results

obtained without the obstruction in place. It is clear that the levels and also the pattern of asymmetry do not change with different inlet flow conditions.

The evolution of the velocity profiles along the pipe, with obstruction in the transitional regime (Re_W = 7120) is shown in **Figures 7.11** and **7.12** for the horizontal and vertical planes, respectively. Again, the velocity profiles are basically symmetric until a certain axial location between x/D = 65 and x/D = 160 and then downstream become asymmetric (see **Figure 7.13**). It might be expected to see highly asymmetric velocity profiles for the farthest upstream location (x/D = 15) due to the presence of the obstruction, exhibiting higher velocity in the "side" between θ = 135° and θ = 315°. This was not the case, possible because the effect of the obstruction was limited to a region much closer to the inlet.

To conclude, inlet conditions do not influence the velocity profile asymmetry, the only influence observed was the earlier onset of transition due to the obstruction at the entrance, therefore the smoother the entrance condition the greater delay in transition is observed, in agreement with Leite (1959), amongst others.

7.4 – Other effects

As discussed in Escudier et al (2005), one other influence which could lead to velocity profile asymmetry is the curvature of the pipe axis. Dean (1927) investigated this influence and proposed the parameter, now termed the Dean number, and defined here as Dn to determine the strength of secondary flows due to curvature:

$$Dn = Re\left(\frac{D}{2R_A}\right)^{1/2} \tag{7.1}$$

where R_A is the radius of curvature of the pipe axis.

The longitudinal curvature of the pipe becomes important when Dn exceeds 40, which is not the case of the present study. For our pipe flow, a Dn value of 40 requires a R_A value lower than 139 m for a Reynolds number of 2110 (lowest Re_1). The maximum longitudinal curvature of our pipe is equal to 10^6 m (calculated in **Appendix**), which corresponds to a Dn less than 0.47. So, the longitudinal curvature of the pipe is too weak to induce asymmetry in our experiments.

The influence of the Coriolis acceleration due to combined effects of the Earth's rotation and the parallel flow is to generate a component of acceleration perpendicular to the pipe axis which leads to a distortion of the velocity profile (Draad and Nieuwstadt (1998)) but only in fully-developed laminar pipe flow. For transitional pipe flow conditions the inertia forces starts to play a role in the fluid-dynamics, thus, under such flow conditions the distortion of the velocity profile can-not be attributed to the Earth's rotation.

Temperature variations within the flow could influence the velocity profile shape (see for example Leite (1959)) due to buoyancy effects which occurs when a sustained uniform temperature gradient exists in the vicinity of the pipe, but we have monitored closely the temperature of the fluid inside the pipe and the temperature in the laboratory. During the experiments the temperature of the fluid varied between

18 and 22 °C and the difference between the temperature in the laboratory and the fluid was always lower than 5 °C. Therefore, distortions of the velocity profile observed in our study are not due to thermal effects. Also repetition of nominally identical runs, but at slightly different temperatures due to ambient conditions, produced identical asymmetries.

In addition none of the above effects (i.e. curvature, Coriolis and temperature) is consistent with the fact that all of the flows initially develop essentially axisymmetrically before the asymmetry sets in some distance downstream.

7.5 – Conclusions

In this chapter we presented experimental results obtained after changes to the upstream and downstream geometry of the pipe facility in order to be able to study the influence of each particular change on the axial velocity profiles. Unfortunately after all of these changes we could not pinpoint the exact cause which leads to asymmetry in the transitional flow regime for non-Newtonian liquids. We do not know the causes of the velocity profile asymmetries in non-Newtonian pipe flow within transitional flow, but now we do know what is most definitely not causing these asymmetries. The next chapter summarises the contents of this work and gives some conclusions in an attempt to better understanding the mechanism which leads to asymmetry and gives some recommendations for further investigations in this subject.

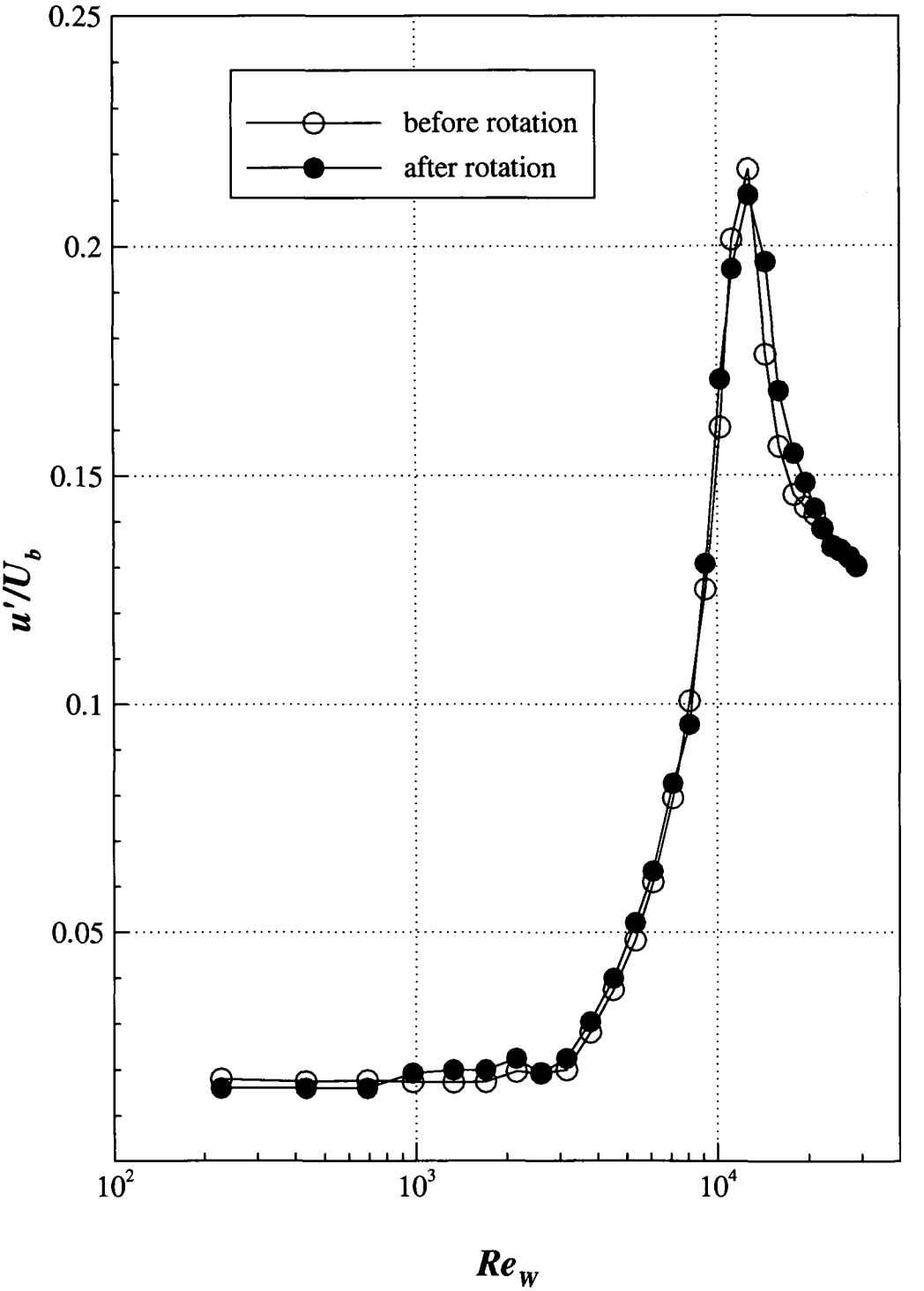

Figure 7.1 – Velocity fluctuations (u'/U_b) *versus* wall Reynolds number (Re_W) at r/R = - 0.8 for two different outlet conditions, for 0.15% XG

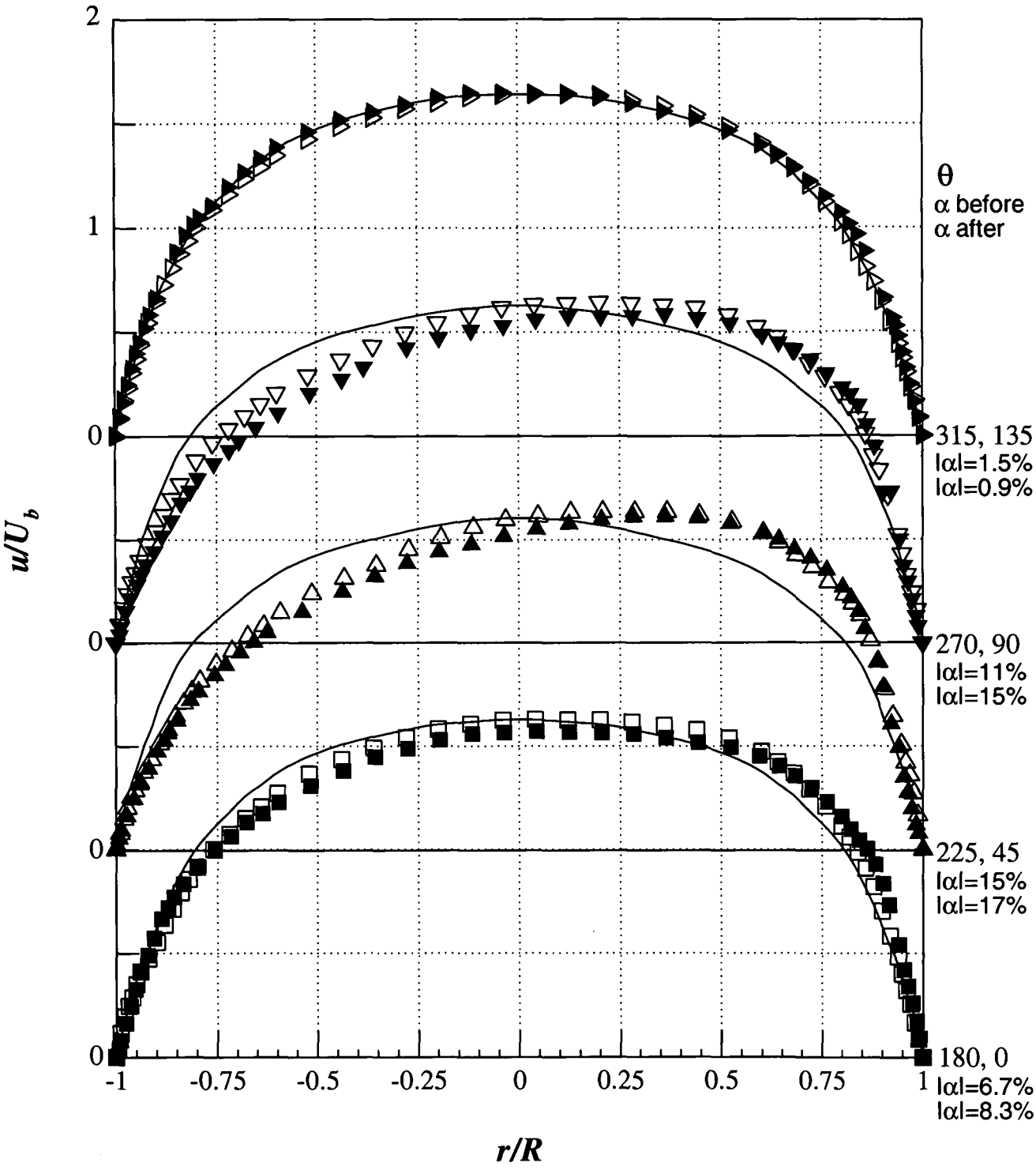

Figure 7.2 – Velocity profiles comparison between two different outlet conditions (before rotation: open symbols; after rotation: filled symbols), for different angles (θ) at Re_w = 10260 and x/D = 220, including averages (continuous lines), for 0.15% XG

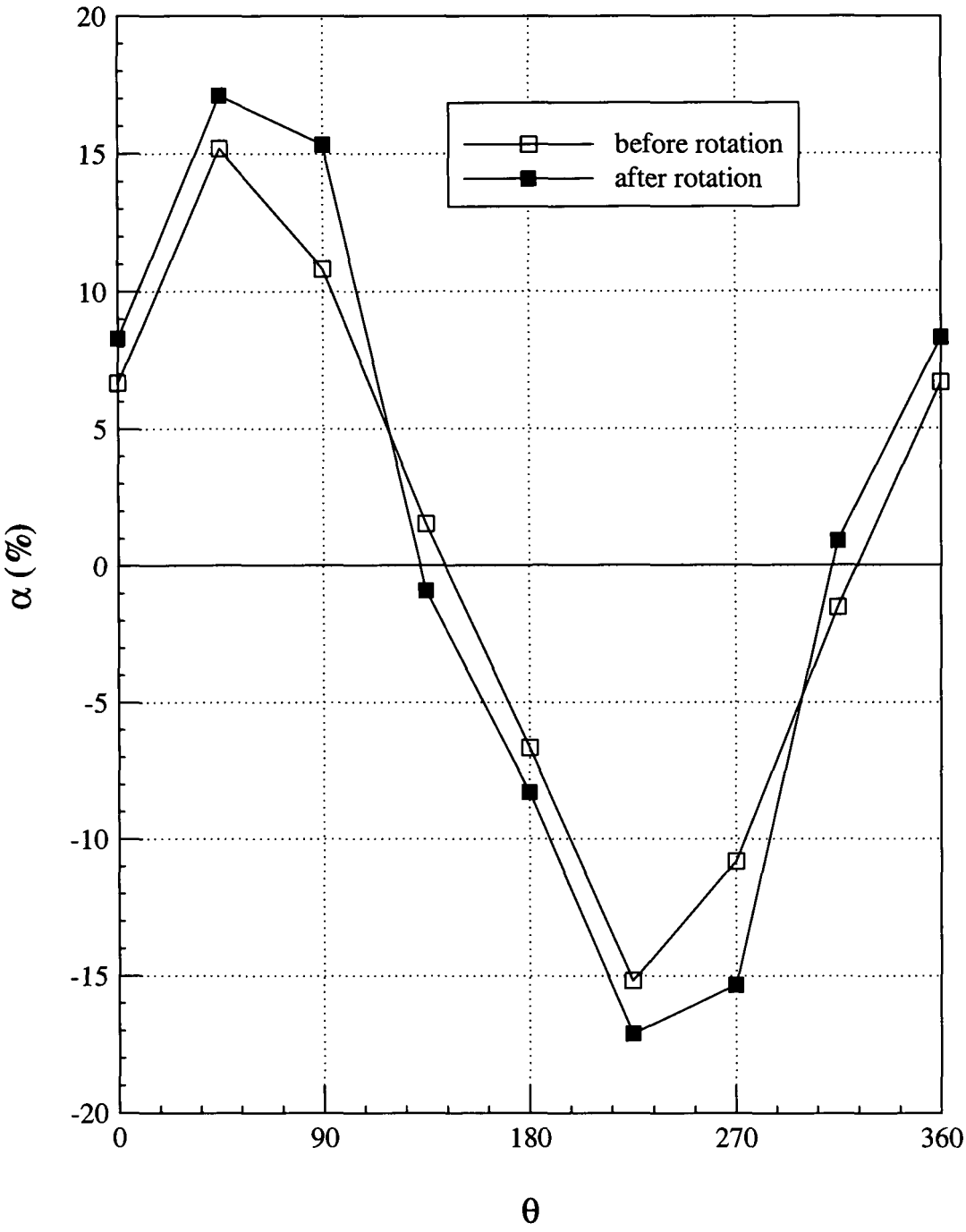

Figure 7.3 – Asymmetry comparison between different outlet conditions at Re_w = 10260 and x/D = 220, for 0.15% XG

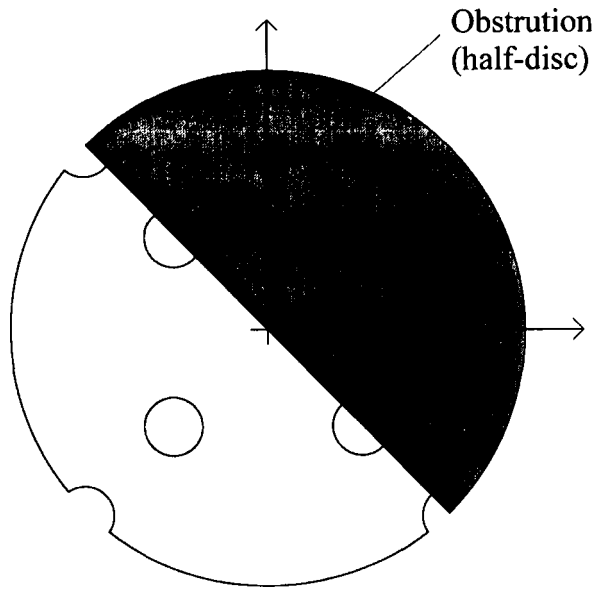

Figure 7.4 – Schematic of the obstruction in the plenum-chamber (flow into the page through the holes)

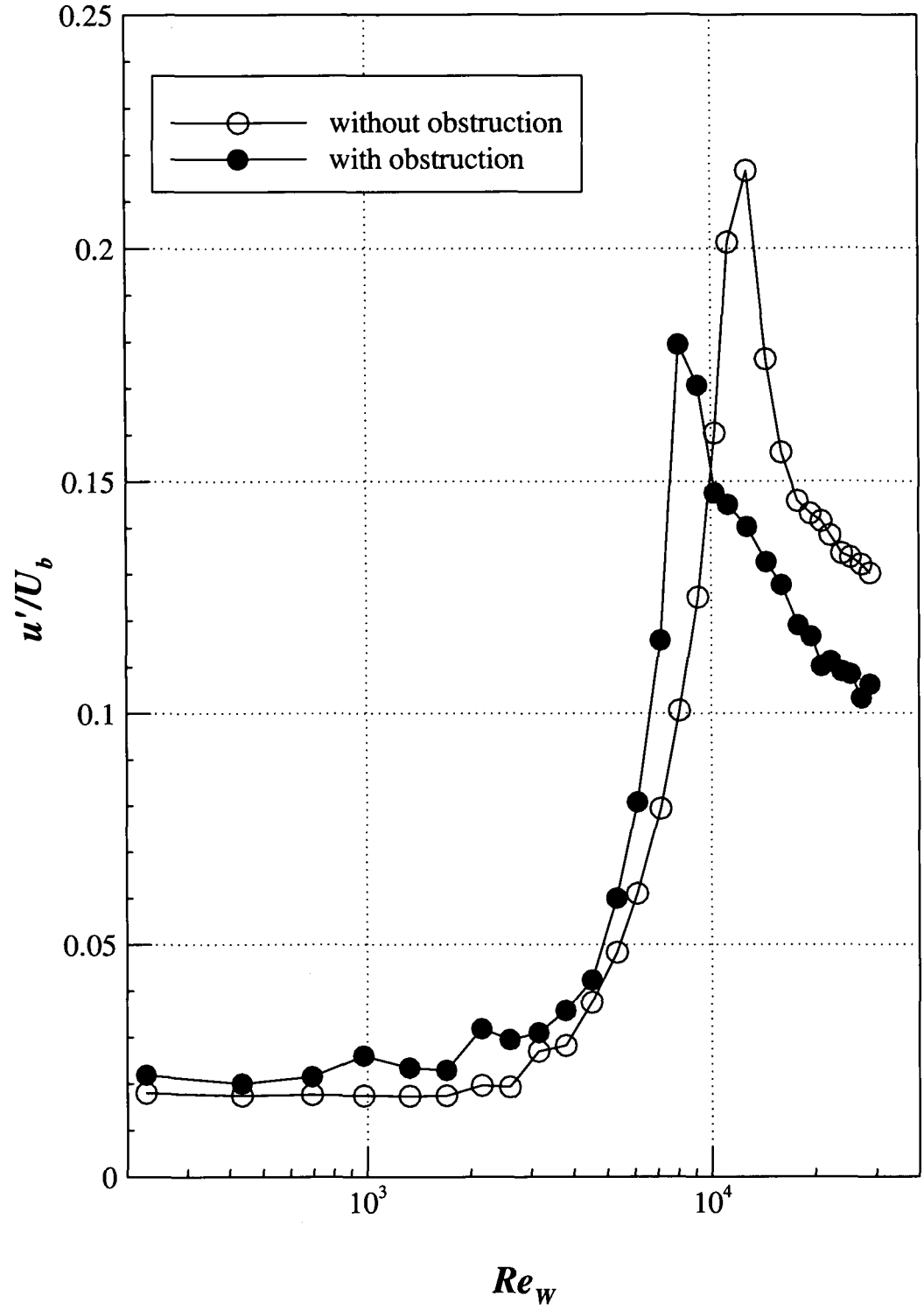

Figure 7.5 – Velocity fluctuations (u'/U_b) *versus* wall Reynolds number (Re_W) at r/R = - 0.8 for two different inlet conditions, for 0.15% XG

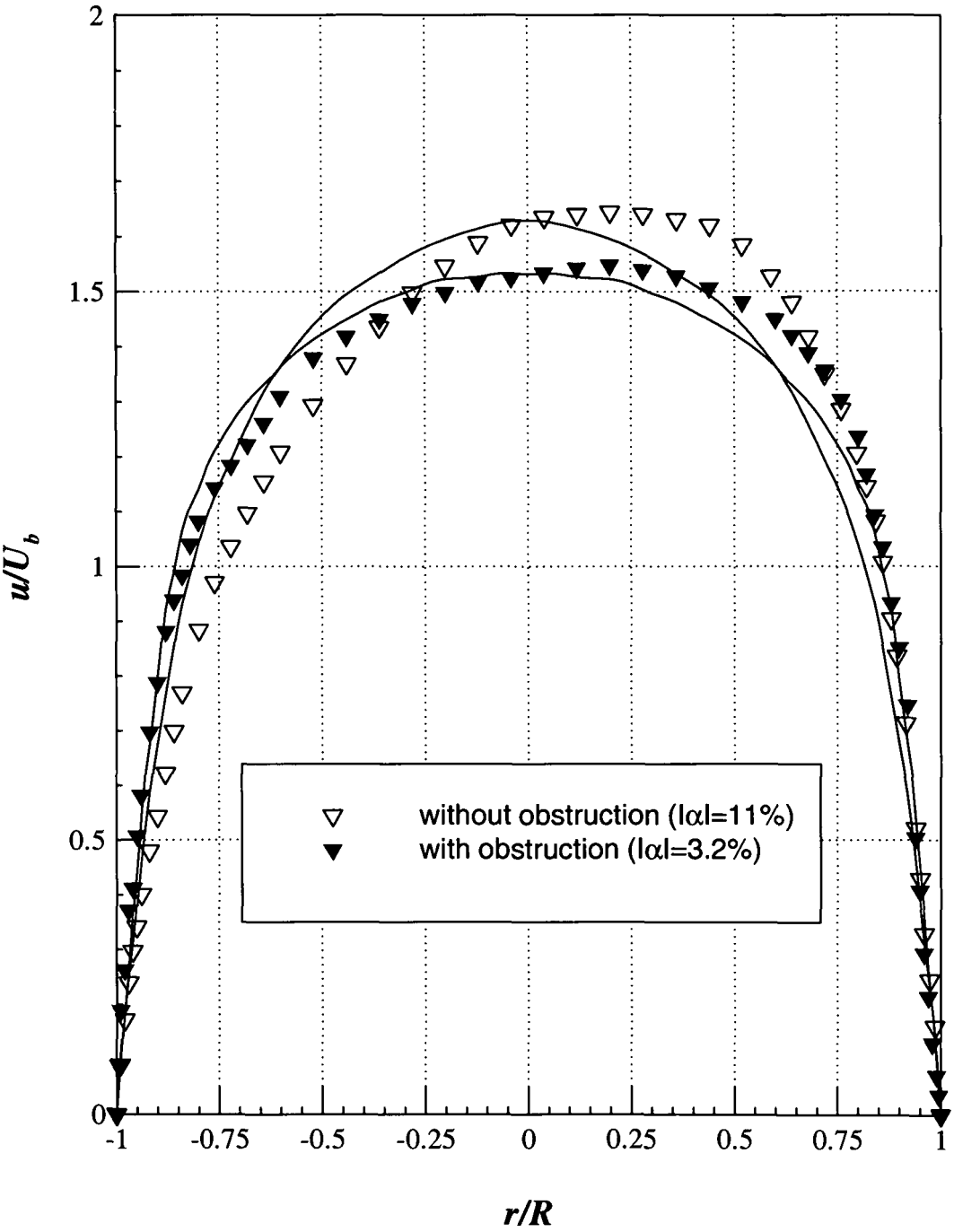

Figure 7.6 – Horizontal (θ = 90°, 270°) velocity profile comparison for different inlet conditions at Re_w = 10260 and x/D = 220, including averages (continuous lines), for 0.15% XG

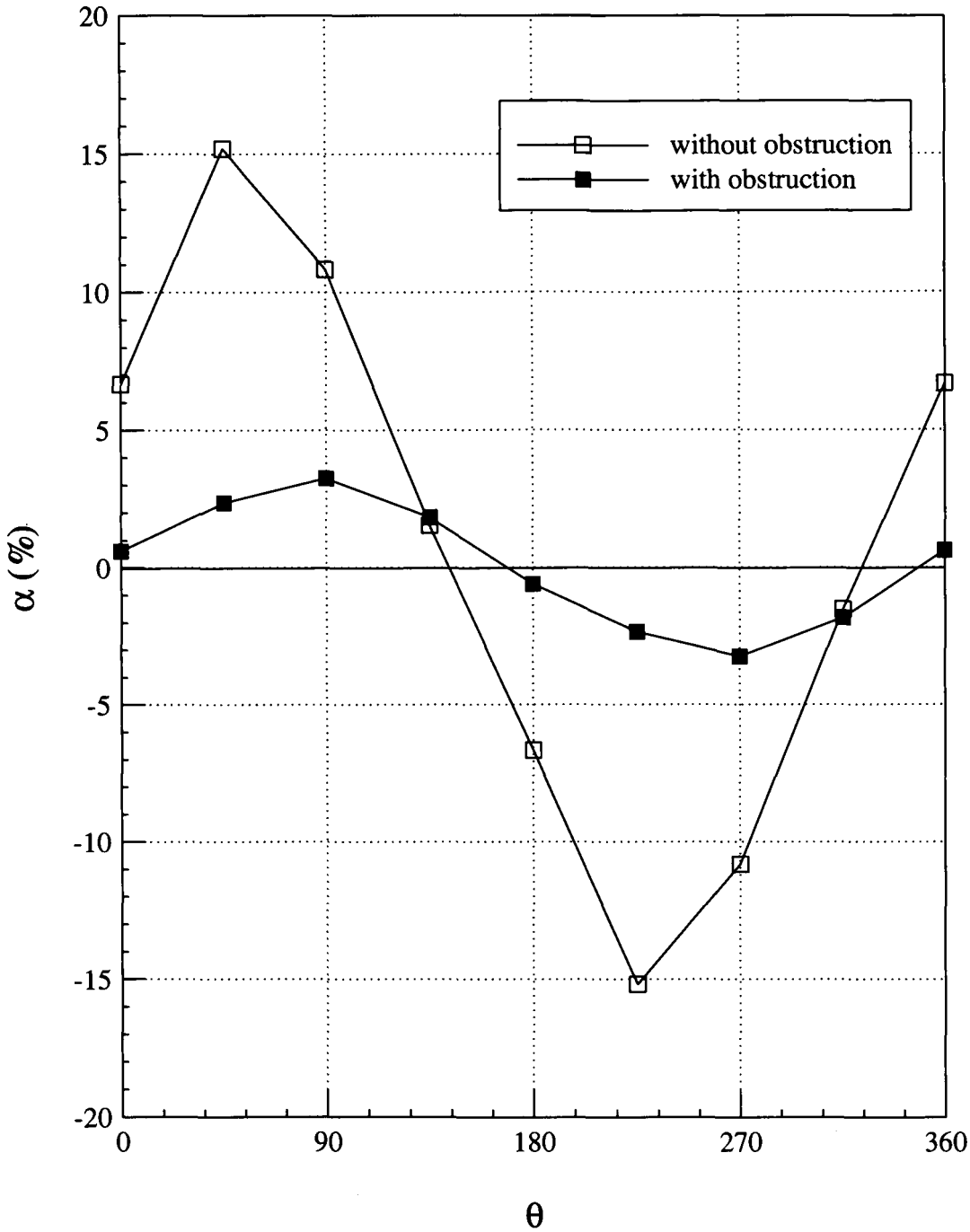

Figure 7.7 – Asymmetry comparison between two different inlet conditions at Re_w = 10260 and x/D = 220 D, for 0.15% XG

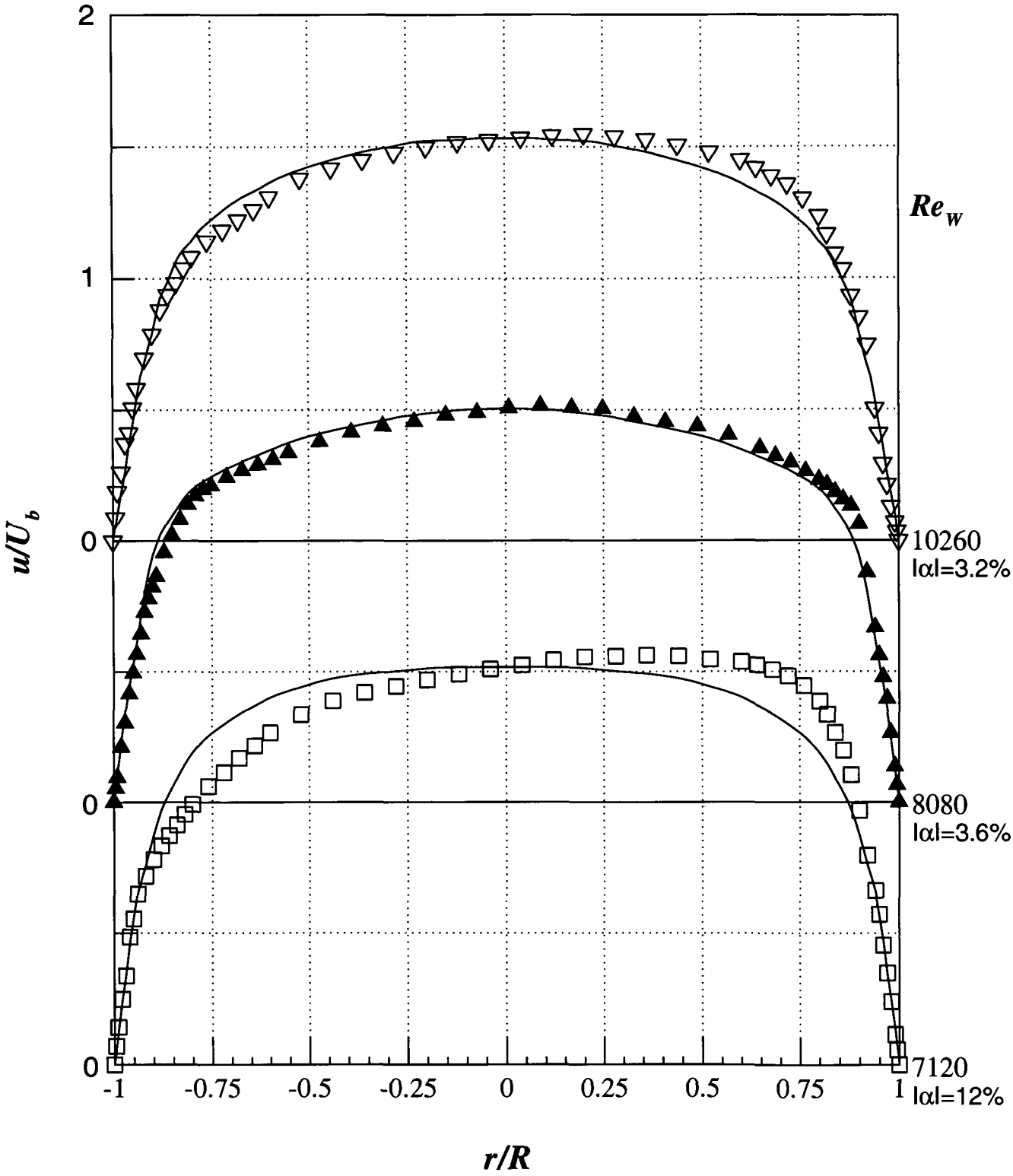

Figure 7.8 – Horizontal (θ = 90°, 270°) velocity profiles for different Reynolds number at x/D = 220 with obstruction at entrance, including average (continuous lines), for 0.15% XG

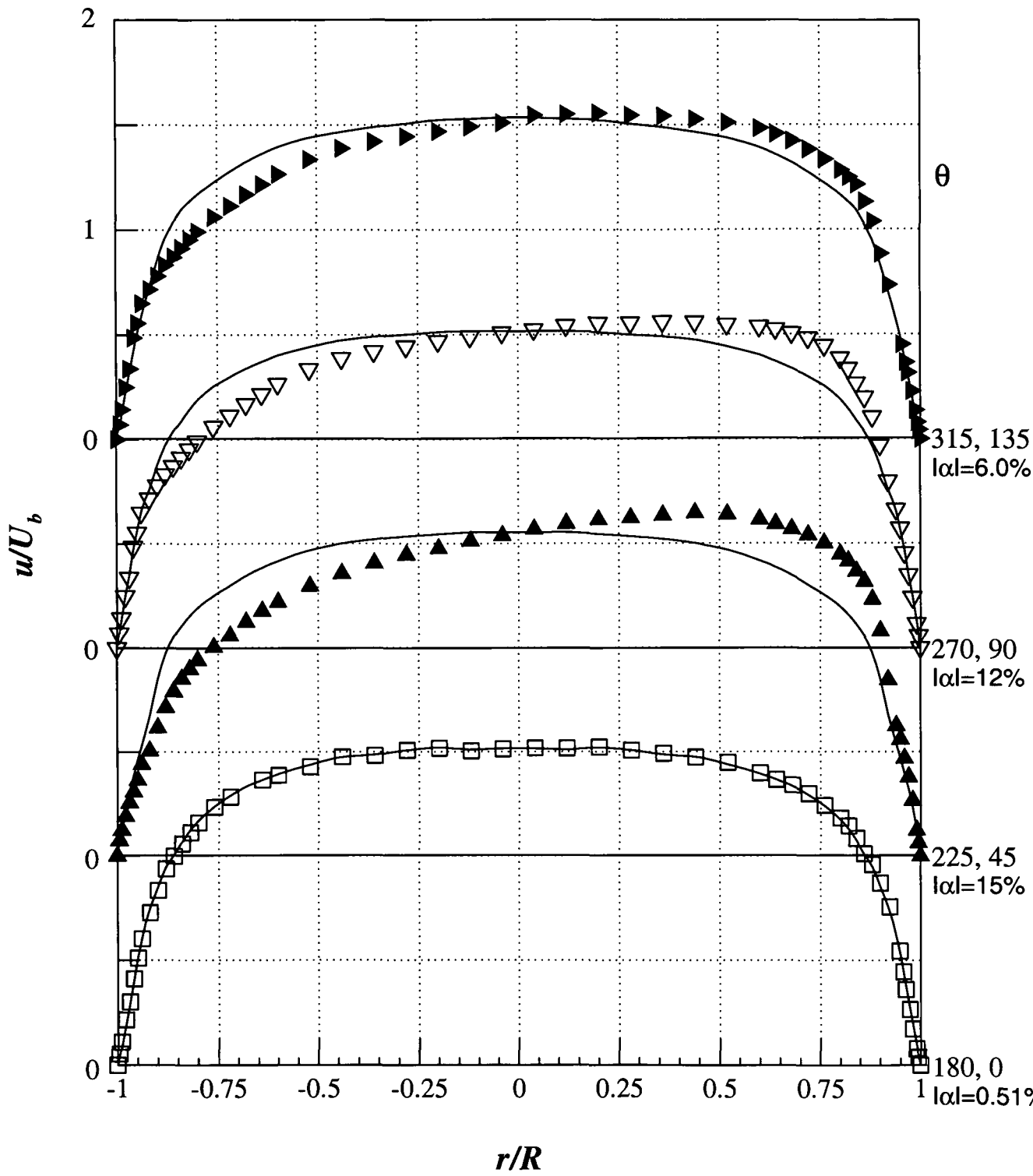

Figure 7.9 – Velocity profiles for different angles (θ) at Re_w = 7120 and x/D = 220, with obstruction at entrance, including averages (continuous lines), for 0.15% XG

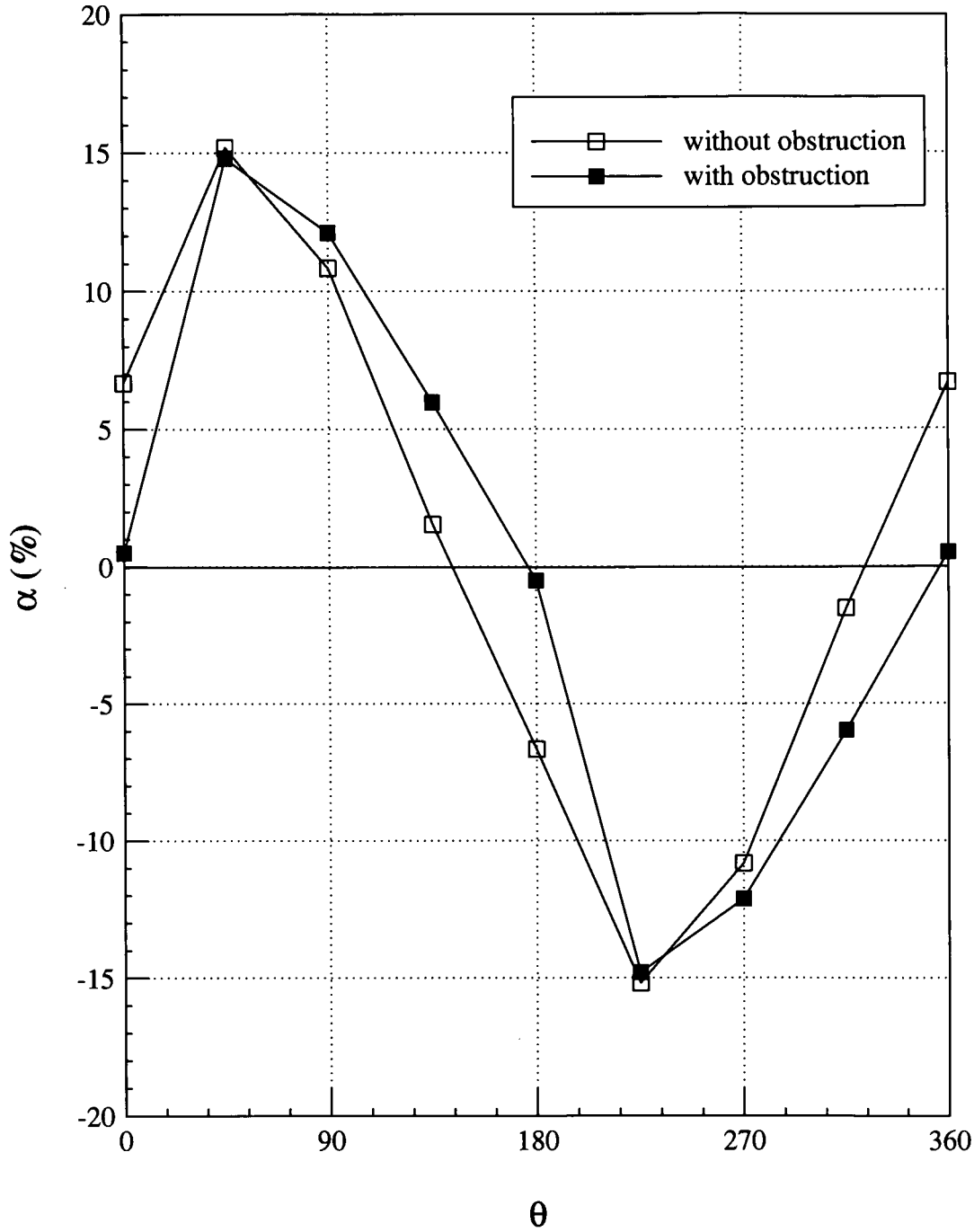

Figure 7.10 - Asymmetry comparison between different inlet conditions (with and without obstruction, Re_w = 7120 and Re_w = 10260, respectively) at x/D = 220, for 0.15% XG

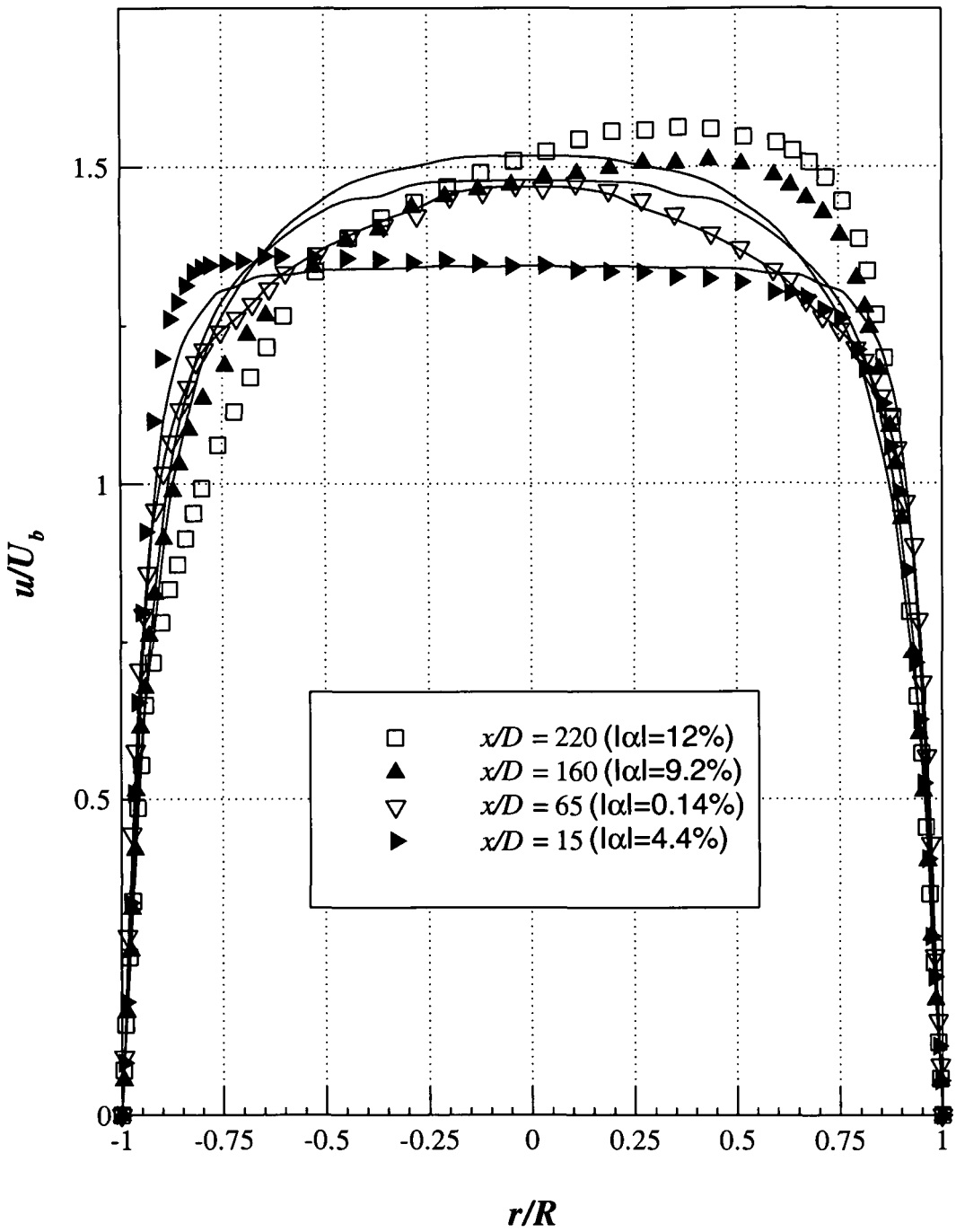

Figure 7.11 – Horizontal (θ = 90°, 270°) velocity profiles for different axial locations (x) at Re_w = 7120, with obstruction at entrance, including averages (continuous lines), for 0.15% XG

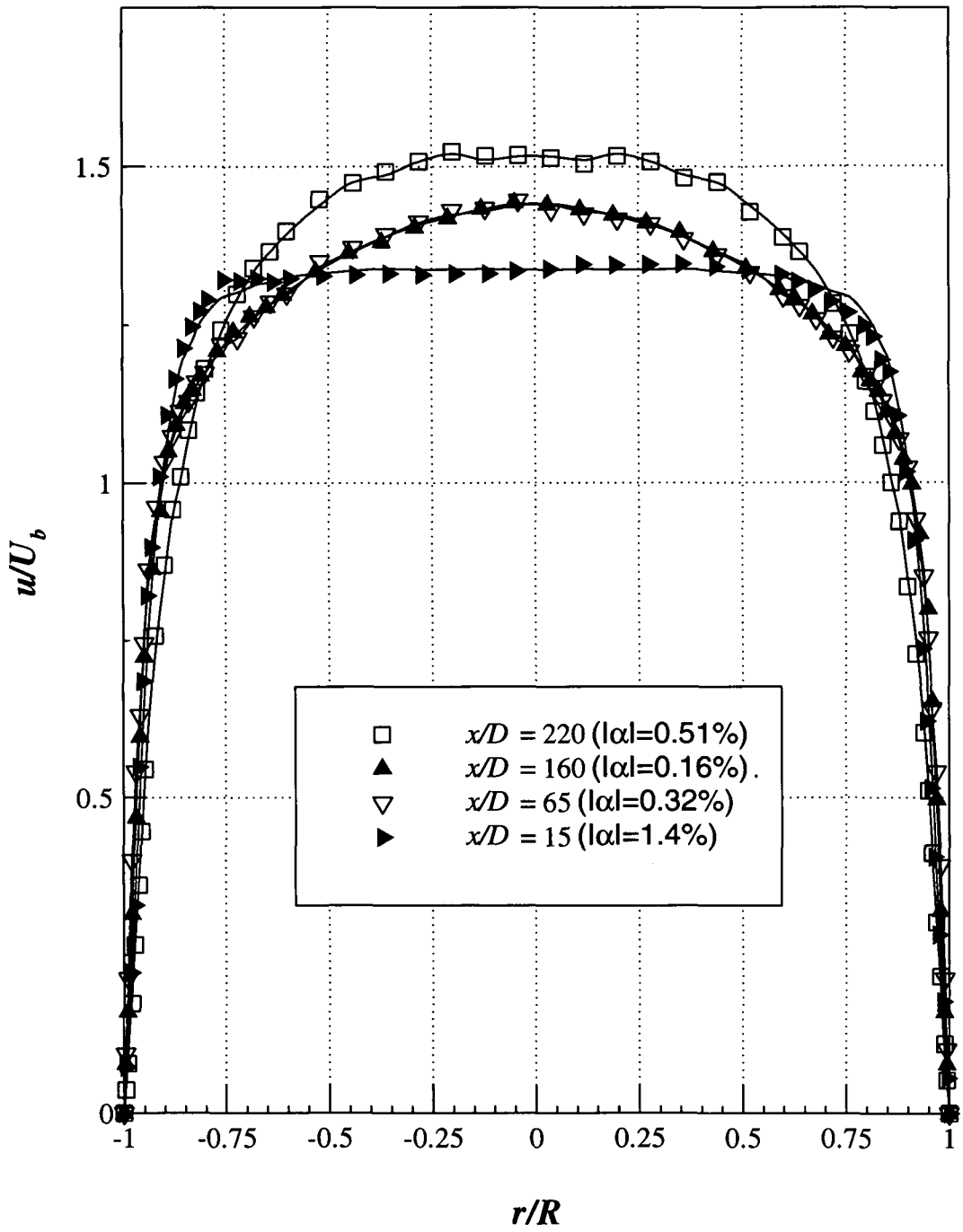

Figure 7.12 – Vertical (θ = 0°, 180°) velocity profiles for different axial locations (x) at Re_w = 7120, with obstruction at entrance, including averages (continuous lines), for 0.15% XG

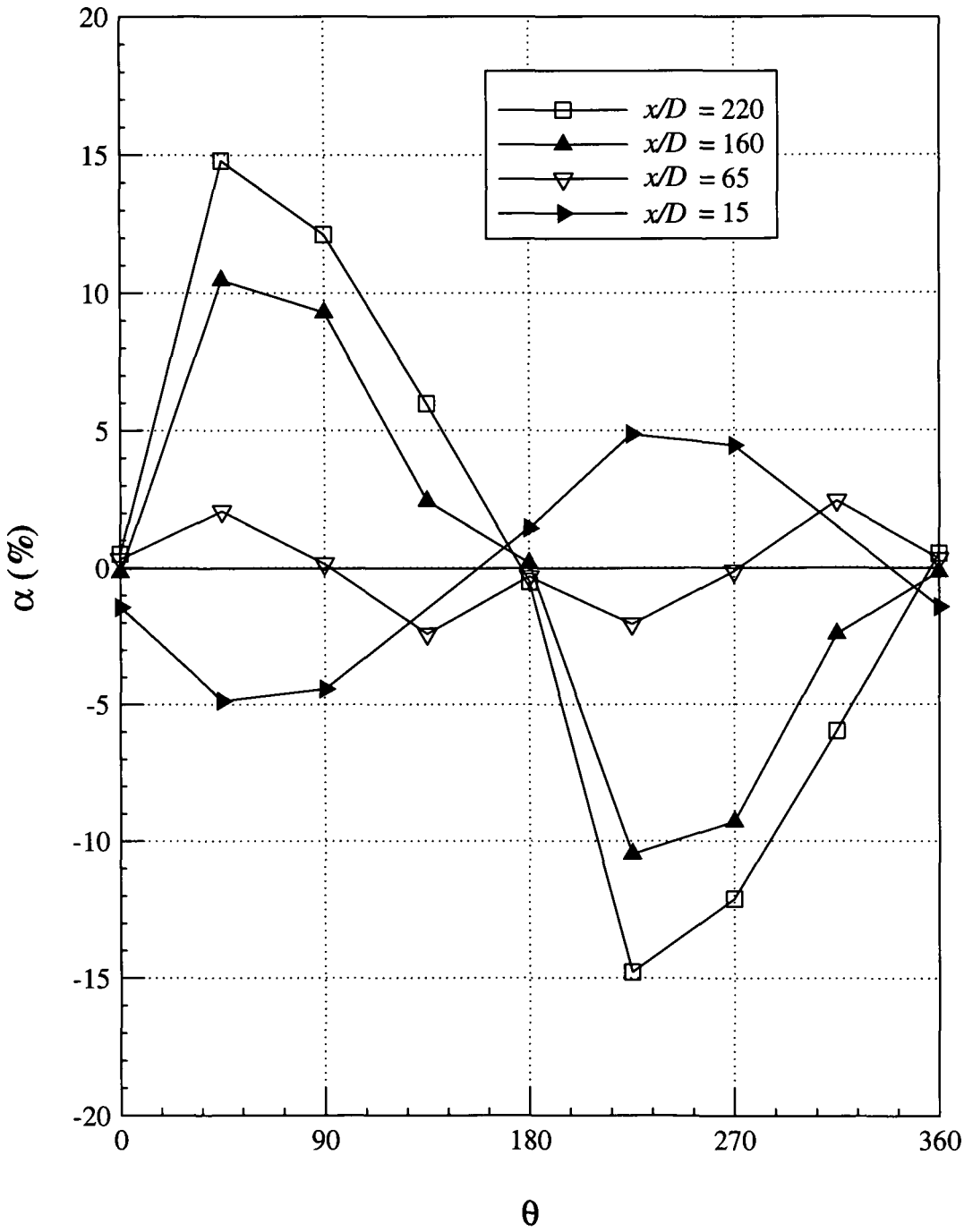

Figure 7.13 – Asymmetry for different axial locations (x) at Re_w = 7120, with obstruction at entrance, for 0.15% XG

8 – Conclusions

8.1 – Introduction

This chapter summarises the contribution of this thesis to the knowledge of transitional pipe-flow behaviour of non-Newtonian fluids. The next section provides a brief overview of the rheological assessments carried out for all working fluids. In Section 8.3 the main findings and achievements of this investigation are summarised, based on the pipe-flow measurements presented and discussed in Chapters 5 to 7. Finally, Section 8.4 presents some ideas with the intention of better understanding the mechanism which leads to the velocity profile asymmetry and identifies those areas in which further work should proceed.

8.2 – Working fluids

All non-Newtonian liquids investigated displayed time-independent shear-thinning characteristics, well represented by the Carreau-Yasuda model. The 0.03% PAA solution exhibited a shear-thinning characteristic of lower magnitude than the 0.125% PAA and 0.15% XG solutions. The 0.15% XG solution was chosen because it has a similar viscometric flow curve to 0.125% PAA but with markedly different elasticity. Comparing the viscometric flow curves of 0.125% PAA and 0.15% XG (see **Figure 2.4**) it is possible to conclude that both solutions have similar shear-thinning behaviour, however it is well known that PAA has a higher elastic behaviour than XG. In contrast with 0.125% PAA, the elastic component N_1 for

0.15% XG was so low that it could not be measured as it was below the resolution of the rheometer.

The working fluids selected for this study were reasonably resistant to degradation effects, showing negligible changes in viscosity before and after each test. They are also non-toxic and optically clear (transparent).

8.3 – Measurements

Transition from laminar to turbulent flow could be consistently detected by the axial velocity fluctuation measured at a fixed radial location (0.8 times the pipe radius). This method is particularly valuable when the non-Newtonian liquid has a high degree of drag reduction with little, or no, indication of transition from the $f - Re_w$ curve. Nevertheless, this method to detect transition is not perfect because it does not takes into account the fact that, for an asymmetric flow, the axial velocity measured at a fixed radial location (r/R = 0.8), varies with the azimuthal angle (θ) and consequently the associated velocity fluctuation (u') also varies. For example, for a particular Re close to transition, the level of velocity fluctuation measured at the horizontal plane can indicate that the flow is still within the laminar regime; however, at a different plane with higher level of velocity fluctuation would suggest already the presence of the transitional regime. Our measurements also highlight the dangers of assuming axisymmetric flow based on measurements in a single plane.

A strong mean-flow asymmetry was observed in the transition regime and only for non-Newtonian fluids. This effect was not seen for the Newtonian liquid or for the laminar and turbulent regimes ($Re < Re_1$ and $Re > Re_2$), where the mean axial velocity profiles remained symmetrical. For non-Newtonian liquids, at low Reynolds number the flow remained laminar and the velocity profiles symmetric, but as the Reynolds number increased, leaving laminar and entering the transitional regime, a progressive asymmetry developed, and then progressively decreased returning to symmetric flow as the turbulent regime was reached.

The peak velocity profile was shifted to the right quadrant of the pipe, around 45°, with a corresponding maximum negative shift in velocity profile in the bottom left quadrant. This variation of the asymmetry with azimuthal angle was observed for all non-Newtonian fluids investigated and all of them followed the same pattern of degree of asymmetry.

Outlet and inlet conditions do not have an influence on velocity profile asymmetry, hence different inlet and outlet conditions produced the same intensity and pattern of asymmetry, and other effects such as the Earth's rotation, curvature of the pipe and temperature also had a negligible influence.

The degree of asymmetry is shear-thinning dependent, because non-Newtonian liquids with similar shear-thinning and different elastic behaviour, 0.125% PAA and 0.15% XG, showed similar values of asymmetry, but higher than 0.03% PAA, suggesting that asymmetry increases with shear-thinning behaviour. Elasticity does not influence the degree of symmetry of the velocity profiles, the higher elastic

behaviour of the 0.125% PAA solution produced the same degree of asymmetry as the 0.15% XG solution.

It is also worthwhile for us to highlight here that this experimental work produced consistent and reproducible results. This can be confirmed by the excellent reproducibility of the axial velocity at the centreline of the pipe, sometimes with time differences between experiments longer than two months. Despite the insights that the investigation reported in this thesis offers, clearly much further work needs to be conducted before the full understanding of the mechanism of transition from laminar to turbulent pipe flow of non-Newtonian fluids can be approached.

8.4 - Further work

All non-Newtonian liquids exhibit a centreline peak velocity shifted to the upper right quadrant of the pipe and none shifted to the left. This suggests that the stability of the mean velocity profiles (degree of symmetry) could be associated with some slight pipe misalignments. Therefore, this point must be investigated further by producing different misalignments of the pipe and checking asymmetries.

Further investigation using a wide range of non-Newtonian fluids is required to better understand the influence of the rheological characteristics on the dynamics of the transitional regime. This investigation indicates that the velocity profile asymmetry is somehow linked with the shear viscosity and not with the elasticity of the liquid.

References

R. J. Adrian (1983), *Laser velocimetry in fluid mechanics measurements.* Ed R. J. Goldstein, Springer-Verlag.

A. Argumedo, T. T. Tung and K. I. Chang (1978), *Rheological property measurements of drag-reducing Polyacrylamide solutions.* Journal of Rheology, 22(5), 449.

H. A. Barnes, J. F. Hutton and K. Walters (1989), *An introduction to rheology.* Elsevier, Amsterdam.

H. A. Barnes (2000), *A Handbook of elementary rheology.* Institute of Non-Newtonian Fluid Mechanics, University of Wales, Aberystwyth.

R. B. Bird, R. C. Armstrong and O. Hassager (1996), *Dynamics of polymeric liquids.* Volume 1, John Wiley & Sons.

D. V. Boger (1977), *A highly elastic constant-viscosity fluid.* Journal of Non-Newtonian Fluid Mechanics, 3, 87.

R. P. Chhabra and J. F. Richardson (1999), *Non-Newtonian flow in process industries: fundamentals and engineering applications.* Butterworth-Heinemann, Oxford.

S. U. S. Choi, Y. I. Cho and K. E. Kasza (1992), *Degradation effects of dilute polymer solutions on turbulent friction and heat transfer behaviour.* Journal of Non-Newtonian Fluid Mechanics, 41, 289.

J. S. Chung and W. P. Graebel (1972), *Laser anemometer measurements of turbulence in non-Newtonian pipe flows.* The Physics of Fluids, 15, 546.

M. Collins and W. R. Schowalter (1963), *Behavior of non-Newtonian fluids in the inlet region of a channel.* AIChE Journal, 9, 98.

M. M. Cross (1965), *Rheology of non-Newtonian fluids: a new flow equation for pseudo-plastic systems.* Journal of Colloid Science, 20-5, 417.

A. G. Darbyshire and T. Mullin (1995), *Transition to turbulence in constant-mass-flux pipe flow.* Journal of Fluid Mechanics, 289, 83.

W. R. Dean (1927), *Note on the motion of a fluid in a curved pipe.* Philosophical Magazine, 4, 208.

C. D. Dimitropoulos, R. Sureshkumar and A. N. Beris (1998), *Direct numerical simulation of viscoelastic turbulent channel flow exhibiting drag reduction: effect of the variation of rheological parameters.* Journal of Non-Newtonian Fluid Mechanics, 79, 433.

P. Dimotakis (1976), *Single scattering particle laser-Doppler measurements of turbulence.* Applications of non intrusive instrumentation in fluid flow research, Agard conference, N. 193, paper 10.

D. W. Dodge and A. B. Metzner (1959), *Turbulent flow of non-Newtonian systems.* AIChE Journal, 5-2, 189.

A. A. Draad (1996), *Laminar-turbulent transition in pipe flow for Newtonian and non-Newtonian fluids.* PhD thesis, Delft University of Technology, Netherlands.

A. A. Draad and F. Nieuwstadt (1998), *The Earth's rotation and laminar pipe flow.* Journal of Fluid Mechanics, 361, 297.

A. A. Draad, G. D. C. Kuiken and F. T. M. Nieuwstadt (1998), *Laminar-turbulent transition in pipe flow for Newtonian and non-Newtonian fluids.* Journal of Fluid Mechanics, 377, 267.

F. Durst, A. Melling and J. H. Whitelaw (1981), *Principles and practise of laser Doppler anemometry.* Academic Press (London), second edition.

F. Durst, R. Haas and W. Interthal (1982), *Laminar and turbulent flows of dilute polymer solutions: a physical model.* Rheologica Acta, 21, 572.

F. Durst, S. Ray, B. Unsal and O. A. Bayoumi (2005), *The development lengths of laminar pipe and channel flows.* Journal of Fluids Engineering, 127, 1154.

B. Eckhardt, T. M. Schneider, B. Hof and J. Westerweel (2007), Turbulence t*ransition in pipe flow.* Annual Review of Fluid Mechanics, 39, 447.

S. Eliahou, A. Tumin and I. Wygnanski (1998), *Laminar-turbulent transition in Poiseuille pipe flow subjected to periodic perturbation emanating from the wall.* Journal of Fluid Mechanics, 361, 333.

W. D. Ernst (1966), *Investigation of the turbulent shear flow of dilute aqueous CMC solutions.* AIChE Journal, 12-3, 581.

M. P. Escudier, D. M. Jones and I. W. Gouldson (1992), F*ully developed pipe flow of shear-thinning liquids.* Sixth International Symposium on Applications of Laser Techniques to Fluid Mechanics, Lisbon, 1.3.1.

M. P. Escudier and F. Presti (1996), *Pipe flow of a thixotropic liquid.* Journal of Non-Newtonian Fluid Mechanics, 62, 291.

M. P. Escudier, F. Presti and S. Smith (1999), *Drag reduction in the turbulent pipe flow of polymers.* Journal of Non-Newtonian Fluid Mechanics, 81, 197.

M. P. Escudier, I. W. Gouldson, A. S. Pereira, F. T. Pinho and R. J. Poole (2001), *On the reproducibility of the rheology of shear-thinning liquids.* Journal of Non-Newtonian Fluid Mechanics, 97, 99.

M. P. Escudier, P. J. Oliveira and F. T. Pinho (2002), *Fully developed laminar flow of purely viscous non-Newtonian liquids through annuli, including the effects of eccentricity and inner-cylinder rotation.* International Journal of Heat and Fluid Flow, 23, 52.

M. P. Escudier, R. J. Poole, F. Presti, C. Dales, C. Nouar, C. Desaubry, L. Graham, and L. Pullum (2005), *Observations of asymmetrical flow behaviour in transitional pipe flow of yield-stress and other shear-thinning liquids.* Journal of Non-Newtonian Fluid Mechanics, 127, 143.

A. Esmael and C. Nouar (2008), *Transitional flow of a yield-stress fluid in a pipe: evidence of a robust coherent structure.* Physical Review E, 77, 057302.

H. Faisst and B. Eckhardt (2004), *Sensitive dependence on initial conditions in transition to turbulence in pipe flow.* Journal of Fluid Mechanics, 504, 343.

J. Ferguson and K. Walters (1990), *Shear and extensional flow of polyacrylamide solutions.* Rheologica Acta, 29, 571.

J. D. Ferry (1980), *Viscoelastic properties of polymers.* Wiley, third edition.

R. E. Franklin and J. M. Wallace (1970), *Absolute measurements of static-hole error using flush transducers.* Journal of Fluid Mechanics, 42, 33.

G. G. Fuller, C. A. Cathey, B. Hubbard and B. E. Zebrowski (1987), *Extensional viscosity measurements for low-viscosity fluids.* Journal of Rheology, 31, 235.

I. Fyrippi, I. Owen and M. P. Escudier (2004), *Flowmetering of non-Newtonian liquids.* Flow Measurement and Instrumentation, 15, 131.

M. T. Ghannam and M. N. Esmail (1998), *Rheological properties of aqueous polyacrylamide solutions.* Journal of Applied Polymer Science, 69, 1587.

I. W. Gouldson (1997), *The flow of Newtonian and non-Newtonian fluids in an annular geometry.* PhD Thesis, Department of Engineering, The University of Liverpool.

A. Gyr (1984), *Direct evidence that drag reduction is an effect of the elongation of the polymer molecules in drag reduction.* Third International Conference on Drag Reduction, Bristol, B, 10-1.

R. W. Hanks (1962), *The laminar-turbulent transition for fluids with a yield stress.* AIChE Journal, 9-3, 306.

J. L. Herrin and J. C. Dutton (1993), *An investigation of LDA velocity bias correction techniques for high-speed separated flows.* Experiments in Fluids, 14, 354.

B. Hof, A. Juel and T. Mullin (2003), *Scaling of the turbulence transition threshold in a pipe.* Physical Review Letters, 91, 244502.

B. Hof, J. Westerweel, T. Schneider and B. Eckhardt (2006), *Finite lifetime of turbulence in shear flows.* Nature (London), 443, 59.

K. D. Housiadas, A.N. Beris and R.A. Handler (2005), *Viscoelastic effects on higher order statistics and on coherent structures in turbulent channel flow.* Physics of Fluids, 17, 035106.

J. W. Hoyt (1972), *The effect of additives on friction factor.* Journal of Basic Engineering, 94, 258.

A. Japper-Jaafar (2008), Private communication.

A. Jeanes, J. E. Pittsley and F. R. Senti (1961), *Polysaccharide B-1459: A new hydrocolloid polyelectrolyte produced from glucose by bacterial fermentation.* Journal of Applied Polymer Science, 5-17, 519.

F. Keegan (2008), Private communication.

R. Lapasin and S. Pricl (1995), *Rheology of industrial polysaccharides: theory and applications.* Chapman & Hall, first edition.

J. Laufer (1954), The structure of turbulence in fully developed pipe flow. National Bureau of Standards Report, Report 1174, 1.

R. J. Leite (1959), *An experimental investigation of the stability of Poiseuille flow.* Journal of Fluid Mechanics, 5, 81.

J. L. Lumley (1969), *Drag reduction by additives.* Annual Reviews of Fluid Mechanics, 1, 367.

H. R. E. van Maanen (1999), *Retrieval of turbulence and turbulence properties from randomly sampled laser-Doppler anemometry data with noise.* PhD Thesis, Technical University of Delft.

E. F. Matthys (1991), *Heat transfer, drag reduction and characterisation for turbulent flow of polymer solutions: recent results and research needs.* Journal of Non-Newtonian Fluid Mechanics, 38, 313.

D. K. McLaughlin and W. G. Tiederman (1973), *Biasing for individual realization of laser anemometer.* Physics of Fluids, 16, 2082.

F. Mellibovsky and A. Meseguer (2006), *The role of streamwise perturbations in pipe flow transition.* Physics of Fluids, 18, 074104.

A. B. Metzner and J. C. Reed (1955), *Flow of non-Newtonian fluids - correlation of laminar, transition and turbulent-flow regions.* AIChE Journal, 1-4, 434.

A. B. Metzner and M. G. Park (1964), *Turbulent flow characteristics of viscoelastic fluids.* Journal of Fluid Mechanics, 20, 291.

P. Mishra and G. Tripathi (1971), *Transition from laminar to turbulent flow of purely viscous non-Newtonian fluids in tubes.* Chemical Engineering Science, 26, 915.

T. Moussa and C. Tiu (1994), *Factors affecting polymer degradation in turbulent pipe flow.* Chemical Engineering Science, 49-10, 1681.

A. Nakano and Y. Minoura (1975), *Effects of solvent and concentration on scission of polymers with high-speed stirring.* Journal of Applied Polymer Science, 19, 2119.

C. Nouar and I. A. Frigaard (2001), *Nonlinear stability of Poiseuille flow of a Bingham fluid: theoretical results and comparison with phenomenological criteria.* Journal of Non-Newtonian Fluid Mechanics, 100, 127.

P. Orlandi (1995), *A tentative approach to the direct simulation of drag reduction by polymers.* Journal of Non-Newtonian Fluid Mechanics, 60, 277.

J. T. Park, R. J. Mannheimer, T. A. Grimley and T. B. Morrow (1989), *Pipe flow measurements of a transparent non-Newtonian slurry.* Journal of Fluids Engineering, 111, 331.

V. C. Patel and M. R. Head (1969), *Some observations on skin friction and velocity profiles in fully developed pipe and channel flows.* Journal of Fluid Mechanics, 38, 181.

R. W. Paterson and F. H. Abernathy (1972), *Transition to turbulence in pipe flow for water and diluted solutions of polyethylene oxide.* Journal of Fluid Mechanics, 51, 177.

J. Peixinho, C. Nouar, C. Desaubry and B. Théron (2005), *Laminar, transitional and turbulent flow of yield stress fluid in a pipe.* Journal of Non-Newtonian Fluid Mechanics, 128, 172.

J. Peixinho and T. Mullin (2006), *Decay of turbulence in pipe flow.* Physical Review Letters, 96, 094501.

A. S. Pereira and F. T. Pinho (1994), *Turbulent pipe flow characteristics of low molecular weight polymer solutions.* Journal of Non-Newtonian Fluid Mechanics, 55, 321.

F. T. Pinho (1990), *Velocity characteristics of polymer solutions in ducts.* PhD Thesis, Department of Mechanical Engineering, Imperial College of Science, Technology and Medicine, University of London.

F. T. Pinho and J. H. Whitelaw (1990), *Flow of non-Newtonian fluids in a pipe.* Journal of Non-Newtonian Fluid Mechanics, 34, 129.

R. J. Poole (2002), *Turbulent flow of Newtonian and non-Newtonian liquids through sudden expansions.* PhD Thesis, Department of Engineering, The University of Liverpool.

R. J. Poole and M. P. Escudier (2004), *Turbulent flow of viscoelastic liquids though an axisymmetric sudden expansion.* Journal of Non-Newtonian Fluid Mechanics, 117, 25.

F. Presti (2000), *Investigation of transition and turbulent pipe flow of non-Newtonian fluids.* PhD Thesis, Department of Engineering, The University of Liverpool.

P. K. Ptasinski, F. T. M. Nieuwstadt, B. H. A. A. Van Den Brule and M. A. Hulsen (2001), *Experiments in turbulent pipe flow with polymer additives at maximum drag reduction.* Flow, Turbulence and Combustion, 66, 159.

G. V. Reddy and R. P. Singh (1985), *Drag reduction effectiveness and shear stability of polymer-polymer and polymer-fibres mixtures in recirculatory turbulent flow of water.* Rheologica Acta, 24, 296.

O. Reynolds (1883), *An experimental investigation of the circumstances which determine whether the motion of water shall be direct or sinuous, and of the law of resistance in parallel channels.* Philosophical Translations of the Royal Society of London A, 174, 935.

W. E. Rochefort and S. Middleman (1987), *Rheology of xanthan gum: salt, temperature and strain effects in oscillatory and steady shear experiments.* Journal of Rheology, 31(4), 337.

A. B. Rodd, D. E. Dunstan and D. V. Boger (2000), *Characterisation of xanthan gum solutions using dynamic light scattering and rheology.* Carbohydrate Polymers, 42, 159.

L. E. Rodd, T. P. Scott, D. V. Boger, J. J. Cooper-White and G. H. McKinley (2005), *The inertio-elastic planar entry flow of low-viscosity elastic fluids in microfabricated geometries.* Journal of Non-Newtonian Fluid Mechanics, 129, 1.

M. J. Rudd (1972), *Velocity measurements made with a laser dopplermeter on the turbulent pipe flow of a dilute polymer solution.* Journal of Fluid Mechanics, 51(4), 673.

N. W. Ryan and M. M. Johnson (1959), *Transition from laminar to turbulent flow in pipes.* AIChE Journal, 5, 433.

R. G. Shaver and E. W. Merrill (1959), *Turbulent flow of pseudoplastic polymer solutions in straight cylindrical tubes.* AIChE Journal, 5-2, 181.

M. L. Sheely (1932), *Glycerol viscosity tables.* Industrial and Engineering Chemistry, 24(9), 1060.

P. T. Slatter (1999), *The laminar-turbulent transition prediction for non-Newtonian slurries.* International Conference on Problems in Fluid Mechanics and Hydrology, Prague, 1, 247.

S. E. Smith (2000), *Turbulent duct flow of non-Newtonian liquids.* PhD Thesis, Department of Engineering, The University of Liverpool.

J. R. Stokes, L. J. W. Graham, N. J. Lawson and D. V. Boger (2001), *Swirling flow of viscoelastic fluids. Part 1. – Interaction between inertia and elasticity.* Journal of Fluid Mechanics, 429, 67.

R. Sureshkumar, A. N. Beris and R. A. Handler (1997), *Direct numerical simulation of the turbulent channel flow of a polymer solution.* Physics of Fluids, 9, 743.

K. C. Tam and C. Tui (1993), *Improved correlation of shear-dependent viscosity of polyelectrolytes solutions.* Journal of Non-Newtonian Fluid Mechanics, 46, 275.

W. G. Tiederman (1989), *The effect of dilute polymer solutions on viscous drag and turbulence structure.* IUTAM Symposium of Turbulence and Drag Reduction, Springer-Verlag, New York, 187.

B. A. Toms (1949), *Some observations on the flow of linear polymer solutions through straight tubes at large Reynolds numbers.* First International Congress on Rheology, North Holland, Amsterdam, 2, 135.

J. M. J. den Toonder, F. T. M. Nieuwstadt and G. D. C. Kuiken (1995), *The role of elongational viscosity in the mechanism of drag reduction by polymer additives.* Applied Scientific Research, 54, 95.

J. M. J. den Toonder, M. A. Hulsen, G. D. C. Kuiken and F. T. M. Nieuwstadt (1997), *Drag reduction by polymer additives in a turbulent pipe flow: numerical and laboratory experiments.* Journal of Fluid Mechanics, 337, 193.

C. Tropea (1995), *Laser Doppler anemometry: recent developments and future challenges.* Measurement Science and Technology, 6, 605.

P. S. Virk, H. S. Mickley and K. A. Smith (1970), *The ultimate asymptote and mean flow structure in Tom's phenomenon.* Journal of Applied Mechanics, 37, 488.

P. S. Virk (1975), *Drag reduction fundamentals.* AIChE Journal, 21, 625.

K. Walters, A. Q. Bhatti and N. Mori (1990), *The influence of polymer conformation on the rheological properties of aqueous polymer solutions.* Recent Developments in Structured Continua, Vol. 2 Eds: D. De Kee and P. N. Kaloni, Pitman.

K. Weissenberg (1949), *Flow of liquids under actions of stationary shear in gaps.* First International Congress on Rheology, Amsterdam, 2, 114.

F. M. White (1994), *Fluid mechanics.* McGraw-Hill, Inc., third edition.

I. J. Wygnanski and F. H. Champagne (1973), *On transition in a pipe. Part 1. The origin of puffs and slugs and the flow in a turbulent slug.* Journal of Fluid Mechanics, 59-2, 281.

I. J. Wygnanski, M. Sokolov and D. Friedman (1975), *On transition in a pipe. Part 2. The equilibrium puff.* Journal of Fluid Mechanics, 69-2, 283.

W. J. Yanta and R. A. Smith (1973), *Measurements of turbulence-transport properties with a laser-Doppler velocimeter,* 11th Aerospace Science Meeting, Washington, paper 73, 169.

K. Yasuda, R. C. Armstrong and R. E. Cohen (1981), *Shear flow properties of concentrated solutions of linear and star branched polystyrenes.* Rheologica Acta, 20, 163.

J. L. Zakin, C. C. Ni, R. J. Hansen and M. M. Reischman (1977), *Laser Doppler velocimetry studies of early turbulence.* Physics of Fluids, 20-10, S85.

Appendix

Calculation of the maximum longitudinal curvature of the pipe axis R_A

Considering the total length of the glass tube equal to be 22.22 m and a linear alignment within 0.2 mm (Section 3.2), as represented in the figure,

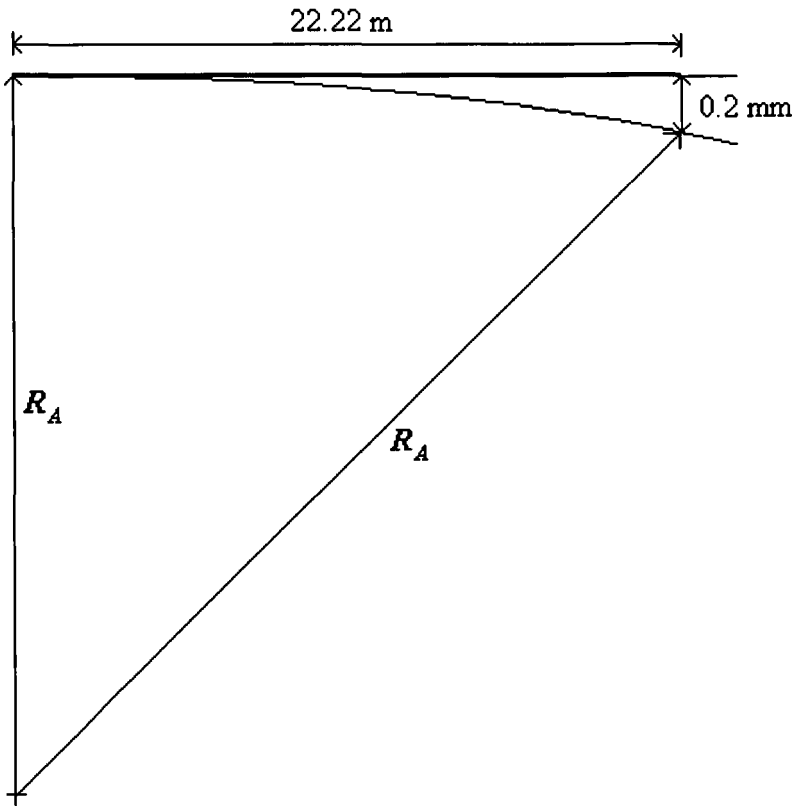

the maximum R_A is given by:

$$R_A{}^2 = (R_A - 0.0002)^2 + 22.22^2$$

$$R_A = \frac{\left(0.0002^2 + 22.22^2\right)}{0.0004} \approx 10^6 \text{ m}$$